



THE HONG KONG
POLYTECHNIC UNIVERSITY

香港理工大學

Pao Yue-kong Library

包玉剛圖書館

Copyright Undertaking

This thesis is protected by copyright, with all rights reserved.

By reading and using the thesis, the reader understands and agrees to the following terms:

1. The reader will abide by the rules and legal ordinances governing copyright regarding the use of the thesis.
2. The reader will use the thesis for the purpose of research or private study only and not for distribution or further reproduction or any other purpose.
3. The reader agrees to indemnify and hold the University harmless from and against any loss, damage, cost, liability or expenses arising from copyright infringement or unauthorized usage.

IMPORTANT

If you have reasons to believe that any materials in this thesis are deemed not suitable to be distributed in this form, or a copyright owner having difficulty with the material being included in our database, please contact lbsys@polyu.edu.hk providing details. The Library will look into your claim and consider taking remedial action upon receipt of the written requests.

**WIDE AREA MONITORING SYSTEM
AND ITS APPLICATION ON POWER SYSTEM
LOW-FREQUENCY OSCILLATION
SUPPRESSION**

ZHANG PENG

Ph.D

The Hong Kong Polytechnic University

2012



The Hong Kong Polytechnic University

Department of Electrical Engineering

**WIDE AREA MONITORING SYSTEM
AND ITS APPLICATION ON POWER SYSTEM
LOW-FREQUENCY OSCILLATION
SUPPRESSION**

ZHANG PENG

A thesis submitted in partial fulfilment of the
requirements for the degree of Doctor of

Philosophy

September 2011

CERTIFICATE OF ORIGINALITY

I hereby declare that this thesis is my own work and that, to the best my knowledge and belief, it reproduces no material previously published or written or material which has been accepted for the award of any other degree or diploma, except where due acknowledgement has been made in the text.

_____ (Signed)

_____ ZHANG Peng _____ (Name of student)

ABSTRACT

As modern electric power systems are transforming into smart grids, real-time wide area monitoring system (WAMS) has become an essential tool for power system operation and control. Though many WAMS based stability analysis and control schemes have been proposed in recent years, their practicality is often limited since important WAMS characteristics such as synchronization accuracy and signal time delay are often not considered in the design. Now, there is an urgent and necessary need for a comprehensive, systematic and quantitative analysis of WAMS characteristics. This thesis not only embarks on the analysis of WAMS characteristics but also investigates their influence on the power system stability analysis and control.

Synchronization accuracy and signal time delay are two of the inherent WAMS characteristics which have to be considered in any WAMS based real-time applications. The control effectiveness of a well-designed wide-area controller which performs well in an ideal system could be badly deteriorated once these two WAMS characteristics are taken into account. In this thesis, synchronization accuracy and signal time delay are systematically studied and quantitatively calculated for the first time. Recommendations have been made to improve the synchronization accuracy and reduce the signal time delay of synchronized phasors supplied by WAMS.

With the increasing applications of WAMS for on-line stability analysis and control in smart grids, it is also imperative to quantitatively evaluate the reliability of WAMS so as to identify the critical components for ensuring the secure and reliable operation of a smart grid. This thesis proposes a comprehensive reliability evaluation scheme for WAMS and its components based on Monte Carlo fault tree (MCFT) analysis. WAMS is a complex system consisting of many component devices and special communication networks

which can be divided to five functional sub-systems for PMUs, PDC, local and wide area communication networks, and control center. A reliability model for each sub-system will first be constructed using the fault tree (FT) modeling method and then be analyzed using the Monte Carlo simulation approach to evaluate a set of reliability indices. Lastly, the FT modeling method will be applied again to construct the reliability model of WAMS and evaluate its reliability using the sub-system results. The validity and advantages of this MCFT reliability evaluation method applied on WAMS have been verified with simulation and comparison studies. A simple example based on an adaptive wide-area damping control scheme has also been given to show the application of the proposed WAMS reliability evaluation method.

The restructuring of the modern electric power systems has had profound effects on the operation of the power grid. Traditional control strategies could become ineffective under the new system structure and new control strategies would be needed as a result. As an important information platform in modern power grid, WAMS with different topology structures would have large impacts on the design of these new control strategies. In this thesis, an in-depth investigation on the relative merits of centralized and distributed WAMS has been conducted to find the most suitable WAMS topology for on-line monitoring and control of the Shandong power grid. Various aspects including investment, signal time delay, operation reliability and risk have been systematically analyzed and compared for the centralized and distributed WAMS. An improved Minimum Spanning Tree (MST) algorithm has been proposed for the construction of communication networks with minimum investment in both centralized and distributed WAMS of Shandong power grid. Though the investment needed for a centralized or distributed WAMS in Shandong power grid is almost the same, the distributed WAMS has shorter signal time delay, higher reliability, and lower risk

than the centralized one.

Last but not least, a novel WAMS based adaptive wide-area low frequency oscillation damping control scheme has been proposed as a rational and logical application of the WAMS because of its relative long operation time frame. Practical issues including signal transmission time delay, changes in system operation conditions and uncertainties in system configuration and parameters have been fully considered in the design to ensure the damping effectiveness and the practicality of the control scheme. The core control algorithm consists of stochastic subspace identification (SSI), wide-area input signal formulation, and signal time delay compensation. Frequency deviation in each generator will be measured and collected via the WAMS to identify the low frequency oscillation modes using SSI and generate a wide-area control signal for each oscillation mode. The superiority of SSI over other identification methods lies in its ability to identify the oscillation modes collectively from all the measured signals instead of individual ones and high resistance to measurement noise. For each identified mode, the corresponding generator cluster will be identified to produce a wide-area control signal to combine with the local input signal as the new input signal of PSSs installed in the generators participating in this oscillation mode. Signal time delays are measured and compensated locally at the generators using GPS time services and adaptive time delay compensators. The effectiveness and robustness of the proposed adaptive wide-area damping control scheme have been verified with simulation studies on the IEEE 4-generator 2-area and IEEE 16-generator 5-area test systems under a number of disturbance scenarios.

ACKNOWLEDGEMENT

First and foremost, I would like to express my sincere gratitude and appreciation to my supervisor, Dr. Ka Wing Chan, for his invaluable guidance and constant encouragement throughout the challenging path towards a doctoral degree. His enthusiasm and guidance were strong sources of inspiration. He is always available for me in spite of his busy schedule and duties. It has been an honor to work under his supervision.

Obtaining a degree called Doctor of Philosophy is a life changing experience. I honestly never thought it would be this intellectually challenging, but fun and satisfying. I have a wonderful time at my department – Department of Electrical Engineering.

I am grateful to all staff of the Department of Electrical Engineering for their support and help. I would like to acknowledge the help that I received from my friends and coworkers as well.

I reserve special thanks to my wife, my parents and other family members who encourage me so much in life and helped me become the person I am today. They are always being supportive. They shower me with love and care, which is why I feel so lucky to have been blessed with the family.

3.2.2	Signal Transmission Error	41
2.2.3	Errors From Power System.....	42
3.3	Signal Time Delay.....	43
3.4	Summary	46
CHAPTER IV RELIABILITY EVALUATION OF WAMS		47
4.1	Introduction.....	47
4.2	FT Modeling Method and Monte Carlo Simulation Approach.....	49
4.2.1	FT Modeling Method.....	50
4.2.2	Monte Carlo Simulation Approach.....	51
4.2.3	Monte Carlo Simulation Approach for FT Logic Gates	55
4.3	Architecture and Reliability Model of WAMS	63
4.4	Reliability Evaluation of PMU.....	65
4.4.1	Reliability Modeling of PMU	66
4.4.2	Reliability Evaluation Flow Chart of PMU	75
4.4.3	Reliability Indices of PMU	77
4.5	Reliability Evaluation of PDC and Control Center.....	85
4.6	Reliability Evaluation of Communication Network	87
4.6.1	Reliability Modeling of WACN.....	88
4.6.2	Reliability Modeling of LACN.....	94
4.6.3	Reliability Indices of Communication Networks	97
4.7	Reliability Evaluation of WAMS	103
4.8	Applications of WAMS Reliability in Power System Stability Analysis and Control.....	104
4.9	Summary	105
CHAPTER V A QUANTITATIVE AND COMPREHENSIVE INVESTIGATION OF WAMS ARCHITECTURE.....		107
5.1	Introduction.....	107

5.2	WAMS Architecture	109
5.2.1	Centralized WAMS	109
5.2.2	Distributed WAMS.....	110
5.2.3	Communication Network.....	112
5.3	The Comparison Criteria of CN.....	112
5.3.1	Investment.....	113
5.3.2	Signal Time Delay	113
5.3.3	Reliability.....	115
5.3.4	Risk	116
5.3.4.1	Calculation of Occurrence Probability of CN Incident	116
5.3.4.2	Quantitative Calculation of Consequence.....	117
5.4	Construction of Communication Network.....	122
5.5	Study Case.....	124
5.5.1	WAMS in Shandong Power Grid.....	124
5.5.2	Centralized WAMS in Shandong Power Grid	125
5.5.3	Distributed WAMS in Shandong Power Grid.....	126
5.5.4	Comparison of Centralized and Distributed CNs	127
5.6	Summary	132

CHAPTER VI SSI ALGORITHM FOR ON-LINE POWER		
SYSTEM LOW-FREQUENCY OSCILLATION		
IDENTIFICATION.....		134
6.1	Introduction.....	134
6.2	Feasibility of Applying SSI Algorithm for Identification of Power System Low-Frequency Oscillation	136
6.3	Analysis of the SSI Algorithm	138
6.3.1	Stochastic State-Space Model.....	138
6.3.2	Solving of Stochastic State-Space Model.....	139

6.3.3	Identification of Oscillation Mode Parameters and Shape	141
6.3.4	Merits of SSI Algorithm	142
6.4	Validity Verification for SSI Algorithm	142
6.5	Case Studies	144
6.5.1	Application of SSI in Low-Frequency Oscillation analysis	144
6.5.2	4-Generator 2-Area Test System.....	145
6.5.3	16-Generator 5-Area Test System.....	150
6.6	Summary	154
CHAPTER VII ADAPTIVE WIDE-AREA DAMPING CONTROL		
SCHEME WITH SSI AND SIGNAL TIME DELAY		
COMPENSATION		
		155
7.1	Introduction	155
7.2	Adaptive Wide-Area Damping Control Scheme.....	156
7.3	Wide-Area Input Signal Formulation.....	159
7.4	Signal Time Delay Compensation.....	159
7.5	Control Flow of Adaptive Wide-Area Damping Control Scheme	161
7.6	Case Studies	163
7.6.1	4-Generator 2-Area Test System.....	163
7.6.2	16-Generator 5-Area Test System.....	167
7.7	Implementation Issues.....	174
7.8	Summary and Future Work	175
CHAPTER VIII CONCLUSION.....		
		176
APPENDICES		
		181
Appendix A	IEEE 4-Generators 2-Area System Parameters.....	181
Appendix B	IEEE 16-Generator 68-Bus System Parameters.....	183
REFERENCE		
		195

LIST OF FIGURES, TABLES, AND ABBREVIATIONS

LIST OF FIGURES

- Fig. 3.1 Functional blocks of a PMU
- Fig. 3.2 Time sequence of PPS and PMU internal clock
- Fig. 3.3 Typical structure of a WAMS
- Fig. 4.1 Changing curve of $F(t)$ and $1-F(t)$ with time t
- Fig. 4.2 Symbol of OR gate
- Fig. 4.3 Possible state-time diagrams of OR gate
- Fig. 4.4 Symbol of AND gate
- Fig. 4.5 Possible state-time diagrams of AND gate
- Fig. 4.6 Symbol of voting gate
- Fig. 4.7 Transformation from voting gate to the combination of OR and AND gate
- Fig. 4.8 Symbol of PAND gate
- Fig. 4.9 Possible state-time diagrams of PAND gate
- Fig. 4.10 Symbol of CSP gate
- Fig. 4.11 Possible state-time diagrams of CSP gate
- Fig. 4.12 Symbol of FDEP gate
- Fig. 4.13 Possible state-time diagram of FDEP gate
- Fig. 4.14 Architecture of multilayer WAMS
- Fig. 4.15 FT reliability model of multilayer WAMS
- Fig. 4.16 Functional structure of PMU
- Fig. 4.17 Sub-FT reliability model of data collection module
- Fig. 4.18 Operation mechanism of GPS
- Fig. 4.19 Sub-FT reliability model of GPS module
- Fig. 4.20 Sub-FT reliability model of CPU module

- Fig. 4.21 Sub-FT reliability models of communication and power source module
- Fig. 4.22 Complete FT reliability model of PMU
- Fig. 4.23 Flow chart of reliability evaluation of PMU
- Fig. 4.24 Convergence factor β against Monte Carlo simulation time for both Case 1 and 2
- Fig. 4.25 Sensitivity analysis of the basic components in GPS and CPU modules
- Fig. 4.26 Structure of a PDC
- Fig. 4.27 WAMS for IEEE 14-bus test system
- Fig. 4.28 FT reliability model of WACN
- Fig. 4.29 Sub-FT₁ for WACN failure caused by PFF and ADM switching failure
- Fig. 4.30 Sub-FT₂ for WACN failure caused by single section PFF
- Fig. 4.31 Sub-FT₃ for WACN failure caused by two or more sections PFF
- Fig. 4.32 Sub-FT₄ for WACN failure caused by single section CCFF and ADM switching failure
- Fig. 4.33 Sub-FT₅ for WACN failure caused by single section CCFF
- Fig. 4.34 Sub-FT₆ for WACN failure caused by two or more sections CCFF
- Fig. 4.35 Sub-FT₇ for WACN failure caused by ADM failure
- Fig. 4.36 5-node U-SHRN/2 structure of LACN₁
- Fig. 4.37 7-node U-SHRN/2 structure of LACN₂
- Fig. 4.38 3-node U-SHRN/2 structure of LACN₃
- Fig. 4.39 Convergence factor β against simulation count for Case 1 and 2
- Fig. 5.1 Architecture and data flow of centralized WAMS
- Fig. 5.2 Architecture and data flow of distributed WAMS
- Fig. 5.3 Geographical distribution of PMUs in WAMS of Shandong Power

Grid

- Fig. 5.4 Centralized WAMS in Shandong Power Grid
- Fig. 5.5 Distributed WAMS in Shandong Power Grid
- Fig. 6.1 Application of SSI algorithm in power system stability control
- Fig. 6.2 IEEE 4-generator 2-area test system
- Fig. 6.3 Generator rotor speed under different SNR
- Fig. 6.4 COI power angle between Area 1 and Area 2 under different SNR
- Fig. 6.5 Effects of noise on power system low-frequency oscillation mode shape
- Fig. 6.6 IEEE 16-generator 5-area test system
- Fig. 6.7 SSI identification mode shapes in Case A
- Fig. 6.8 SSI identification mode shapes in Case B
- Fig. 7.1 Adaptive wide-area damping control Scheme
- Fig. 7.2 Exciter model of one generator participating in a specific inter-area oscillation mode with PSS combining local and wide-area input signals
- Fig. 7.3 Scheme of signal time delay compensator
- Fig. 7.4 Time delay modeling and compensation
- Fig. 7.5 Flow chart of the proposed adaptive wide-area damping control scheme
- Fig. 7.6 Active powers from area 1 to 2 in Case a and b
- Fig. 7.7 Active powers from area 1 to 2 in Case a and b with signal time delay
- Fig. 7.8 Rotor speed deviations of G12 and G13 in Case a and b under operation scenario 1
- Fig. 7.9 Rotor speed deviations of G12 in Case a and b under operation scenario 1 with signal time delay
- Fig. 7.10 Rotor speed deviations of G12 and G13 in Case a and b under

operation scenario 2

Fig. 7.11 Rotor speed deviations of G12 in Case a and b under operation scenario 2 with signal time delay

Fig. A.1 Single line diagram of IEEE 4-generator 2-area system

Fig. A.2 IEEE type 1 rotating excitation system model

Fig. B.1 Single line diagram of IEEE 16-generator 68-bus system

Fig. B.2 IEEE Type 1 rotating excitation system model

LIST OF TABLES

- Table 3.1 Demand of synchronization accuracy in synchronized phasors for various real-time applications
- Table 4.1 Reliability parameters of basic components in PMU
- Table 4.2 Reliability indices of PMU and seven function modules in PMU
- Table 4.3 Comparison of reliability indices of PMU from different methods
- Table 4.4 Importance analysis of function modules in PMU
- Table 4.5 Importance analysis of basic components in GPS and CPU modules
- Table 4.6 Change of reliability indices of PMU with redundancy design of basic components in GPS and CPU modules
- Table 4.7 Reliability parameters of two different-scaled WACN
- Table 4.8 Comparison of reliability indices of WACN for different reliability evaluation methods
- Table 4.9 Importance analysis of fiber sections in WACN
- Table 4.10 Reliability parameters of LACN₁
- Table 4.11 Reliability parameters of LACN₂
- Table 4.12 Reliability parameters of LACN₃
- Table 4.13 Reliability indices of LACNs for IEEE 14-bus test system
- Table 5.1 The 1~9 scale rule in AHP algorithm
- Table 5.2 *RI* value
- Table 5.3 Risk grade of each risk factor
- Table 5.4 Investment for centralized and distributed CNs
- Table 5.5 Signal time delay of centralized and distributed CNs
- Table 5.6 Reliability of centralized and distributed CNs
- Table 6.1 Eigenvalues of the four-order system obtained with eigenvalue analysis and SSI algorithm
- Table 6.2 Identification results without noise

- Table 6.3 Identification results with noise (SNR=90)
- Table 6.4 Identification results with noise (SNR=80)
- Table 6.5 Identification results with noise (SNR=70)
- Table 6.6 Inter-area oscillation modes of IEEE 16-generator 5-area test system
- Table 6.7 SSI identification results of Case A (Bus 33)
- Table 6.8 SSI identification results of Case A (Bus 12 and Bus 28)
- Table 6.9 SSI identification results of Case B (Bus 17)
- Table 6.10 SSI identification results of Case B (Bus 1 and Bus 48)
- Table 7.1 Identification results for IEEE 4-generator 2-area test system
- Table 7.2 Identification results for IEEE 16-generator 5-area test system in Scenario 1
- Table 7.3 Identification results for IEEE 16-generator 5-area test system in Scenario 2
- Table B. 1 Bus data of IEEE 16-generator 68-bus system
- Table B.2 Branch data of IEEE 16-generator 68-bus system
- Table B.3 Generator data of IEEE 16-generator 68-bus system
- Table B.4 Exciter data of IEEE 16-generator 68-bus system
- Table B.5 PSS data of IEEE 16-generator 68-bus system

LIST OF ABBREVIATIONS

WAMS	Wide Area Measurement System
PMU	Phasor Measurement Unit
PDC	Phasor Data Concentrator
WACN	Wide Area Communication Network
LACN	Local Area Communication Network
GPS	Global Positioning System
PSS	Power System Stabilizer
HVDC	High Voltage Direct Current
FACTS	Flexible AC Transmission Systems
FFT	Fast Fourier Transformation
SWFT	Sliding Window Fourier Transformation
HHT	Hilbert-Huang Transformation
AR	Auto-Regressive
ARMA	Auto-Regressive Moving Average
SVD	Singular Value Decomposition
UPFC	Unified-Power-Flow Controller
LMI	Linear Matrix Inequality
FT	Fault Tree
DFT	Dynamic Fault Tree
SSI	Stochastic Subspace Identification
CSG	China Southern Power Grid
WACS	Wide-area Control System
OTSCPS	On-line Transient Stability Control Pre-decision System
WECC	Western Electric Coordinating Council
BPA	Bonneville Power Administration
DSA	Dynamic Security Assessment

PPS	Pulse-Per-Second
UTC	Universal Time Coordinated
CT	Current Transformer
PT	Potential Transformer
CPN	Colored Petri Nets
RBD	Reliability Block Diagrams
SEQ	Enforcing Gate
PAND	Priority-AND Gate
FDEP	Functional Dependency Gate
CSP	Cold Spare Gate
WSP	Warm Spare Gate
HSP	Hot Spare Gate
MTBF	Mean Time between Failures
MTTR	Mean Time to Repair
SONET	Synchronous Optical Network
SDH	Synchronous Digital Hierarchy
SSP	Synchronous Sampling Pulse
STS	Synchronous Time Signal
FEP	Front End Processor
RTDB	Real Time Data Base
HisDB	History Data Base
SHR	Self-Healing Ring
U-SHR/2	2-Fiber Unidirectional SHR
ADM	Add-Drop Multiplexers
PFF	Primary Fiber Failure
SFF	Spare Fiber Failure
CCFF	Common Cause Fiber Failure

CVA	Canonical Variate Algorithm
COI	Centre of Inertia
SNR	Signal-to-Noise Ratio
LPSS	Local Power System Stabilizer
WADC	Wide-Area Damping Controller
LIS	Local Input Signal
WAIS	Wide-Area Input Signal

CHAPTER I INTRODUCTION

1.1 BACKGROUND AND MOTIVATION

From 1960s', several blackouts [1-4], which seriously affect the normal production and living of people, have taken place. All of these blackouts, which cause large area power outage, have made power system engineers and researchers better recognize that the local information based traditional power system control and protection schemes cannot satisfy the demand of modern interconnected smart grids for oscillation control, system protection and dynamic security protection. With the development of technologies especially electronic, computer and communication technologies, Wide Area Monitoring System (WAMS) has now emerged acts as an advanced and reliable information platform for power system real-time monitoring and control [5,6].

The advancement of WAMS has enabled the use of real-time and dynamic measurement data of power system operation state for on-line security assessment and real-time control of power system. Recently, the WAMS based real-time dynamic monitoring system and its advanced applications have become the hot research topics in the field of power system monitoring and control and have drawn a wide concern in the community of power system engineering.

As the information platform of power system, WAMS has its own inherent characteristics including synchronization accuracy, signal transmission time delay, and operation reliability. While the utilization of WAMS can enhance the observability and strengthen the security of power system, it does have negative effects too, mainly caused by the poor characteristic of WAMS such as poor synchronization accuracy, large signal time delay and bad reliability. In order to take the full advantages of WAMS and have it operating at best performance, it is therefore necessary to thoroughly analyze and improve the characteristics of

WAMS.

Synchronization accuracy is the time difference among the synchronized phasors supplied by WAMS. Synchronized phasors with high synchronization accuracy is essential to the practical applications of WAMS based stability analysis and control schemes in practical power systems. Poor synchronization accuracy may lead to suboptimum or even wrong analysis results and causes wrong control instructions to be produced in WAMS based analysis and control schemes. The mal-operation or refused operation of control equipments will lead to serious consequence, even the blackout of the whole power system.

In WAMS, obvious signal time delay will be introduced during signal transmission, exchange and processing. Large signal time delay can compromise the effectiveness of wide-area controllers, which work well in no delayed input systems, and even may cause disastrous accidents.

Reliability is a performance characteristic of WAMS that reflects the ability of WAMS to operate successfully long enough to supply enough synchronized phasors for the monitoring and control of power system. Concern on the reliability of the existing WAMS has been one of the major reasons for the slow pace of synchro-phasor adoption for real-time applications. In order to upgrade the existing WAMS to a production-grade system capable of meeting cyber-security requirement and the reliability needs of real-time controls and situational awareness applications, it is now absolutely essential to comprehensively and quantitatively to evaluate the reliability of WAMS. Especially, when WAMS based stability analysis and control schemes are applied to real power systems, sole consideration of the advantages offered by the WAMS alone is not sufficient whilst the risks involved are neglected. Although WAMS has been established in many countries [7,8], the utilization of WAMS information is often the main research focus and hardly any qualitative evaluation, not to

mention quantitative reliability evaluation, of WAMS has been conducted. It is not until very recently that two papers have been published on the reliability evaluation of WAMS [9,10]. In both papers, the traditional Markov method was used to construct a reliability model of WAMS, in which components of WAMS were represented as equivalent two-state model first and then Markov state transition diagram was used to depict the dynamic logic relationship between WAMS and its components. The main concern of this approach is the large state space cardinality which precludes not only the model solution but also the generation of the transition rate matrix [11]. In order to simplify the Markov state transition diagram, only single fault pattern in the failure of WAMS was therefore considered while multiple fault patterns were ignored. Furthermore, during the reliability evaluation of WAMS, only the reliability of Phasor Measurement Unit (PMU) measurements uploading from PMUs to control center was considered, while reliability of control instructions downloading from control center to PMUs was ignored. Without an accurate reliability model of WAMS, it would be difficult to derive accurate reliability indices.

Once a reliability model of WAMS is constructed, an analytical algorithm would be needed to evaluate the reliability indices. State enumeration technique was used in [10] to analyze the Markov based reliability model of WAMS. However, numerous states will be resulted as the system size grows and prohibit its practical use in large-scale WAMS. In [9], state transfer diagram was used to analyze the reliability model of WAMS and the same combination explosion problem exists.

Pioneer studies mostly focus on the utilization of synchronized phasors supplied by WAMS to analyze and control the stability and security of power system. However, the influence of WAMS characteristics including investment,

synchronization accuracy, signal time delay and reliability on power system stability analysis and control has not researched thoroughly yet.

For a modern inter-connected smart grid, it's safe and stable operation depends heavily on the real-time data transmitted in WAMS. When a power grid suffers a severe incident, if WAMS cannot supply enough real-time data to the control center, the incident could escalate and cause the power grid to lose its stability. The effects of the WAMS to the safe operation of the power grid shall therefore also be considered in the evaluation of the WAMS. However, at present the safety assessment on WAMS is based mostly on its reliability and focuses on the probability of WAMS being in failure or operation condition while the consequences of WAMS incidents to power grid are ignored.

With the deregulation and increasing complexity of power industries, new control strategies should be adopted. As an important carrier of the control strategy in power grid, WAMS with different structures would be resulted for better execution of different control strategies. The communication network (CN) is a bottleneck in the architecture of WAMS since the quality of data from PMU is highly dependent on the architecture of CN. The design of a high-performance CN with a better architecture is crucial to the performance of WAMS. CNs with different architecture possess different characteristics including investment, signal time delay, reliability and risk items. So far, little research has been done on this important area which is very important to the selection of CN structure in practical WAMS projects.

As mentioned above, different WAMS characteristics would have different degree of influence on power system stability analysis and control. Among all, signal time delay would be most influential. Even for a small time delay as little as 25 ms, its effect could be fatal on a power system controller with good performance when the signal time delay is ignored [12]. Compared with transient

stability or other kinds of stability problems, low-frequency oscillation is a relative slow change process with time frame ranged from 10s to 20s or more [13]. With the current state-of-art technology, WAMS based wide-area damping control would be a timely WAMS application which would compensate the signal time delay in synchronized phasors and uses them to control low-frequency oscillation. Though various kinds of WAMS based control schemes have been proposed for suppressing low-frequency power oscillations, many of them, if not all, are either ignoring the signal time delay problem or using fixed power system models, parameters, and topology. In case signal time delay was considered, very complex and time consuming compensation methods were adopted. Their practicability is therefore limited. So far, there is still a need for a practical on-line wide-area low-frequency oscillation control scheme which could be applied in practical power systems.

1.2 PRIMARY CONTRIBUTIONS

As a promising technology, WAMS has become the key of smart grid. Though many WAMS based stability analysis and control schemes have been proposed, the influences of WAMS characteristics such as synchronization accuracy, signal time delay and the reliability on power system stability analysis and control are seldom considered.

The objectives of this thesis are threefold. Firstly, the characteristics of WAMS are systematically and quantitatively analyzed. Secondly, the investment, signal time delay, reliability and risk of WAMS are taken as comparison criteria to investigate which WAMS structure would have higher performance in the monitoring and control of power system. Finally, an on-line adaptive wide-area damping control scheme with signal time delay compensation is proposed to suppress power system low-frequency oscillations.

To be more specific, the contributions of this thesis are summarized into the following three aspects:

(1) WAMS characteristics including synchronization accuracy, signal time delay and reliability are systematically studied and quantitatively calculated. Adjustments, compensations and optimizations are proposed and applied to improve or minimize the effects caused by various WAMS characteristics. A comprehensive reliability evaluation scheme based on Monte Carlo simulation and fault tree (FT) analysis is proposed for quantitative evaluation of WAMS reliability. The main advantage for using the fault tree modeling method to construct the reliability model of WAMS is that it allows multiple fault patterns in WAMS to be considered in the reliability evaluation conveniently. Furthermore, the reliability of both PMU measurements uploading from PMUs to the control center and control instructions downloading from the control center to PMUs could be considered in the construction of reliability model of WAMS. The problem of state space explosion is overcome with the use of Monte Carlo simulation for evaluating the FT reliability model of WAMS. Not only the reliability indices of WAMS can be evaluated more accurately, but also additional reliability indices such as importance indices, which cannot be easily obtained otherwise, can be deduced via the Monte Carlo simulation.

(2) The investment, signal time delay, reliability and the risk of WAMS are taken as the comparison criteria to find out, between the centralized and distributed WAMS, which WAMS structure would have better performance in the monitoring and control of power grid. WAMS established in the Shandong Power Grid is taken as a case study for conducting this investigation. An improved MST algorithm is proposed to construct the communication

networks with minimum investment in both centralized and distributed WAMS of the Shandong power grid. The investigation concludes that, in the condition with almost the same investment, the distributed WAMS has shorter signal time delay, higher reliability, and lower risk to the power grid than the centralized WAMS.

- (3) A novel adaptive wide-area damping control scheme with Stochastic Subspace Identification (SSI) and signal time delay compensation is proposed. SSI is a recent robust identification algorithm firstly used in civil engineering. In this thesis, it is adopted to identify the low-frequency oscillation modes on-line. Based on the SSI results, wide-area input signals would be calculated and combined with local input signal to act as the input signal of the PSS. A simple and practical signal time delay compensation algorithm is proposed to measure and compensate the time delay in each wide-area input signal so as to eliminate the effects of signal time delay on the proposed adaptive wide-area damping control scheme. The effectiveness and robustness of proposed adaptive wide-area damping control scheme have been extensively verified with simulation studies on the IEEE 4-generator 2-area and IEEE 16-generator 5-area test systems under various disturbance scenarios.

1.3 ORGANIZATION OF THIS THESIS

In this thesis, eight chapters are included and the main contents of these eight chapters are as follows:

In Chapter I, the background and motivation of WAMS characteristics analysis and wide-area damping control are stated first, and then the primary contributions in this thesis are introduced. Lastly, the organization of this thesis and a list of publications on this research work are presented.

In Chapter II, firstly, a literature review on WAMS applications and characteristics as well as wide-area damping control is conducted. Then, WAMSs established in the world are briefly introduced.

In Chapter III, a quantitative analysis of WAMS characteristics including synchronization accuracy and signal time delay is conducted.

In Chapter IV, firstly, FT modeling method and Monte Carlo simulation approach are introduced. Secondly, multilayer FT reliability model of WAMS is constructed to decompose the WAMS into sub-systems. Thirdly, based on the structure and functional features of PMU, FT reliability model of PMU is constructed and analyzed to derive the reliability indices of PMU using Monte Carlo simulation. While importance analysis is conducted to find the weak links in PMU, sensitivity and redundancy design analysis are conducted to find the best measures to improve the reliability of PMU. Fourthly, similar reliability evaluation method as PMU is used to analyze the reliability of PDC and control center. Fifthly, WAMS for the IEEE 14-bus test system is taken as an example to evaluate the reliability of WAMS. The reliability evaluation of communication network including WACN and LACN is conducted with the proposed MCFT reliability evaluation method. Finally, the reliability indices of PMU, PDC, communication networks and control center are combined to calculate the reliability indices of the WAMS.

In Chapter V, firstly, structures of the centralized and distributed WAMS are introduced. Secondly, the investment, signal time delay, reliability, and the risk of CN to the power grid are systematically analyzed and quantitatively calculated. Thirdly, through the comparison of the investment, signal time delay, reliability and risk of CN, WAMS established in the Shandong Power Grid is taken as an example to investigate, between the centralized and distributed CN, which CN structure would have better performance in the monitoring and control of power

grid. An improved MST algorithm is proposed to construct the CNs with minimum investment in the centralized and distributed WAMS.

In Chapter VI, SSI algorithm is employed to identify oscillation modal parameters and modal shape of power system low-frequency oscillations. Firstly, the mathematical corelationship between power system low-frequency oscillation and oscillation of mechanical system is analyzed to verify the applicability of SSI algorithm in the oscillation identification of power system. Secondly, the analysis process of SSI algorithm is depicted and a fourth order system is taken as an example to verify the validity of SSI algorithm. Thirdly, the IEEE 4-generator 2-area test system and IEEE 16-generators 5-area test system are taken as examples to test the effectiveness of SSI algorithm in the identification of oscillation modal parameters and modal shape. Lastly, signals with different noise intensity are used to test the effectiveness of SSI algorithm under a noisy environment.

In Chapter VII, a novel adaptive wide-area damping control scheme with SSI and signal time delay compensation is proposed. Firstly, the wide-area input signal of PSS is calculated based on the low-frequency oscillation mode identified by the SSI algorithm. Secondly, a simple and practical signal time delay compensation algorithm is proposed to measure and compensate the time delay in each wide-area input signal so as to eliminate the effects of signal time delay on the proposed adaptive WADC. Thirdly, simulations on IEEE 4-generator 2-area and IEEE 16-generators 5-area test systems are studied to substantiate the effectiveness and robustness of proposed adaptive wide-area damping control scheme.

Last but not least, Chapter VIII presents the conclusion of this thesis.

1.4 LIST OF PUBLICATIONS

1. P. Zhang, K.W. Chan, and D.Y. Yang, “In Depth Analysis on Synchronized Phasor Measurements for Wide-Area Stability Analysis and Control,” International Conference on Advances in Power System Control, Operation and Management 2009, Hong Kong, 8 – 11 Nov 2009.
2. J.G. Yang, K.W. Chan, H.M. Ma, P. Zhang, and D.Z. Fang “Preventive Transient Stability Control Using Constrained Optimal Power Flow,” International Conference on Advances in Power System Control, Operation and Management 2009, Hong Kong, 8 – 11 Nov 2009.
3. P. Zhang, D.Y. Yang, K.W. Chan, Y.T. Zhang, and G.W. Cai, “Self-adaptive Wide-area Damping Control Based on SSI and WAMS,” International Conference on Electrical Engineering, Korea, 11-14 Jul 2010.
4. Y. T. Zhang, D. Y. Yang, K. W. Chan, P. Zhang, and G.W. Cai, “Short-term Wind Forecasting Based on EMD and Statistical Models,” International Conference on Electrical Engineering, Korea, 11-14 Jul 2010.
5. D.Y. Yang, P. Zhang, and K.W. Chan, “The Monitoring of Modal for Power System Low-Frequency Oscillation Based on Measured Signal,” in preparation for journal submission.
6. P. Zhang, K.W. Chan, and D.Y. Yang, “Adaptive Wide-area Damping Control with Stochastic Subspace Identification and signal time delay compensation”, provisionally accepted by IET Generation, Transmission & Distribution, Manuscript ID: GTD-2011-0680, 2 Apr 2012.
7. P. Zhang and K.W. Chan, “Reliability Evaluation of Phasor Measurement Unit Using Monte Carlo Dynamic Fault Tree Method,” accepted for

publication by IEEE Transactions on Smart Grid, Manuscript ID: TSG-00259-2011, 12 Dec 2011.

8. P. Zhang and K.W. Chan, “Comprehensive Reliability Evaluation of Wide Area Monitoring System Using Monte Carlo Fault Tree Analysis,” submitted to IET Generation, Transmission & Distribution, Manuscript ID: GTD-2011-0838.
9. P. Zhang and K.W. Chan, “A Quantitative and Comprehensive Investigation of WAMS Architecture,” submitted to IEEE Transactions on Smart Grid, Manuscript ID: TSG-00338-2012.

CHAPTER II LITERATURE REVIEW

2.1 WAMS

WAMS is a new generation of power system dynamic monitoring and control system based on the synchronized phasor technology which includes synchronized phasor measurement, transmission, analysis and application technology. Firstly, the key idea of WAMS is that, based on Global Positioning System (GPS), WAMS can synchronously collect the real-time state parameters (including all kinds of phasor parameters) of wide-area power system. Secondly, by using high-speed communication network, all the distributed phasor data can be gathered and the dynamic information, which is under a unifying time coordinated system, of the whole power system can be snapped. Thirdly, based on this dynamic information, the real-time dynamic progress of power system operation can be monitored, and then the automatic control, security and stability of the power system can be significantly improved with the help of WAMS.

So far, many researches have been conducted on the utilization of WAMS. These researches mainly cover the following aspects:

(1) State estimation

PMU can measure the amplitude and phase angle of the voltage of the nodes where PMUs are installed directly. For on-line applications, this could replace the iteration process of power flow calculation and state estimation [14,15]. The precision of PMU measurements is very high and this can be combined with existing SCADA system to increase the precision of power system state estimation [16]. In [17], a power system harmonic state estimation based on phasor measurements has been proposed to transform the harmonic state estimation of the whole power system into state estimation of many single-bus systems.

(2) Wide-area dynamic monitor, record and replay

In WAMS, when the power system is subjected to a disturbance, all of the PMUs installed in nodes of the interconnected power system can acquire the dynamic information of the whole power system at the same time. To an extent, the WAMS can be regarded as a large fault recorder. Recording the dynamic process of the whole power system is the basic function of WAMS. Over the world, many power systems have installed WAMS to monitor the dynamic process of power system [18-22]. The real-time dynamic process information recorded by WAMS provides valuable data to the analysis of dynamic characteristics, analysis of the cause of accident, dispatcher training, etc.

(3) Model/Parameter identification and simulation validation

An accurate power system dynamic model is the starting point of any dynamic analysis and control to all power systems. At present, there are many analysis and researches based on established models, but there are relative less works on verifying the validity of those models. For example, the WSCC blackout on 10.08.1996 can be recreated with computer simulation based on the established power system model [23].

(4) Transient stability prediction and control

So far, the application of WAMS for transient stability control is still mostly in theoretically discussions rather than practical implementation. In WAMS, the dynamic real-time operation state of power system can be used as the initial condition for existing methods, such as Extended Equal Area Criteria (EEAC), Auto-Regression (AR) method, and so on. Once real-time WAMS data is readily available, transient stability control would be one of the important WAMS applications in the future [24,25].

(5) Voltage and frequency stability monitoring and control

Relative to transient stability, static voltage stability and frequency stability

are slow dynamic process. WAMS can therefore be more easily to be applied in monitoring and control of static voltage stability and frequency stability. In [26], voltage phasor acquired via the WAMS was used to divide the system into a two-point-system, and the voltage stability margin can then be derived quickly. In [27], busbar voltage angle differences and generator reactive power outputs provided by the WAMS was use to assess the system voltage security level. In [28], WAMS information was used to identify power system dynamic model so as to analyze and predict the voltage stability of power system. Currently, much research work has been focused on the application of WAMS information on the monitoring and prediction of voltage stability while the control of voltage stability is often ignored.

(6) Oscillation stability

Depending on oscillation scale and the number of generators oscillating with each other, power system oscillation can be divided into local oscillation mode and inter-area oscillation mode. By using the real-time measured data, various identification algorithms such as characteristic equation, recursive least squares, least mean squares, Prony method, and AR method Kalman filter technique have been proposed to estimate the oscillation parameters. In [29], a small signal stabilization controller with PSS was proposed. Once oscillations were detected from the WAMS data, SVCs and TCSCs installed on important tie lines would be used to suppress the power oscillations. Case study showed that black out in USA on 10 Aug.1966 could be prevented by the proposed control scheme.

(7) Wide-area relay

Recent blackouts showed that power system would lose its stability, even if relays worked well according to their designed logic. This is mainly because traditional relays just utilize the local information. When power system is in fault condition, these traditional relays would only eliminate the faulted components

or their protected tie lines while the effects to the whole power grid were not considered. For example, when the power grid is under stress with heavy load, the elimination of the faulty line would lead to the load to be transferred to another line which in turn could be switched out as well because of overload. In this condition, cascading trips would take place and cause a heavy blackout. If these relays do not just eliminate the faulted or overload transmission lines before the thermal limits but determine which lines should be eliminated first based on the WAMS information so as to stop the spread of fault and prevent the cascading trips.

The advent of WAMS has made the design of wide-area protection scheme possible and researches on this direction are currently on-going [30-32]. In order to prevent cascading trips, the best approach would be to monitor the whole power grid and identify the cause of overloads. If the overload of one transmission line is caused by flow transfer, the backup relay of this line should be blocked until the thermal limit of this line is reached.

Notably, in the wide-area protection scheme, the design logic of the main relay should not be changed. One reason is that: the signal time delay in WAMS data could postpone the tripping signal of the main relay and compromises the security and stability of power grid. The other reason is that the complicated wide-area control scheme will greatly deduce the reliability of the main relay.

WAMSs established in different power grids would have different investment, synchronization accuracy, signal time delay, reliability and risk characteristics; and all of them would have great influence on both the construction and application of WAMS in power system [33]. So far, there is little systematic analysis on these aspects and investigation on their influence to the power system stability analysis and control neither in the industry nor academic research. In the following subsections, more details on these aspects will be presented.

2.1.1 INVESTMENT, SYNCHRONIZATION ACCURACY AND SIGNAL TIME DELAY

The investment for fiber-based communication network in power system is analyzed in [34,35]. In [35], the whole investment for the communication network was calculated by the accumulation of the cost for its components. The synchronization accuracy of WAMS has been evaluated in both laboratory environments and under field operation conditions in [36,37]. The evaluation result was that the synchronization accuracy of WAMS meets the requirements for synchronized phasors supplied by WAMS as specified in IEEE C37.118-2005. Much research has covered the analysis of signal time delay and its effect to stability analysis and control [12,13,29]. However, a systematic and comprehensive signal time delay analysis is still lacking.

2.1.2 RELIABILITY EVALUATION

Reliability evaluation is a top research topic received wide attention in various research fields. At present, most of the reliability evaluation methods can acquire various kinds of reliability indices by using the probability and statistics theory to analyze the failure and experiments data of the system and its components. The qualitative and quantitative reliability evaluation methods mainly can be divided into three categories as follows:

- (1) The classic analysis methods, such as Reliability Block Diagrams (RBD), Failure Mode and Effects Analysis (FMEA), Fault Tree Analysis (FTA), etc.
- (2) The state analysis methods, such as Markov, Petri Nets, etc.
- (3) The intelligent evaluation methods, such as Bayesian Networks, Neural Network Model, Monte Carlo Simulation, etc.

Among these reliability evaluation methods, the traditional reliability evaluation methods, such as RBD, FMEA, FTA, etc., have been mature enough

to be widely used in the engineering domain. Brief descriptions on each of the common reliability evaluation methods are given as follows:

(1) Classic analysis methods

1) RBD

RBD [38-40] is the most basic and earliest designed reliability evaluation method. This method uses the graphical way to depict the logic relationship between the failures of system and its components. The reliability model constructed by RBD is very visual and easy. However, it is very difficult to use RBD to construct the reliability model of the large-scale complex system. Furthermore, the effects of human and environment cannot be considered clearly during the construction of reliability model using RBD.

2) FMEA

FMEA [41-43] is a widely used reliability analysis method. In FMEA, all the failure states of each system component are firstly analyzed in detail, and then the effects of each failure state to the whole system are determined based the severity degree and probability of these failure states. FMEA usually uses analysis form to analyze the reliability of system in the way from the subsystem to the whole system. The analysis progress of this method is very clear, simple and easy to master. However, FMEA can only analyze single failure mode while the reliability of system with multiple failure modes cannot be catered.

3) FTA

FTA [43-45] is first proposed by H. A. Wilson in Bell laboratory to conduct the reliability analysis, safety analysis and risk evaluation of the large-scale complex system. It can provide a mathematical and graphical representation of the combinations of events that can lead to system

failure. By using FT modeling method, the potential fault of system can be found and the probability of the system failure can be predicted. FTA is usually used to analyze the reliability of the complex system. It can flexibly reflect the effects of the external factors (such as environmental factor, human factor, and so on) to the failure of system. Through FTA, all the failure states of system can be acquired.

(2) State analysis methods

1) Markov

Markov [46-48] is first proposed by the Soviet Union mathematician Markov and be introduced to the reliability analysis field in 1951. The fundamental idea of this method is that: based on the discrete or continue probability of system or component in operation or failure state, Markov can estimate the probability of system or component in a certain state at some point in the future. In this method, the transforming probability between two states of system or component must remain constant and the future state is independent on the past states except the latest one.

Compared with the classic analysis methods, Markov method is a dynamic analysis method and can be used to the repairable system or other dynamic systems which are difficult to be depicted by using FMEA and FTA. The disadvantage of Markov is that the scale of Markov model exponentially increases with number of components and make it not suitable for the modeling of complex system.

2) Petri Nets

The concept of Petri Nets [49,50] is first proposed by C. A. Petri in 1962. This method can be used to construct the reliability model of a dynamic system with the limitation of binary state. The complexity of

this reliability model constructed by Petri Nets is much simpler than that constructed by Markov method. Though Petri Network has many advantages in the construction of reliability model of the dynamic system over FMEA and FTA methods, this method is mainly used in the theory research and has not widely been used in the practical engineering domain yet. This is mainly because the solution of reliability indices using Petri Network is based on the Markov theory, thus leading to the same state space explosion problem as Markov method. Furthermore, too many different expansion forms of Petri Nets make a uniform criterion hardly be formed.

(3) Intelligent evaluation methods

1) Bayesian Networks

Bayesian Networks [51,52] can graphically depict the relationship between the probability of system and its components. Bayesian Networks can avoid the solution of the minimal cuts in fault tree and make the reliability evaluation more visible and flexible. By using this method, not only the reliability indices of system can be acquired but also the effects of each component or several components to the whole system can be easily obtained.

2) Monte Carlo Simulation

Monte Carlo [53-56] simulation method is first proposed and used in 1940s. It is based on the probability and statistic theory. During the reliability analysis of system, through the simulation of system life, Monte Carlo Simulation can be used to evaluate the reliability of system. Based on the different system characteristics, Monte Carlo Simulation can be divided into static simulation and dynamic simulation. Monte Carlo Simulation can be used to evaluate the reliability of dynamic system

because Monte Carlo Simulation can conquer the state space explosion problem. Since 1960s, Monte Carlo Simulation has been widely used in the reliability analysis. It is mainly used to solve the high-dimension problem, non-Markov problem, structural reliability problem, and so on.

The above mentioned is the current general research state of reliability evaluation. As to the reliability evaluation of WAMS, so far only two papers have been published [9,10].

In [9], WAMS was divided into two sub-systems, namely monitor center system and data acquisition system. Based on Markov method, the evaluation procedure of the monitor center system was obtained. In the availability analysis of communication system, Markov state transfer diagram was used to calculate the probability of communication system in fault condition. While the source of reliability parameters of equipments was not disclosed and the characteristics of the communication system, which was composed of self-healing ring of SDH, were also not considered.

A hierarchical WAMS structure and a quantified reliability evaluation method for the backbone communication network were proposed in [10]. Markov method was used to construct the reliability model of WAMS first, and then state enumeration method was used to evaluate the reliability indices of WAMS.

In both [9] and [10], Markov method is used to construct the reliability model of WAMS. When the system size is large enough, in Markov method, there will be an infamous state space explosion problem [11]. In order to conquer this problem, only single fault pattern rather than multiple fault patterns were considered. Furthermore, only reliability of PMU measurement uploading to control center was considered while control instruction downloading from control center to PMU was ignored.

2.1.3 RISK EVALUATION

WAMS has become an essential tool for power system operation and control in smart grids. A typical WAMS is composed of PMUs, PDC, communication network, and control center. The communication network can be further divided into local area communication network and wide area communication networks which also contain many components such as fiber sections, routers and repeaters. All of these WAMS components are combined together to form a complex WAMS with multiple layers. The failure of each component in WAMS will affect the service quality of WAMS or even threaten the safe and stable operation of power system. Therefore, the evaluation of the risk of WAMS has become an imperative task.

Presently, risk evaluation has attracted intensive concern in the industry. According to the quantization degree of the risk indices, risk evaluation methods can be divided into two categories: qualitative risk evaluation and quantitative risk evaluation.

(1) Qualitative risk evaluation method

Qualitative risk evaluation method is the most widely used risk evaluation method. The main functions of this method are that: first finding the varieties of system consequences and the corresponding risk factors to these consequences, and then finding the conditions, under which these risk factors would lead to the consequences, and the severity degree of these consequences to the system, finally determining the control measures to prevent these consequences. In qualitative risk evaluation method, the determination of the system risk degree mainly depends on the risk evaluators' knowledge, experience, and so on. The traditional qualitative risk evaluation method mainly includes Safety Checklist (SCL), Preliminary Hazard Analysis (PHA), Hazard and Operability (HAZOP). The qualitative risk evaluation method is easy to operate and master. The

evaluation progress and result of this method is intuitive. The limitation of this method lies in that the evaluation result cannot be quantified.

i) SCL

SCL [57,58] indicates a set of questions to guide the analysis to determine the system state. These questions are mainly related with the environment, devices, operation, management. SCL is effective in identifying additional variations and commonalities. In [58], a safety checklist was organized for use on four-variable requirements models for real-time process-control systems.

ii) PHA

PHA [59-61] was developed in 1960s in the aeronautical and military fields. In the design process of a project, PHA can serve as a safety analysis method to identify the risks. Through the estimation and collection of the probability and severity of each risk, designers can evaluate the risk level and provide a suggestion to eliminate or mitigate these risks.

iii) HAZOP

In the late 1960s, HAZOP [62-64] was originated in the heavy organic chemicals division of imperial chemical industries, and developed as a multidisciplinary team approach for hazard and problem identification. The HAZOP team is normally composed of several individuals with varying background and expertise. The team is headed by a leader who should chair the HAZOP meetings. In the HAZOP meetings, through a collective brainstorming effort that stimulates creativity and new ideas, a thorough review of the process is made to identify and evaluate hazards as well as operability problem.

(2) Quantitative risk evaluation method

Quantitative risk evaluation method is using the quantity indices to indicate the risk degree of system. In this method, the probability of a specific incident is calculated first, and then the risk of system can be calculated by combining the quantitative consequences caused by this incident. The quantitative risk evaluation method mainly includes Fault Tree Analysis (FTA) as outlined in Section 2.1.2, Event Tree Analysis (ETA) and Analytic Hierarchy Process (AHP). Through the quantitative risk evaluation, quantitative risk indices of system can be calculated to find out the security vulnerabilities in system and then formulate the corresponding measures to reduce the risk and improve the system security. The limitation of this method lies in that accurate and enough initial data are needed.

1) ETA

ETA [65,66] is generally used to identify the consequences caused by the occurrence of a potentially hazardous event. At present, this method was applied in risk assessments not only for the nuclear industry but also other industries, such as traffic carrying trade, construction industry. Event tree is an inductive method to examine all the possible responses to the initiating event. In this event tree, the branch points represent the success and failure of system and its subsystems which are related to the initiating event.

2) AHP

AHP [67-70] method was first proposed by Saaty in 1970s. It is a quantitative risk evaluation method with multi-criteria and multi-objective. This method divides the unsolved problem into three layers: target layer, criteria layer and index layer. Based on the analysis, comparison and solution of the weights of each risk factor in the index

layer, AHP method can resolve the unsolved problem layer by layer until the final analysis result is obtained.

The above mentioned is the current research state of risk evaluation. As to the risk evaluation of WAMS, so far only one paper covers the security assessment of WAMS information based on evidence theory [71]. In this paper, a framework was proposed to assess the security of WAMS communication system. The WAMS communication system was first divided into several subsystems, and then AHP method was used to build the assessment hierarchy and determine the index weights, finally D-S algorithm was used to aggregate all the data of these subsystems. The security assessment conducted in this paper can be considered as an integration of qualitative and quantitative risk evaluation. However, because of the application of too many expert evaluations, accurate and convincing risk indices cannot be evaluated.

2.2 LOW-FREQUENCY OSCILLATION

After a disturbance, power oscillations would occur in a power system and the modes of oscillation can be divided into two distinct types, namely local mode and inter-area mode. In local oscillation mode, only one generator or a group of generators oscillate against the rest generators in the system. In inter-area oscillation mode, groups of generators oscillate against each other. The typical frequency of inter-area oscillation modes is between 0.1-2.5 Hz.

Inter-area oscillation modes are mainly caused by the heavy power transmission across weak tie-lines [72]. So, when there is an inter-area oscillation mode in power system, the amount of power transmission in the tie-lines, which connect the regions oscillating with each other, will be heavily limited. Following the interconnection of power systems, inter-area low-frequency oscillation occurs more and more often and has become more and more difficult

to suppress.

The traditional and effective control method for low-frequency oscillation is to install power system stabilizer (PSS) to provide supplementary control through the exciter of generators. Recent years, new technologies or equipments such as High Voltage Direct Current (HVDC) transmission system and Flexible AC Transmission Systems (FACTS) devices have been used to damp down low-frequency oscillation. All of these conventional damping controllers using the local information are effective in controlling the local low-frequency oscillation modes, but they often perform poorly in the control of inter-area low-frequency oscillation modes. It is mainly because those local controllers lack the global observation of inter-area low-frequency oscillation modes.

Following the advent and maturity of WAMS, WAMS based low-frequency oscillation control scheme has a great potential to overcome the shortcomings of local damping controller. Many researches have applied WAMS information to control low frequency oscillation and promising results have been reported.

The difficulties of the wide-area oscillation control mainly lie in the following aspects:

- i) Identification of the low-frequency oscillation modes
 - ii) Choice of wide-area feedback signals and controller location
 - iii) Structure of the wide-area oscillation control scheme and design of the wide-area oscillation controller
 - iv) Processing method to overcome the signal time delay
- (1) Identification of the low-frequency oscillation modes

Through the application of WAMS information, the low-frequency oscillation identification methods can acquire the oscillation frequency, damping, even the oscillation mode shape. These identification methods mainly can be divided into non-parametric model identification method and parametric model identification

method.

1) Non-parametric mode identification

Non-parametric mode identification method refers to using the system input and output signals to estimate the non-parametric model of system [73]. Fourier Transformation (FT) [74], Fast Fourier Transformation (FFT) [75] and Sliding Window Fourier Transformation (SWFT) [76,77] are the main methods for the identification of non-parametric model of system. It shall be noted that Fourier Transformation based identification methods can handle stationary signals only. However, power system is a nonlinear system with high dimension; small disturbances could lead to drastic change in system characteristics. Recently, Wavelet algorithm [78] and Hilbert-Huang Transformation (HHT) algorithm [79,80] have become popular as they can be used to identify non-stationary signals.

2) Parametric model identification

Parametric model identification method builds a parametric model of system first, and then optimization method can be used to calculate the model parameters based on the sampling data.

i) Regression analysis

Frequency and damping of low-frequency oscillation modes can be acquired with the Auto-Regressive (AR) [81] and Auto-Regressive Moving Average (ARMA) [82] methods. In [83], ARMA was used to depict the input and output data first, and then least-squares method was adopted to get the system transfer function.

ii) Prony algorithm

Prony algorithm can calculate the signal frequency, amplitude and attenuation directly. In [84], adaptive sampling window was used in Prony method to acquire faster monitoring rate with acceptable

accuracy in practical implementation. In [85], a method was proposed to obtain the transfer functions of PSS based on Prony signal analysis.

iii) Subspace method

Subspace model identification first forms a Hankel matrix using the input and output data, and then the system model parameters can be derived from the row subspace and column subspace of the projection of Hankel matrix [86].

(2) Choice of wide-area feedback signals and controller location

Different wide-area feedback signals to the oscillation controllers and different controllers' location have different control effectiveness to the same oscillation mode. In order to have the best control effectiveness, wide-area feedback signals and controllers' location shall be chosen carefully.

In recent years, many researchers have covered the choice of wide-area feedback signals and controllers' location. Residue method [87], dominant mode ratio [88], the controllability and observability of mode shape [89], Singular Value Decomposition (SVD) [90] and many more have been proposed to select the optimum wide-area feedback signals and location for the wide-area oscillation controllers.

(3) Structure of the wide-area oscillation control scheme and design of the wide-area oscillation controller

The distributed excitation control has the advantage that system could maintain its stability even if the excitation of one generator is out of control. It is therefore in the recent research on wide-area oscillation control scheme, a multilayer approach is commonly adopted in which PSS would act as the first layer in the multilayer structure while the wide-area oscillation controller acts as the second layer.

In [89], WAMS based hierarchical controller was first regarded as a question

of H_2/H_∞ output-feedback control and regional pole placement, and then the Linear Matrix Inequality (LMI) approach is used to solve this question.

[91] proposed a two-level wide-area oscillation control scheme to enhance the transfer capability of interconnected power systems. In this scheme, multiple supplementary excitation control loops using wide-area feedback signals were coordinated.

[92] proposed a controller with two-level hierarchical structure to improve the stability of a multi-machine power system. In this controller, the remote signals from all generators were used to decouple the control signals to improve the local controllers' performances.

Based on the research of the structure of wide-area oscillation control scheme, linear optimal control [93], nonlinear optimal control [94,95], robust control [96-98], adaptive control [99,100] and intelligent control [101-103] methods can be used to design various kinds of wide-area oscillation controllers.

(4) Processing method to overcome the signal time delay

Because of the long distance transmission, signals from WAMS contain time delay ranged from tens to hundred milliseconds [104].

LMI theory is widely used for the analysis of the upper limit of time delay and the design of robust controller considering signal time delay [105-109]. In [108], a power system model considering time delay was constructed through system identification and Pade approximation. Based on this time-delay system model, a robust damping controller was designed by employing mixed-sensitivity- H_∞ control theory and pole placement approach in LMI framework. In [109], a predictor based H_∞ control design strategy was discussed for the time-delayed systems.

In [110], a wide-area oscillation controller design method is proposed. This method combined LMI theory and gain schedule method to guarantee the

stability of system in different operation state and different time delay.

General speaking, present researches on wide-area oscillation controller with time delay considered mainly focus the fixed time delay while random time delay has been rarely researched. Furthermore, all the time delay analysis methods are very complex with limited practicality for on-line implementation.

2.3 BRIEF SURVEY OF WAMSs AROUND THE WORLD

Because of the advantages of WAMS compared with the traditional SCADA in the monitoring of the dynamic behaviors and the stability control of power system, many countries have established WAMS to guarantee the security and stability of their power grids. Here, a brief survey on the WAMSs established around the world is presented.

(1) Wide-area control system in CSG

China Southern Power Grid (CSG) system [111,112] is characterized by its parallel HVDC-HVAC transmission system, high rate of load growth, major generation resources remote from the load center and multi-circuit HVDC transmission lines system.

The project named “wide-area coordinated control of multiple HVDC system” (WACCH) was started in 2005 by CSG to construct a closed-loop control system to modulate active power of HVDC with feedback signals from WAMS. With the efforts of the researchers and engineers, WACCH has archived significant accomplishments in the past three years.

WACCH was used to damp inter-area low frequency oscillation through modulating the multiple HVDC systems. WACCH also developed an adaptive control algorithm based on on-line Prony analysis. Simulation and field test results have validated the effective and efficiency of the proposed Wide-area Control System (WACS).

So far, more than 140 plants and stations across CSG have PMUs installed, including most of the 500kV stations and large power plants. All PMUs communicate with the central station through a digital fiber optic network at a rate of 100 times per second (one every 10 ms).

(2) OTSCPS in Jiangsu power grid

The Jiangsu power system [113] is one of the most important power systems in southeast china. The backbone grid comprises 220kV and 500kV networks. It is connected with Shanghai power grid through a 500kV transmission line.

WAMS constructed in Jiangsu power system includes several PMUs, data concentrators and central analysis servers. The whole project has finished its second stage. It can independently monitor several important power plants and substations. Based on WAMS and the existed EMS, state estimation is accomplished first. Based on the results of the state estimation, transient stability assessment is then conducted using an On-line Transient Stability Control Pre-decision system (OTSCPS). This system enhances the adaptability and precision of preventive and emergency control of Jiangsu power system.

(3) Wide-area measurement and control system in Mexico

During the 1990's, Mexico's Federal Electricity Commission [114] envisioned a project which included the deployment of a synchronized phasor measurement system for contingency analysis and visualization of the operational state of the National Electrical System. At the initial stage of this project, fifteen PMUs were installed in two of the four subsystems. Largest generation complexes, major load points, and critical power transfer interfaces were used as the installation criteria. In the first stage, most of the focus was put on the post-fault analysis and model validation of power system simulator models. In the second stage, for the safe operation of the electric power system in Mexico, a synchronized phasor measurement system was proposed.

(4) Wide-area monitoring and control at Hydro-Québec

Wide-area measurements at Hydro-Québec [115] started in 1976 when a team of IREQ researchers successfully measured the voltage angle shift between Arnaud (northeast Québec) and Boucherville (south shore of Montreal), two 735kV substations separated by more than 1000 km. A precise number of zero-crossing of the voltage was used to obtain this angle shift. The synchronizing error was less than 46 μ s, which represented about 1° electrical angle of the 60-Hz fundamental phasor.

Currently, eight-PMU-based wide-area monitoring system commissioned in 2004 is on-line. This system brings GPS-synchronized angles, frequencies, and harmonic distortion measurements from key 735kV busses to the EMS. Hydro-Québec is now actively investigating possible application of wide-area voltage measurements to enhance long-term stability through secondary voltage control.

(5) Wide-area oscillation monitoring in Nordic power system

The Nordic power system [116] comprises the inter-connected power systems in Finland, Sweden, Norway and East Denmark (the Nordic synchronous area) and West Denmark (being synchronously connected to the union for the coordination of transmission of electricity system). Iceland is also part of the Nordel cooperation, but has an isolated power system. In 2006, the total electricity consumption in the Nordel area was 405 TWh. The peak load was 67 GW. There are four dominating inter-area modes in Nordic power system. Both frequency and damping of the oscillatory modes show significant variations depending on the actual operating point.

Prototype installations have been performed to introduce WAMS applications in the Scandinavian power transmission system. The most important functions and applications to be included in this WAMS installation were identified and

selected in close collaboration with operators at the Norwegian TSO, Statnett. The modal analyses were applied to the full (large-scale) Scandinavian power system model and used among other criteria (such as practical accessibility of the corresponding geographic locations as well as availability of fast Internet access) as a basis for selecting the sites for the PMU installations. Finally, four locations were selected according to the observability of all critical oscillations in Norway.

(6) Application of Campus WAMS in Japan

In Japan [117], a PMUs-based Campus WAMS has been started to construct since several years ago. At present, the Campus WAMS totally encompasses 12 PMUs. Nine of them are installed in the area of Western Japan 60Hz system and another three are installed in the area of Eastern Japan 50Hz system. In Japan, there are ten independent power companies who operate their own power supply area as well as the tie-lines that link the adjacent companies. Therefore, the Campus WAMS is in fact a unique wide-area system which covers the power supply area of all ten power companies and continuously provides synchronized phasor measurements of the complete system. With application of the Campus WAMS, the inter-area oscillation modes that occur in Western Japan 60Hz power system have been successfully detected and the corresponding eigenvalue property has been estimated.

(7) WAMS implementation in North America

PMU was first deployed in the Western Electric Coordinating Council (WECC, formerly the WSCC) in 1988 by the Bonneville Power Administration (BPA) [118]. BPA has conducted both lab and field tested on prototype units developed in the Power Lab at Virginia Polytechnic Institute. In 1994, the first commercial PMUs were installed in the WECC as part of an EPRI research project.

Progress in the development and use of the WECC WAMS has been reported roughly once a year. By the end of 2004, the WECC WAMS has reached the

following size:

- 11 PDC units, operated by 9 data owners.
- 53 integrated PMUs
- 7 stand-alone PMUs
- ~23 PPSM units
- ~10 monitor units of other kinds

On 2 July and 10 August, 1996, the western North American power system undergo a severe breakups, WAMS of WSCC provided real-time data. So far, the WAMS in WECC has obtained the following accomplishments:

- PMUs and PDCs technologies have been maturing.
- The dynamics of power system can be modeled better.
- The dynamic performance of power system can be observed and tested directly.

(8) "Defence Plan" in France power grid

Since the early seventies France power grid [119] has been operating a policy for countering loss of synchronism which involves isolating the zone at fault in order to prevent propagation of the disturbance. This policy, known as the "Defence Plan" is currently implemented by the local automatic systems responsible for detecting loss of synchronism and isolating the faulty zone accordingly. A new Defence Plan for protecting the electricity supply system against loss of synchronism is being considered to cope with the future system. This new Defence Plan is based on the following precepts:

- Reliable detection of any zone suffering from loss of synchronism;
- Very rapid isolation (within about one second) by open-circuiting the EHV lines leading to the faulty zone;
- If the isolated zone exports a lot of energy, the cut-out must be accompanied by simultaneous load-shedding from the HV-MV and EHV-MV substations

in non-affected zones in order to prevent collapse.

The required sensitivity and selectivity is obtained based on measuring the voltage phase angle in PMUs located at the centre of each zone and comparing results pair by pair in a central computer. The Research Center of France power grid, in collaboration with the company PSC, has been working on a "PMU" capable of performing phase angle measurements of this type.

(9) DSA in Korea

The growth of the power system in Korea [120] is very rapid. The power consumption in Korea has increased from 4,800 MW in 1976 to 41,000 MW in 1997. But, because of the finance and environment, the construction of new transmission lines for the growing load encountered many problems. With the restructuring of power system, Korea power grid cannot operate as the traditional manner any more. The continuous monitoring of the system operation state and on-line dynamic security assessment (DSA) are needed to predict the uncertainty of operation state.

Configuration of WAMS in Korea power system is composed of one master system and 24 local units. The functions of this master system lie in data acquisition, system monitoring, bringing serious disturbance to the attention of the operator and DSA. In Korea WAMS, PMUs are installed at the major generating stations and 345/765 kV substations. Each PMU can measure 3-phase voltages and 3-phase currents of fourteen feeders.

2.4 CENTRALIZED AND DISTRIBUTED WAMS

Based on the different control strategies adopted in the countries' power grids and the future development plan of WAMS, WAMS established in several countries has different topology structure. Generally, there are mainly two kinds of WAMS topology structures: centralized WAMS and distributed WAMS.

Among all WAMS established in the world, CSG, Wide-area Measurement and Control System in Mexico, Wide-area Oscillation Monitoring in Nordic Power System and WAMS implementation in North America adopt distributed structure, while the other WAMSs adopt centralized structure. The differences of centralized and distributed WAMS lie in various aspects such as investment, signal time delay, reliability and risk. In Chapter V, all of these aspects are taken as the comparison criteria to investigate which WAMS structure has better performance in the monitoring and control of power system.

2.5 SUMMARY

In this chapter, a literature review on various aspects of WAMS including investment, synchronization accuracy, signal time delay, reliability and risk is presented. Meanwhile, the current state of the art on the application of WAMS in power system stability analysis and control especially in the identification and control of power system low-frequency oscillation is described. Furthermore, WAMSs established in the world including China, Mexico, North America, Nordic, Japan, France, and Korea are briefly surveyed. Finally, the topology structure of WAMS is generally introduced.

CHAPTER III SYNCHRONIZATION ACCURACY AND SIGNAL TIME DELAY OF WAMS

3.1 INTRODUCTION

Power system stability analysis and control is the most important tools for securing the operation of a power system. For effective monitoring and control of power system stability over a large power system network, WAMS has been proposed and constructed in many countries over the world. WAMS is capable of collecting synchronized real-time operation state over a wide-area power system network through a high speed communication network for on-line power system stability analysis and control.

Synchronized phasors with high synchronization accuracy are essential to the practical applications of WAMS based stability analysis and control schemes in practical power systems. Table 3.1 summarizes the demand of synchronization accuracy in synchronized phasors for various real-time applications [121].

Table 3.1 Demand of synchronization accuracy in synchronized phasors for various real-time applications

Applications	Degree accuracy/ $^{\circ}$	Time accuracy/ μ s
State estimation (static)	0.5	25
State estimation (dynamic)	1.5	75
Stability monitoring and control	1	50
Phase angle measurement	0.1	5
Adaptive relay	0.1	5

As shown in Table 3.1, the required synchronization accuracy of synchronized phasors in phase angle measurement is a tenth of degree, i.e. 5μ s.

Since the foundation of wide-area stability analysis and control is built by the synchronized phasors which compose of both magnitude and phase angle, the synchronization accuracy of synchronized phasors must be within $5\mu\text{s}$.

Like any other measurement equipments, PMU can bring errors to the synchronized phasors which would compromise the stability analysis. In addition, data transmission delays, namely signal time delay in the WAMS, will affect the execution accuracy of stability control action as well [122].

Existing research mostly focuses on the utilization of real-time information supplied by WAMS to analyze power system stability or instability [123-125]. A few papers have proposed control actions to allow the power system to recover from power system instability. However, most papers do not consider the effect of errors introduced by synchronized phasor measurement equipment and the data transmission delays in the power system stability analysis and control.

In this chapter, through a qualitative and quantitative analysis of synchronization accuracy and signal time delay, the effect of each part of synchronized phasor measurement and transmission to wide-area stability analysis and control will be systematically studied and examined such that recommendations could be made to improve the synchronization accuracy and reduce the signal time delay of synchronized phasors supplied by WAMS to meet the demand of wide-area stability analysis and control.

3.2 ANALYSIS OF SYNCHRONIZATION ACCURACY

The major functional blocks of a PMU are shown in Fig. 3.1. GPS receiver first receives the Pulse-Per-Second (PPS) signal from the satellite and then transmits it to the locked oscillator which generates the synchronized sampling pulse to trigger the A/D converter to sample the voltage and current signal captured by CT/PT with anti-aliasing filtering. The discrete A/D samples are

transmitted to a microcomputer to calculate the synchronized phasor using the discrete Fourier transform method. The synchronized phasor is then labeled with time stamp and transmitted to the phasor data concentrator.

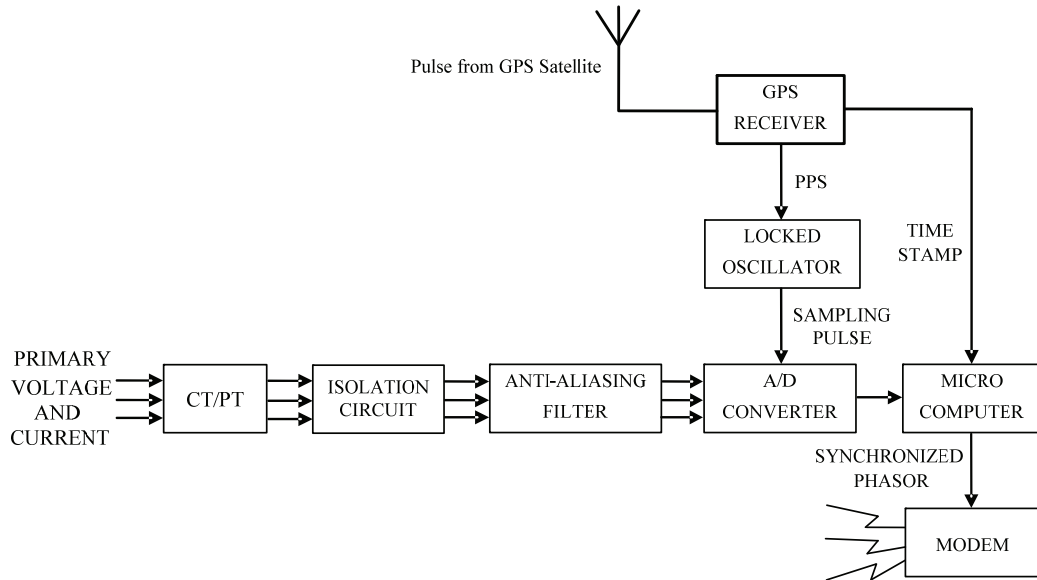


Fig. 3.1 Functional blocks of a PMU

Since the accuracy of the synchronization GPS pulse is within $0.5\mu\text{s}$ and $1.1\mu\text{s}$ for 92% and 99.9% of time, respectively; the synchronization accuracy of GPS pulses is considered as $1\mu\text{s}$ for simplicity in the following analysis. This potential level of accuracy, however, cannot simply be translated as the accuracy of the synchronized phasors produced by the PMU in field installation, and it would be a misunderstanding to consider the synchronized phasors being used in real-time applications would have the same level of synchronization accuracy, i.e. $1\mu\text{s}$, as the GPS pulse. This is because during the build-up process of the synchronous clock of the whole network, each part of timing system and the signal transmission of measurement will introduce time error and delay.

PMU synchronization is essential for synchronized phasor measurements to capture system dynamic behaviors [126]. However, poor synchronization can occur due to the synchronous clock error, signal transmission error and errors from the power system.

3.2.1 SYNCHRONOUS CLOCK ERROR

The main use of GPS in power system applications is to use its PPS signal to develop a highly accurate synchronous clock system. This synchronous clock system is used to label the synchronized phasor measurements with highly accurate synchronized time. The synchronous clock error means the difference between the PPS signal and synchronous sampling pulse which is used to trigger the A/D converter to sample the signal being measured. The following are the main sources of errors in the synchronous clock.

- (1) There is an error between the rising edge of PPS signal produced by the GPS receiver and Universal Time Coordinated (UTC) real-time clock. This error is about 80 ns.
- (2) There is a random error between the rising edges of PPSs produced by any two GPS receivers. Through test measurement, this error is between 50 ns to 100 ns.
- (3) There is an error between the rising edge of PPS and the rising edge of the internal clock pulse of PMU. That means that the internal clock can receive PPS signal until the next rising edge comes. Fig. 3.2 shows the time sequence of PPS and the internal clock pulse of PMU.

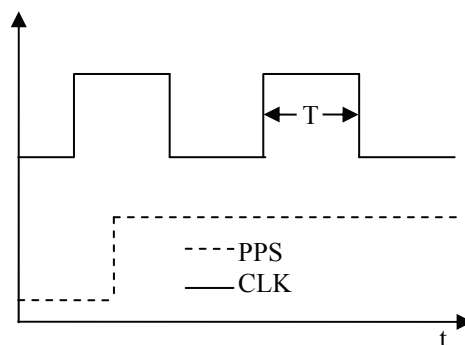


Fig. 3.2 Time sequence of PPS and PMU internal clock

- (4) Error will be introduced when the PPS signal is transmitted. If GPS receiver is installed on the system support plate directly, this error can be neglected.

However, in order to have a better satellite signal reception, the GPS receiver is mostly installed in the open air while the rest of PMU parts are installed in the switch cabinet with other intelligent equipments. This means that a cable is needed to connect the GPS receiver and PMU parts together, and as a result, large error will be introduced because of the long connection cable and the device used to isolate and process signal. This error will be 215ns when the cable length is 1m and 810ns when the cable length is 100m.

(5) Error will also be introduced during the data processing and recording of time by the micro-computer due to the time delay from the execution of CPU instructions.

(6) The accuracy and reliability of crystal oscillator of GPS receiver has obvious effect on the system timing accuracy. This error is reflected as time lead or lag when the time of one system compares to the time of another system.

With all the error sources of the synchronous clock being considered, some error elimination methods based on the improvement of software and hardware of PMU should be taken such that the error of sampling pulse used to trigger the A/D converter to sample can be restricted to satisfy the demand of, for example, on-line transient stability analysis.

Through test, the maximum difference between two synchronous sampling pulses produced by any two PMU is less than $5\mu\text{s}$. This means the difference between the synchronized phasor phases will be less than 0.1 degree and the synchronization accuracy can reach 0.1 degree.

Additional synchronization error will be introduced if the PMUs in WAMS are made by different manufacturers since different manufacturers use different design approaches that result in variable performance among PMUs [127]. Test results indicated that measurements from PMUs made by different manufacturers can be mixed in applications with steady state or slowly varying dynamic

conditions at the fundamental frequency [128,129]. The results also showed that operation at 10% or less of the nominal value will greatly increase the magnitude and phase errors. Test also revealed that data from different PMUs of different manufacturers cannot be combined for off-nominal frequency operation or to capture the fast variable power system state when power system is in transient process.

3.2.2 SIGNAL TRANSMISSION ERROR

Before the A/D converter samples the power signal such as voltage and current, the signal pass through the CT/PT, isolation circuit and anti-aliasing filters. Each of these three parts as well as the connection cables will introduce time errors into the signal.

- (1) Transformer delay: Study shows that the phase shift error of typical CT and PT is about 0.1 degree which is equivalent to $5\mu\text{s}$.
- (2) The effect of cable: Often there is a long distance between CT/PT and PMU and long cable is hence needed to connect the two equipments. Large error will be introduced as a result from the long cable and device used to isolate and process signal.
- (3) Isolation circuit: There is an isolation circuit between CT/PT and anti-aliasing filter. Isolation circuit is used to suppress noise interference and will introduce a little phase shift error.
- (4) Anti-aliasing filter: Each input channel must be equipped with an anti-aliasing filter to preclude unwanted frequency components in the captured signal. This filter will introduce an equivalent phase shift of about 6 degrees. However with the use of stable resistor/capacitor, this phase shift will be suppressed to 0.01 degree.

All in all the signal transmission error would be large than $8\mu\text{s}$ and is the

dominant factor in determining the overall synchronization error in the synchronized phasors when it is compared with the synchronous clock error. Though transformer delay, which is the main contributor in the signal transmission delay, can be largely reduced by compensation methods, the exact amount of improvement is still in doubt because of the complexity of power signal involved and the variations in the characteristics of CTs and PTs from different manufacturers.

2.2.3 ERRORS FROM POWER SYSTEM

The following are the main sources of errors from the power system.

- (1) Along with the increasing use of electronic equipments in power system, more and more harmonics and Direct Current (DC) components are introduced in power signal. This will prohibit the accurate calculation of synchronized phasors by the discrete Fourier transform. The following is the discrete Fourier transform.

$$\begin{aligned} \bar{X}(1) = X_c - jX_s = & \frac{\sqrt{2}}{N} \sum_{k=0}^{N-1} X_k \cos \left[\frac{2\pi}{N} k \right] \\ & - j \frac{\sqrt{2}}{N} \sum_{k=0}^{N-1} X_k \sin \left[\frac{2\pi}{N} k \right] \end{aligned} \quad (3.1)$$

$$\begin{aligned} \bar{X}(r) = \bar{X}(r-1) + j \frac{\sqrt{2}}{N} (X_{n+r} - X_r) e^{-j \frac{2\pi}{N} (r-1)} \\ r = 2, 3, \dots, \end{aligned} \quad (3.2)$$

where $\bar{X}(r)$ and $\bar{X}(r-1)$ are the r^{th} and $(r-1)^{\text{th}}$ phasor measurements, N is the number of samples per cycle. Through the discrete Fourier transform, both the DC and harmonics components can be eliminated from the original power signal.

- (2) Wide-area stability analysis and control is executed when power system suffers large disturbance. In such a case, the state of power system changes drastically. The decaying aperiodic component will be introduced in generator

stator circuit and transmission line. The effect of decaying aperiodic component can be eliminated for example by including two extra sample points into the data window of the discrete Fourier transform [130].

- (3) Drastically changing power system state would cause the signal frequency to change drastically as well. PMU which measures voltage and current phasors using the discrete Fourier transform can detect transients or surges within milliseconds of their occurrence [131]. A sampling rate of 12 times the nominal power system frequency, i.e. 600Hz for a 50Hz power system, has been found to be advantageous in relaying and measurement functions. If the network frequency undergoes a change characterized by a small frequency offset Δf , it has been shown that the synchronized phasor will also undergo a change [132]. However, if fixed sampling frequency is used continuously to sample the signal for the discrete Fourier transform when the network frequency changes, spectrum leakage will occur due to the sampling frequency become not an integral multiple of the signal frequency. The practical and effective solution is to design effective frequency tracking circuit to make the sampling frequency track the fundamental frequency of signal in real-time [133]. That is to make sure the sampling interval based on the fundamental frequency ready to sample and the spectrum leakage can be eliminated completely.

3.3 SIGNAL TIME DELAY

The typical structure of a WAMS is illustrated in Fig. 3.3. Synchronized phasors acquired by dispersive PMUs are transmitted to Phasor Data Concentrator (PDC) via the communication links [134]. The preconditioned synchronized phasors are then transmitted to the application software for system monitoring and control.

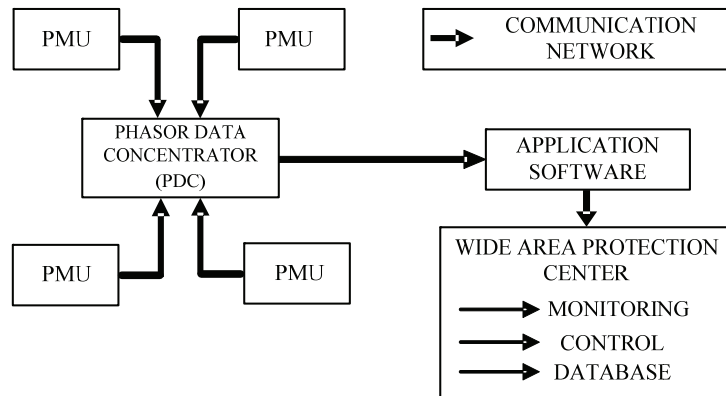


Fig. 3.3 Typical structure of a WAMS

PMUs are distributed over power system network on large utilities and substations. They are often far away from the PDC, so fast and reliable communication links are needed to transmit the synchronized phasors to the PDC. Therefore, the communication network is a key component of WAMS. Data transmission over long distance can be based on fiber, microwave, and satellite. When taking into account of bandwidth, robust, and time delay, fiber is the best choice. An experiment study showed that the time delays caused by different communication links are different, but all of the delays are more than 25ms [104]. The delay could even be larger when there are a large number of signals being routed or signals from different areas are waiting for synchronizing.

Normally, synchronized phasors from various locations in the power grid is required to determine the wide-area control actions. Synchronized phasors from different locations experience different amount of delays before they reach the control center.

Signal time delay in WAMS mainly includes PMU time delay, serial time delay, routing time delay, propagation time delay and repeating time delay.

PMU time delay indicates the time between the input analog voltage and electricity measurements and the output voltage and electricity synchronized phasors. It includes synchronization delay, synchronized sampling delay, phasor calculation delay and data encapsulation delay. While synchronization delay, also

known as synchronization accuracy, has been analyzed in the last section, synchronized sampling delay refers to A/D transformation delay and phasor calculation delay refers to discrete Fourier transform algorithm delay. The time delay caused by the data encapsulation depends on the quantity of the data and the efficiency of the data processing unit. In short, PMU time delay mainly depends on the hardware and software in PMU. Through the impact on synchronization delay, GPS signal also has a certain impact on PMU time delay

Serial time delay indicates the delay of having one bit being sent one after another. It is equal to the data packet divided by the communication rate of the communication medium.

Routing time delay indicates the time required for data to be sent through a router, and sent to another location.

Propagation time delay indicates the time required to transmit data over a particular communications medium. It depends on the network transmission media and transmission distance. It is equal to the length of transmission line by the velocity of the transmission media.

Repeating time delay indicates the time required for data to be received by a repeater, and compensated to transmit continue in the long communication link.

The total signal time delay in WAMS can be expressed as follows:

$$T = T_{\text{PMU}} + T_s + T_{\text{ro}} + T_p + T_{\text{re}} \quad (3.3)$$

$$T_s = \frac{P_s}{D_r} \quad (3.4)$$

$$T_p = \frac{l}{v} \quad (3.5)$$

where T_{PMU} is the PMU time delay, T_s is the serial time delay, T_{ro} is the routing time delay, T_p is the propagation time delay, T_{re} is the repeating time delay, P_s is the size of the packet (bits/packet), D_r is the data rate of the communication network, l is the length of the communication media, and v is the velocity at which

the data are sent through the communication media.

The quantitative analysis of signal time delay in WAMS is conducted in chapter V.

3.4 SUMMARY

Wide-area stability analysis and control is capable to recover power system from large disturbance and accident. However, the synchronization accuracy of synchronized phasors and signal time delay, which are two of the inherent characteristics of WAMS, would have large impacts on the effectiveness of wide-area stability analysis and control. During the process of the design of WAMS based stability analysis and control schemes, these two characteristics must be considered.

This chapter first discusses the causes and effects of synchronization inaccuracy and signal time delay, and then the synchronization accuracy and signal time delay are systematically studied and examined such that some recommendations are made to improve the synchronization accuracy and reduce the signal time delay to meet the demand of wide-area stability analysis and control in practical use.

Following the maturity of WAMS technology and application of WAMS based stability analysis and control schemes, the quantitative analysis of synchronization accuracy and signal time delay will play as the foundation of these WAMS based schemes.

CHAPTER IV RELIABILITY EVALUATION OF WAMS

4.1 INTRODUCTION

As modern electric power systems are transforming into smart grids, real-time WAMS has become an essential tool for operation and control [135, 136]. Despite practical WAMS has already been established in many countries [7], pioneer studies focused mostly on the utilization of WAMS information rather than quantitative evaluation of its reliability. In fact, the concerns on reliability of WAMS are one of the main factors contributed to the slow pace of synchro-phasor adoption for real-time applications [137]. It is now urgent and necessary to comprehensively and quantitatively evaluate the reliability of WAMS to ensure its availability and reliability meeting the requirements for real-time analysis and control.

Reliability indices of WAMS can be derived either from the statistical data collected in operation or from a reliability model. As WAMS is still an emerging technology, statistical data available for reliability evaluation would be little and the most convenient approach would be to first construct a reliability model of WAMS and then to evaluate the reliability indices of this model using a comprehensive reliability method.

In [9,10], traditional Markov method was used to construct a reliability model of WAMS, in which components of WAMS were represented as equivalent two-state model first and then Markov state transition diagram was used to depict the dynamic logic relationship between WAMS and its components. The main concern of this approach is the large state space cardinality which precludes not only the model solution but also the generation of the transition rate matrix [11]. In order to simplify the Markov state transition diagram, only single fault pattern in

the failure of WAMS was therefore considered while multiple fault patterns were ignored. Furthermore, during the reliability evaluation of WAMS, only the reliability of PMU measurements uploading from PMUs to control center was considered, while reliability of control instructions downloading from control center to PMUs was ignored. Without an accurate reliability model of WAMS, it would be difficult to derive accurate reliability indices.

Once a reliability model of WAMS is constructed, an analytical algorithm would be needed to evaluate the reliability indices. State enumeration technique was used in [10] to analyze the Markov based reliability model of WAMS. However, numerous states will be resulted as the system size grows and prohibit its practical use in large-scale WAMS. In [9], state transfer diagram was used to analyze the reliability model of WAMS and the same combination explosion problem exists.

In this chapter, a comprehensive reliability evaluation scheme based on Monte Carlo (MC) simulation and Fault Tree (FT) analysis is proposed for quantitative evaluation of WAMS reliability. The main advantage for using the fault tree modeling method to construct the reliability model of WAMS is that it allows multiple fault patterns in WAMS to be considered in the reliability evaluation conveniently. Furthermore, the reliability of both PMU measurements uploading from PMUs to the control center and control instructions downloading from the control center to PMUs could be considered in the construction of reliability model of WAMS. The problem of state space explosion is overcome with the use of Monte Carlo simulation for evaluating the FT reliability model of WAMS. Not only the reliability indices of WAMS can be evaluated more accurately, but also additional reliability indices such as importance indices, which cannot be easily obtained otherwise, can be deduced via the Monte Carlo simulation.

This chapter is organized as follows: section 4.2 introduces the FT modeling

method and the Monte Carlo simulation approach. In section 4.3, a multilayer FT reliability model of WAMS is constructed. In section 4.4, a FT reliability model of PMU is constructed and analyzed with Monte Carlo simulation to calculate the reliability indices of PMU. In section 4.5, reliability of PDC and control center is evaluated. In section 4.6, reliability of communication networks including WACN and LACN is evaluated. In section 4.7, reliability indices of the complete WAMS are generated. In section 4.8, a simple example based on an adaptive wide-area damping control scheme with consideration of signal time delay is given to show the application of the proposed WAMS reliability evaluation method. Lastly, a conclusion is conducted in section 4.9.

4.2 FT MODELING METHOD AND MONTE CARLO SIMULATION APPROACH

There are many methods for constructing a reliability model such as FT analysis, Bayes method, Colored Petri Nets (CPN), RBD, Markov and so on [138-142]. Among all of them, FT modeling method is the most popular technique in industrial applications for the construction of reliability model [143-146].

Many methods [142,147-152] such as minimal cut sets, network reduction method and Monte Carlo simulation approach have been proposed to analyze FT based reliability model. However, with the increase of system scale and complexity, it is difficult for the minimal cut sets method to find the minimal cut sets in FT based reliability model. Network reduction method can equivalently simplify the system reliability model through reducing the network nodes. But because of such simplification, accurate reliability indices cannot be reached. Comparatively, Monte Carlo simulation approach would be more flexible and easier to obtain accurate reliability indices.

4.2.1 FT MODELING METHOD

FT modeling method was firstly proposed by H. A. Wilson in Bell laboratory. It can provide a mathematical and graphical representation of the combinations of events that can lead to system failure [151,153-155], and therefore, is an effective method for the reliability evaluation of WAMS. By using FT modeling method, the potential fault of WAMS can be found and the probability of the WAMS failure can be predicted.

FT can be classified as static or dynamic FT depending on the types of the gates being used. FT composed by basic logic gates such as OR/AND gates, XOR gate, voting gate and so on is called Static FT (SFT). FT composed by at least one dynamic logic gates including Sequence Enforcing gate (SEQ), Priority-AND gate (PAND), Functional Dependency gate (FDEP), Cold Spare gate (CSP), Warm Spare gate (WSP) and Hot Spare gate (HSP) is called Dynamic FT (DFT) [156,157].

In the FT based reliability model, the basic events usually refer to the failure of basic components or the misoperation of operator, and the top event usually refers to the system failure. The interaction between the basic events and the top event is described by logic gates. In this way a whole FT based reliability model could be constructed. The modeling procedures of FT based reliability model of WAMS are as follows:

- (1) Defining WAMS failure as the top event.
- (2) Analyzing the logic relationships between the basic components in WAMS and the top event.
- (3) Describing these logic relationships with logic gates in FT.
- (4) Constructing the whole FT based reliability model of WAMS by the combination of all the logic relationships.

4.2.2 MONTE CARLO SIMULATION APPROACH

Monte Carlo simulation approach is a very valuable method which is widely used in the solution of practical engineering problems in many fields. With the increase in the scale of WAMS, it is difficult to use any analytical methods (e.g. minimal cut sets, network reduction method) to analyze the FT based reliability model of WAMS so as to calculate accurate reliability indices. Monte Carlo simulation approach based the FT analysis method can overcome this problem and is able to derive accurate reliability indices of WAMS including the importance indices which cannot be easily obtained with analytical methods.

Monte Carlo simulation approach evaluates the reliability indices by simulating the actual process and random behavior of WAMS based on its FT reliability model. This method treats the basic events in the FT reliability model of WAMS as a series of real experiments. It evaluates the probability and other indices by counting the failure counts and recording the failure and repair time of the top event during all the experiments. The required information for this method is the Probability Density Functions (PDF) for time to failure and repair of all basic components in WAMS [146].

(1) Sampling method of Monte Carlo simulation approach [146]

Consider that the PDF for time to failure $f(t)$ of component is following exponential distribution with parameter λ . Thus, $f(t)$ and life distribution function $F(t)$ are given by:

$$\begin{aligned} f(t) &= \lambda \exp(-\lambda t) \\ F(t) &= \int_0^t f(t) dt = 1 - \exp(-\lambda t) \end{aligned} \quad (4.1)$$

Fig. 4.1 shows the change of $F(t)$ and $1-F(t)$ over time with $\lambda=1$, i.e. the failure rate of this component is once every year.

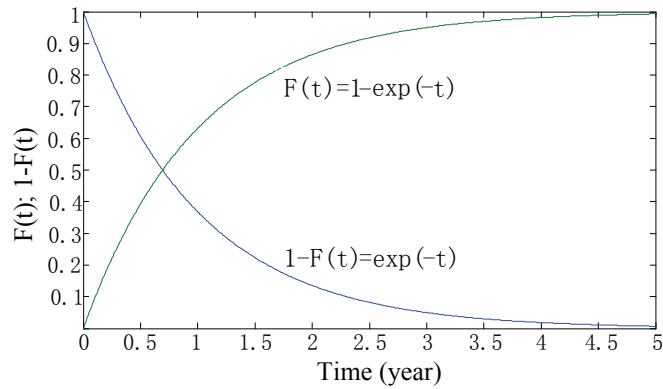


Fig. 4.1 Changing curve of $F(t)$ and $1-F(t)$ with time t

The inverse function of $F(t)$ can be expressed by:

$$t = G(F(t)) = -\frac{1}{\lambda} \ln(1 - F(t)) \quad (4.2)$$

where t is the failure time of component. As shown in Fig. 4.1, $1-F(t)$ distributes between 0 and 1. Based on Equation (4.2), the random failure time of component can be sampled using direct sampling method of Monte Carlo as follows:

$$ft = -\frac{1}{\lambda} \ln \varepsilon_1 \quad (4.3)$$

where ε_1 is a uniform distribution between 0 and 1. The random repair time of component is:

$$rt = -\frac{1}{\mu} \ln \varepsilon_2 \quad (4.4)$$

where ε_2 is also a uniform distribution between 0 and 1.

(2) Reliability indices

Reliability indices mean the parameters which can indicate the reliability degree of system from different aspects. Traditionally, reliability indices include Mean Time between Failures (MTBF), Mean Time to Repair (MTTR), availability, unavailability, basic cell importance and basic cell module importance.

MTBF is the mean working time between two failures. MTTR is the mean time for the repair of faulted system. MTBF and MTTR can be expressed by the method of Monte Carlo simulation approach, respectively:

$$\begin{aligned}
MTBF &= \frac{1}{N} \sum_{i=1}^N ft_i \\
MTTR &= \frac{1}{N} \sum_{i=1}^N rt_i
\end{aligned}
\tag{4.5}$$

where N is the failure count of system in the whole simulation time, ft_i and rt_i are the failure and repair time of system, respectively, in the i^{th} Monte Carlo simulation.

According to the MTBF and MTTR of WAMS, the availability and unavailability of system can be described as [155]:

$$\begin{aligned}
A &= \frac{MTBF}{MTBF + MTTR} \\
U = 1 - A &= \frac{MTTR}{MTBF + MTTR}
\end{aligned}
\tag{4.6}$$

Component importance indices are used to arrange the components in order of increasing or decreasing importance. Among all the existing component importance indices such as Birnbaum's reliability importance, Fussell-Vesely's measure of importance, Criticality importance, the interruption cost based importance index, Maintenance potential and Failure criticality importance index, the failure criticality importance index is best suited for the Monte Carlo simulation approach adopted in this chapter as no extra Monte Carlo simulation cycle would be needed. In failure criticality importance indices, the basic cell importance $W(Z)$ of component Z reflects the probability of the failure of PMU arising from the failure of component Z . $W(Z)$ can be defined as [149]:

$$W(Z) = \frac{NS_z}{N_z}
\tag{4.7}$$

where NS_z is failure count of system caused by the failure of its basic component Z and N_z is the failure count of component Z . The basic cell importance of component Z mainly depends on the logic location of component Z in the FT reliability model of system.

Another key index in failure criticality importance indices is the basic cell module importance $W_N(Z)$, which reflects the proportion of the failure count of PMU arising from the failure of component Z in all failure counts of PMU. $W_N(Z)$ can be expressed as[149]:

$$W_N(Z) = \frac{NS_Z}{NS} \quad (4.8)$$

where NS is the failure count of system. Components with high basic cell module importance would be the components which have high impact on the reliability of system. The basic cell module importance of component Z mainly depends on the failure rate of component Z .

(3) Convergence analysis [54,55]

Monte Carlo simulation approach is a numerical method based on probability theory to compute the results with repeated random sampling. In the solution process of the reliability indices of complex system, the convergence of the Monte Carlo simulation results must be assessed to determine the termination condition. Here, standard error is used to assess the simulation convergence, and the convergence factor β is defined as:

$$\beta = \frac{\sigma}{\sqrt{N}} \leq \varepsilon_r \quad (4.9)$$

where

$$\sigma = \sqrt{V(ft)} \quad (4.10)$$

$$V(ft) = \frac{1}{N-1} \sum_{i=1}^N (ft_i - E(ft_i))^2 \quad (4.11)$$

$$E(ft) = \frac{1}{N} \sum_{i=1}^N ft_i \quad (4.12)$$

N is the failure count of system in the whole simulation time, ε_r is pre-specified fraction, ft is the failure time of system in one simulation, $V(ft)$ is the variance of failure time of system and σ is the standard error of failure time of system.

4.2.3 MONTE CARLO SIMULATION APPROACH FOR FT LOGIC GATES

Since there will be a large amount of logic gates in the FT reliability model of WAMS, nonsequential Monte Carlo simulation approach [158] is therefore adopted to analyze the FT logic gates such as OR gate, AND gate, voting gate, PAND gate, CSP gate, and FDEP gate [146].

During the Monte Carlo simulation reliability evaluation process of WAMS, basic components in WAMS are simulated as a series of experiments for depicting the duration of available (operation) state, which means that components are available or in operation state, and the duration of unavailable (failure) state, which means that components are unavailable or in failure state. As operation and failure states will come and change with time in experiments, they are called state-time diagrams [146]. Durations of these two states depend on the PDFs of time to failure and time to repair.

(1) OR gate

The symbol of OR gate is shown in Fig. 4.2. Assuming OR gate has two basic events, A and B, and one top event C. In one experiment, basic events A and B can be either in operation state or failure state. When at least one of them reaches failure state, the top event C will reach failure state.

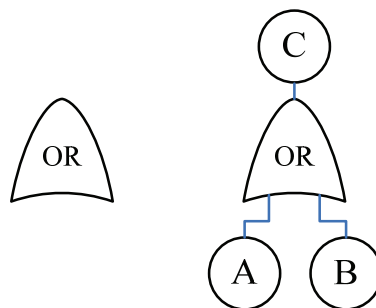


Fig. 4.2 Symbol of OR gate

By employing the direct sampling method of Monte Carlo mentioned above, the failure and repair time of basic events A and B can be obtained from their PDFs

of time to failure and repair as follows:

$$\begin{aligned}
 ft_A &= -\frac{1}{\lambda_A} \ln \varepsilon_1 & ft_B &= -\frac{1}{\lambda_B} \ln \varepsilon_3 \\
 rt_A &= -\frac{1}{\mu_A} \ln \varepsilon_2 & rt_B &= -\frac{1}{\mu_B} \ln \varepsilon_4
 \end{aligned}
 \tag{4.13}$$

All the possible state-time diagrams of OR gate are shown in Fig. 4.3, in which ft_A, ft_B and ft_C denote the failure time of basic events A, B and the top event C, respectively, and rt_A, rt_B and rt_C denote the repair time of basic events A, B and the top event C, respectively.

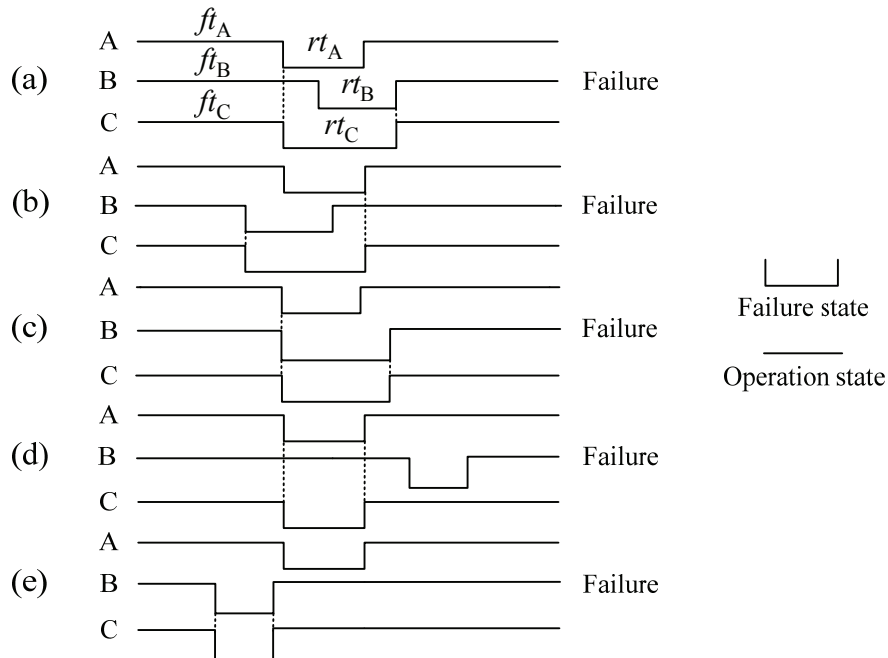


Fig. 4.3 Possible state-time diagrams of OR gate

In all the possible state-time diagrams, top event C is in failure state and $ft_C = \min(ft_A, ft_B)$. In (a), $rt_C = ft_B + rt_B - ft_A$. In (b), $rt_C = ft_A + rt_A - ft_B$. In (c), $rt_C = \max(rt_A, rt_B)$. In (d) and (e), rt_C is the repair time of the basic event which has the minimum failure time. The failure counts N of top event C will cumulate when top event C is in failure state in one experiment. After the convergence criterion is satisfied, MTBF and MTTR of top event C can be calculated as:

$$T_{MTBF} = \frac{1}{N} \sum_{i=1}^N f_{Ci}$$

$$T_{MTTR} = \frac{1}{N} \sum_{i=1}^N r_{Ci}$$
(4.14)

(2) AND gate

The symbol of AND gate is shown in Fig. 4.4. Assuming AND gate has two basic events, A and B, and one top event C. In one experiment, when both basic events A and B reach failure state, the top event C will reach failure state.

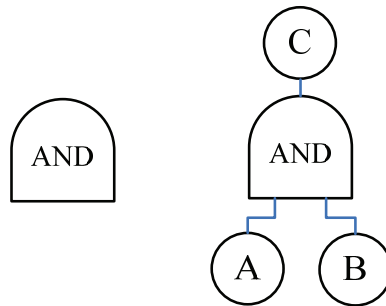


Fig. 4.4 Symbol of AND gate

Base on the sampling method in Equation (4.13), all the possible state-time diagrams of AND gate are shown in Fig. 4.5.

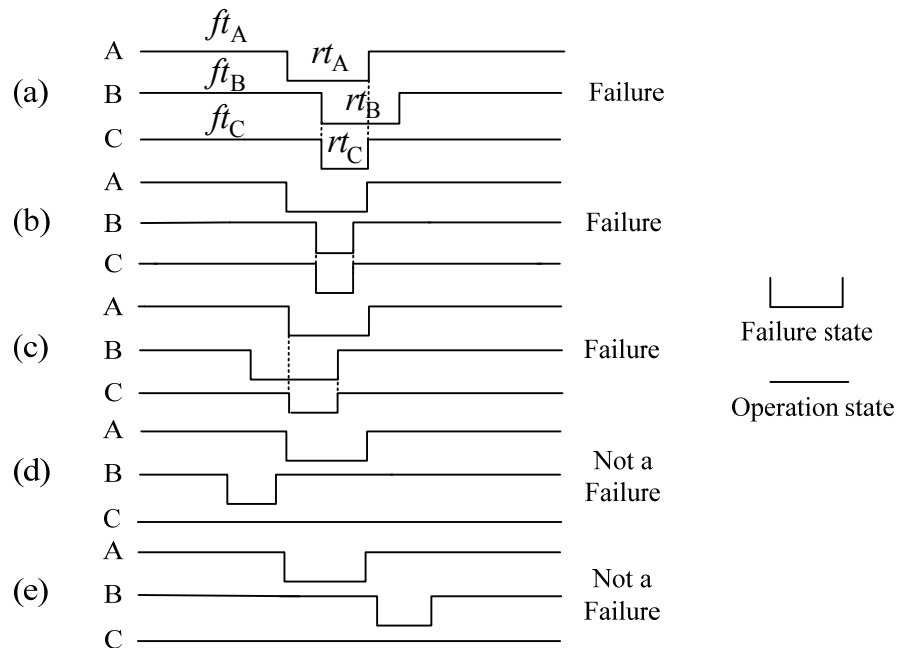


Fig. 4.5 Possible state-time diagrams of AND gate

In state-time diagram (a), (b) and (c), top event C is in failure state and failure counts N will cumulate. In (d) and (e), top event C is in operation state and the basic events A and B will be sampled again until top event C reaches failure state, then failure counts N of top event C will cumulate.

In (a), $ft_C = ft_B$ and $rt_C = ft_A + rt_A - ft_B$. In (b), $ft_C = ft_B$ and $rt_C = rt_B$. In (c), $ft_C = ft_A$ and $rt_C = ft_B + rt_B - ft_A$. In (d) and (e), ft_C and rt_C will cumulate until the top event C changes to failure state. Similarly, MTBF and MTTR of the top event C can be calculated with Equation (4.14).

(3) Voting gate

The symbol of voting gate is shown in Fig. 4.6. Assuming voting gate has three basic events, A, B and D, and one top event C. In one experiment, when at least two of the basic events reach failure state, the top event C will reach failure state.

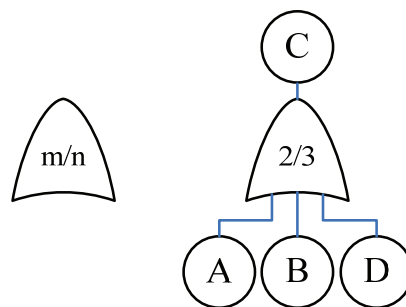


Fig. 4.6 Symbol of voting gate

It is difficult to analyze voting gate through Monte Carlo simulation approach directly because there are too many possible state-time diagrams in voting gate. In order to facilitate the analysis, voting gate can be transformed to the combination of OR and AND gates as shown in Fig. 4.7 based on the principle of equivalence.

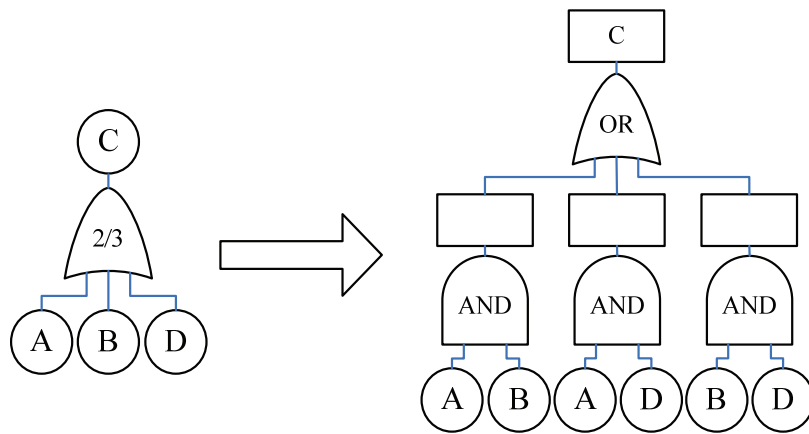


Fig. 4.7 Transformation from voting gate to the combination of OR and AND gate

After the transformation, voting gate is composed of OR and AND gates, which can be analyzed as above, and Monte Carlo simulation approach can be applied to the voting gate as combination of OR and AND gates.

(4) PAND gate

The symbol of PAND gate is shown in Fig. 4.8. Assuming PAND gate has two basic events, A and B, and one top event C. In one experiment, when basic events A and B reach failure state in a pre-assigned order, usually from left to right, the top event C will reach failure state.

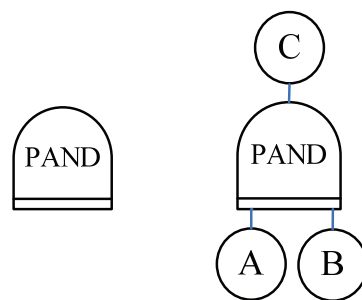


Fig. 4.8 Symbol of PAND gate

Base on the sampling method in Equation (4.13), all the possible state-time diagrams of PAND gate are shown in Fig. 4.9.

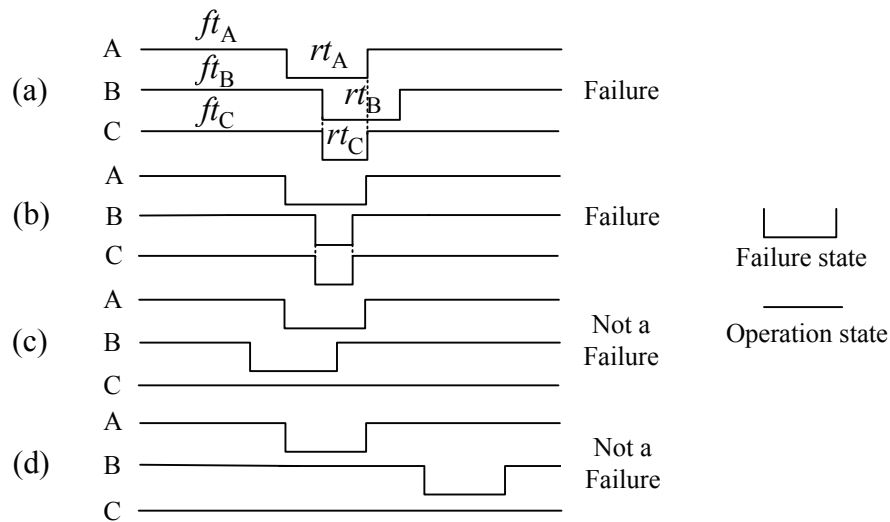


Fig. 4.9 Possible state-time diagrams of PAND gate

In state-time diagram (a) and (b), top event C is in failure state and failure counts N will cumulate. In (c) and (d), top event C is in operation state and the basic events A and B will be repeatedly sampled until top event C changes to failure state, then N will cumulate.

In (a), $ft_C = ft_B$ and $rt_C = ft_A + rt_A - ft_B$. In (b), $ft_C = ft_B$ and $rt_C = rt_B$. In (c) and (d), ft_C and rt_C will cumulate until top event C changes to failure state. Similarly, MTBF and MTTR of the top event C can be calculated with Equation (4.14).

(5) CSP gate

The symbol of CSP gate is shown in Fig. 4.10. CSP gate has an active basic event A and a standby basic event B. In normal condition, basic event A is in operation state and basic event B is in cold spare state. When basic event A changes to failure state, basic event B will change to operation state from cold spare state. When both basic events A and B reach failure state, the top event C will reach failure state.

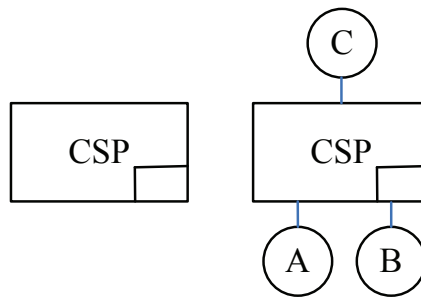


Fig. 4.10 Symbol of CSP gate

Base on the sampling method in Equation (4.13), all the possible state-time diagrams of CSP gate are shown in Fig. 4.11.

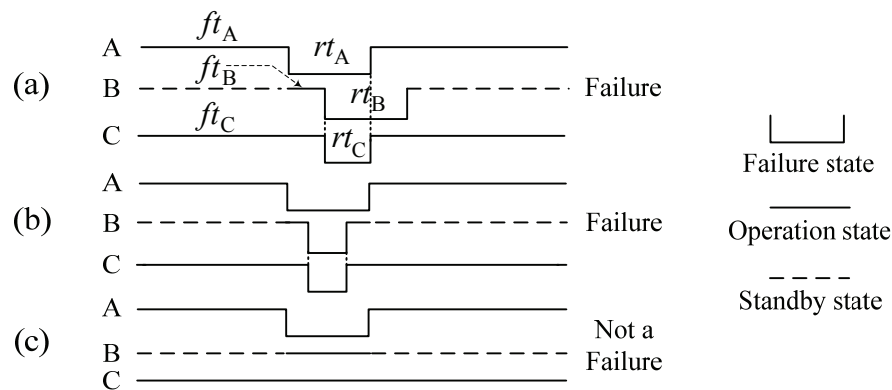


Fig. 4.11 Possible state-time diagrams of CSP gate

In state-time diagram (a) and (b), top event C is in failure state and failure counts N will cumulate. In (c), top event C is in operation state and the basic events A and B will be repeatedly sampled until top event C changes to failure state, then N will cumulate.

In (a), $ft_C = ft_A + ft_B$ and $rt_C = rt_A - ft_B$. In (b), $ft_C = ft_A + ft_B$ and $rt_C = rt_B$. In (c), failure time ft_C and repair time rt_C will cumulate until the top event C changes to failure state. Similarly, MTBF and MTTR of top event C can be calculated with Equation (4.14).

(6) FEDP gate

The symbol of FDEP gate is shown in Fig. 4.12. FDEP gate has a trigger event

T and a basic event A. The basic event A is functionally dependent on the trigger event T. When the trigger event T reaches failure state, the dependent basic event A will be forced to fail and top event C will reach failure state. When trigger event T is in operation state, event C will also reach failure state following the failure of basic event A.

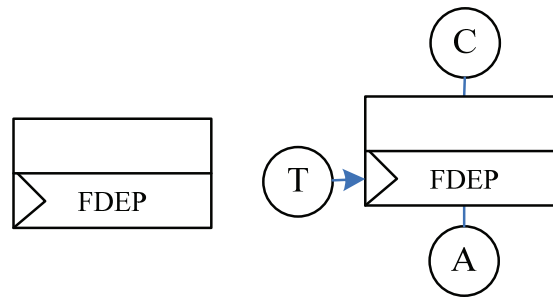


Fig. 4.12 Symbol of FDEP gate

Base on the sampling method in Equation (4.13), all the possible state-time diagrams of FDEP gate are shown in Fig. 4.13, in which ft_T and rt_T denote the failure time and repair time of triggering event T, respectively.

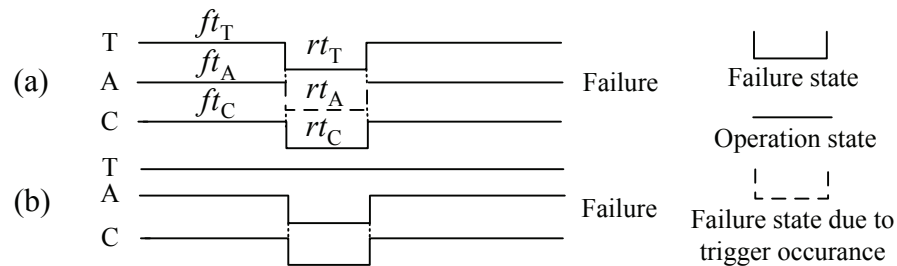


Fig. 4.13 Possible state-time diagram of FDEP gate

In Fig. 4.13, state (a) and state (b) are the failure states of top event C and failure times N of top event C will cumulate. In (a), $ft_C=ft_T$ and $rt_C=rt_T$. In (b), $ft_C=ft_A$ and $rt_C=rt_A$. Similarly, MTBF and MTTR of top event C can be calculated with Equation (4.14).

4.3 ARCHITECTURE AND RELIABILITY MODEL OF WAMS

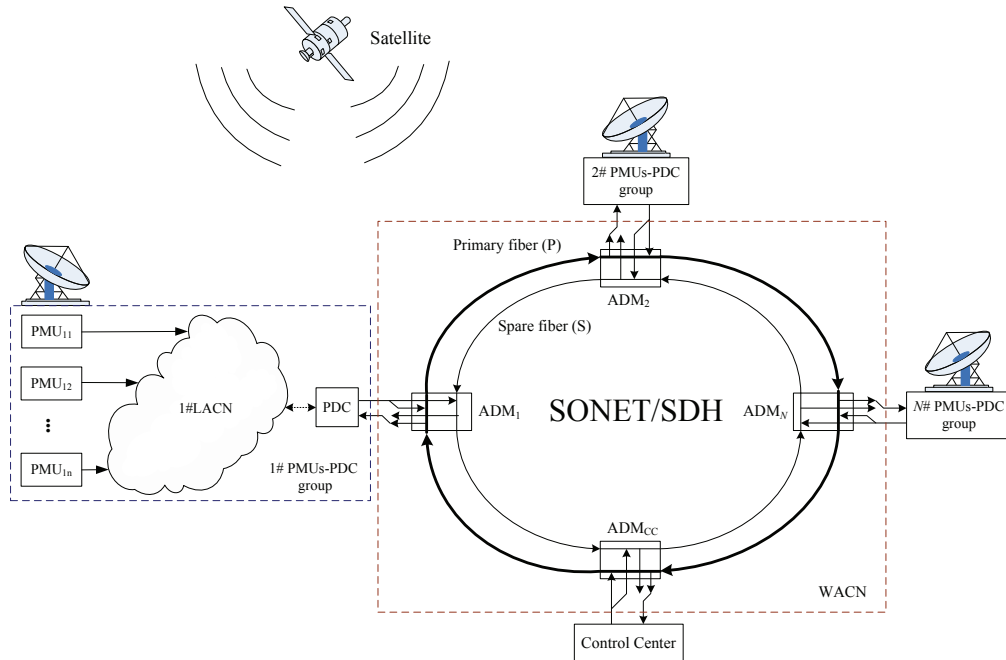


Fig. 4.14 Architecture of multilayer WAMS

Typical structure of WAMS consists of PMUs, PDC, communication networks including Wide-Area Communication Network (WACN) and Local-Area Communication Network (LACN), and control center. Based on the distribution and structure of these components, various WAMS architectures have been proposed over the years [7]. Here, a common multilayer WAMS architecture is adopted as shown in Fig.4.14.

In this WAMS architecture, dispersed PMUs would send the synchronized phasors to PDC via LACN. LACN, PDC and PMUs in the same region would form a PMUs-PDC group, and many PMUs-PDC groups are linked up with the control center via WACN.

For the reliability evaluation of this multilayer WAMS, an accurate and comprehensive reliability model can be constructed using the FT modeling method as shown in Fig. 4.15.

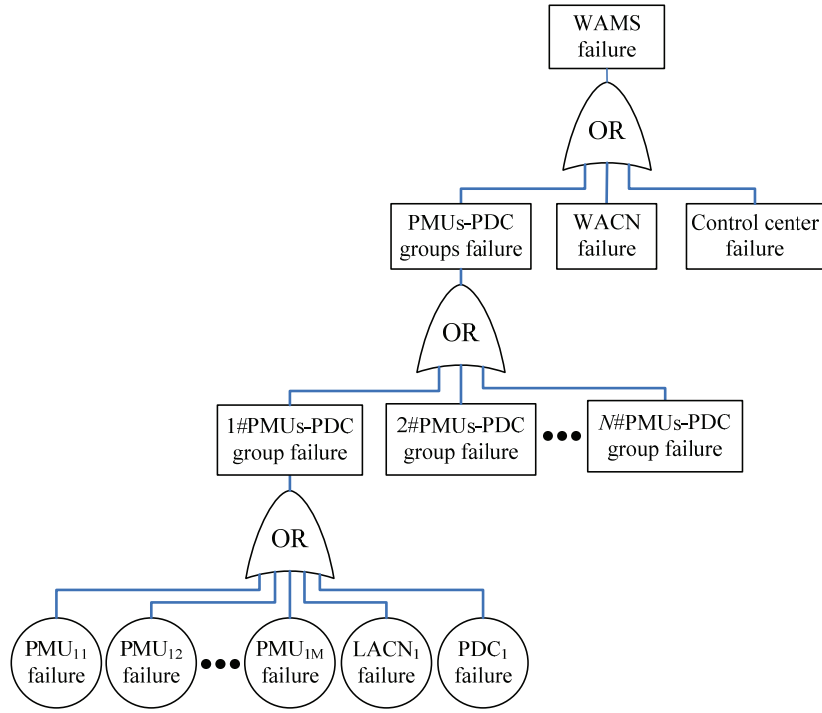


Fig. 4.15 FT reliability model of multilayer WAMS

In Fig. 4.15, the FT reliability model of WAMS is divided into several levels based on the multilayer WAMS architecture. The top event is WAMS failure, the sublevel events consist of the failure of PMUs-PDC groups, WACN and control center, the third level is the failure of N PMUs-PDC groups and the basic level events are the failure of M PMUs, LACN and PDC, which are the components of one PMUs-PDC group. The availability of WAMS can be calculated as follows [159]:

$$A_{\text{WAMS}} = \left(\prod_{i=1}^N A_{\text{PMUs-PDC}_i} \right) \cdot A_{\text{WACN}} \cdot A_{\text{Control-Center}} \quad (4.15)$$

where

$$A_{\text{PMUs-PDC}_i} = \left(\prod_{j=1}^{M_i} A_{\text{PMU}_{ij}} \right) \cdot A_{\text{LACN}_i} \cdot A_{\text{PDC}_i} \quad (4.16)$$

A_{WACN} is the availability of WACN; $A_{\text{Control-Center}}$ is the availability of control center; $A_{\text{PMUs-PDC}_i}$ is the availability of i^{th} PMUs-PDC group; $A_{\text{PMU}_{ij}}$, A_{LACN_i} and A_{PDC_i} are the availability of j^{th} PMU, LACN and PDC in the i^{th} PMUs-PDC group, respectively; N is the number of PMUs-PDC groups and M_i is the number of PMUs

in i^{th} PMUs-PDC group.

In the following subsections, reliability of PMU, PDC, control center and communication networks including WACN and LACNs will first be evaluated and the reliability of WAMS will then be calculated from the reliability of its components.

4.4 RELIABILITY EVALUATION OF PMU

The reliability evaluation of WAMS inevitably needs to analyze the function and characteristic of its components. Since PMU is the core component of WAMS [5], the evaluation of its reliability is a primary key in the reliability evaluation of WAMS. For instance, availability assessments were conducted in [159] for assessing the proposed applications of WAMS in power system monitoring and control but with typical availability of PMU assumed only.

Reliability model of PMU has been constructed in [160,161] using the traditional Markov method, in which the reliability indices of PMU were evaluated from fixed and uncertain reliability parameters of the basic components in PMU. In Markov method, the basic components of PMU are first represented as equivalent two-state models and then Markov state transition diagram is used to depict the logic relationship between PMU and its basic components. However, logic relationship between PMU and its basic components would be too complicated to be depicted accurately in the Markov state transition diagram. Furthermore, in order to simplify Markov state transition diagram as in [160,161], only single fault pattern was considered while multiple fault patterns were ignored. Without an accurate reliability model of PMU, the accuracy of the reliability indices would be compromised.

In order to overcome these problems in the Markov method, FT modeling method [108,112], which can accurately depict the complex logic relationship

between PMU and its basic components, is proposed to construct an accurate reliability model of PMU in which multiple fault patterns are considered. This FT reliability model of PMU can then be analyzed with various methods such as network reduction method [162], minimal cut sets [163], and Monte Carlo simulation approach. Compared with other two methods, Monte Carlo simulation approach can evaluate the reliability indices of PMU more easily and accurately.

4.4.1 RELIABILITY MODELING OF PMU

Fig. 4.16 shows the general structure of a PMU with seven function modules [160] including various basic components.

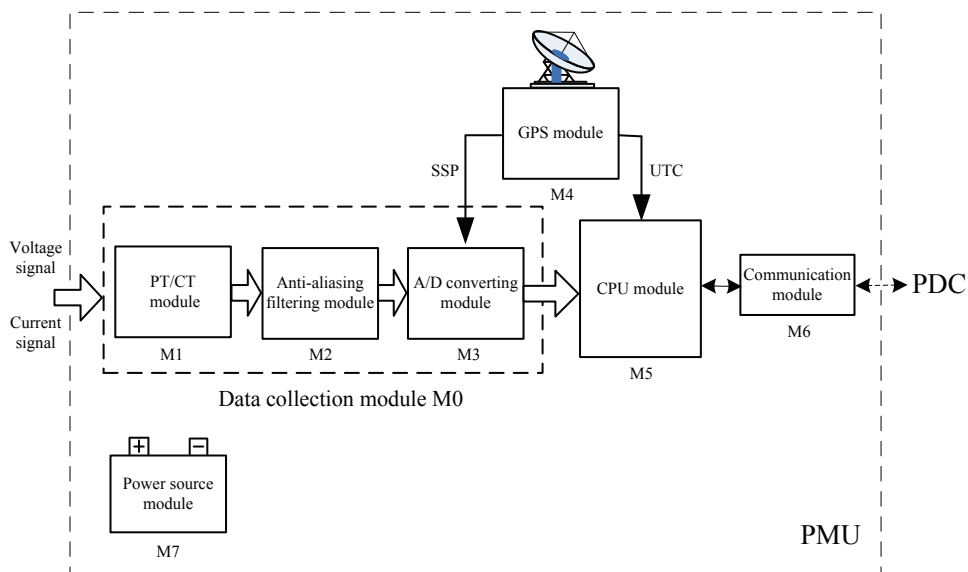


Fig. 4.16 Functional structure of PMU [160]

Through the PT/CT module (M1), large analog three-phase voltage and current signals are transformed into small analog voltage and current signals which will then be passed to the anti-aliasing filtering module (M2) to eliminate any high frequency noise. The A/D converting module (M3), whose synchronous sampling pulse (SSP) is supplied by the GPS module (M4), is used to convert the scaled and filtered analog inputs to digital signals. In the CPU module (M5), the

phasors of phase voltages and currents are computed via these digitized signals and stamped with coordinated universal time (UTC) supplied by the GPS module (M4), and then sent to phasor data concentrator (PDC) and control center by the communication module (M6) through communication network. The power of PMU is supplied by the power source module (M7).

Highly available PMU should be designed to automatically detect, isolate, and recover from failure. To achieve the fastest possible recovery, service is often restored onto redundant modules or components that are in standby and ready to rapidly accept service from a failed module or component. High-availability PMU should also be designed by architecting redundant arrangements of all critical modules or components so that no single module or component failure will produce a service outage. Therefore, in PMU, each type of field-replaceable hardware unit can be duplicated.

In China, there are three main manufacturers of commercial PMU including NR Electric Co. Ltd., Beijing Sifang Automation Co. Ltd., and China Electric Power Research Institute. The models of PMU produced by these three manufacturers are SMU-2 [164], CSS-200/1 [165], and PAC-2000 [166], respectively. Though the structures of these three PMUs are different, many common redundancy designs are used to improve the reliability of these three PMUs. For example, in all of these three PMUs, several AC, DC, or digital plug-in boards are used to allow multiple input signals and form redundancy. Furthermore, several identical 10M/100M Ethernet interfaces are used to allow PMU to communicate with multiple equipments and form redundancy. Individually, further redundancy designs are also incorporated including dual-cpu-board, dual-hot-pluggable power supply, etc.

Since PMUs designed and produced by different manufacturers do have different structure, a generic PMU structure proposed in [160] was therefore

adopted in this chapter. While simpler PMU structures could be easily derived from this model, this model also offers the opportunity for the reliability results obtained in this chapter to be comparable with published results in [160].

In the FT reliability model of PMU, the complex logic relationship between PMU and its basic components is accurately depicted through dynamic logic gates including Sequence Enforcing gate (SEQ), Priority-AND gate (PAND), Functional Dependency gate (FDEP), Cold Spare gate (CSP), Warm Spare gate (WSP) and Hot Spare gate (HSP).

PMU is a complex device which can be divided into seven function modules (M1~M7) based on their functional features. Each module, which could contain a small or large number of basic components, is first constructed as a sub-DFT reliability model, and then the complete DFT reliability model of PMU is constructed by combining these sub-DFT reliability models. This approach can significantly reduce the PMU modeling complexity and computational effort required by the following Monte Carlo simulation.

(1) Sub-FT reliability model of data collection module

Data collection module (M0) is used to transform large voltage and current signals to small signals, filter noise and random disturbances, and convert the analog input signals to digital ones. It consists of three function modules: PT/CT module (M1), anti-aliasing filtering module (M2) and A/D converting module (M3) as shown in Fig. 4.16.

In each of the three function modules, there are two parallel circuit boards (one is active and the other operates as cold standby). The sub-FT reliability model of this data collection module is shown as Fig. 4.17 in which λ_{M1A} , λ_{M1B} , λ_{M2A} , λ_{M2B} , λ_{M3A} , λ_{M3B} , μ_{M1A} , μ_{M1B} , μ_{M2A} , μ_{M2B} , μ_{M3A} and μ_{M3B} denote the failure and repair rate of circuit boards in module M1, M2 and M3.

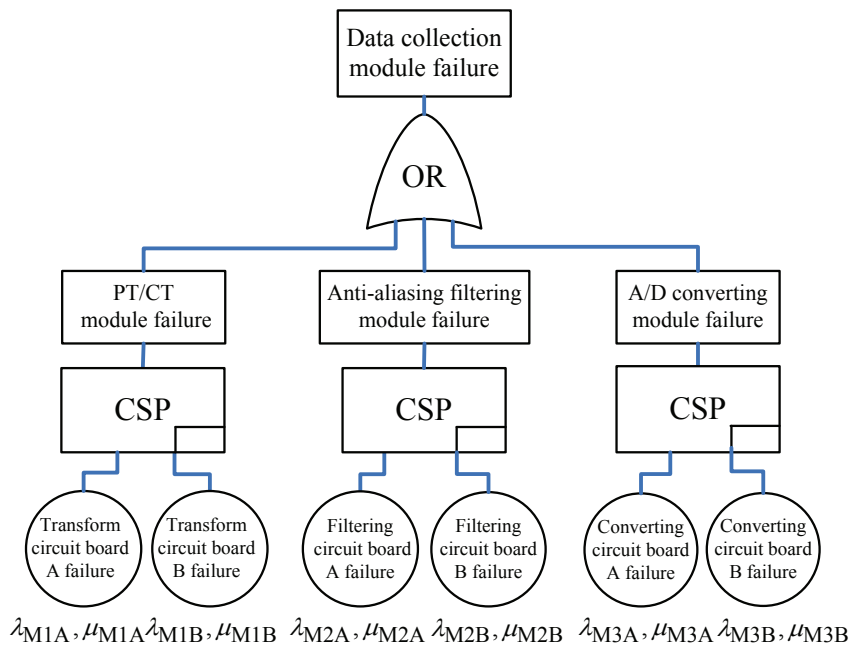


Fig. 4.17 Sub-FT reliability model of data collection module

In sub-FT based reliability model of data collection module, dynamic logic gate CSP is used to depict the spare mutual relationship between the two circuit boards, which are standby to each other, in module M1, M2 and M3.

(2) Sub-FT reliability model of GPS module

The construction of the sub-FT reliability model of GPS module is the key in the construction of reliability model of PMU. Thus, it is necessary to properly analyze the operation mechanism of GPS module shown in Fig. 4.18.

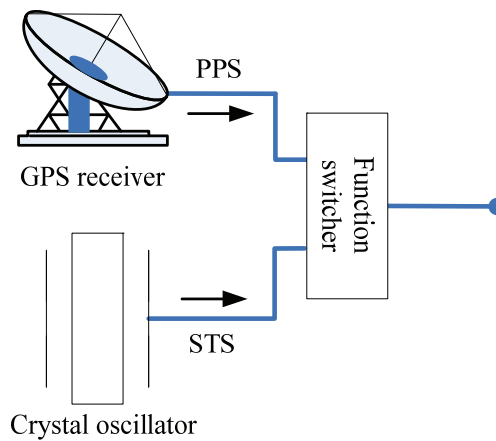


Fig. 4.18 Operation mechanism of GPS

In GPS, the functions of the crystal oscillator are twofold. The first function is to supply the high precision sampling clock pulses for the A/D converting module. The other function, which is the by-product of the crystal oscillator, is to preserve the precise time reference during the loss of GPS signal.

GPS may temporarily lose its signal because of various causes no matter how strong the observability of the current GPS satellites is. The following are the common causes for the loss of GPS signal:

- 1) Poor placement of the GPS antenna.
- 2) The loose connections at either end of the GPS antenna cable or the IRIG-B cables.
- 3) Temporary physical blockage due to a large bird landing on or building a nest over the antenna.
- 4) Interference or jammed signal at the receiver from various sources, such as:
 - a. Solar storms with large solar flares
 - b. Terrible weather with thick cloud
 - c. Unintentional interference from nearby RF transmitters
 - d. Intentional interference to disable the GPS receiver

Each of the above situations can result in the loss of precise timing and some of them are not avoidable even if GPS is well designed or installed. A field experience and assessment of stability of GPS signal in [167] showed that GPS does lose its signal from time to time.

For PMUs, the inaccuracy and missing data caused by the GPS signal loss is a big issue for the smart grid whose operation and control heavily depends on the quality and reliability of PMU synchronized phasor. Therefore, to address the short periods of GPS signal loss, PMU should allow the clock to maintain accurate time over a period of time when it is not receiving a GPS signal. Crystal

oscillator is the cheapest, simplest and the most practical method to achieve this objective.

According to the standard PMU definition/basic specification set by the Regional Transmission Organization (MISO), for the hardware requirements of a PMU, PMU shall automatically switch to local clock in case of loss of GPS signal, and shall resynchronize automatically when GPS signal is available [168]. This means all commercial PMUs should have some kind of built-in time reference keeping mechanism after the loss of GPS signal. For the SIMEAS R-PMU produced by Siemens, if the GPS signal is interrupted, it will enter a holdover mode with quartz oscillator [169]. For SEL-487E produced by Schweitzer Engineering Laboratories, when satellite lock is failed, its operation mode will turn to holdover mode operating on the internal oscillator [170]. For the three main PMUs currently in production in China, the time reference keeping mechanism is designed to keep the precise time reference when GPS signal is lost. For SMU-2 PMU produced by NR Electric Co. Ltd, internal high stable Oven Controlled Crystal Oscillator is used to keep the accurate time reference during the loss of GPS signal [164]. When GPS signal is lost, through internal high precision crystal oscillator, CSS-200/1 PMU produced by Beijing Sifang Automation Co. Ltd. can keep the synchronization error being less than 0.5 degree within two hours [165]. This can greatly improve the usability of CSS-200/1 PMU. For PAC-2000 produced by China Electric Power Research Institute, high precision crystal oscillator and time keeping circuit are adopted to keep the synchronous sampling error be less than 30 μ s within 2 hours [166].

Therefore, in this chapter, when the GPS signal is lost, the crystal oscillator will take over the GPS receiver to supply the Synchronous Time Signal (STS), and the GPS module would enter backup clock operation mode.

Under backup clock operation mode, the time accumulation error in STS

cannot be eliminated but would be less than $1\mu\text{s/h}$ [171]. According to IEEE Std. C37.118-2005, the Total Vector Error (TVE) needs to be less than 1% which corresponds to a maximum time error of $\pm 26\mu\text{s}$ for a 60Hz system. After the loss of GPS signal, GPS will enter backup clock operation mode and synchronous phasor from PMU can maintain its synchronization accuracy for up to 26 hours depending on the other sources of error contributed to the TVE before the recovery of GPS signal.

Fig. 4.19 shows the sub-FT reliability model of GPS module in which λ_{CO} , $\lambda_{\text{GPS-R}}$ and λ_{BC} denote the failure rate of crystal oscillator, GPS receiver and backup clock operation mode, respectively, μ_{CO} and $\mu_{\text{GPS-R}}$ denotes the repair rate of crystal oscillator and GPS receiver, respectively, and q_s denotes the probability of unsuccessful operation of function switcher.

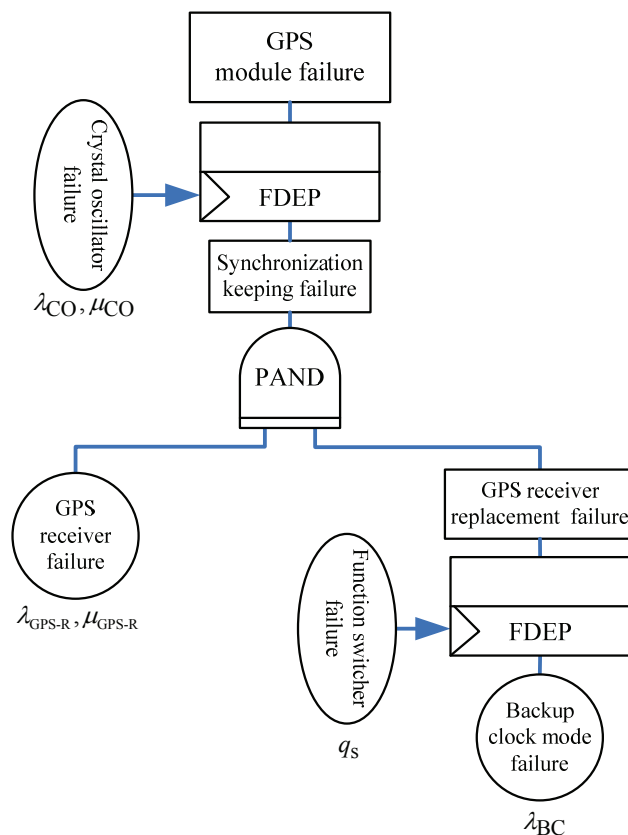


Fig. 4.19 Sub-FT reliability model of GPS module

In sub-FT reliability model of GPS module, two dynamic logic gates FDEP are used to depict the functional dependence relationship between crystal oscillator failure and synchronization failure and between function switcher failure and backup clock mode failure, and a PAND gate is used to depict the events sequence relationship between GPS receiver failure and GPS replacement failure.

(3) Sub-FT reliability model of CPU module

CPU module consists of hardware and software. Hardware is the carrier of software to accomplish the designed PMU functions such as phasor calculation, frequency estimation and so on. The reliability evaluation of software is totally different from that of hardware. Firstly, the failure of hardware is associated with the physical failure, but the failure of software mainly associates with the failure of its function because of the code error. Secondly, due to aging, reliability of hardware will gradually decrease while the reliability of software will increase due to the unceasing optimization of its code.

Among all the reliability models of software, logarithmic exponential model is commonly used to analyze the reliability of software [172]. The failure rate of software is given by

$$\lambda(u)=\lambda_0e^{-\theta u} \quad (4.17)$$

where λ_0 is the initial failure rate, θ is the failure decay parameter, and u is the number of failures found.

Fig. 4.20 shows the sub-FT reliability model of CPU module in which λ_{sw} , λ_{hw} , μ_{sw} and μ_{hw} denote the failure rate and repair rate of software and hardware in CPU module.

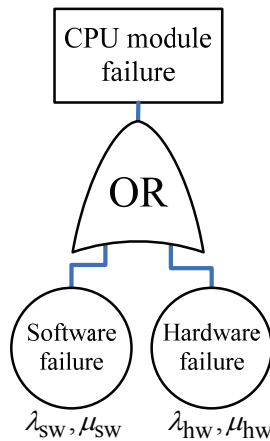


Fig. 4.20 Sub-FT reliability model of CPU module

In sub-FT based reliability model of CPU module, basic logic gate OR is used to depict the relationship between software and hardware in CPU module.

(4) Sub-FT reliability model of communication module and power source module

In PMU, there are two parallel communication ports which are spare mutually. There is also a standby power source module to improve the reliability of power supply.

The sub-FT reliability models of communication module and power source module are described in Fig. 4.21, in which $\lambda_{M6A}, \lambda_{M6B}, \lambda_{M7A}, \lambda_{M7B}, \mu_{M6A}, \mu_{M6B}, \mu_{M7A}$ and μ_{M7B} denote the failure rate and repair rate of network ports in communication module and two alternate power source modules

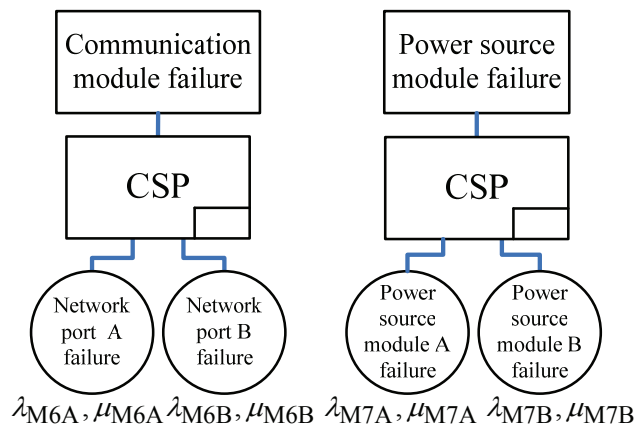


Fig.4.21 Sub-FT reliability models of communication and power source module

Like the sub-FT reliability model of data collection modules, dynamic logic gate CSP is used to depict the alternate relationship between two communication ports in communication module and between two power source modules.

(5) Complete FT reliability model of PMU

It can be seen from Fig. 4.16 that the failure of any function module will result in PMU failure. From a reliability point of view, all the modules are called in series. Therefore, basic logic gate OR is used to combine all the sub-FT reliability models associated with the seven function modules of PMU to obtain the complete FT reliability model of PMU as shown Fig. 4.22.

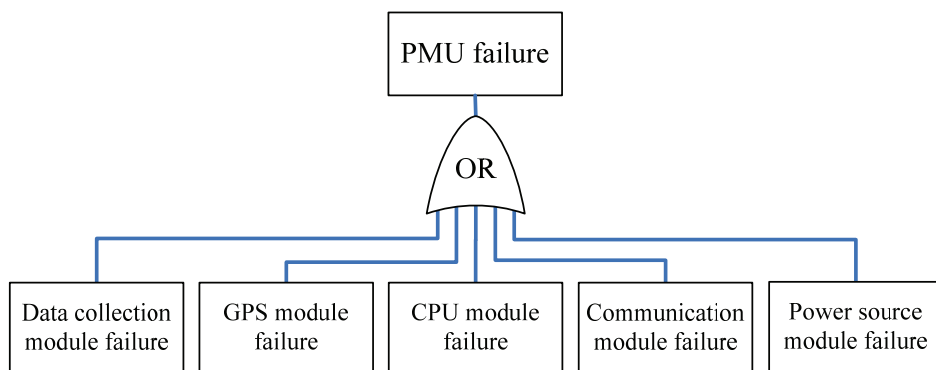


Fig. 4.22 Complete FT reliability model of PMU

Once the complete FT reliability model of PMU is constructed, Monte Carlo simulation would be used to determine the reliability indices of PMU accurately.

4.4.2 RELIABILITY EVALUATION FLOW CHART OF PMU

Flow chart of reliability evaluation of PMU using the proposed MCFT reliability evaluation method is shown in Fig. 4.23 where N indicates the count of down state (failure) of PMU in simulation, ε_r indicates the pre-set convergence criterion of Monte Carlo simulation, T_1 indicates the array of failure time of PMU, T_2 indicates the array of repair time of PMU. Some equations are included to describe the failure and repair time of PMU and its function modules in Monte

Carlo simulation. For example, $(ft_{M6}, rt_{M6})=CSP(M6A, M6B)$ means that the failure time and repair time of communication module (M6) are evaluated through the Monte Carlo simulation of CSP gate which is used to construct the sub-FT reliability model of communication module, $(ft_{M4}, rt_{M4})=Crystal\ oscillator$ means that failure and repair time of GPS module (M4) are determined by those of crystal oscillator.

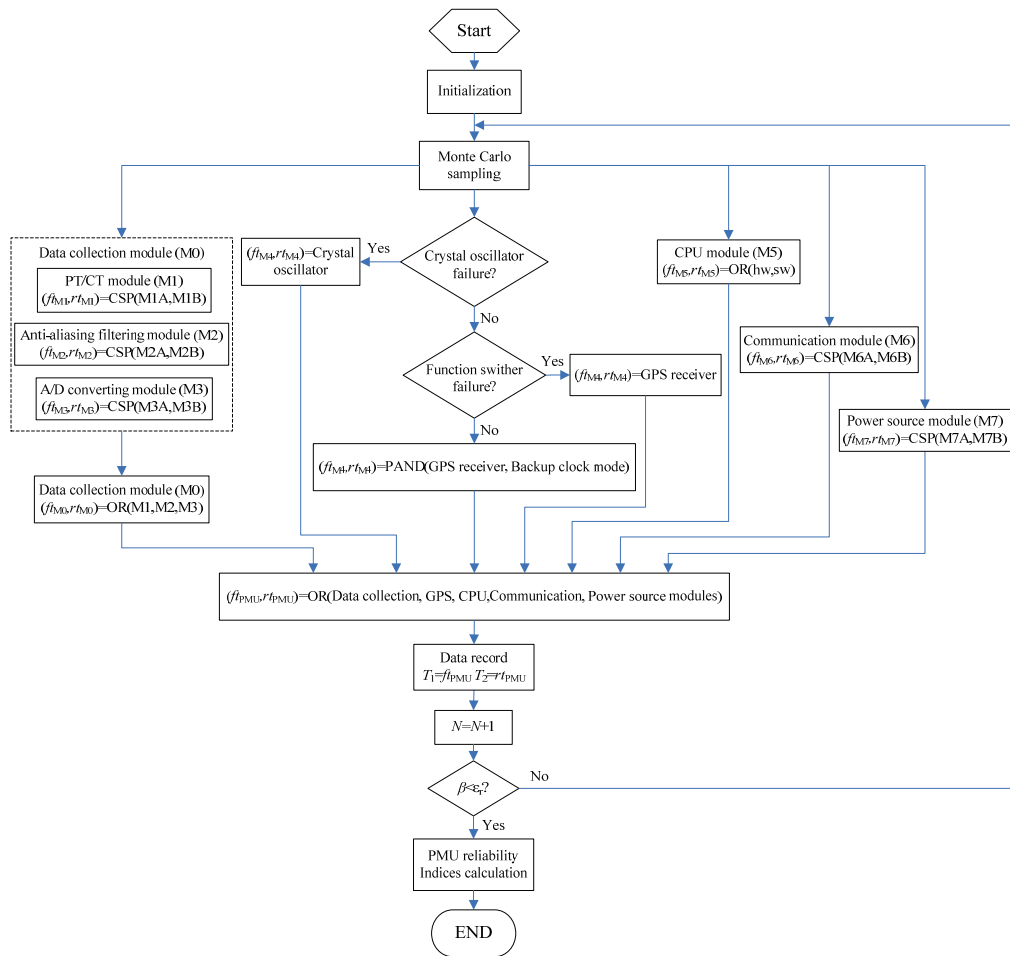


Fig. 4.23 Flow chart of reliability evaluation of PMU

In the start of simulation, parameters N , ϵ_r , T_1 and T_2 are firstly initialized. Secondly, Monte Carlo samples the failure and repair time of each basic component in PMU. Thirdly, failure and repair time of the seven function modules in PMU are evaluated. Fourthly, one set of failure and repair time of PMU are evaluated and stored in array T_1 and T_2 , then PMU failure count will be

incremented and convergence analysis will be conducted using array T_1 and T_2 to determine whether reliability indices of PMU have reached pre-set accuracy or not. If Monte Carlo simulation result has reached pre-set accuracy, reliability indices of PMU can be calculated; otherwise, another round of Monte Carlo simulation will be conducted until the convergence criterion is satisfied.

4.4.3 RELIABILITY INDICES OF PMU

Table 4.1 Reliability parameters of basic components in PMU

Parameters (M1)	Value	Parameters (M2)	Value	Parameters (M3)	Value
λ_{M1A}	0.4155	λ_{M2A}	0.1923	λ_{M3A}	0.1383
μ_{M1A}	673.85	μ_{M2A}	547.5	μ_{M3A}	438
λ_{M1B}	0.4155	λ_{M2B}	0.1923	λ_{M3B}	0.1383
μ_{M1B}	673.85	μ_{M2B}	547.5	μ_{M3B}	438
Parameters (M5)	Value	Parameters (M6)	Value	Parameters (M7)	Value
λ_{hw}	0.2368	λ_{M6A}	0.0228	λ_{M7A}	0.2751
μ_{hw}	365	μ_{M6A}	17520	μ_{M7A}	365
λ_{sw}	0.0657	λ_{M6B}	0.0228	λ_{M7B}	0.2751
μ_{sw}	1460	μ_{M6B}	17520	μ_{M7B}	365
Parameters (M4)	Value	Parameters (M4)	Value	Parameters (M4)	Value
λ_{CO}	0.0188	λ_{GPS-R}	0.7727	q_s	0.75%
μ_{CO}	312.88	μ_{GPS-R}	365	λ_{BC}	273.75

Note: unit of λ is in failures/year and unit of μ is in repairs/year

Basic components in PMUs supplied by different manufacturers would have different reliability parameters. Most often accurate reliability parameters would

not be available from the manufacturers to the public or even users. In this work, the reliability parameters of PMU basic components were either collected or derived from [173,174] as shown in Table 4.1. Although these data is not absolutely accurate, it is sufficient for demonstrating the proposed PMU reliability evaluation method and the subsequent analysis.

4.4.3.1 CONVERGENCE ASSESSMENT

Fig. 4.24 plots the convergence factor β against Monte Carlo simulation time for Case 1 and 2 (details of Case 1 and 2 will be described in next subsection). It is clear that in both Case 1 and 2 the convergence factor β remains almost unchanged when the simulation time is over 200,000 years. The corresponding convergence factor 0.35% for Case 1 and 0.14% for Case 2 were therefore selected as the termination condition for Monte Carlo simulations for ensuring the convergence and accuracy of the reliability indices in evaluating the reliability of PMU in the following studies.

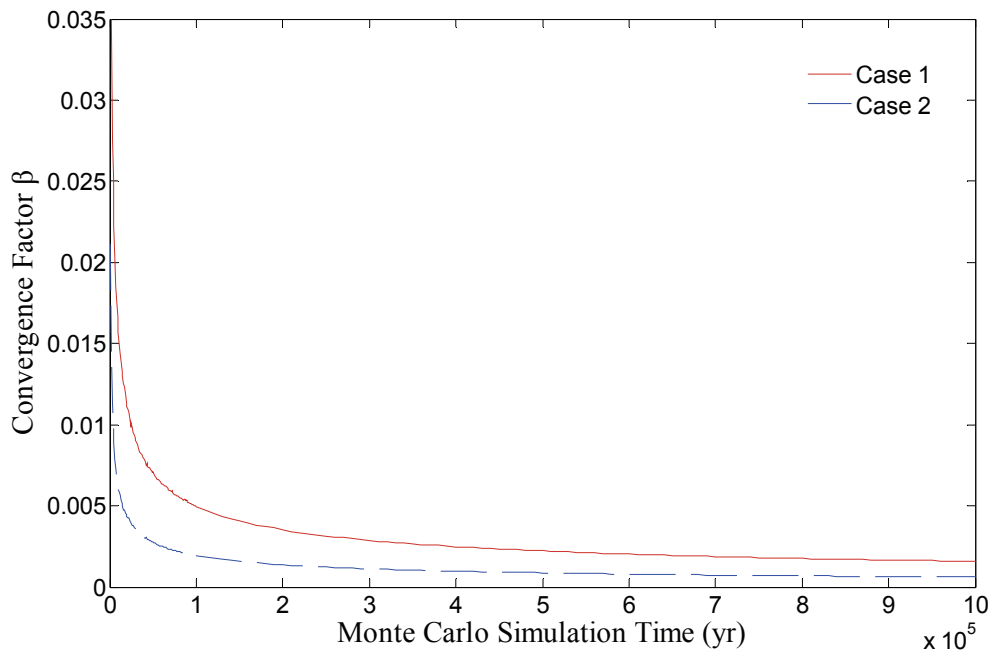


Fig. 4.24 Convergence factor β against Monte Carlo simulation time for both Case 1 and 2

4.4.3.2 RELIABILITY INDICES OF PMU

Table 4.2 lists the reliability indices evaluated with the proposed MCFT reliability evaluation method.

Table 4.2 Reliability indices of PMU and seven function modules in PMU

Module	Reliability indices			
	<i>A</i>	<i>U</i>	<i>MTBF</i> (yr)	<i>MTTR</i> (hr)
M1	1.0000	1.8639e-7	3.9418e3	6.4913
M2	1.0000	6.2536e-8	1.4926e4	8.0589
M3	1.0000	4.3698e-8	2.308e4	9.8283
M4	0.9989	1.0987e-3	2.8281	27.2812
M5	0.9992	7.8756e-4	3.2123	22.5309
M6	1.0000	8.2635e-13	4.1731e7	0.2594
M7	1.0000	2.8936e-7	4.7753e3	11.9803
PMU	0.9982	0.0018	1.4635	23.1168

It can be seen from Table 4.2 that:

- (1) Availability of PMU reaches 0.9982 which means PMU is unavailable about 15.8 hr/yr.
- (2) Among the seven function modules of PMU, availability of GPS module (M4) and CPU module (M5) have the highest impact on the availability of PMU, and availability of other modules is extremely high due to their redundancy design.

PMUs supplied by different manufacturers do have different reliability. The differences are mainly caused by the different reliability parameters of their basic components, especially the basic components in GPS module (M4) and CPU

module (M5). Here, two cases with different sets of reliability parameters of basic components in PMU are used to show how different the reliability indices could be in different makes of PMUs. In Case 1, reliability parameters of basic components in PMU are same as listed in Table 4.1. In Case 2, failure rate of components in GPS module (M4) and CPU module (M5) is five times larger while failure rate of components in other modules remains unchanged. The validity and advantage of proposed MCFT method are further checked in Table 4.3 with a comparison of the reliability indices of PMU for the above two cases acquired with Markov [161] and the proposed MCFT method.

Table 4.3 Comparison of reliability indices of PMU from different methods

Case	Reliability evaluation method	A_{PMU}	$MTBF_{PMU}$	$MTTR_{PMU}$
Case 1	Markov	0.9983	1.5230	22.2894
	MCFT	0.9982	1.4635	23.1168
Case 2	Markov	0.9932	0.4847	29.0693
	MCFT	0.9918	0.4429	32.0738

In both Case 1 and 2, there are differences between reliability indices of PMU acquired by the two methods. Those differences are mainly due to the fact that more accurate reliability model of PMU is constructed and multiple fault patterns rather than only single fault pattern were considered in the proposed MCFT method.

In Case 1, because of the low failure rate of PMU components, there are just only a few multiple fault patterns in all the failure patterns of PMU. The difference between availability of PMU acquired by the two methods is small, $\Delta A_{PMU} = 0.0001$, i.e. about 0.8 hr/yr for the unavailable time. This concludes that the results obtained with the proposed MCFT reliability evaluation method is

in-line with the benchmarking Markov method for PMU with low failure rate.

In Case 2, there are a significant number of multiple fault patterns in all the failure patterns of PMU because of the high failure rate of PMU components. The difference between availability of PMU acquired by the two methods is expectedly large, $\Delta A_{PMU} = 0.0014$, which means the difference between the unavailable time is up to 12.3 hr/yr. This indicates that the proposed MCFT method is superior as it could construct more accurate reliability model and deal with multiple fault patterns.

4.4.3.3 IMPORTANCE ANALYSIS

As a complex system, PMU consists of seven function modules which in turn composes of numerous basic components whose reliability degree have different impact on the reliability of PMU. In order to find out the most critical basic components which would have high impact on the reliability of PMU and its improvement, importance analysis of basic components in PMU should be conducted.

Importance analysis is first conducted on the seven function modules, and then importance analysis is conducted on the basic components in the function modules with high impact on the reliability of PMU. Table 4.4 and 4.5 summarize the results.

It can be seen from Table 4.4 that the value of basic cell importance of all function modules is 1 because of the series relationship between PMU and its seven function modules, and GPS (M4) and CPU modules (M5), which possess high basic cell module importance, have high impact on the reliability of PMU. The same conclusion has also been reached from the analysis of Table 4.2. GPS and CPU modules are the two function modules which will be analyzed further on their basic components.

Table 4.4 Importance analysis of function modules in PMU

Modules	Importance indices		Rank by	
	Basic cell importance W	Basic cell module importance W_N	W	W_N
PT/CT module	1	0.042%	1	3
Anti-aliasing filtering module	1	0.006%	1	6
A/D converting module	1	0.010%	1	5
GPS module	1	53.624%	1	1
CPU module	1	46.289%	1	2
Communication module	1	0%	1	7
Power source module	1	0.029%	1	4

Table 4.5 Importance analysis of basic components in GPS and CPU modules

Module	Component	Importance indices		Rank by	
		Basic cell importance W	Basic cell module importance W_N	W	W_N
GPS module	GPS receiver	42.2057%	50.757%	2	1
	Crystal oscillator	1	2.867%	1	4
CPU module	Software in CPU	1	9.998%	1	3
	Hardware in CPU	1	36.29%	1	2

Table 4.5 summaries the importance analysis conducted on the basic components in the GPS and CPU modules. When GPS receiver fails, GPS module

will enter backup clock operation mode and PMU will not fail immediately, so the basic cell importance of GPS receiver is just 42.2057% which is smaller than the basic cell importance of the other basic components in GPS and CPU modules. Due to the high failure rate, GPS receiver has the highest basic cell module importance, which indicates that GPS receiver has the highest impact on the reliability of PMU.

Once the basic components which have high impact on PMU reliability have been identified, two measures could be applied to improve the reliability of PMU [175]:

- (1) Increase the reliability of basic components with high impact on the reliability of PMU. This measure can be achieved through either reducing the failure rate or raising the repair rate of the basic components.
- (2) Adopt redundancy design of the basic components with high impact on the reliability of PMU. Though both measures can improve the reliability of PMU, their effectiveness and economy are different.

4.4.3.4 SENSITIVITY ANALYSIS

The effectiveness and economy of the first PMU reliability improvement measure mentioned in previous section can be assessed with the help of sensitivity analysis. The changes of availability of PMU with the change of failure rate or repair rate of the basic components in GPS and CPU modules are plotted in Fig. 4.25.

It can be seen that the availability of PMU will increase linearly with the decrease of the failure rate of basic components in GPS and CPU modules. However, the availability of PMU will not reach 1 even if the failure rate decreases to zero which is technically infeasible. Also, the availability of PMU will be saturated when the repair rate is higher than a certain value.

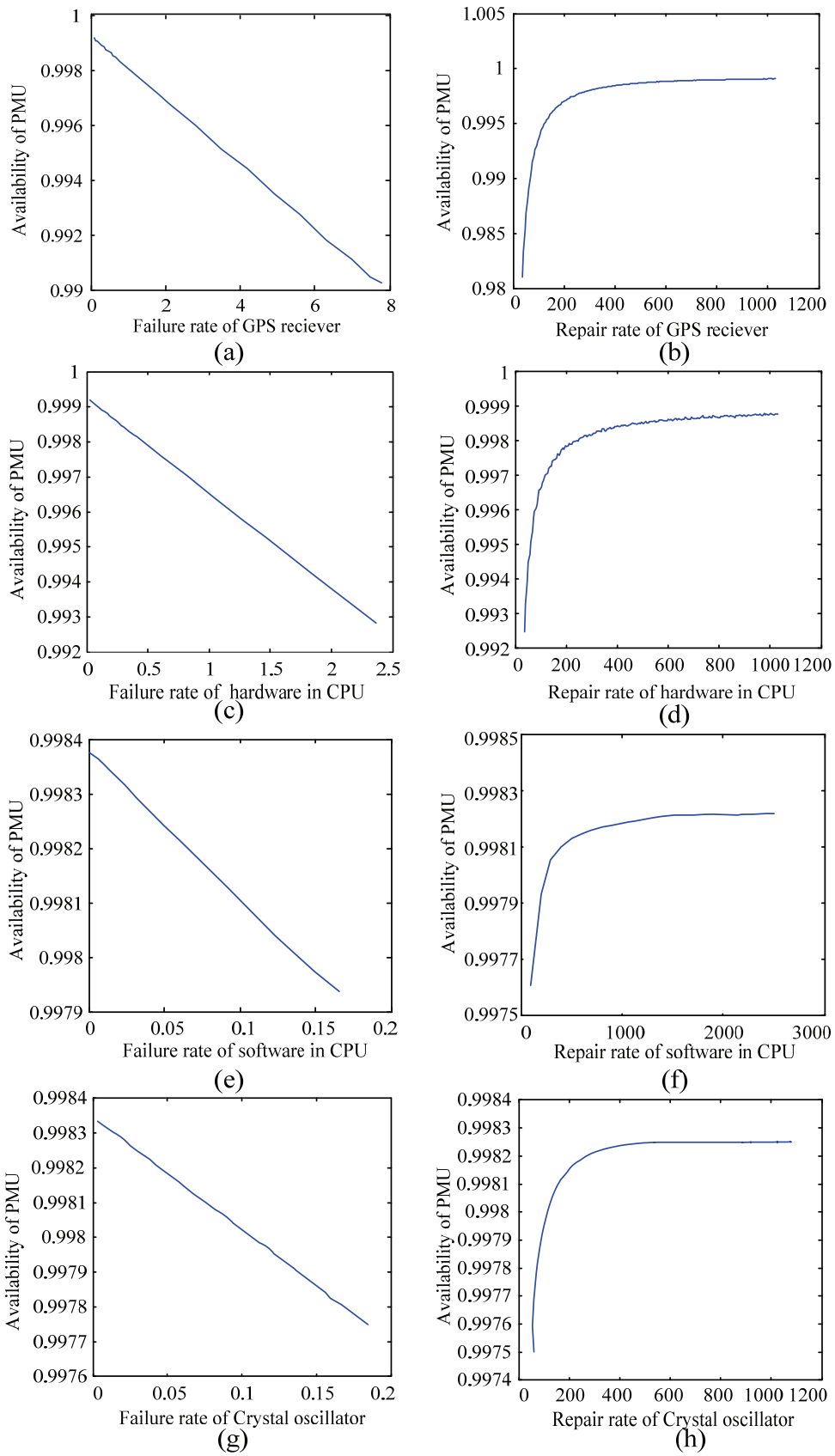


Fig. 4.25 Sensitivity analysis of the basic components in GPS and CPU modules

4.4.3.5 REDUNDANCY DESIGN ANALYSIS

Cold standby components were added to the GPS and CPU modules to test the effectiveness of the second PMU reliability improvement measure. The change of reliability of PMU with the redundancy design of basic components in GPS and CPU modules is shown in Table 4.6.

Table 4.6 Change of reliability indices of PMU with redundancy design of basic components in GPS and CPU modules

Cold standby component	$MTBF_{PMU}$	$MTTR_{PMU}$	A_{PMU}	ΔA_{PMU}
GPS receiver	2.8555	22.5332	0.9991	0.0009
CPU hardware	2.3196	22.3766	0.9989	0.0007
Crystal oscillator	1.5108	22.5372	0.9983	0.0001

Availability of PMU does improve significantly with redundancy added. The biggest improvement would be the redundancy design of GPS receiver which has the highest basic cell module importance.

Compared with the improvement shown in the sensitivity analysis done in previous section for the first PMU reliability improvement measure, the second measure with redundancy design on GPS receiver and CPU hardware is more practical and cost effective with larger PMU reliability improvement.

4.5 RELIABILITY EVALUATION OF PDC AND CONTROL CENTER

The main function of PDC is to first collect and resynchronize the phasor data from PMUs belong to the same PMUs-PDC working group as PDC, and then transmit the resynchronized data to the control center. Modern PDC can

accomplish many functions, such as real-time monitoring of power system state and manipulating and analyzing history data. In order to accomplish these functions which can only be accomplished in control center before, PDC needs to have similar structure as the control center. Reliability evaluation of PDC and control center is therefore very similar with that of PMU, and detailed reliability evaluation of PDC and control center will not be conducted in here again.

Fig. 4.26 shows the detailed PDC structure, in which, based on the function feature of PDC, PDC is divided into six function modules (M8~M13). M8 is power source module, M9 is Front End Processor (FEP) module which collects synchronized phasor data from different PMUs, M10 is Real Time Database (RTDB) module which handles the real-time data, M11 is History Database (HisDB) module which handles the history data, M12 is gateways module which transmits synchronized phasor data to control center and M13 is the workstation which coordinates the operation of all modules in PDC.

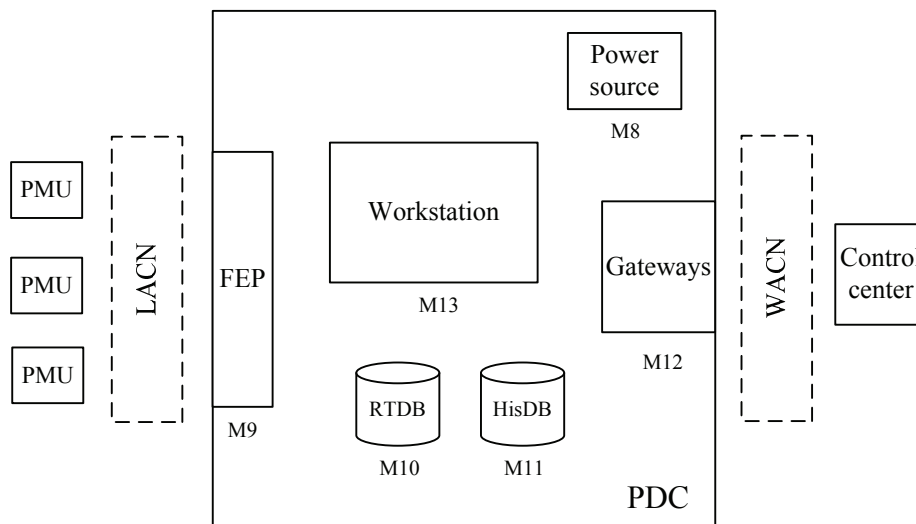


Fig. 4.26 Structure of a PDC

It can be seen from Fig. 4.26 that the structure of PDC has a striking similarity with that of PMU, and the proposed MCFT reliability evaluation method can be applied to evaluate the reliability of PDC and control center.

4.6 RELIABILITY EVALUATION OF COMMUNICATION NETWORK

For illustration, WAMS for the IEEE 14-bus test system shown in Fig. 4.27 would be used as an example to fully explore the proposed reliability evaluation method.

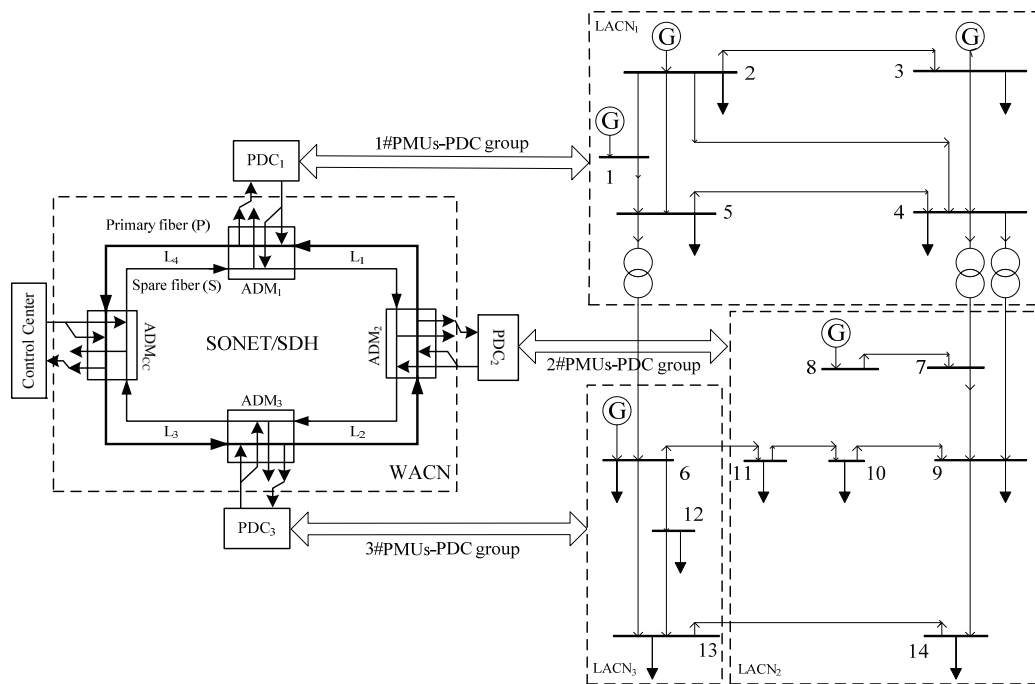


Fig. 4.27 WAMS for IEEE 14-bus test system

Speed, robustness and reliability are the basic requirements of communication networks in WAMS. Since Synchronous Optical Network / Synchronous Digital Hierarchy (SONET/SDH) possesses high speed data communication and high operation reliability, it has become commonly adopted as the main structure of communication networks in WAMS [176]. In most of the existing WAMS, the main structure of SONET/SDH communication network is a 2-fiber Unidirectional Self-Healing Ring Network (U-SHRN/2) [7,177] whose merits mainly lie in the low cost for network construction, less failure recovery time, and highly reliable 1+1 data communication protection.

Compared with conventional reliability evaluation methods [9,10,178,179], the proposed Monte Carlo fault tree (MCFT) reliability evaluation method for communication networks has following advantages:

- (1) Multiple fault patterns, instead of single fault pattern only, in the failure of communication networks are considered.
- (2) The reliability of both PMU measurements uploading from PMUs to control center and control instructions downloading from control center to PMUs is considered.
- (3) Additional reliability indices, especially the importance indices which are very useful for improving the reliability of communication networks, can be generated.

4.6.1 RELIABILITY MODELING OF WACN

The WACN for IEEE 14-bus test system as shown in Fig. 4.27 is in a 4-node U-SHRN/2 structure which contains four Add-Drop Multiplexers (ADM) dividing the WACN into four fiber sections L_1 - L_4 . In WACN, there are two optic fiber rings. One is the primary fiber ring (P) transmitting data in anti-clockwise direction and the other is the spare fiber ring (S) transmitting data in clockwise direction. Uploading PMU measurements from PMUs would be sent to both primary and spare fiber ring via the ADM. In normal operation, PMU measurements transmitted in the primary fiber ring would be selected as the working data uploading to the control center. In case of failure in the primary fiber ring, PMU measurements in the spare fiber ring would be selected as the working data through successful switching operation of ADM_{CC} . The downloading of control instructions has a similar operation mechanism as the uploading of PMU measurements. In the reliability evaluation of WAMS, not only the reliability of uploading PMU measurements but also the reliability of downloading control

instructions should be considered.

Before the FT reliability model of WACN can be constructed, a clear definition of a working WACN is firstly needed. When a WACN is in a working state, not only the control center can receive all the uploading PMU measurements but also PMUs could receive all the downloading control instructions from the control center via either the primary or spare fiber ring. The criteria of a working WACN can be summarized as follows:

- (1) All failures occur on the primary fiber ring and ADM could switch successfully.
- (2) All failures occur on the spare fiber ring.
- (3) When there are failures on both primary and spare fiber rings simultaneously in the same fiber section L_i and ADM can switch successfully, control center can still receive all the PMU measurements and PMUs can still receive the control instructions from control center due to the U-SHRN/2 structure of WACN. There are two kinds of simultaneous failures: one is caused by a common cause, which is referred as common cause failure and is the main failure pattern of communication networks with U-SHRN/2 structure, whilst the other is not.

With the above criteria, all the states of failure for different fault locations can be derived and constructed as sub-FTs which can then be combined to build the complete reliability model of WACN as shown in Fig. 4.28.

For the construction of FT reliability model of WACN, the following three types of failures are considered: (1) Primary Fiber Failure (PFF) - failure occurs on primary fiber section $L_i(P)$, (2) Spare Fiber Failure (SFF) - failure occurs on spare fiber section $L_i(S)$, and (3) Common Cause Fiber Failure (CCFF) - common cause failure occurs on fiber section $L_i(P\&S)$.

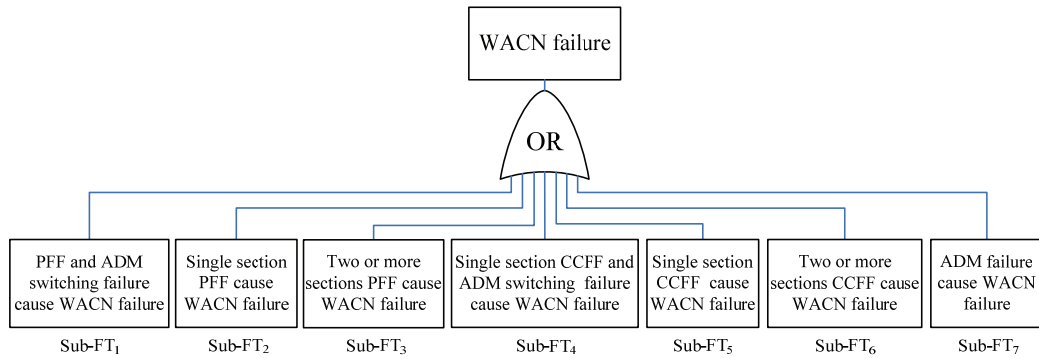


Fig. 4.28 FT reliability model of WACN

(1) Sub-FT₁

In Sub-FT₁ as shown in Fig. 4.29, the failure condition of WACN is that failures just occur on the primary fiber ring and ADM could not switch successfully.

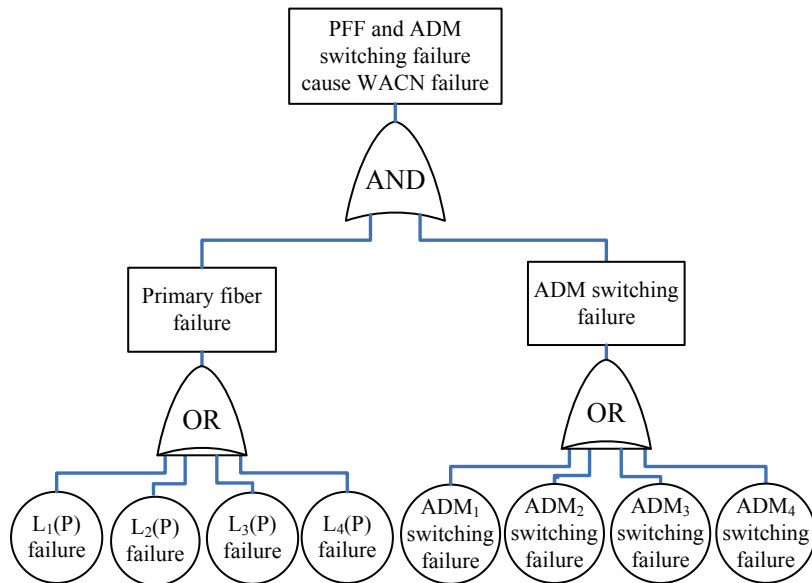


Fig. 4.29 Sub-FT₁ for WACN failure caused by PFF and ADM switching failure

In this failure condition, when primary fiber ring fails because of unsuccessful switching of ADM, either uploading PMU measurements or downloading control instructions in spare fiber ring cannot be selected as the working data.

(2) Sub-FT₂

In Sub-FT₂ as shown in Fig. 4.30, the failure condition of WACN is that failures occur on just one section of primary fiber and one or more sections of

spare fiber which are not on the same section where the primary fiber failure occurs.

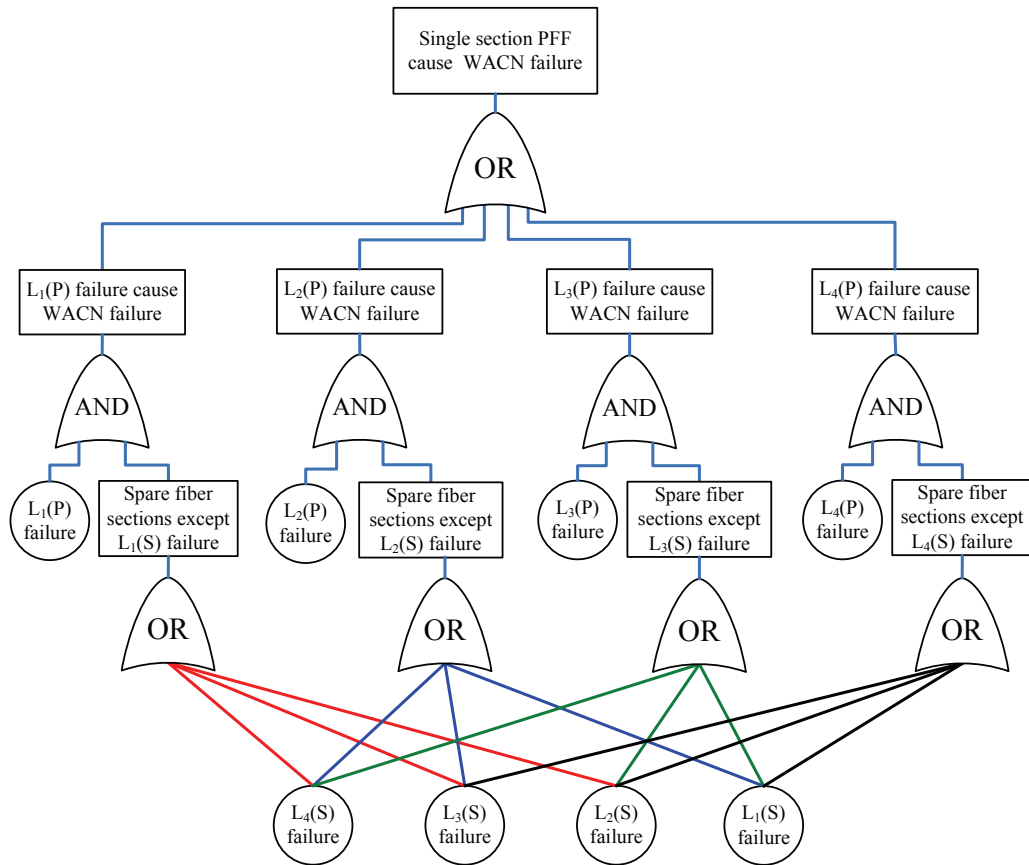


Fig. 4.30 Sub-FT₂ for WACN failure caused by single section PFF

Since there are failures in different sections and in both the primary and spare fiber ring, either the control center cannot receive the uploading PMU measurements from PMUs or PMUs cannot receive the downloading control instructions from the control center, or even both, no matter the switching of ADM is successful or not.

Failure conditions of WACN in Sub-FT₃ to Sub-FT₆ have the similar failure mechanism as Sub-FT₂.

(3) Sub-FT₃

In Sub-FT₃ as shown in Fig. 4.31, the failure condition is that failures occur on two or more sections of primary fiber and one or more sections of spare fiber.

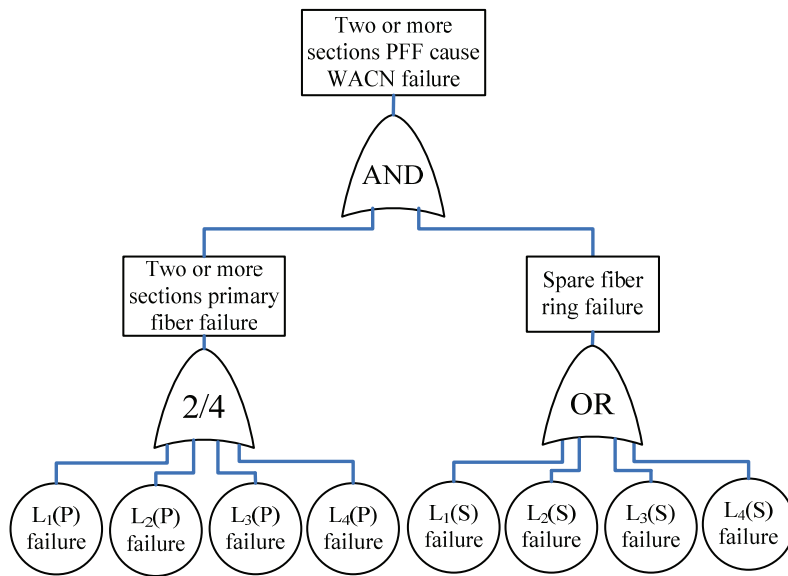


Fig. 4.31 Sub-FT₃ for WACN failure caused by two or more sections PFF

(4) Sub-FT₄

In Sub-FT₄ as shown in Fig. 4.32, the failure condition is that common cause failure occurs on one fiber section and ADM could not switch successfully.

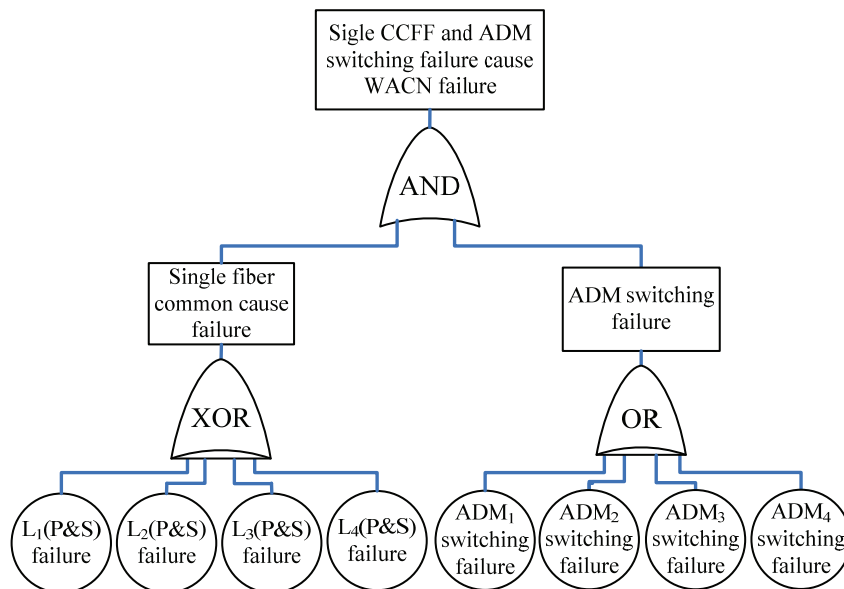


Fig. 4.32 Sub-FT₄ for WACN failure caused by single section CCFF and ADM switching failure

(5) Sub-FT₅

In Sub-FT₅ as shown in Fig. 4.33, the failure condition is that common cause

failures occur on one fiber section and failures occur on one or more sections of both primary fiber and spare fiber, which are not in the same section as the one with common cause failures.

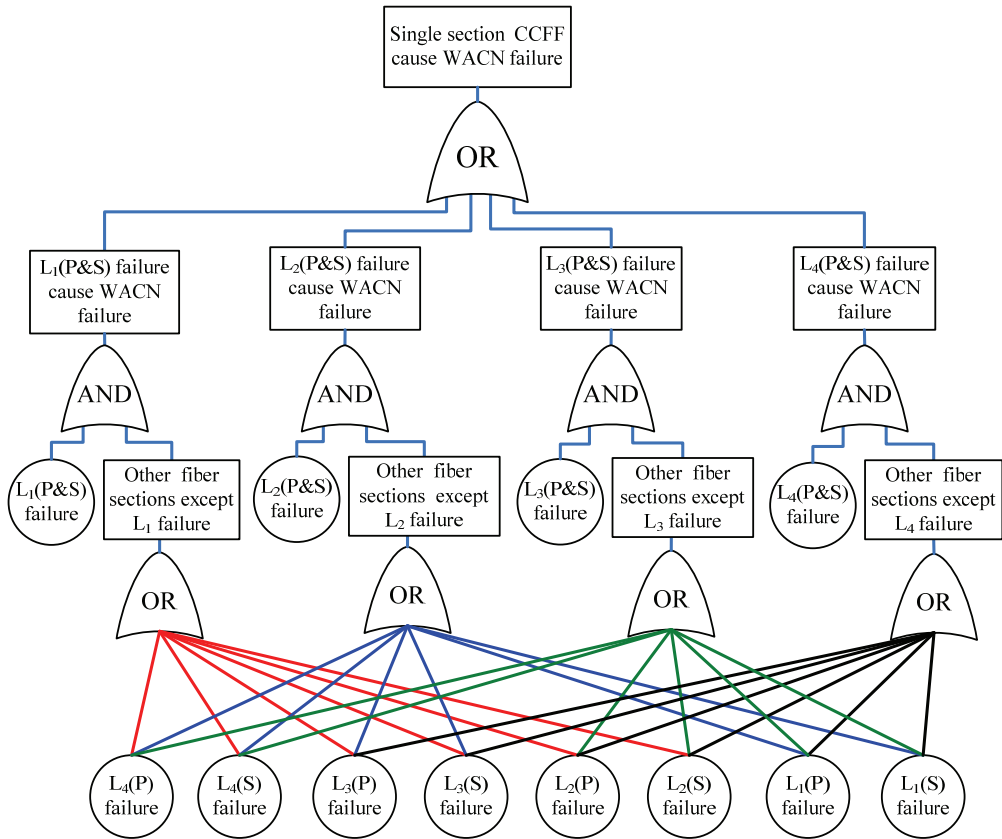


Fig. 4.33 Sub-FT₅ for WACN failure caused by single section CCF

(6) Sub-FT₆

In Sub-FT₆ as shown in Fig. 4.34, the failure condition is that common cause failures happen on two or more sections of fiber.

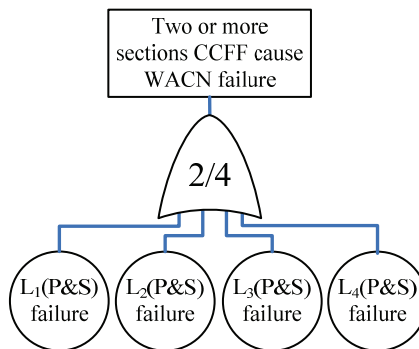


Fig. 4.34 Sub-FT₆ for WACN failure caused by two or more sections CCF

(7) Sub-FT₇

In Sub-FT₇ as shown in Fig. 4.35, the failure condition of WACN is that failures occur on one or more ADMs. In this failure condition, due to the failure of ADMs, PMUs-PDC groups linking with WACN through the faulty ADMs cannot exchange information with the control center.

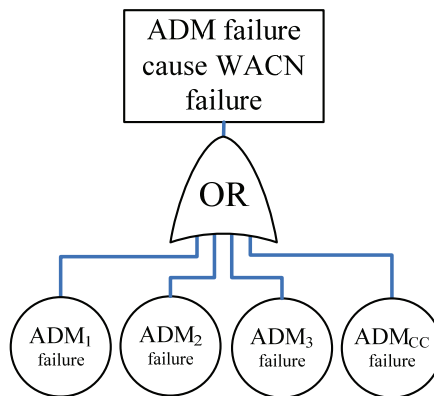


Fig. 4.35 Sub-FT₇ for WACN failure caused by ADM failure

In sub-FT₇, failure condition of WACN is that failures happen on one or more ADMs. In this failure condition, because of the failure of ADMs, PMUs-PDC groups linking with WACN through the fault ADMs cannot exchange information with control center.

By combining Sub-FT₁ to Sub-FT₇, which depicts all the failure states of WACN, the complete FT reliability model of WACN can be constructed as shown in Fig. 4.28.

4.6.2 RELIABILITY MODELING OF LACN

Often power grids are distributed and geographically dispersed in large-scale. Many LACNs are therefore needed to transmit dispersed PMUs data to respective PDC. In [10], carrier wave and microwave communication channel was used to construct the LACN. However, because of the limitations of such communication channel mediums in reliability, scalability and robustness, most often this kind of

LACN cannot fully satisfy the requirements of WAMS based stability analysis and control schemes for the real-time wide-area information [179]. LACN could be in star or ring structure. The reliability of LACN with star structure is low and can be evaluated easily. In the near future, following the increasing requirement for the reliability, LACN with star structure will be replaced by LACN with ring structure whose reliability is very high. Therefore, in this chapter, in order to guarantee the real-time and reliability of data transmission, in modern WAMS, similar to WACN, U-SHRN/2 structure is also utilized to construct the LACN.

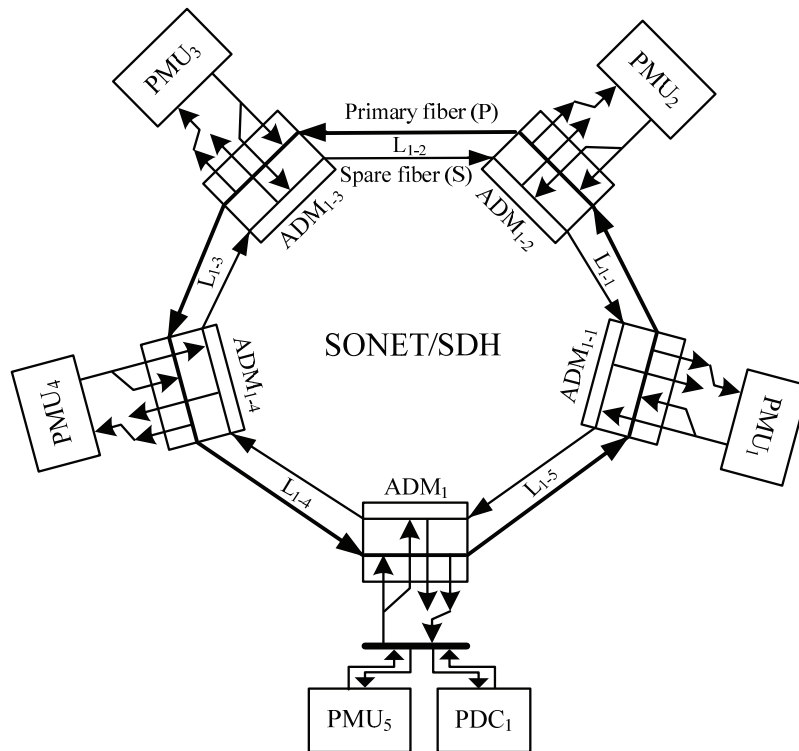


Fig. 4.36 5-node U-SHRN/2 structure of LACN₁

Based on the voltage level and geographical location, WAMS for IEEE 14-bus test system is divided into 3 subsystems and each forms a PMUs-PDC group. Since 1#PMUs-PDC group contains 5 PMUs and one PDC, a 5-node U-SHRN/2 is used to construct LACN₁. 2#PMUs-PDC group contains 6 PMUs and one PDC, a 7-node U-SHRN/2 is therefore used to construct LACN₂. 3#PMUs-PDC group

contains 3 PMUs and one PDC, so a 3-node U-SHRN/2 is used to construct LACN₃. Structure of LACN₁, LACN₂ and LACN₃ is shown in Fig. 4.36, 4.37 and 4.38, respectively.

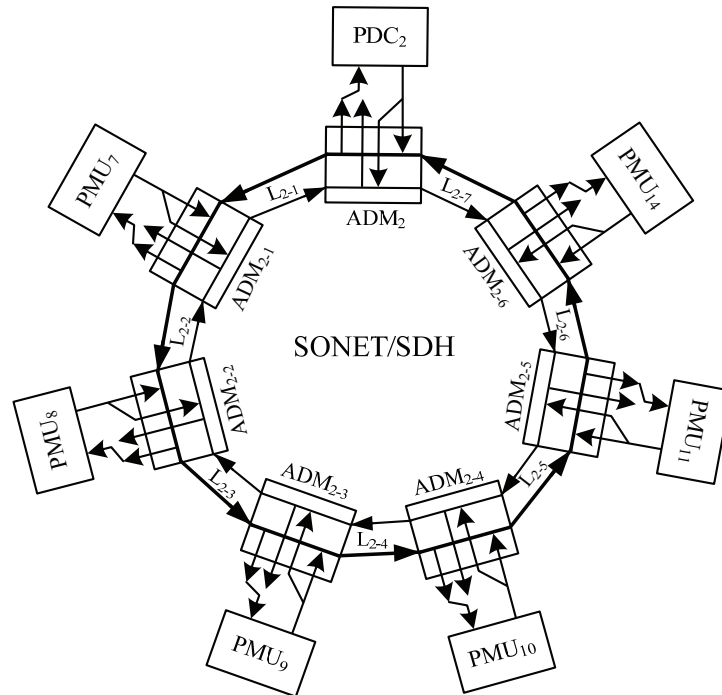


Fig. 4.37 7-node U-SHRN/2 structure of LACN₂

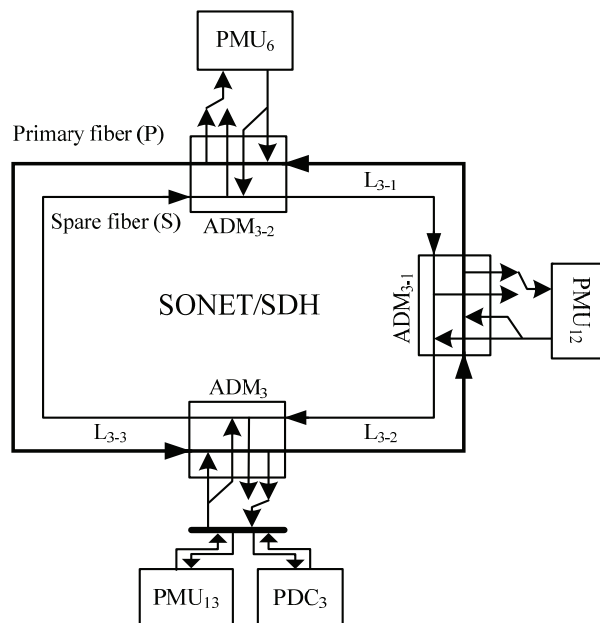


Fig. 4.38 3-node U-SHRN/2 structure of LACN₃

Since LACN has a similar structure as WACN, the approach previously described for WACN can be applied again to construct the reliability model of LACN.

4.6.3 RELIABILITY INDICES OF COMMUNICATION NETWORKS

4.6.3.1 RELIABILITY INDICES OF WACN

The scale of WAMS and its communication networks do vary with the size of power grid. In order to better evaluate the reliability of different sized WACN, two cases for the IEEE 14-bus test system were prepared as listed in Table 4.7. Whilst Case 1 represents a small scale WACN detailed in [174], Case 2 represents a large WACN based on Case 1 and scaled with a large fiber network. Units of λ and μ are failures/year and repairs/year respectively. The unsuccessful switching probability of ADM q_s is set to 0.75%.

Table 4.7 Reliability parameters of two different-scaled WACN

Case	Fiber section	L ₁	L ₂	L ₃	L ₄
	Parameters				
Case 1	Length (km)	180	90	120	150
	λ_{L_i} (P) or λ_{L_i} (S)	0.5256	0.2628	0.3504	0.4380
	μ_{L_i} (P) or μ_{L_i} (S)	146	262	197	155
	λ_{L_i} (P&S)	2.6280	1.314	1.752	2.19
	μ_{L_i} (P&S)	109.5	207	155	146
Case 2	Length (km)	1080	540	720	900
	λ_{L_i} (P) or λ_{L_i} (S)	3.1536	1.5768	2.1024	2.628
	μ_{L_i} (P) or μ_{L_i} (S)	127	218	153	136
	λ_{L_i} (P&S)	15.768	7.884	10.512	13.14
	μ_{L_i} (P&S)	88.6	168	127	113

For the given sets of reliability parameters for Case 1 and 2, the proposed MCFT reliability evaluation method was applied to evaluate the reliability indices of WACN. In order to examine the convergence of the Monte Carlo simulations, the convergence factor β in Case 1 and 2 is plotted against simulation time in Fig. 4.39.

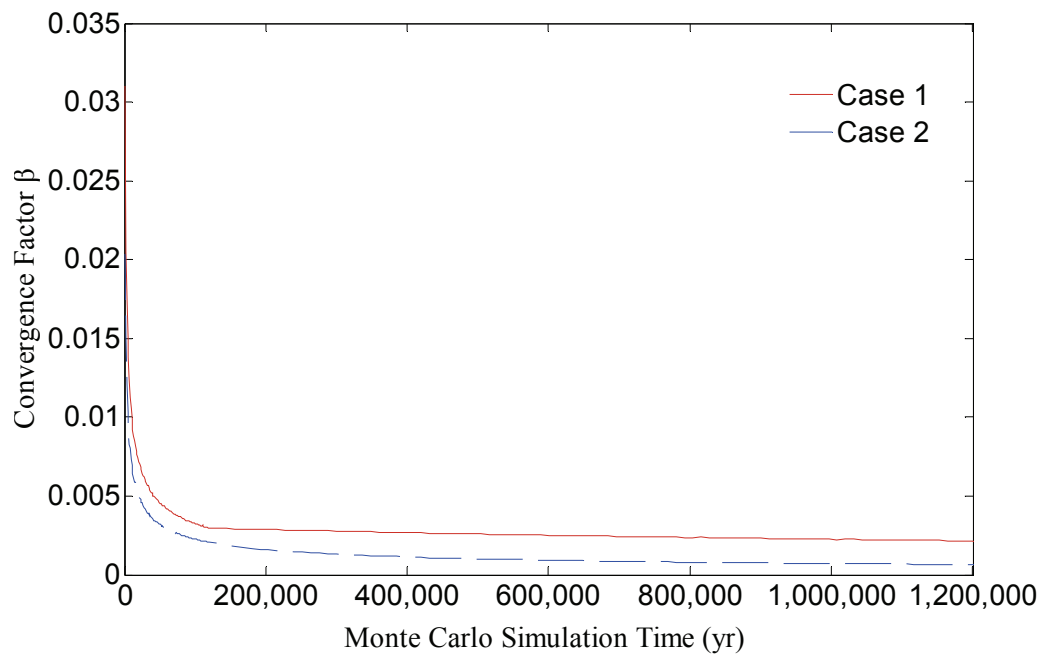


Fig. 4.39 Convergence factor β against simulation time for Case 1 and 2

It is clear that in both Case 1 and 2 the convergence factor β remains virtually unchanged when the simulation time is over 200,000 years. For the following studies, the corresponding convergence factors 0.29% for Case 1 and 0.16% for Case 2 are therefore selected as the termination condition for Monte Carlo simulations so as to ensure the accuracy of the reliability indices in evaluating the reliability of WACN.

Table 4.8 lists the reliability indices of WACN obtained for Case 1 and 2 together with the ones obtained with the Markov-Enumeration method. In both Case 1 and 2, differences do exist between the results obtained with the proposed MCFT and the benchmarking Markov-Enumeration methods. The differences are

mainly due to the fact that only single fault pattern rather than multi-fault patterns is considered in Markov-Enumeration method in order to reduce the state space. Furthermore, in Markov-Enumeration method, only the reliability of PMU measurements uploading from PMUs to control center is considered while the reliability of control instructions downloading from control center to PMUs is ignored.

Table 4.8 Comparison of reliability indices of WACN for different reliability evaluation methods

Case	Indices		A_{WACN}	U_{WACN}	$MTBF_{WACN}$ (yr)	$MTTR_{WACN}$ (hr)
	Methods					
1	Markov-Enumeration		0.9978	0.0022	1.1489	21.7473
	MCFT		0.9976	0.0024	1.1220	23.6448
2	Markov-Enumeration		0.9396	0.0604	0.0458	25.7819
	MCFT		0.9239	0.0761	0.0503	36.2684

In Case 1, the availability of WACN obtained with the proposed MCFT method is $A_{WACN} = 0.9976$. This means that WACN is unavailable for about 21 hr/yr. Since the scale of WACN is small with low failure rate, there are just only a few multiple fault patterns in all the failure patterns of WACN. The difference between the availability of WACN obtained with both methods is small, $\Delta A_{WACN} = 0.0002$, i.e. about 1.7 hr/yr for the unavailable time. Furthermore, the difference between MTBF and MTTR of WACN obtained with both methods is also small. This concludes that the results obtained with the proposed MCFT reliability evaluation method is in-line with the benchmarking Markov-Enumeration method for small scale WACN with low failure rate.

In Case 2, the parameter set represents a large-scale WACN with high failure rate, there are significant number of multiple fault patterns in all the failure

patterns of WACN. The difference between availability of WACN obtained with the proposed MCFT and the Markov-Enumeration methods is expected to be large, $\Delta A_{\text{WACN}} = 0.0157$ which means the difference between the unavailable time is up to 137.5 hr/yr. Furthermore, there is also a distinct difference between MTBF and MTTR of WACN obtained with both methods. This indicates that the proposed MCFT method is superior as it could deal with multiple fault pattern as well as the different reliabilities in uploading PMU measurements to the control center and downloading control instructions to PMU.

4.6.3.2 IMPORTANCE ANALYSIS OF FIBER SECTIONS IN WACN

In order to identify the most critical fiber section which would have high impact on the reliability and its improvement of WACN, importance analysis of fiber sections in WACN is conducted with results tabulated in Table 4.9.

Table 4.9 Importance analysis of fiber sections in WACN

Fiber section \ Importance	Basic cell importance W (%)				Basic cell module importance W_N (%)			
	L ₁	L ₂	L ₃	L ₄	L ₁	L ₂	L ₃	L ₄
L _i (P&S)	6.58	4.12	5.16	5.67	45.27	27.98	35.41	39.19
L _i (P)	1.53	0.77	1.06	1.35	10.39	5.39	7.25	9.41
L _i (S)	1.26	0.64	0.89	1.15	8.72	4.53	6.12	7.88
Rank	4	3	1	2	4	3	1	2

It can be seen from Table 4.9 that:

- (1) Because of the higher failure rate, common cause fiber has higher importance than primary and spare fiber in the same fiber section;
- (2) Primary fiber sections have higher importance than spare fiber sections because, in normal condition, primary fiber ring is in working states

while spare fiber ring is in cold standby condition;

- (3) The importance ranking indicates that longer fiber section has higher importance.

Hence, one measure to improve the reliability of WACN is to decrease the failure rate of common cause failure which is the main failure pattern of fiber section while the other measure is to avoid long fiber section as much as it could.

4.6.3.3 RELIABILITY INDICES OF LACN

Table 4.10 Reliability parameters of LACN₁

Parameters Fiber section	$\lambda_{LACN_{1-i}}$ (P or S)	$\mu_{LACN_{1-i}}$ (P or S)	$\lambda_{LACN_{1-i}}$ (P & S)	$\mu_{LACN_{1-i}}$ (P & S)
LACN ₁₋₁ (80km)	0.2336	295	1.168	232.5
LACN ₁₋₂ (100km)	0.2920	236	1.460	186
LACN ₁₋₃ (120km)	0.3504	197	1.7520	155
LACN ₁₋₄ (90km)	0.2628	262	1.314	207
LACN ₁₋₅ (100km)	0.2920	236	1.460	186

Table 4.11 Reliability parameters of LACN₂

Parameters Fiber section	$\lambda_{LACN_{2-i}}$ (P or S)	$\mu_{LACN_{2-i}}$ (P or S)	$\lambda_{LACN_{2-i}}$ (P & S)	$\mu_{LACN_{2-i}}$ (P & S)
LACN ₂₋₁ (9km)	0.2628	262	1.314	207
LACN ₂₋₂ (80km)	0.2336	295	1.168	232.5
LACN ₂₋₃ (100km)	0.2920	236	1.460	186
LACN ₂₋₄ (70km)	0.2044	337	1.022	266
LACN ₂₋₅ (80km)	0.2336	295	1.168	232.5
LACN ₂₋₆ (90km)	0.2628	262	1.314	207
LACN ₂₋₇ (120km)	0.3504	197	1.7520	155

Table 4.12 Reliability parameters of LACN₃

Parameters Fiber section	$\lambda_{LACN_{3-i}}$ (P or S)	$\mu_{LACN_{3-i}}$ (P or S)	$\lambda_{LACN_{3-i}}$ (P & S)	$\mu_{LACN_{3-i}}$ (P & S)
LACN ₃₋₁ (70km)	0.2044	337	1.022	266
LACN ₃₋₂ (90km)	0.2628	262	1.314	207
LACN ₃₋₃ (80km)	0.2336	295	1.168	232.5

Because LACNs (LACN₁, LACN₂ and LACN₃) for IEEE 14-bus test system do have similar structure as WACN, the MCFT reliability evaluation method proposed for WACN could also be applied to evaluate the reliability of LACNs.

The reliability parameters of LACN₁, LACN₂ and LACN₃ for IEEE 14-bus test system are respectively listed in Table 4.10, 4.11 and 4.12.

The corresponding reliability indices of them are detailed in Table 4.13.

Table 4.13 Reliability indices of LACNs for IEEE 14-bus test system

Reliability indices LACN	A_{LACN}	U_{LACN}	$MTBF_{WACN}$ (yr)	$MTTR_{WACN}$ (hr)
LACN ₁	0.9990	0.0010	3.1959	28.0242
LACN ₂	0.9982	0.0018	2.4649	38.9362
LACN ₃	0.9994	0.0006	4.3085	22.6590

It can be seen from Table 4.8 and 4.13 that communication networks, including WACN and LACNs, do have high availability which is close to 1. Therefore, the designed structures of communication networks have sufficient reliability for IEEE 14-bus test system in which the reliability and number of PMUs would play an important rule.

4.7 RELIABILITY EVALUATION OF WAMS

For the reliability evaluation of WAMS for IEEE 14-bus test system, it is assumed that all the PMUs are uniform and the availability of each PMU is 0.9982 which is calculated in section 4.4 while the availability of WACN in Case 1, 2 and LACNs is determined as described in section 4.6. WACN in Case 1 is taken as an illustration example in this section. From Equation (4.15) and (4.16), the availability of WAMS for IEEE 14-bus test system can be calculated with the following availabilities.

$$A_{\text{PMUs-PDC}_1} = \left(\prod_{j=1}^5 A_{\text{PMU}_{1j}} \right) \cdot A_{\text{LACN}_1} \cdot A_{\text{PDC}_1} = 0.9905 \quad (4.18)$$

$$A_{\text{PMUs-PDC}_2} = \left(\prod_{j=1}^6 A_{\text{PMU}_{2j}} \right) \cdot A_{\text{LACN}_2} \cdot A_{\text{PDC}_2} = 0.9881 \quad (4.19)$$

$$A_{\text{PMUs-PDC}_3} = \left(\prod_{j=1}^3 A_{\text{PMU}_{3j}} \right) \cdot A_{\text{LACN}_3} \cdot A_{\text{PDC}_3} = 0.9943 \quad (4.20)$$

$$A_{\text{WAMS}} = \left(\prod_{i=1}^3 A_i^{\text{PMUs-PDC}} \right) \cdot A_{\text{WACN}} \cdot A_{\text{Control-Center}} = 0.9708 \quad (4.21)$$

Though the reliability of each individual component in the WAMS for the IEEE 14-bus test system is high enough, the availability of the overall WAMS is quite low, $A_{\text{WAMS}} = 0.9708$. This means WAMS will be unavailable for about 255.8 hr/yr mainly because of the large number of PMUs. Therefore, the reliability of PMU is the key to the success application of WAMS, especially for those WAMS based stability analysis and control scheme where PMU measurements at all buses are required.

On the other hand, for many WAMS based stability analysis and control schemes, only partial WAMS information is required. Suppose that a wide-area differential relay is installed on transmission line bus13-bus14. In this wide-area protection scheme, only PMU measurements in bus 13 and bus 14 are required.

Reliability of WAMS for this wide-area differential relay scheme can be calculated as follows:

$$A_{\text{PMUs-PDC}_2} = A_{\text{PMU}_{14}} \cdot A_{\text{LACN}_2} \cdot A_{\text{PDC}_2} = 0.9965 \quad (4.22)$$

$$A_{\text{PMUs-PDC}_3} = A_{\text{PMU}_{13}} \cdot A_{\text{LACN}_3} \cdot A_{\text{PDC}_3} = 0.9977 \quad (4.23)$$

$$A_{\text{WAMS}} = \left(\prod_{i=2}^3 A_i^{\text{PMUs-PDC}} \right) \cdot A_{\text{WACN}} \cdot A_{\text{Control-Center}} = 0.9919 \quad (4.24)$$

Therefore, the reliability of WAMS for these WAMS based stability analysis and control schemes requiring only partial WAMS information is much higher than those requiring global WAMS information. Though different schemes would require different WAMS information and have different degree of reliability, the following measures should be taken to improve the reliability of WAMS.

- (1) The amount of WAMS information being used in any WAMS based stability analysis and control schemes shall be minimized.
- (2) For those buses whose electrical quantities are required by most of the WAMS based stability analysis and control schemes, backup PMU should be installed to increase the availability.
- (3) Among all the improvement measures, the most important and fundamental is to improve the reliability of PMUs and communication networks, WACN and LACNs.

4.8 APPLICATIONS OF WAMS RELIABILITY IN POWER SYSTEM STABILITY ANALYSIS AND CONTROL

Reliability of PMU must be considered in any WAMS based stability analysis and control schemes whose reliability needs to be guaranteed prior to live operation. Here, an adaptive wide-area damping control scheme proposed in [180] is taken as an example to demonstrate how the availability of PMU is utilized.

For simplicity it is assumed that this damping control scheme operates on an

IEEE 14-bus test system (seen as Fig. 4.27), the input signals are the five generator rotor speeds measured by five PMUs. Through the corresponding communication networks including LACN and WACN, generator rotor speeds are transmitted to PDC and control center where this damping control scheme is operated.

Reliability of PMU and communication networks including LACN and WACN has been evaluated in the previous sections. The PDC and control center generally have very high reliability and their availabilities (A_{PDC} and $A_{Control-Center}$) are assumed to be 1.0 in this example [10]. From the perspective of reliability, these devices are in series and the availability of this damping control scheme can be calculated by the product of their availability [159]. Assuming all the PMUs are uniform, the availability of WAMS for this damping control schemes in IEEE 14-bus test system can be calculated as follows:

$$A_{WAMS} = \left(\prod_{j=1}^5 A_{PMU_j} \right) \cdot \left(\prod_{j=1}^3 A_{LACN_j} \right) \cdot \left(\prod_{j=1}^3 A_{PDC_j} \right) \cdot A_{WACN} \cdot A_{Control-Center} \quad (4.25)$$

$$= 0.9858$$

In other words, this adaptive wide-area damping control scheme in IEEE 14-bus test system will be unavailable for about 124.4 hr/yr and therefore would not be sufficiently reliable for practical use. However, it should be noted that the availability was calculated with the reliability parameters of the WAMS basic components collected or derived from published papers which are not necessary realistic enough for practical assessment of the availability of WAMS. Furthermore, the availability could be improved by optimizing the structure of the WAMS such that the number of PMUs involved in the control scheme could be reduced for example.

4.9 SUMMARY

In this chapter, a comprehensive reliability evaluation method based on Monte Carlo Fault Tree Analysis is proposed for WAMS. Fault tree modeling method is

first used to construct an accurate reliability model of WAMS, in which multiple fault patterns rather than single fault pattern are considered and both the reliability of PMUs measurements uploading to control center and control instructions downloading to PMUs are considered. Monte Carlo simulation approach is then used to evaluate the reliability indices of WAMS as well as some importance indices which cannot be easily obtained otherwise and are essential in identifying the critical links in WAMS.

WAMS is composed of PMUs, PDC, communication networks including LACN and WACN, and control center. In this chapter, the reliability of all of these components of WAMS is evaluated by employing the proposed MCFT reliability evaluation method.

Comparison studies with the Markov-Enumeration method showed that the proposed reliability evaluation method is superior, in terms of both correctness and functionality, in particular for large-scale WAMS with high failure rate. This paper also provides a general guideline to improve the reliability of WAMS for online stability analysis and control. A simple example based on an adaptive wide-area damping control scheme has also been given to show the application of the proposed WAMS reliability evaluation method.

CHAPTER V A QUANTITATIVE AND COMPREHENSIVE INVESTIGATION OF WAMS ARCHITECTURE

5.1 INTRODUCTION

Power industries around the world are experiencing a profound deregulation aiming to provide electricity customers with better services at a cheaper cost [181]. A large number of small and geographically dispersed power generation units (e.g., wind turbines, solar cells, plug-in electric cars) are gradually replacing large centralized power plants. The operation and control of power system is becoming more complex because of the distributed nature, multiple interactions and uncertainties. Accordingly, the control strategy of power system shall also be changed from the traditional centralized control to distributed control. Generally, the structure of the control strategies is determined by the location of data resources, control center and the controllable devices [181, 182].

As an information infrastructure with monitoring, control, and protection functions in modern transmission grid, WAMS has become an important system component to carry the centralized and distributed control strategies of power system and guarantee the security and stability of power systems [10]. WAMS is responsible for the synchronized phasors acquisition and data (including synchronized phasors and control instructions) exchange among PMUs, control centers and controllable devices. As a carrier of the control strategy, WAMS would have the same structure as the control strategy. The communication network (CN) is a bottleneck in the architecture of centralized and distributed WAMS since the quality of data from PMU is highly dependent on the architecture of CN [183]. The design of a high-performance CN with a better architecture is crucial to the performance of WAMS [184, 185].

CNs with different architecture possess different characteristics including investment, signal time delay, reliability and risk items; and among them, reliability and risk are used to assess the security level of CN. Different from the traditional reliability-based security assessment, risk-based security assessment would consider the likelihood and severity of CN incident and quantify the risk indicator [186]. Risk assessment is a key function that shall be performed in advance of the design of CN [187].

Research on CN architecture and the corresponding four characteristics items have been conducted for some time [176, 187-190]. While most of the work focused on the design of CN with high-performance in one or two characteristic items to satisfy the requirement of a specific application, a quantitative and comprehensive investigation of CN considering all of the characteristic items is still lacking. In [191], a comparison between communication infrastructures of centralized and distributed WAMS is conducted with latency, reliability and cost as the criteria represented as function of number of routers and length of media. Furthermore, the risk evaluation which is an essential function to the design of CN is missing.

In this chapter, the investment, signal time delay, reliability and risk for centralized and distributed CNs are quantitatively calculated and taken as the comparison criteria to comprehensively investigate which CN architecture has a better performance in monitoring and control of power grid. Monte Carlo dynamic fault tree reliability evaluation method proposed in Chapter IV is used to evaluate the reliability of CN with complex but practically used SDH ring structure. In this chapter, for the first time, a hybrid multiple criteria decision-making (MCDM) approach combined with analytic hierarchy progress (AHP) and risk ranking technology is proposed to quantitatively evaluate the risk of CN incident to the power grid.

In the simulation case, a practical WAMS in Shandong Power Grid is taken as a platform to demonstrate the comparison scheme proposed in this chapter. Given the particularity of the investment for CN, an improved Minimum Spanning Tree (MST) algorithm is proposed to construct the optimal centralized and distributed CN with minimum investment in WAMS of Shandong Power Grid.

This chapter is organized as follows. Section 5.2 defines the centralized and distributed WAMS. The comparison criteria of CNs with different architecture are presented in detail in Section 5.3. In Section 5.4, an improved MST algorithm is proposed to construct the optimal CN with minimum investment. WAMS in Shandong Power Grid is taken as a platform to illuminate the proposed CN performance comparison in Section 5.5. Finally, a conclusion is reached in Section 5.6.

5.2 WAMS ARCHITECTURE

A typical WAMS includes three basic components: 1) PMUs which are used to measure the synchronized phasors of voltage or current; 2) PDC which acts as the central center (CC) to collect and process the PMU data; 3) Communication network which is responsible for the information exchange between PMUs or controllable devices and PDC.

Corresponding to the control strategies adopted by the power system operators, WAMS mainly has two architectures: centralized and distributed which are distinguished by the data flow among the locations of PMUs, control center and controllable devices.

5.2.1 CENTRALIZED WAMS

The architecture and data flow of centralized WAMS is shown in Fig. 5.1

[182] in which remote nodes consist of PMUs and controllable devices.

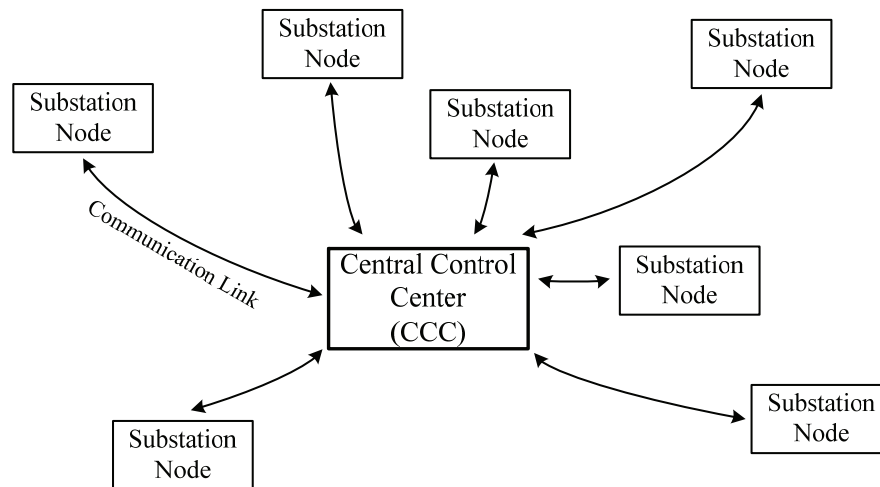


Fig. 5.1 Architecture and data flow of centralized WAMS

In centralized WAMS, a Central Control Center (CCC) is responsible for the monitoring and control of the entire power grid. All synchronized phasors measured by PMUs are routed up to CCC through high speed CN. The CCC processes all of these synchronized phasors to decide if control actions are required and generates those control instructions. Then, these control instructions from CCC are routed down to the controllable devices installed in the remote nodes.

5.2.2 DISTRIBUTED WAMS

The architecture and data flow of distributed WAMS is shown in Fig. 5.2 [182, 191]. In distributed WAMS, power grid is divided into several control areas. In each control area, an Area Control Center (ACC) is responsible for the monitoring and control of the regional system. In each control area, PMUs send synchronized phasors to their ACC, and ACC processes these synchronized phasors just as what the CCC in centralized WAMS does. In order to control the entire power grid, ACCs share their data with each other through CN in WAMS.

Usually, one of the ACCs should be selected as CCC to communicate with the other ACCs to monitor and control the entire power grid.

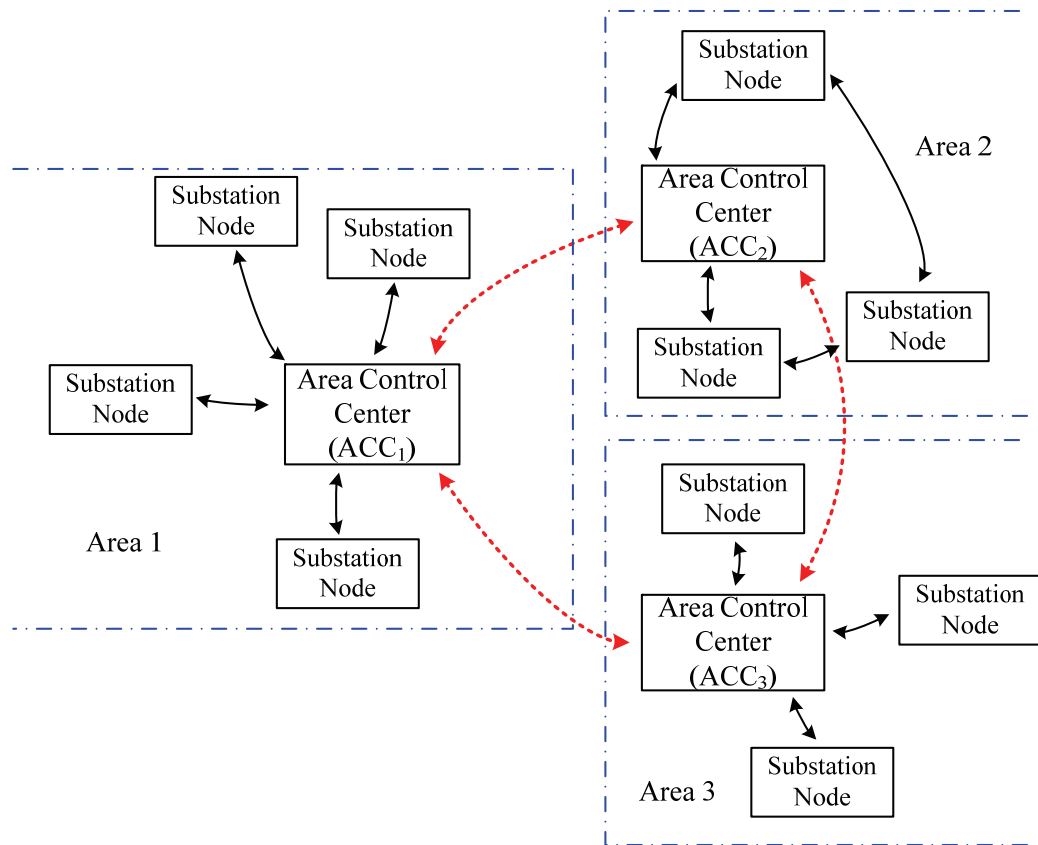


Fig. 5.2 Architecture and data flow of distributed WAMS

As it can be seen from Fig. 5.1 and 5.2, the main difference between centralized and distributed control strategies lies in the location of the control centers including CCC and ACCs, and because of this difference, communication networks with different structures would be constructed to meet the different information exchange requirements with different economy, security, reliability and control performance. Furthermore, since the existing regional dispatching and communication centers in the location of CCC and ACCs can be served as the CCC and ACCs, the investment for CCC and ACCs is not considered in the following calculation of the investment for communication network .

5.2.3 COMMUNICATION NETWORK

The CN is an important component in the architecture of a WAMS. This is because in WAMS, a high-performance CN is needed to connect PMUs geographically distributed in the entire power grid with the CCC or several ACCs. The CN is a bottleneck in the architecture of WAMS since the quality of PMU data is highly dependent on the architecture of CN. As a result, great attention shall be paid to the architecture of CN which is related with the architecture of WAMS.

Considering the real-time performance and reliability of WAMS, IP over synchronous digital hierarchy (SDH) in optical fiber networks with multi-protocol label switching (MPLS) is becoming the mainstream for communication network [188]. For a high-performance CN, economy, speed, reliability and security are the basic requirements which would be seriously influenced by the transmission media and architecture of CN. These basic requirements for CN manifest in the investment for CN, signal time delay introduced by CN, reliability of CN, and risk to the power grid caused by CN incident. Thus, in this chapter, the investment, signal time delay, reliability and risk for centralized and distributed CNs are quantitatively calculated and taken as the comparison criteria to comprehensively investigate which CN architecture has the better performance in the monitoring and control of power grid.

5.3 THE COMPARISON CRITERIA OF CN

Centralized and distributed CNs are characterized by different items including investment, signal time delay, reliability and risk. In the following subsections, these four characteristic items will be systematically analyzed and quantitative calculated.

5.3.1 INVESTMENT

In a fiber-based CN, the maximum use of resources is obtained by maximizing both the bandwidth and the distance between the repeaters. Fewer fibers, repeaters and routers are then needed for a given amount of traffic [184]. The investment for a fiber-based CN is mainly composed of three major parts including the investment for the total length of optical fiber cable, the total number of repeaters and routers in CN [34, 35]. Optical fiber cable is the transmission media of WAMS data, router is used to receive and regenerate the WAMS data through O/E/O module in it, and repeater is used to compensate for the optical attenuation and distortion of the WAMS signals transmitted in the long communication link.

The total investment for CN can be represented as [34]:

$$I_{\text{CN}} = L_f \cdot \text{Cost}_f + N_{\text{re}} \cdot \text{Cost}_{\text{re}} + N_{\text{ro}} \cdot \text{Cost}_{\text{ro}} \quad (5.1)$$

where L_f is the total length of optical fiber cable in CN, Cost_f is the cost of optical fiber cable per km, N_{re} and N_{ro} are the number of repeaters and routers in CN, respectively, and Cost_{re} and Cost_{ro} are the cost of one repeater and one router, respectively. The typical values for Cost_f , Cost_{re} and Cost_{ro} are \$346.5 per km (Quotation provided by YOFC), \$2,520 and \$3,780 (Quotation provided by Huawei Technologies Co.), respectively.

5.3.2 SIGNAL TIME DELAY

Synchronized phasors from various locations in the power grid is required to determine the wide-area control actions. Communication of synchronized phasors from different locations experience different amount of time delays before reaching the CC or ACCs. Communication delay is one of the key factors that determine the performance of CN [8].

Like the signal time delay in WAMS expressed by (3.3), the total signal time delay introduced by CN can be represented as follows:

$$T_{\text{CN}} = T_s + T_{\text{ro}} + T_p + T_{\text{re}} \quad (5.2)$$

$$T_s = \frac{P_s}{D_r} \quad T_p = \frac{l}{v} \quad (5.3)$$

where T_s is the serial time delay, T_{ro} is the routing time delay, T_p is the propagation time delay, T_{re} is the repeating time delay, P_s is the size of the packet (bits/packet), D_r is the data rate of optical fiber, l is the length of the optical fiber cable, and v is the velocity at which the data are sent through the optical fiber.

The typical value for the data rate of optical fiber is 2Mb/s [192]. Assuming the data packet is 64 byte which contains 12 synchronized phasors and 16 digital channel states, serial time delay T_s will be calculated as follows:

$$T_s = \frac{P_s}{D_r} = 64 \times 8 \text{b} / 2048 \text{kb} \cdot \text{s}^{-1} = 0.25 \text{ms} \quad (5.4)$$

For a given node in CN, the routing time delay from this node to CC can be expressed as follows:

$$T_{\text{ro}} = \sum_{i=1}^N T_{i^{\text{th}}_{\text{ro}}} \quad (5.5)$$

where N is the number of routers from this node to CC and $T_{i^{\text{th}}_{\text{ro}}}$ is the routing time delay caused by the i^{th} router. The typical value for T_{ro} is 0.375ms [192].

The propagation time delay T_p from this node to CC can be expressed as follows:

$$T_p = \frac{L_{\text{N-C}}}{v} \quad (5.6)$$

where $L_{\text{N-C}}$ is the length of optical fiber cable from this node to CC. The typical value for v is 200 km/ms [192].

The repeating time delay from this node to CC can be expressed as follows:

$$T_{\text{re}} = \sum_{i=1}^N T_{i^{\text{th}}_{\text{re}}} \quad (5.7)$$

where N is the number of repeaters from this node to CC and $T_{i^{\text{th}}_{\text{re}}}$ is the repeating time delay caused by the i^{th} repeater. By employing the Erbium-doped fiber amplifier (EDFA) technology in the repeater, the value for T_{re} can reach nanosecond (ns) scale which can be neglected in the calculation of signal time delay introduced by CN [193].

5.3.3 RELIABILITY

Reliability is the most important characteristic of CN [177]. Any performance improvement to the other characteristic items of CN such as investment and signal time delay can only be conducted on the condition that the high reliability of CN is maintained. In order to improve the operation reliability and coordinate with the control strategy in power system, in most of the existing WAMS, 2-fiber unidirectional self-healing ring network (U-SHRN/2) has become commonly adopted as the main structure of CNs in WAMS [177]. Reliability evaluation of CN with such structure is rather a challenging task for the existing algorithms.

In this chapter, Monte Carlo dynamic fault tree reliability evaluation method proposed in Section IV is used to conduct the reliability evaluation of CN with centralized and distributed architecture. With this reliability evaluation method, multiple fault patterns in CN could be considered. Furthermore, the reliability of both synchronized phasors uploading from PMUs to the CC and control instructions downloading from the CC to control devices through CC could be considered.

The typical value of the failure rate λ_f and repair rate μ_f for optical fiber cable is 0.0147 failures/year per km and 150 repairs/year, respectively. The typical value of the failure rate λ_{ro} and repair rate μ_{ro} for router is 0.0053 failures/year and 17520 repairs/year, respectively [174].

Both centralized and distributed WAMS require all synchronized phasors measured by PMUs to be transmitted to the CCC or ACCs through communication network within a stringent period. This implicates that the communication network in WAMS should function properly; otherwise, the CCC or ACCs would fail.

5.3.4 RISK

The root of CN risk lies in its intrinsic probabilistic behavior. Generally, WAMS operation personnel cannot control the CN components' random failures [184]. Consequences of CN incident to power grid range from the extra signal time delay to the damage to the safety and stability of the power grid. Today, the risk evaluation of CN has become a challenging but necessary task. It is essential to conduct a quantitative risk evaluation of CN so as to generate indices which could represent the degree of risk involved. As a comprehensive risk index, not only the probability of incident but also the consequences caused by this incident should be considered. In other words, the risk evaluation of CN should consider both the probability of failure events and the severity level of their consequences.

Therefore, risk of WAMS can be defined quantitatively as follows [194]:

$$R = C \cdot P \quad (5.8)$$

where R indicates the risk of a specific CN incident; C and P indicate the consequences and the occurrence probability of this incident.

5.3.4.1 CALCULATION OF OCCURRENCE PROBABILITY OF CN INCIDENT

Routers and repeaters are two important components in CN. Their operation and failure state probability can be expressed as follows:

$$P_0 = \frac{\mu}{\lambda + \mu} \quad P_1 = \frac{\lambda}{\lambda + \mu} \quad (5.9)$$

where λ and μ are the failure rate and repair rate of these components, respectively.

As for the communication link, its operation and failure state probability calculation is very different from other components. Most modern CNs adopt a 2-fiber structure. One fiber is in working condition while the other serves as the standby fiber. For such communication link, there are two kinds of failures: one fiber failure and two fibers failure. The second failure type can be further divided into two types: the common cause failure and the independence failure. Individual modeling method, which constructs the reliability model of the communication link as independence failure models and common cause failure model, can be used to analyze the state probability of such communication link [195]. Here, the communication link L_i is taken as an example to analyze its state probability as follows:

The probability of no fiber failure can be expressed as:

$$P_0(L_i) = \frac{\mu_{L_{iC}}}{\lambda_{L_{iC}} + \mu_{L_{iC}}} \frac{\mu_{L_i}}{\lambda_{L_i} + \mu_{L_i}} \frac{\mu_{L_i}}{\lambda_{L_i} + \mu_{L_i}} \quad (5.10)$$

The probability of one fiber failure can be expressed as:

$$P_1(L_i) = 2 \cdot \frac{\mu_{L_{iC}}}{\lambda_{L_{iC}} + \mu_{L_{iC}}} \frac{\mu_{L_i}}{\lambda_{L_i} + \mu_{L_i}} \frac{\lambda_{L_i}}{\lambda_{L_i} + \mu_{L_i}} \quad (5.11)$$

The probability of two fibers failure can be expressed as:

$$P_2(L_i) = \frac{\lambda_{L_{iC}}}{\lambda_{L_{iC}} + \mu_{L_{iC}}} + \frac{\mu_{L_{iC}}}{\lambda_{L_{iC}} + \mu_{L_{iC}}} \frac{\lambda_{L_i}}{\lambda_{L_i} + \mu_{L_i}} \frac{\lambda_{L_i}}{\lambda_{L_i} + \mu_{L_i}} \quad (5.12)$$

where $\lambda_{L_{iC}}$ and $\mu_{L_{iC}}$ are the common cause failure rate and repair rate of the communication link L_i , respectively; λ_{L_i} and μ_{L_i} are the failure rate and repair rate of one fiber in communication link L_i , respectively.

5.3.4.2 QUANTITATIVE CALCULATION OF CONSEQUENCE

The consequences caused by CN incident to power grid are reflected in many

risk factors such as signal time delay, data loss, control instruction, economy loss and power grid security. These five risk factors are described in detail as follows:

(1) Signal time delay

Any kind of CN incident would more or less add extra signal time delay to both the data uploading from PMUs to the control center and the instruction downloading from the control center to PMUs and the control devices.

(2) Data loss

In the condition of CN incident, the control center may not be able to receive part or all the uploading data.

(3) Control instruction

After all the WAMS data is sent to the control center, the WAMS based stability analysis and control schemes will analyze these data to produce an optimal stability control instruction. This control instruction will be sent to the control devices, which are distributed among the power grid, to maintain the stable and safe operation of power system after an incident. The signal time delay and data loss caused by the CN incident would deteriorate the real-time and accuracy of the control instruction.

(4) Economy loss

Time delayed and inaccurate control instruction may impair the efficiency of generators or increase the power loss of power grid.

(5) Power grid safety

Due to the loss of real-time and accurate control of power grid after an incident, the safety of power grid will be affected.

The above five risk factors are ranked by not only their degree of importance but also their time sequence. They can indicate how severely the CN incident affects the power grid.

In order to quantitatively and systematically test the importance degree of

each risk factor in the consequences, the specific weight of each risk factor should be evaluated during the risk evaluation. Here, the well-known AHP algorithm is used to evaluate the specific weight of each risk factor. AHP algorithm is first proposed by T. L. Saaty, an American operations researcher [196]. It is an algorithm used for dealing with problems which involve the consideration of multiple criteria simultaneously [197]. It is unique in its ability to deal with intangible attributes and to monitor the consistency with which a decision maker makes his decisions.

In order to quantify these risk factors after their respective importance to the consequences is acquired, a risk ranking technology is needed to rank these risk factors according to their respective severity level.

In this chapter, a hybrid MCDM approach combined with AHP and risk ranking technology is proposed to comprehensively and quantitatively calculate the consequences of CN incident to the power grid. The detail steps to be followed are as follows:

- Step 1: Set up a decision hierarchy by breaking down the consequences of CN incident into a hierarchy of interrelated risk factors including signal time delay, data loss, control instruction, economy loss, and grid security.
- Step 2: Collect input data by pairing comparisons of these risk factors using 1~9 scale rule in AHP algorithm as shown in Table 5.1 to construct the comparison matrix.
- Step 3: Use the eigenvalue method to calculate the relative importance weights of these five risk factors to the total consequences.
- Step 4: Classify these risk factors to 5 grades using 1~5 grade rule in risk ranking technology with each grade representing the consequence with different severity degree as shown in Table 5.3.
- Step 5: Calculate the value of consequences of CN incident.

Table 5.1 The 1~9 scale rule in AHP algorithm

Scale	Definition
1	Factor i and factor j are of the equal importance
3	Factor i is moderately more important than factor j
5	Factor i is essentially more important than factor j
7	Factor i is strongly more important than factor j
9	Factor i is extremely more important than factor j
2,4,6,8	Intermediate values between the two adjacent scales
Reciprocals	If factor i has one of the above scales when compared with factor j , then factor j has the reciprocal value when compared with factor i .

The comparison matrix can be constructed by using the typical 1~9 scale rule in AHP algorithm. This 1~9 scale rule is shown in Table 5.1. Each factor in the comparison matrix is acquired from the comparison of risk factor i and j . This comparison matrix reflects the understanding of the risk evaluation personnel to the relative importance degree of each risk factor in the consequences.

Next, the eigenvalue method will be used to calculate the weights of risk factors.

If matrix W is defined as $W = (w_1, w_2, w_3, \dots, w_n)^T$, equation $AW = \lambda_{\max} W$ can be obtained, in which λ_{\max} is the largest eigenvalue to the comparison matrix A and W is the eigenvector associated with λ_{\max} .

λ_{\max} and W can be calculated by solving the characteristic equation:

$$\det(\lambda I - A) = |\lambda I - A| = 0 \quad (5.13)$$

The weights vector \bar{W} for all the risk factors can then be calculated by normalizing W . Because the comparison matrix A is constructed according to the understanding and judgment of the risk evaluation personnel, some subjective

factors can hardly be avoided. Therefore, the consistency of the comparison matrix A must be tested. If the comparison matrix A is not consistent, the weight vector \bar{W} of risk factors cannot reflect the relative importance of each risk factor. Here, the consistency index (CI) is defined as:

$$CI = \frac{\lambda_{\max} - n}{n - 1} \quad (5.14)$$

where n is the order of the comparison matrix A .

The consistency ratio (CR) can be defined as:

$$CR = \frac{CI}{RI} \quad (5.15)$$

where RI is the random index whose typical values are illustrated in Table 5.2.

Table 5.2 RI value

Order	1	2	3	4	5	6	7	8	9
RI	0.00	0.00	0.58	0.96	1.12	1.24	1.32	1.41	1.45

If $CR < 0.1$, the comparison matrix A has sufficient consistency; if not, the comparison matrix A should be adjusted until $CR < 0.1$ is satisfied.

In order to quantitatively evaluate the value of the consequences of CN incident, the risk grade of each risk factor in the consequences must be ranked with risk ranking technology after the importance weight of each risk factor to the total consequences is obtained.

Following the 1~5 grade rule in [198], the risk grade of each risk factor can be classified as Table 5.3. In this table, the risk grade of data loss is classified according to the data loss ratio among all the data in a specified time period.

Finally, the value of the consequences of CN incident can be quantitatively calculated as follows [198]:

$$C = \sum_{i=1}^n \bar{W}_i G_i \quad (5.16)$$

where n is the number of considered risk factors.

Table 5.3 Risk grade of each risk factor

Risk factor	Risk grade				
	1	2	3	4	5
Signal time delay	Almost no increase	a little increase	a great increase	extreme increase	Communication breakdown
Data loss	<0.1‰	Between 0.1‰ and 1‰	Between 1‰ and 1%	>1%	Cannot be received at all
Control instruction	Accuracy nearly not be effected	Accuracy is effected a little	Accuracy is greatly effected	Accuracy is bad	Cannot be obtained at all
Economy loss	Nearly no loss	A little loss	A moderate loss	A great loss	A severe loss
Power grid safety	Nearly not be impacted	Be impacted slightly	Be effected greatly	Be effected severely	Be destroyed totally

5.4 CONSTRUCTION OF COMMUNICATION NETWORK

For conducting the performance comparison scheme, centralized and distributed CNs with minimum investment shall be constructed first. The construction of CN can be applied as an optimization problem with the optimization target as the minimum investment. Minimum Spanning Tree (MST) algorithm is one of the most efficient algorithms for the construction of CN [176, 199-201]. By employing MST algorithm, CN connecting all the nodes with minimum investment can be constructed.

In MST algorithm, CN construction problem can be modeled with a connected, undirected graph $G=(V, E, W)$, where V is the set of nodes, E is the set of communication links between pairs of nodes, and W is the weigh matrix. For each communication link $(u,v) \in E$, a weight $w(u,v)$ can be used to specify the cost to connect nodes u and v . In order to find an acyclic subset $T \subseteq E$ that connects all of the nodes and whose total weight $w(T) = \sum_{(u,v) \in T} w(u,v)$ is minimized. The problem of determining the tree T can be called the MST problem. Prim's algorithm is used here to solve the MST problem.

The weight of the i^{th} communication link can be expressed as follows:

$$w_i = L_i \cdot \text{Cost}_f + N \cdot \text{Cost}_{re} \quad (5.17)$$

where L is the length of optical fiber cable in the i^{th} communication link and N is the number of repeaters needed in the i^{th} communication link.

In traditional MST algorithm, with the weight of each communication link expressed as (5.17), only CN with minimum investment for optical fiber cable and repeaters can be constructed. However, the investment for CN includes not only the investment for optical fiber cable and repeaters but also the investment for routers which are used to connect multiple communication links. The investment for optical fiber and repeaters depends on the total length of communication links, while the investment for routers depends on the number of them which can only be determined after the construction of CN. Therefore, traditional MST algorithm cannot be used directly for the construction of optimal CN. As a remedy, an improved MST algorithm is proposed in this chapter to construct the optimal CN with minimum investment. With this algorithm, the total investment for optical fiber, repeaters and routers in CN can be minimized.

Assuming $G = (V, E, W)$, where V , E , and W are respectively the set of all nodes, the set of all possible communication links and the set of the weights of all communication links in CN, define new sets T and S which respectively represent the set of communication links and the set of all router nodes (the node with router) in the MST of CN.

The construction procedures of optimal CN with minimum investment using the proposed improved MST algorithm are as follows:

Step 1: Initialization. Set the initial value of V , E , and W . Each element in set W is the weight of each possible communication link expressed as (5.17). Set the initial value of n , which is used to indicate the number of router nodes in set S , as 1.

Step 2: Select n nodes from V as the router nodes and put them into set S . There are $C_{|V|}^n$ kinds of possible selection combinations of selecting n nodes from V , so there will be also $C_{|V|}^n$ kinds of S .

Step 3: For each kind of S , using MST algorithm to construct CN with S as the router nodes. In this way, $C_{|V|}^n$ kinds of CNs with n router nodes can be acquired. From these $C_{|V|}^n$ kinds of CNs, select one with minimum investment as the optimal CN with n router nodes and record the communication links of this CN in T .

Step 4: If $n=1$, $n=n+1$ and go to Step 2. If not, go to Step 5.

Step 5: Compare the investments of CNs with $n-1$ and n router nodes. If the difference between investments is less than $cost_{to}$, CN with $n-1$ router nodes can be selected as the optimal CN with minimum investment. If not, $n=n+1$ and go to Step 2.

5.5 STUDY CASE

5.5.1 WAMS IN SHANDONG POWER GRID

Here, a commercial WAMS established in Shandong Power Grid is taken as a platform for testing the validity and practicality of the performance comparison scheme of centralized and distributed CNs. Shandong Power Grid possessed 36 500kV substations and 206 220kV substations. WAMS project for Shandong Power Grid started from August 2005. Until 2010, 20 PMUs were installed on 18 500kV substations and 2 power plants to form the backbone WAMS. 2.5 Gbit/s SDH optical fiber network is used to construct the CN of WAMS in Shandong Power Grid. Normally, in 2.5 Gbit/s SDH network, by employing EDFA technology, the longest transmission distance of single mode optical fiber cable can reach up to 200 km without a repeater [193]. The geographical distribution of PMUs in WAMS of Shandong Power Grid is shown in Fig. 5.3.

In the centralized WAMS, Jinan as the capital city of Shandong province must be selected as the CCC. The synchronized phasors measured by PMUs will first be sent to Jinan through CN, and then the control instructions will be sent back from Jinan to the control devices. During the construction, as CCC, Jinan should always be selected as one of the router nodes.

5.5.3 DISTRIBUTED WAMS IN SHANDONG POWER GRID

In the distributed WAMS, Jinan is also the CCC of the entire distributed WAMS of Shandong Power Grid. Based on the coherency identification and geographical location, WAMS in Shandong Power Grid is divided into three control areas including North-West Lu, South-Western Lu and Eastern Lu [202]. Following the method proposed in [203], Jinan, Luzhong and Weifang are selected as the ACCs of these three control area, respectively. For each control area, proposed improved MST algorithm is used to construct the optimal area CN with minimum investment. The architecture and data flow of the distributed WAMS in Shandong Power Grid is shown in Fig. 5.5.

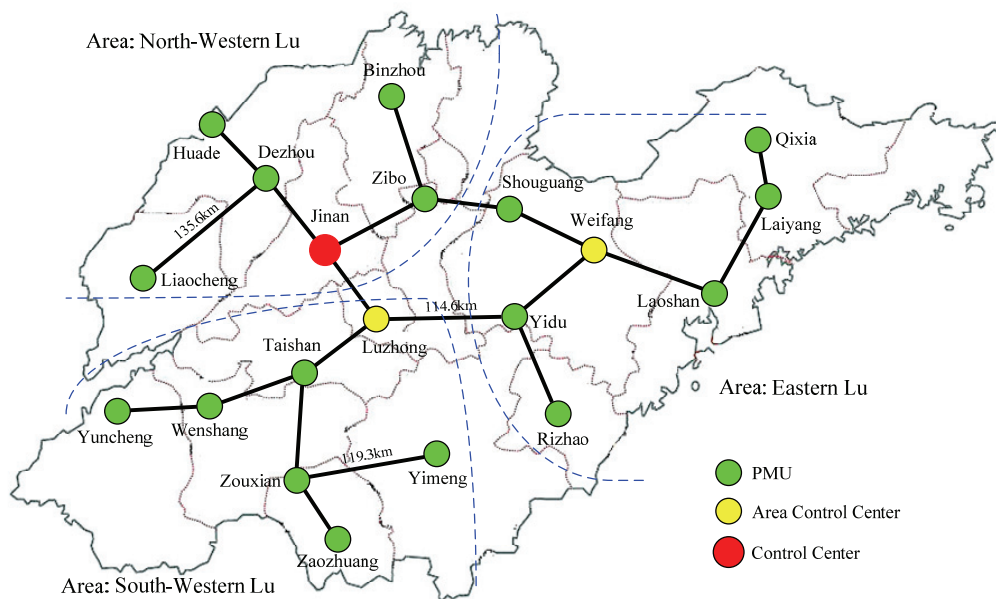


Fig. 5.5 Distributed WAMS in Shandong Power Grid

PMUs send the synchronized phasors to the ACC in their control area to monitor and control their own control areas. In order to monitor and control the entire Shandong Power Grid, these three ACCs are connected with each other to form a ring network to exchange data with each other. In this way, these three area CNs are connected to form the entire CN with minimum investment in distributed WAMS of Shandong Power Grid. During the construction of each area CN, each ACC should always be selected as one of the router nodes.

5.5.4 COMPARISON OF CENTRALIZED AND DISTRIBUTED CNS

(1) Investment comparison

After the centralized and distributed CNS of WAMS in Shandong Power Grid with minimum investment are constructed, the investments for these two CNS can be calculated according to Equation (5.1). The calculation results are shown in Table 5.4.

Table 5.4 Investment for centralized and distributed CNS

CN	Centralized	Distributed
Total fiber cable length (km)	1,427	1,573
Optical fiber investment (USD)	449,219.6	495,180.4
Repeater number	0	0
Repeater investment (USD)	0	0
Router number	13	12
Router investment (USD)	49,108.8	288,000
Total investment (USD)	3,166,000	3,434,000

Because the lengths of all the communication links in both centralized and distributed CNS are less than 200 km, there is no need to install repeater. The

difference of investment between centralized and distributed CNs is quite small relative to the total investment. Thus, the investments for CNs of centralized and distributed WAMS in Shandong Power Grid can be regarded as almost the same.

(2) Signal time delay comparison

According to the theory of barrel, the signal time delay in CN depends on the maximum signal time delay which can be calculated using Equation (5.2). Different from the centralized CN, each ACC in the distributed CN can monitor and control its own control area. Thus, most random disturbances in individual control areas would be processed locally to minimize its impact on other control areas [181]. When the data of the entire power grid is needed, all ACCs would send their data to CCC. Therefore, the signal time delay in the distributed CN should be divided into two parts. One is the signal time delay from PMUs to their own ACCs in the area communication networks while the other is the signal time delay from PMUs to CCC in the entire CN. The signal time delay in the centralized and distributed CNs of WAMS in Shandong Power Grid is shown in Table 5.5.

Table 5.5 Signal time delay of centralized and distributed CNs

CN	Signal time delay (ms)
Centralized	4.325
Distributed	4.325
Area: North-Western Lu	1.63
Area: South-Western Lu	1.9685
Area: Eastern Lu	1.9465

From Table 5.5 it can be seen that because the CCCs of the centralized and distributed CNs are both in Jinan, centralized and distributed CNs have the same signal time delay for the entire CN. However, in the distributed CN, most of local

random disturbances are handled by ACCs. Thus, the shorter signal time delay in area CNs can ensure ACCs process the disturbances in time to prevent the cascading faults. Furthermore, the control effectiveness of the control devices which are sensitive to the signal time delay will be greatly improved.

(3) Reliability comparison

Just as the signal time delay, the reliability of the distributed CN can be divided into two parts too. One is the reliability of the entire CN while the other is the reliability of the area CNs. Following the proposed Monte Carlo fault tree reliability evaluation method, reliability of the centralized and distributed CNs in WAMS of Shandong Power Grid is calculated as shown in Table 5.6.

Table 5.6 Reliability of centralized and distributed CNs

CN	Reliability indices
Centralized	0.878
Distributed	0.907
Area: North-Western Lu	0.9682
Area: South-Western Lu	0.9679
Area: Eastern Lu	0.9693

From Table 5.6 it can be seen that because of the ring CN between ACCs, the reliability of the distributed CN is much higher than that of the centralized one. The reliability difference is $\Delta A = 0.029$ which means that the different between the unavailable time of the centralized and distributed CNs reaches up to 254.04 hr/year. As the coordinators of the CCC, the ACCs can locally process most of the random disturbances. Thus, the burden of the CCC will be greatly reduced and the reliability of the entire distributed CN will be enhanced further. As a result, the reliability of the monitoring and control for the entire system will be largely enhanced by employing the distributed CN.

(4) Risk comparison

Through the comparison of centralized and distributed CNs in WAMS of Shandong Power Grid, it can be seen that the greatest difference lies in the fact that all the PMUs are linked with CCC through 2-fiber network in centralized CN while all the ACCs are linked up with CCC to form a 2-fiber unidirectional self-healing ring network in distributed CN.

The communication link between Jinan and Zibo (L_{J-Z}) can be taken as an example to conduct the risk evaluation. The reason for selecting L_{J-Z} is that: in centralized CN, L_{J-Z} is just a common communication link, while in distributed CN L_{J-Z} is a communication link in the ring network. In order to facilitate the analysis, $L_{J-Z(C)}$ and $L_{J-Z(D)}$ are used to indicate L_{J-Z} in the centralized and distributed CN, respectively.

The probability of L_{J-Z} failure can be calculated as follows:

$$P(L_j) = P_2(L_j) \left(\prod_{i=1, i \neq j}^n P_0(L_i) \right) \left(\prod_{i=1}^m P_0(ro_i) \right) \left(\prod_{i=1}^p P_0(re_i) \right) \quad (5.18)$$

where n , m , p is the number of communication link, routers, repeaters in the centralized or distributed CNs, respectively.

The reliability parameters of CN are shown in Subsection 5.3.3. By the combination of (5.9-5.12) and (5.18), the probability of $L_{J-Z(C)}$ can be calculated as $P(L_{J-Z(C)}) = 0.768\%$. The probability of $L_{J-Z(D)}$ failure can be calculated as $P(L_{J-Z(D)}) = 0.745\%$.

For this study case, 5 risk factors are proposed to indicate the consequences of the L_{J-Z} failure to the power grid. These 5 risk factors are signal time delay, data loss, control instruction, economy loss, and power grid security, respectively.

According to the 1~9 scale rule shown in Table 5.1, the comparison matrix A can be constructed as:

$$A = \begin{bmatrix} 1 & 1/3 & 1/5 & 1/7 & 1/9 \\ 3 & 1 & 1/4 & 1/5 & 1/8 \\ 5 & 4 & 1 & 1/3 & 1/6 \\ 7 & 5 & 3 & 1 & 1/4 \\ 9 & 8 & 6 & 4 & 1 \end{bmatrix}$$

From the eigenvalue calculation, $\lambda_{\max} = 5.3791$ and the weights vector of these 5 risk factors is $\bar{W} = [0.0339, 0.0619, 0.1347, 0.2334, 0.5361]$.

Consistency test is then conducted to test the rationality of the constructed comparison matrix A , it can be calculated that: $CI = \frac{5.3791 - 5}{5 - 1} = 0.0948$ and

$$CR = \frac{0.0948}{1.12} = 0.0783 < 0.1 \text{ which means the constructed comparison matrix } A \text{ is}$$

reasonable and it can accurately reflect the different importance degree of 5 risk factors in the consequences of L_{J-Z} failure to the power grid.

According to Table 5.3, the risk grade of each risk factor can be determined. For $L_{J-Z(C)}$ failure, the risk grade for the risk factors can be determined as: $G_C = [4, 3, 3, 2, 3]$. For $L_{J-Z(D)}$ failure, the risk grade for the risk factors can be determined as: $G_D = [1, 1, 1, 1, 1]$.

According to Equation (5.16), the value of the consequences of L_{J-Z} failure to the power grid can be calculated as follows:

$$\begin{aligned} C_C &= \sum_{i=1}^5 \bar{W}_i (G_C)_i = 2.8005 \\ C_D &= \sum_{i=1}^5 \bar{W}_i (G_D)_i = 1 \end{aligned} \tag{5.19}$$

where C_C and C_D are the value of consequences caused by $L_{J-Z(C)}$ failure and $L_{J-Z(D)}$ failure to power grid, respectively.

Finally, the risk of L_{J-Z} can be calculated as follows:

$$\begin{aligned} R_C &= P(L_{J-Z(C)}) \cdot C_C = 0.0215 \\ R_D &= P(L_{J-Z(D)}) \cdot C_D = 0.0075 \end{aligned} \tag{5.20}$$

where R_C and R_D are the risk of $L_{J-Z(C)}$ and $L_{J-Z(D)}$, respectively.

It can be seen that the risk of $L_{J-Z(C)}$ is much higher than that of $L_{J-Z(D)}$ failure even though the probability of $L_{J-Z(C)}$ failure and $L_{J-Z(D)}$ failure is nearly the same. This is mainly because $L_{J-Z(C)}$ failure can lead to more severe consequences to the power grid than $L_{J-Z(D)}$ failure. When failure occurs on $L_{J-Z(C)}$ which is near the CCC, nearly 1/3 of the total WAMS data cannot be sent to the CCC. In this condition, the accurate control instruction cannot be acquired, thus leading to the high economy loss and the damage to the power system security. However, when failure occurs on $L_{J-Z(D)}$, because of the 2-fiber unidirectional self-healing ring network structure, all the WAMS data can also be sent to the CCC. Just a little extra signal time delay may be added to a part of the data transmitted through $L_{J-Z(D)}$. In this condition, the accurate control instruction can be used to keep economic and safe operation of power system.

Another important difference in the architecture of centralized and distributed CNs is that only CCC is used to control the whole power grid, but in distributed CN, several ACCs are used to assist the CCC to control the whole power grid. If failure occurs on CCC in centralized CN, WAMS would lose its function and poses a great crisis and risk to the power grid. If failure occurs on CCC in distributed CN, WAMS would only lose part of its function and ACCs can control part of the power grid to reduce the risk and consequences caused by the failure of CCC.

5.6 SUMMARY

With the profound deregulation and the growing integration of renewable energies and intelligent controllers, new control strategies should be adopted to control the increasingly complex power industries. There is an urgent need for high-performance CN which is an essential component of WAMS with different architecture to coordinate with the different control strategies of power systems.

By employing the proposed improved MST algorithm, the optimal communication networks with minimum investment in centralized and distributed WAMS of Shandong Power Grid are firstly constructed to facilitate the quantitative and comprehensive investigation of centralized and distributed CNs. Results from the investigation show that, while the investment is comparable, distributed CN has shorter signal time delay, higher reliability and lower risk than centralized one. This means that distributed CN has better performance in the monitoring and control of power systems than the centralized one.

Through the risk evaluation of centralized and distributed CNs by using MCDM approach combined with AHP and risk ranking technology, it can be seen that the same communication link in CN with different architecture could possess totally different risk to the power grid. This can be used to reduce the risk level of the existing CN and construct the new CN with lowest risk level.

CHAPTER VI SSI ALGORITHM FOR ON-LINE POWER SYSTEM LOW-FREQUENCY OSCILLATION IDENTIFICATION

6.1 INTRODUCTION

Power system oscillations have been observed in power systems ever since synchronous generators were interconnected to provide higher generation capacity and reliability, and have become one of the severe threats for modern interconnected power grids [86]. Power system oscillations triggered by a disturbance, for example, could have two distinct oscillation modes, namely local oscillation mode and inter-area oscillation mode. As their typical oscillation frequency is ranged from 0.1Hz to 2.5Hz, they are commonly referred as power system low-frequency oscillation. Generally, inter-area mode of oscillations is a relative slow change process with time frame ranged from 10s to 20s or more with typical frequency 0.1-0.7Hz, and would involve wider range and more generators compared to local mode of oscillation with typical frequency 0.7-2.5Hz [13]. When there is an inter-area mode of oscillation developed in a power system, the amount of allowable power transfer in the tie-lines will be severely limited. Following the interconnection of power grids, inter-area oscillation has occurred more and more often and has become more and more difficult to suppress. The identification and analysis of inter-area oscillation mode would therefore be the focus of this chapter.

At present, there are mainly two approaches for low-frequency oscillation analysis. The first one is eigenvalue analysis [204] based on state matrix, which is established by linearizing the power system components. This method is more suitable for offline analysis but is often limited by the veracity of component model and parameters of power system. The other one is signal processing based

on measured data, which has been rapidly expanded in recent years with the mature and wide applications of WAMS. Prony [85, 205], ARMA [82] and HHT [79] are the main signal processing methods which have been successfully applied in low-frequency oscillation analysis and control. So far, nearly all of these methods proposed in various papers have employed locally measured data, such as power angle of generator, active power of generator, rotor speed of generator or active power of tie-line for analyzing low-frequency oscillations. Though oscillation mode parameters can be obtained with these methods, oscillation mode shapes which are important for low-frequency oscillation analysis and control cannot be acquired. Furthermore, the identification results of Prony and ARMA are influenced strongly by the signal noise and system order [206] while the process of HHT is complex and time consuming.

Though Stochastic Subspace Identification (SSI) [86] is a well-known parametric time domain estimator, which could be used to obtain both oscillation mode parameters and mode shape, and has been used to analyze the oscillatory stability limit in [207], its unique advantage has not been fully explored and the signal noise has not been taken into consideration.

In this chapter, the SSI algorithm is employed to identify the oscillation mode parameters of low-frequency oscillation, especially the mode shape. The mathematical correlation between low-frequency oscillation and oscillation of mechanical system will first be analyzed to verify the feasibility for applying the SSI algorithm for oscillation identification of power system. The detailed analysis process of SSI algorithm will then be depicted. The validity of SSI algorithm will first be verified with a fourth-order system and then followed by case studies on two test power systems.

6.2 FEASIBILITY OF APPLYING SSI ALGORITHM FOR IDENTIFICATION OF POWER SYSTEM LOW-FREQUENCY OSCILLATION

The SSI algorithm was first introduced by Kung in 1978 [208]. Remarkable advances have been made since then. While the application of this algorithm is mainly on the fields of construction and bridge [209, 210], it is adopted here for identifying the oscillation mode parameters and mode shape of the low-frequency oscillation.

The SSI algorithm was originally developed for the identification of linear system. The structure mode parameters of system can be identified from the structure response referred as the ambient excitation. In this section, the mathematical correlation between the power system oscillation and the oscillation of mechanical system will first be analyzed to examine the feasibility of applying the SSI algorithm for identifying the low-frequency oscillation mode parameters and mode shape.

In a mechanical system, the oscillatory characteristic of particle is determined by the power inflicted on the mechanical system. In the case of a linear dynamical model for the single degree of freedom system, one has the following system of ordinary differential equation [211]:

$$M \frac{d^2 \mathbf{u}(t)}{dt^2} + C \frac{d\mathbf{u}(t)}{dt} + K\mathbf{u}(t) = \mathbf{f}(t) \quad (6.1)$$

where M is the mass, C is the damping, K is the stiffness, $\mathbf{u}(t)$ is the displacement vector and $\mathbf{f}(t)$ is the vector with exciting forces. However, (6.1) cannot be processed by SSI algorithm directly because:

- (1) (6.1) is continuous in time while the practical samplings are discrete.
- (2) There will be unavoidable noise interference in the measuring process.

Meanwhile, (6.1) can be converted to a continuous-time state space model

using the state space theory in control:

$$\frac{d}{dt} \begin{bmatrix} \mathbf{u}(t) \\ \dot{\mathbf{u}}(t) \end{bmatrix} = \begin{bmatrix} 0 & 1 \\ -\frac{K}{M} & -\frac{C}{M} \end{bmatrix} \begin{bmatrix} \mathbf{u}(t) \\ \dot{\mathbf{u}}(t) \end{bmatrix} + \begin{bmatrix} 0 \\ \frac{1}{M} \end{bmatrix} \mathbf{f}(t) \quad (6.2)$$

In a single-machine infinite bus system, the swing equation can be written as follows [5]:

$$\begin{cases} T \frac{d^2 \delta}{dt^2} + K_D \frac{d\delta}{dt} + P_e = P_m \\ \frac{d\delta}{dt} = \omega - 1 \end{cases} \quad (6.3)$$

where δ is the rotor angle, ω is per unit speed, T , K_D , P_e and P_m are the moment of inertia, damping coefficient, electrical power and mechanical power, respectively. In this single-machine infinite bus system, $P_e = \frac{E' E_B}{X_T} \sin \delta$ where E' is the generator terminal voltage, E_B is the infinite bus voltage and X_T is the equivalent resistance. After the linearization, (6.3) can be converted to the following state space form:

$$\frac{d}{dt} \begin{bmatrix} \Delta \delta \\ \Delta \omega \end{bmatrix} = \begin{bmatrix} 0 & 1 \\ -\frac{K_s}{T} & -\frac{K_D}{T} \end{bmatrix} \begin{bmatrix} \Delta \delta \\ \Delta \omega \end{bmatrix} + \begin{bmatrix} 0 \\ \frac{1}{T} \end{bmatrix} \Delta P_m \quad (6.4)$$

where $\Delta \omega = \Delta \dot{\delta}$ and $K_s = \frac{E' E_B}{X_T}$ is the synchronizing torque coefficient.

Though power system oscillation and mechanical system oscillation are two different physical phenomena, their state space models do share the exact same form as shown in (6.2) and (6.4). Therefore, the two different physical problems can be considered as the same mathematical problem and solved by the same mathematical method. Here, methods successfully used in experimental modal analysis for mechanical system are cited to deal with the power system oscillation problem.

6.3 ANALYSIS OF THE SSI ALGORITHM

6.3.1 STOCHASTIC STATE-SPACE MODEL

The behavior of a dynamic power system can be described in following form by using vector-matrix notation:

$$\begin{aligned}\dot{\mathbf{x}} &= f(\mathbf{x}, \mathbf{u}) \\ \mathbf{y} &= g(\mathbf{x}, \mathbf{u})\end{aligned}\tag{6.5}$$

where \mathbf{x} is the state vector, \mathbf{u} is the input vector and \mathbf{y} is the output vector.

After linearization, (6.5) can be converted to continuous-time deterministic state-space model as follows:

$$\begin{aligned}\dot{\mathbf{x}} &= \mathbf{A}\mathbf{x} + \mathbf{B}\mathbf{u} \\ \mathbf{y} &= \mathbf{C}\mathbf{x} + \mathbf{D}\mathbf{u}\end{aligned}\tag{6.6}$$

where \mathbf{A} is the state matrix, \mathbf{B} is the control or input matrix, \mathbf{C} is the output matrix and \mathbf{D} is the feed forward matrix which defines the proportion of input which appears directly in the output. Continuous time means that the expressions can be evaluated at each time instant $t \in \mathbb{R}$ and deterministic means that the input-output quantities $u(t)$, $y(t)$ can be measured exactly. Of course, this is not realistic: measurements are available at discrete time instants $k\Delta t$, $k \in \mathbb{N}$ with Δt , the sample time and stochastic components such as noise are always influencing the data. After sampling, the following discrete-time combined deterministic-stochastic state-space model can be obtained [212]:

$$\begin{aligned}\mathbf{x}_{k+1} &= \mathbf{A}_d \mathbf{x}_k + \mathbf{B}\mathbf{u}_k + \mathbf{w}_k, & \mathbf{A}_d &= e^{\mathbf{A}T_s} \\ \mathbf{y}_k &= \mathbf{C}\mathbf{x}_k + \mathbf{D}\mathbf{u}_k + \mathbf{v}_k\end{aligned}\tag{6.7}$$

where \mathbf{x}_k is the discrete state vector, \mathbf{y}_k is the discrete output vector, T_s is the sampling time. The process noise \mathbf{w}_k and measurement noise \mathbf{v}_k are zero mean noise, namely $E(\mathbf{w}_k) = E(\mathbf{v}_k) = 0$.

Based on (6.7), the stochastic state-space model can be defined as the

following equation without \mathbf{u}_k terms [207,212]:

$$\begin{aligned}\mathbf{x}_{k+1} &= \mathbf{A}_d \mathbf{x}_k + \mathbf{w}_k \\ \mathbf{y}_k &= \mathbf{C} \mathbf{x}_k + \mathbf{v}_k\end{aligned}\quad (6.8)$$

6.3.2 SOLVING OF STOCHASTIC STATE-SPACE MODEL

The measured data are divided into two parts named past and future, and formed as an output block Hankel matrix [212]:

$$\mathbf{Y}_{0|2i-1} = \begin{bmatrix} y_0 & y_1 & \cdots & y_{j-1} \\ y_1 & y_2 & \cdots & y_j \\ \cdots & \cdots & \cdots & \cdots \\ y_{i-1} & y_i & \cdots & y_{i+j-2} \\ y_i & y_{i+1} & \cdots & y_{i+j-1} \\ y_{i+1} & y_{i+2} & \cdots & y_{i+j} \\ \cdots & \cdots & \cdots & \cdots \\ y_{2i-1} & y_{2i} & \cdots & y_{2i+j-2} \end{bmatrix} = \begin{bmatrix} \mathbf{Y}_{0|i-1} \\ \mathbf{Y}_{i|2i-1} \end{bmatrix} = \frac{\mathbf{Y}_p}{\mathbf{Y}_f} \quad (6.9)$$

where $\mathbf{Y}_p = \mathbf{Y}_{0|i-1}$ $\mathbf{Y}_f = \mathbf{Y}_{i|2i-1}$ are the past and future parts respectively in the block Hankel matrix, $i=2m$ (m is the SSI order), j is the number of elements in the discrete output vector. \mathbf{Y}_p (the past inputs) and \mathbf{Y}_f (the future inputs) are defined by splitting $\mathbf{Y}_{0|2i-1}$ in two equal part of i block rows. By shifting the border i in the Hankel matrix, the new past and future parts can be obtained, which are $\mathbf{Y}_p^+ = \mathbf{Y}_{0|i}$ $\mathbf{Y}_f^- = \mathbf{Y}_{i+1|2i-1}$ [86].

Different algorithms can be used to calculate system matrix \mathbf{A}_d and \mathbf{C} . Here, the Canonical Variate Algorithm (CVA) is adopted and its procedure is as below [86,207].

(1) Calculate the orthogonal projections:

$$\begin{aligned}\mathbf{O}_i &= \mathbf{Y}_f / \mathbf{Y}_p \\ \mathbf{O}_{i-1} &= \mathbf{Y}_f^- / \mathbf{Y}_p^+\end{aligned}\quad (6.10)$$

(2) Calculate the singular value decomposition (SVD) of the weighted

projection:

$$\begin{aligned} \mathbf{W}_1 \mathbf{O}_i \mathbf{W}_2 &= \mathbf{U} \mathbf{S} \mathbf{V}^T \\ &= [\mathbf{U}_1 \quad \mathbf{U}_2] \begin{bmatrix} \mathbf{S}_1 & 0 \\ 0 & 0 \end{bmatrix} \begin{bmatrix} \mathbf{V}_1^T \\ \mathbf{V}_2^T \end{bmatrix} \end{aligned} \quad (6.11)$$

where $\mathbf{W}_1 = ((1/j)\mathbf{Y}_f \mathbf{Y}_f^T)^{-(1/2)}$, $\mathbf{W}_2 = [\mathbf{I}]_{j \times j}$, \mathbf{W}_1 and \mathbf{W}_2 are all the weighting matrices. \mathbf{U} and \mathbf{V} are unitary matrices from the *SVD* process. The SSI order m is determined by inspecting the singular values in \mathbf{S} , and the sub-matrix \mathbf{S}_1 (identity matrix $m \times m$) are the cosine of the principal angles related with past outputs \mathbf{Y}_p and future outputs \mathbf{Y}_f .

- (3) Determine the extended observables matrices as:

$$\mathbf{\Gamma}_i = \mathbf{W}_1^{-1} \mathbf{U}_1 \mathbf{S}_1^{1/2} \mathbf{T} \quad (6.12)$$

where $\mathbf{T} \in \mathbb{R}^{n \times n}$ is an arbitrary non-singular matrix representing a similarity transformation.

- (4) The part of the state sequence $\hat{\mathbf{X}}_i$ that lies in the column space of \mathbf{W}_2 can be recovered from:

$$\hat{\mathbf{X}}_i \mathbf{W}_2 = \mathbf{T}^{-1} \mathbf{S}_1^{1/2} \mathbf{V}_1^T \quad (6.13)$$

- (5) The state sequence $\hat{\mathbf{X}}_i$ is equal to:

$$\hat{\mathbf{X}}_i = \mathbf{\Gamma}_i^\dagger \mathbf{O}_i \quad (6.14)$$

- (6) The state sequence $\hat{\mathbf{X}}_{i+1}$ can be calculated as:

$$\begin{aligned} \hat{\mathbf{X}}_{i+1} &= \mathbf{\Gamma}_{i-1}^\dagger \mathbf{O}_{i-1} \\ \mathbf{\Gamma}_{i-1} &= \underline{\mathbf{\Gamma}}_i \end{aligned} \quad (6.15)$$

where $\underline{\mathbf{\Gamma}}_i$ is obtained by deleting the last l rows in $\mathbf{\Gamma}_i$, and l is the number of output in (6.8).

- (7) Finally, system state matrix \mathbf{A}_d and output matrix \mathbf{C} can be solved from:

$$\begin{bmatrix} \mathbf{A}_d \\ \mathbf{C} \end{bmatrix} = \begin{bmatrix} \hat{\mathbf{X}}_{i+1} \\ \mathbf{Y}_{i|i} \end{bmatrix} \hat{\mathbf{X}}_i^\dagger \quad (6.16)$$

It shall be noted that the state matrix \mathbf{A}_d obtained is identified collectively from l measured signals instead of one particular individual signal. This gives SSI the unique advantage of high robustness and high resistance to noise.

6.3.3 IDENTIFICATION OF OSCILLATION MODE PARAMETERS AND SHAPE

Once the system state matrix \mathbf{A}_d and output matrix \mathbf{C} are obtained, power system low-frequency oscillation mode parameters and mode shape can be identified as follows:

- (1) The discrete time state matrix \mathbf{A}_d can be expressed as [213]:

$$\mathbf{A}_d = \mathbf{\Psi} \begin{bmatrix} \eta_1 & & & \\ & \eta_2 & & \\ & & 0 & \\ & & & \eta_m \end{bmatrix} \mathbf{\Psi}^{-1} \quad (6.17)$$

where η_i ($i=1,2,\dots,m$) and $\mathbf{\Psi}$ are the eigenvalues and eigenvector matrix of the discrete time system as (6.8), respectively.

- (2) The continuous time system eigenvalue λ_i could be found from the discrete system eigenvalue η_i by

$$\lambda_i = \ln(\eta_i)/T_s \quad (6.18)$$

- (3) Then the oscillation modal parameters can be calculated as [197]:

$$\begin{aligned} f_i &= \omega_i/2\pi = |\lambda_i|/2\pi \\ \xi_i &= \text{Re}(\lambda_i)/|\lambda_i| \end{aligned} \quad (6.19)$$

where f_i is the oscillation frequency and ξ_i is the damping.

- (4) Finally, the oscillation modal shape matrix can be found from

$$\mathbf{\Phi} = \mathbf{C}\mathbf{\Psi} \quad (6.20)$$

6.3.4 MERITS OF SSI ALGORITHM

The SSI algorithm is founded based on the system identification theory and, in this algorithm, the perturbation is treated as the white noise, so the oscillation mode parameters can be obtained from the measured data with measurement errors effectively be disposed.

In modern power system, the network structure is often complex with areas and tie-lines not clear defined. Often, classical power system low-frequency oscillation analysis methods based on Prony, ARMA, or HHT are employed to analyze the active power of tie-lines. But in practices, it would be a challenge to correctly identify the critical tie-line online as it will vary with the change in the power flow pattern. Following the maturity of WAMS technology, WAMS based SSI algorithm is with great promise for the identification of power system low-frequency oscillation. In WAMS, various signals of generators such as rotor speed and angle are first collected by the local PMU, and then these measured data are sent to PDC for processing and data collection. The pre-processed data from all PDCs will then be sent to the control centre where oscillation mode parameters and mode shape can be identified by employing SSI algorithm based on the measured data collected over the whole system.

6.4 VALIDITY VERIFICATION FOR SSI ALGORITHM

Previous sections showed that it is feasible to use SSI algorithm to identify low-frequency oscillation and how the SSI algorithm works. Here, a fourth order example system is used to further verify the validity of SSI algorithm.

$$\begin{aligned}\dot{\mathbf{x}} &= \mathbf{Ax} + \mathbf{Ke}(t) \\ \mathbf{y} &= \mathbf{Cx} + e(t)\end{aligned}\tag{6.21}$$

where

$$A = \begin{bmatrix} 0.603 & 0.603 & 0 & 0 \\ -0.603 & 0.603 & 0 & 0 \\ 0 & 0 & -0.603 & 0.603 \\ 0 & 0 & 0.603 & -0.603 \end{bmatrix} \quad K = \begin{bmatrix} 0.2820 & -0.3041 \\ -0.7557 & 0.0296 \\ 0.1919 & 0.1317 \\ -0.3797 & 0.6538 \end{bmatrix}$$

$$C = \begin{bmatrix} 0.2641 & -1.4462 & 1.2460 & 0.5774 \\ 0.8717 & -0.7012 & -0.6390 & -0.3600 \end{bmatrix}$$

and the covariance of noise $e(t)$ is

$$\text{cov}(e(t)) = R = \begin{bmatrix} 0.1257 & 0.1166 \\ 0.1166 & 0.2170 \end{bmatrix}$$

For the evaluation of the SSI algorithm, two sets of output data were generated by feeding random input to (6.21). Table 6.1 summaries the eigenvalues calculated directly by the eigenvalue analysis and identified from the output data using the SSI algorithm.

Table 6.1 Eigenvalues of the four-order system obtained with eigenvalue analysis and SSI algorithm

Input data group	Analysis method	Real	Imag	Frequency (Hz)	Damping (%)
-	Eigenvalue analysis	0.603	0.603	0.096	-70.71
1	SSI algorithm	0.6049	0.5968	0.095	-71.19
2	SSI algorithm	-0.6018	0.6031	0.096	70.64

From Table 6.1, it can be seen that the eigenvalues calculated and identified by eigenvalue analysis and SSI algorithm are very close to each other. This shows clearly that the SSI algorithm is effective in identifying system oscillation.

6.5 CASE STUDIES

6.5.1 APPLICATION OF SSI IN LOW-FREQUENCY OSCILLATION ANALYSIS

Fig. 6.1 shows the design of an on-line application of SSI algorithm in power system low-frequency oscillation analysis in which the rotor speeds of generators are collected from the WAMS and used as the input to the SSI algorithm.

By employing SSI algorithm, system state matrix and output matrix are first determined, and then low-frequency oscillation modal parameters and modal shape are calculated and further processed for oscillation control. In other words, power system low-frequency oscillation is monitored on-line and the acquired oscillation modal parameters and modal shape are sent to the control center to derive the control measures, such as adjusting the generator active power and DC modulation, to suppress the power system low-frequency oscillation oscillations.

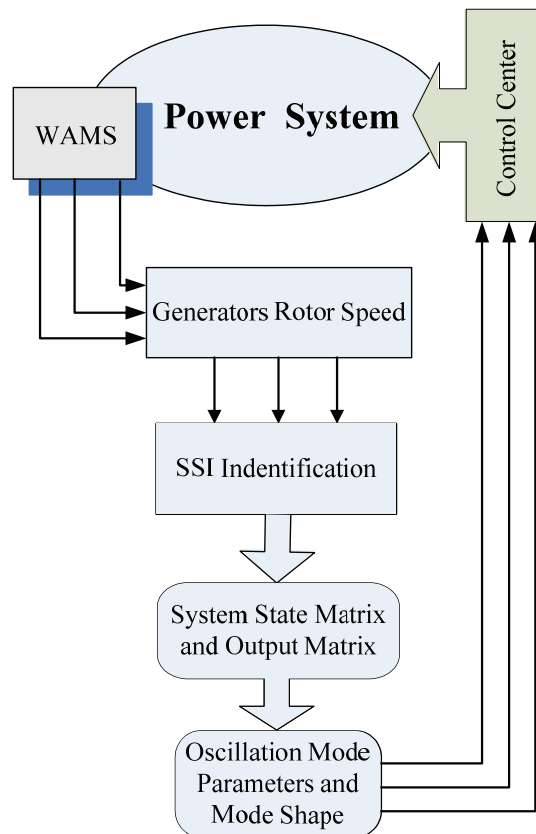


Fig. 6.1 Application of SSI algorithm in power system stability control

6.5.2 4-GENERATOR 2-AREA TEST SYSTEM

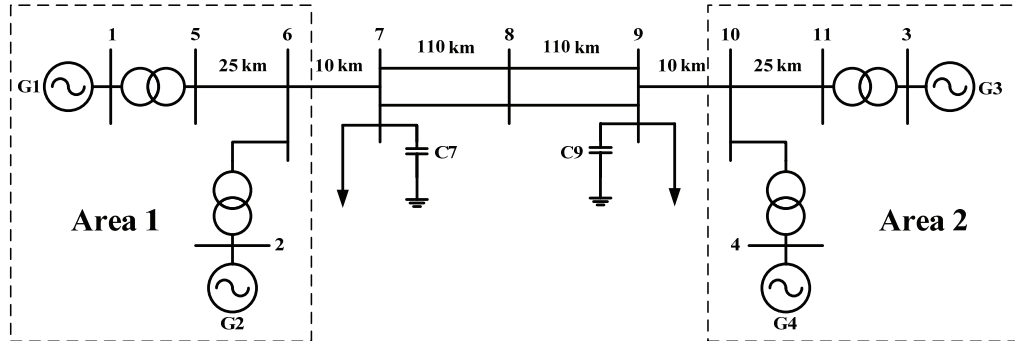


Fig. 6.2 IEEE 4-generator 2-area test system

In order to validate the effectiveness of SSI algorithm in the identification of power system low-frequency oscillation mode parameters and mode shape after a disturbance, IEEE 4-generator 2-area test system shown in Fig. 6.2 is adopted.

Assuming that a three phase fault takes place on bus 6 at time 1s and it is cleared at time 1.05s. In practical power system, the measured data often contains noise which may heavily affect the oscillation identification result. In order to test the ability of SSI algorithm to resist noise, after obtaining the rotor speed, different amount of random noises were added to the ideal signals. Fig. 6.3 and 6.4 show the rotor speed of the four generators and the COI (centre of inertia) power angle between Area1 and Area2 under different signal to noise ratio (SNR). The power angle between Area1 and Area2 is calculated as follows:

$$\delta_{\text{COI}} = \frac{\delta_1 + \delta_2}{M_1 + M_2} - \frac{\delta_3 + \delta_4}{M_3 + M_4} \quad (6.22)$$

where M_i and δ_i are the inertia time constant and power angle of generator i .

It can be seen from Fig. 6.3 that: during and shortly after the three phase fault was applied, the rotor speed oscillated dramatically with a strong nonlinear feature. Data during this period shall therefore not be used by the SSI algorithm for oscillation mode analysis and identification. Afterwards, oscillations settled down

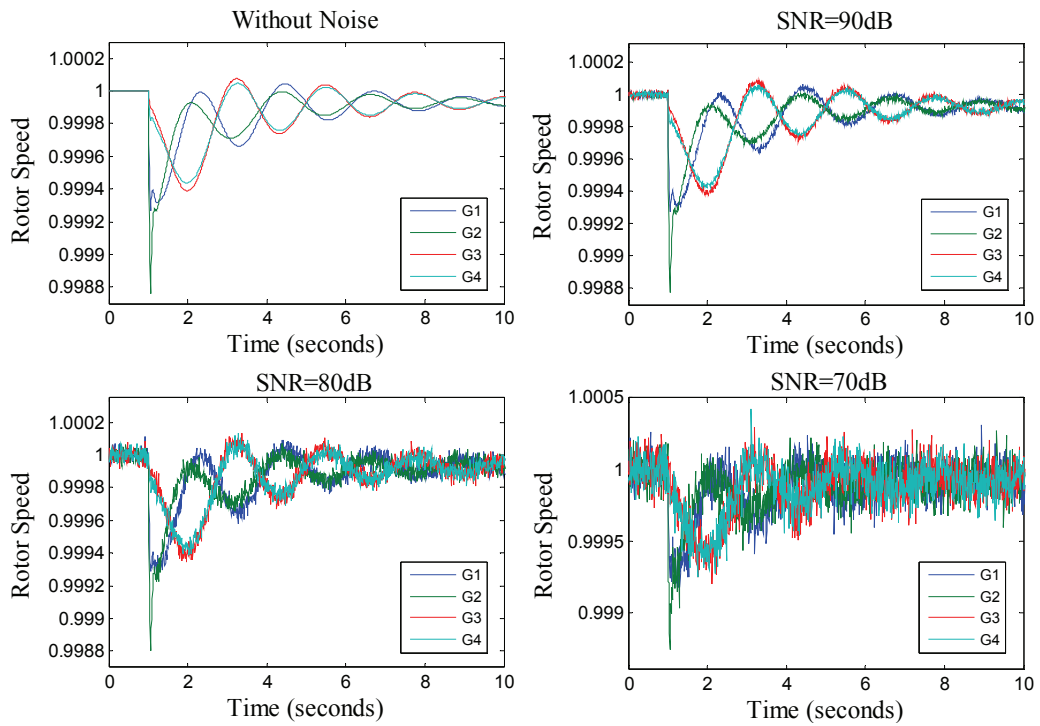


Fig. 6.3 Generator rotor speed under different SNR

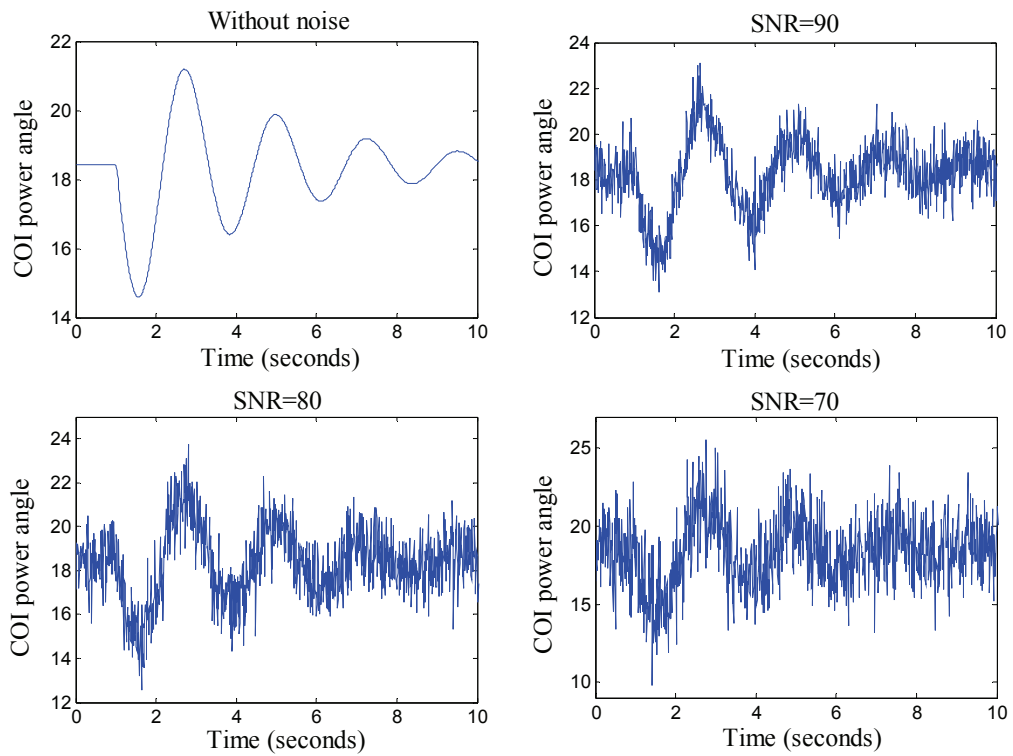


Fig. 6.4 COI power angle between Area 1 and Area 2 under different SNR

slowly. Data during this period can then be used by the SSI algorithm to identify the post-fault oscillation modes in power grid. Therefore, in the following data during fault should be discarded and only the post-fault data should be selected for use in the SSI algorithm.

Table 6.2 Identification results without noise

Method	Signal	Frequency (Hz)	Damping (%)	Elapsed Time (s)
Prony	δ_{COI}	0.4912	0.1495	0.1893
HHT	δ_{COI}	0.4884	0.1460	0.0534
SSI	$\omega_{G1} \sim \omega_{G4}$	0.4920	0.1490	0.0478

The generators' rotor speed is selected as the input of SSI algorithm and, in order to compare with the classical methods, traditional Prony and HHT oscillation identification methods are also employed to analyze the COI power angle between Area1 and Area2. Table 6.2 shows the identification results for inter-area oscillation mode of IEEE 4-generator 2-area test system by using the ideal signal without noise.

The results in Table 6.2 illustrate that the identification results of SSI algorithm is very close to the ones from Prony and HHT. It validates the effectiveness of SSI algorithm in oscillation mode identification using the ideal signal without noise. As for the computation time of those three methods as shown in Table 6.2, it can be seen that SSI is the fastest and HHT is slight slower while Prony is significantly slower. This shows that the SSI algorithm is more efficient than the other oscillation mode identification methods. As for the reliability in identifying the oscillation mode, because these three methods do not involve iteration or simulation, the oscillation mode identified by these three methods is certain.

However, in the real power system, noise is inevitable in measurement data. Investigation shows that the accuracy of Prony and HHT are sensitive to noise while noise brings relatively little impact to the results of SSI algorithm. Table 6.3, 6.4 and 6.5 show the identification results for signals with various amount of white noise added (SNR = 90, 80 and 70).

Table 6.3 Identification results with noise (SNR=90)

Method	Signal	Frequency (Hz)	Damping (%)
Prony	δ_{COI}	0.4879	0.1399
HHT	δ_{COI}	0.5052	0.1422
SSI	$\omega_{G1} \sim \omega_{G4}$	0.4967	0.1490

Table 6.4 Identification results with noise (SNR=80)

Method	Signal	Frequency (Hz)	Damping (%)
Prony	δ_{COI}	0.4643	0.2048
		1.6774	0.0949
HHT	δ_{COI}	0.4294	0.2126
		0.2555	-0.1676
SSI	$\omega_{G1} \sim \omega_{G4}$	0.4970	0.1464

Table 6.5 Identification results with noise (SNR=70)

Method	Signal	Frequency (Hz)	Damping (%)
Prony	δ_{COI}	0.5337	0.1959
		1.8169	0.3503
HHT	δ_{COI}	0.3682	0.2165
		0.4317	-0.0261
SSI	$\omega_{G1} \sim \omega_{G4}$	0.4907	0.1442

Comparing Table 6.3, 6.4 and 6.5 with Table 6.2, the results indicate that the identification accuracy of Prony and HHT gradually reduce with the decrease of SNR. However, since disturbance is treated as white noise in SSI, the SSI algorithm copes well with noise. The results in Table 6.2, 6.3, 6.4 and 6.5 show that the impact of noise on the oscillation mode parameters identified by SSI algorithm is little.

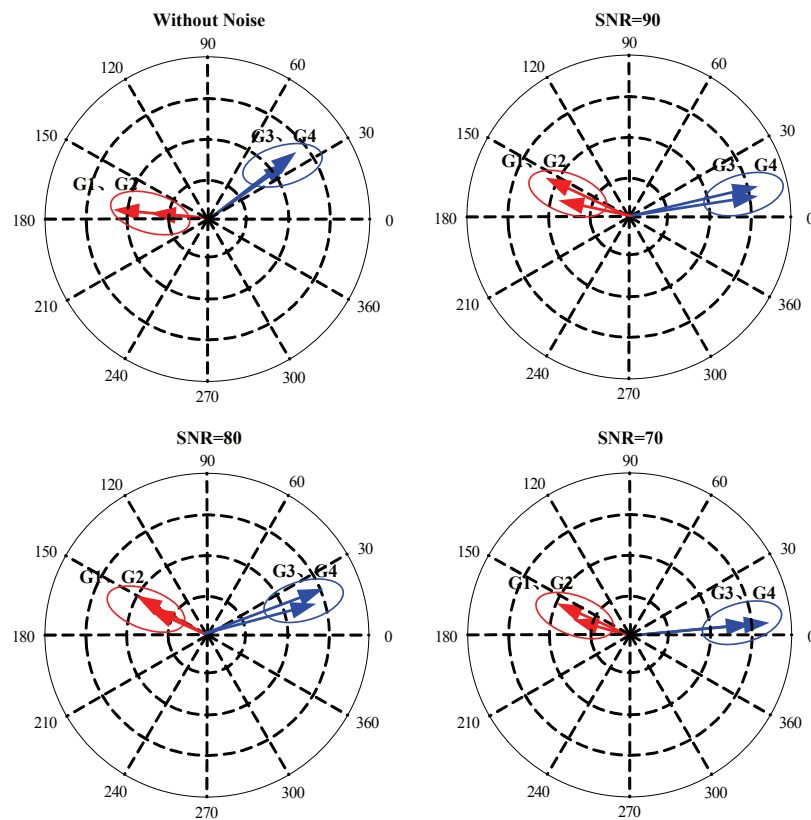


Fig. 6.5 Effects of noise on power system low-frequency oscillation mode shape

By employing SSI algorithm, the oscillation mode shape can be obtained at the same time with the mode parameters. The oscillation mode shapes of IEEE four-generator two area test system for signals with different signal to noise ratio are shown in Fig. 6.5.

In summary, the SSI algorithm can accurately identify the power system low-frequency oscillation mode parameters and oscillation mode shape, and can effectively cope with the noise in measured data.

6.5.3 16-GENERATOR 5-AREA TEST SYSTEM

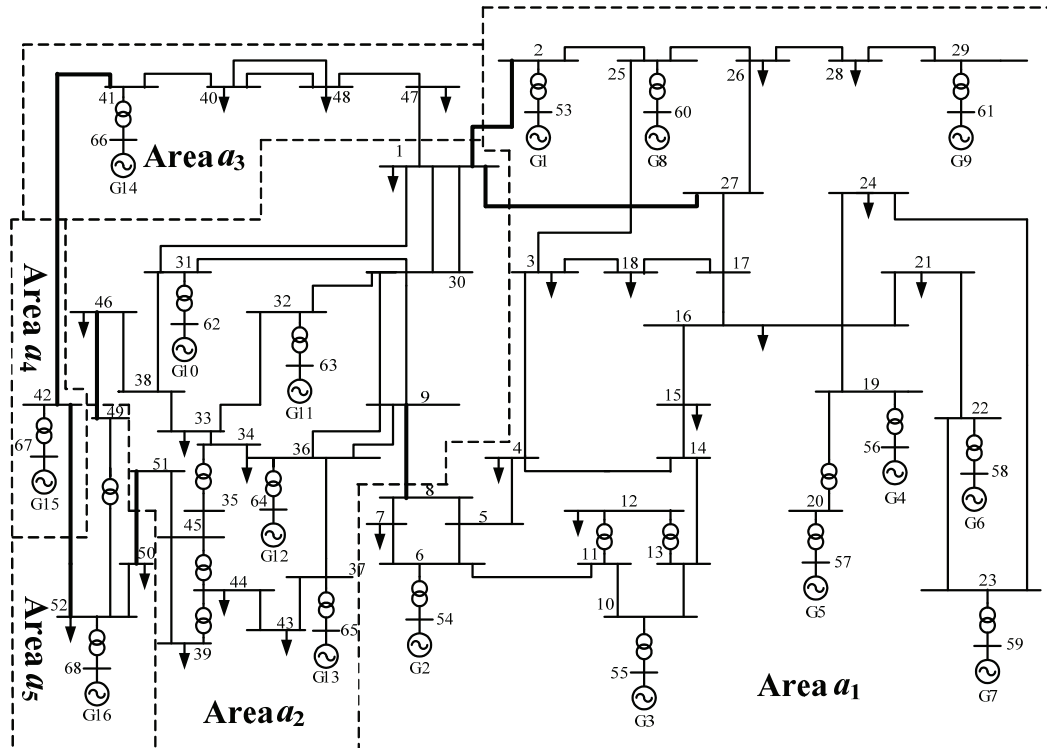


Fig. 6.6 IEEE 16-generator 5-area test system

Fig. 6.6 shows the IEEE 16-generator 5-area test system. Data for this system was taken from [22]. According to the results in [13], this 16 generator system can be divided into 5 areas, namely, a_1 – New England (G1-G9), a_2 – New York (G10-G13), a_3 – Equivalent Generator G14, a_4 – Equivalent Generator G15, and a_5 – Equivalent Generator G16. For simplicity and convenience, only the inter-area oscillation modes would be considered and analyzed here. Table 6.6 shows the eigenvalues of the two inter-area oscillation modes obtained from the small signal stability analysis in the PSASP package.

Table 6.6 Inter-area oscillation modes of IEEE 16-generator 5-area test system

Mode	Real	Imag	Frequency (Hz)	Damping (%)
1	-0.139	2.9412	0.4681	4.72
2	-0.1672	4.8582	0.7732	3.34

Case A: Small Disturbance

In Case A, a small disturbance was introduced on bus 33 by reducing the active power load on bus 33 to half for 1s. By employing the rotor speed of 16 generators and SSI identification method, two inter-area oscillation mode parameters and shapes were obtained and are shown in Fig 6.7 and Table 6.7, respectively.

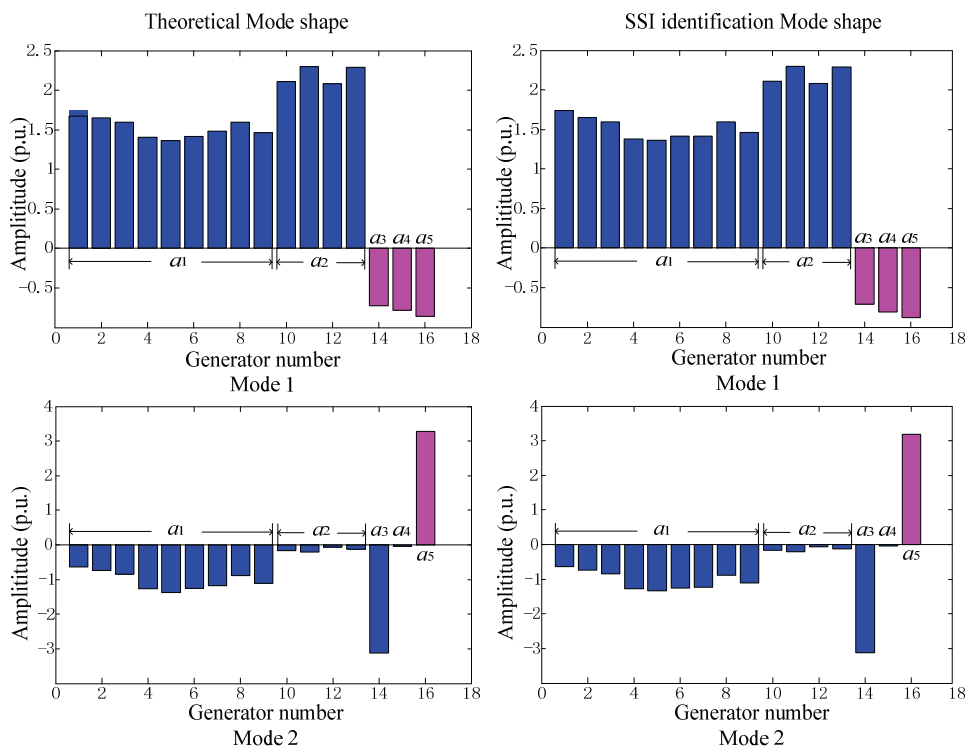


Fig. 6.7 SSI identification mode shapes in Case A

Table 6.7 SSI identification results of Case A (Bus 33)

Mode	Frequency (Hz)	Damping (%)
1	0.4685	4.73
2	0.7734	3.36

Comparing Table 6.6 with Table 6.7, it can be seen that the SSI identification results are very close to the theoretical mode parameters. Fig. 6.7 shows that the inter-area oscillation mode shapes identified by SSI identification method are nearly the same as the theoretical mode shapes.

The same disturbance on bus 33 was applied to bus 12 and 28 in turn. Similar SSI identification results were obtained and are shown in Table 6.8.

Table 6.8 SSI identification results of Case A (Bus 12 and Bus 28)

Mode	Bus 12		Bus 28	
	Frequency (Hz)	Damping (%)	Frequency (Hz)	Damping (%)
1	0.4679	4.68	0.4683	4.71
2	0.7728	3.27	0.7731	3.32

The results indicate that SSI can accurately identify the mode parameters and mode shapes after small disturbance from the generator rotor speed.

Case B: Large Disturbance

In Case B, a three phase ground fault was applied to bus 17 at time 1s and cleared at 1.1s. By employing the rotor speed of 16 generators and SSI identification method, two inter-area oscillation mode parameters were obtained as shown in Table 6.9.

Table 6.9 SSI identification results of Case B (Bus 17)

Mode	Frequency (Hz)	Damping (%)
1	0.4960	3.52
2	0.7969	3.65

It can be seen that the differences between the SSI identification result and theoretical results are slightly larger than that in Case A. Fig. 6.8 shows that between the inter-area oscillation mode shapes identified by SSI identification method and the theoretical mode shapes, the participant generators are the same, but the participant degree of generator is different.

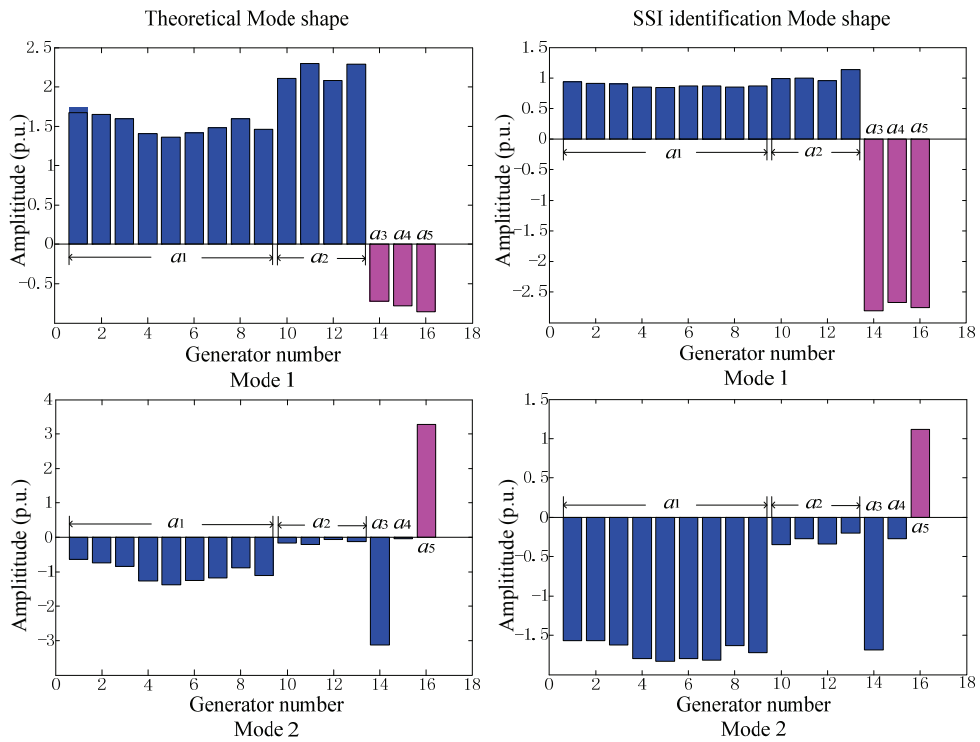


Fig. 6.8 SSI identification mode shapes in Case B

The same fault as applied to bus 17 was then applied to bus 1 and 48 separately instead. Similar identification results were obtained and are shown in Table 6.10.

Table 6.10 SSI identification results of Case B (Bus 1 and Bus 48)

Mode	Bus 1		Bus 48	
	Frequency (Hz)	Damping (%)	Frequency (Hz)	Damping (%)
1	0.4956	3.49	0.4955	3.47
2	0.7962	3.61	0.7965	3.63

The above results indicate that oscillation modes would change in power system for different faults, and therefore, power system low-frequency oscillation should be monitored on-line so that proper control actions can be taken on demand as soon as possible.

6.6 SUMMARY

In this chapter, the SSI algorithm is adopted to analyze the power system low-frequency oscillation using measured data. Based on WAMS and by employing the SSI algorithm, the oscillation mode parameters and mode shape can be accurately obtained. Simulation results showed that the adopted SSI algorithms indeed have high resistance to noise as compared to Prony and HHT methods. The results for the 16-generator 5-area test system showed that the SSI algorithm is a highly effective tool for power system low-frequency oscillation analysis.

With the maturity of WAMS technology, WAMS base SSI algorithm can be used to identify the power system low-frequency oscillation online and would form a solid platform for WAMS based power system low-frequency oscillation analysis and control. In the next chapter, based on the power system low-frequency oscillation identification results by the SSI algorithm, a WAMS based on-line wide-area damping analysis and control scheme is proposed.

CHAPTER VII ADAPTIVE WIDE-AREA DAMPING CONTROL SCHEME WITH SSI AND SIGNAL TIME DELAY COMPENSATION

7.1 INTRODUCTION

With the increasing large interconnection of power grids, low-frequency oscillation has become one of the most severe threats for the safe and economic operation of modern power system [136, 177]. Up to now, the research on Power System Stabilizer (PSS) with local input signal has been of maturity. Though this type of PSS is effective in damping local oscillation modes, its effectiveness in damping inter-area mode is limited [214]. With the advent of PMU, which can offer real-time measurements of power system operation state with a satellite triggered time stamp in time intervals down to 20ms [159], and the rapid development of WAMS, various WAMS based PSSs have been designed to suppress inter-area oscillation modes [105-107, 109, 110, 215-219].

Based on synchronized phasors from WAMS, a coupled vibration model including the effect of PSS has been successfully used to tune PSS in [216]. However, such method based on the exact model of power system could only be used off-line and would provide little information to on-site power system operators. As a remedy, online methods based on Prony [217] and H_∞ [218] analysis have been proposed recently for online low frequency oscillation analysis and control. Nevertheless, these methods cannot effectively identify all the oscillation modes online and have not considered the effect of signal time delay which may severely deteriorate their control performance [107, 219]. Though LMI [105, 110] and H_∞ [106, 109] methods could be used to design PSS accounting for various time delays, complex treatment of time delay would not

only increase the processing time but also reduce the practicability of wide-area damping control.

On-line wide-area PSS design can be categorized into direct and passive approach. Direct tuning refers to online changing of PSS parameters to achieve higher controllability of inter-area oscillations; whereas, passive design focuses on optimizing the observability of the PSS by varying the input signals of PSS. Though both approaches can enhance the stability of inter-area mode, passive designs have not been widely explored yet. Since varying PSS parameters require extensive studies prior to implementation and is a computational exhaustive procedure, the forte of passive strategy is that the control design is less complex. Therefore, the motivation of this chapter is to investigate the possibility of an online PSS control design by solely optimizing the observability towards inter-area oscillations. This is to ensure that modifications to the existing grid could be minimized. The objective is to adaptively adjust the input remote signals being fed into the PSS in accordance to the present grid operating condition.

This chapter presents a novel wide-area damping control scheme in which (1) the robust SSI algorithm is adopted to identify inter-area oscillation modes online so as to derive the wide-area input signal of the PSS, and (2) a simple but practical time delay compensator is designed to eliminate the effects of signal transmission time delay. Simulations on IEEE 4-generator 2-area and IEEE 16-generator 5-area test systems have validated the effectiveness of the proposed adaptive wide-area damping control scheme.

7.2 ADAPTIVE WIDE-AREA DAMPING CONTROL SCHEME

Fig. 7.1 shows the proposed adaptive wide-area damping control scheme with online system identification and consideration of signal time delay. It is built on

the infrastructure established for the wide-area monitoring and control system in smart grid. All PMU equipped generators are monitored with frequency deviation $\Delta\omega$ measured and transmitted to the wide-area damping control center via the PMU data collection system.

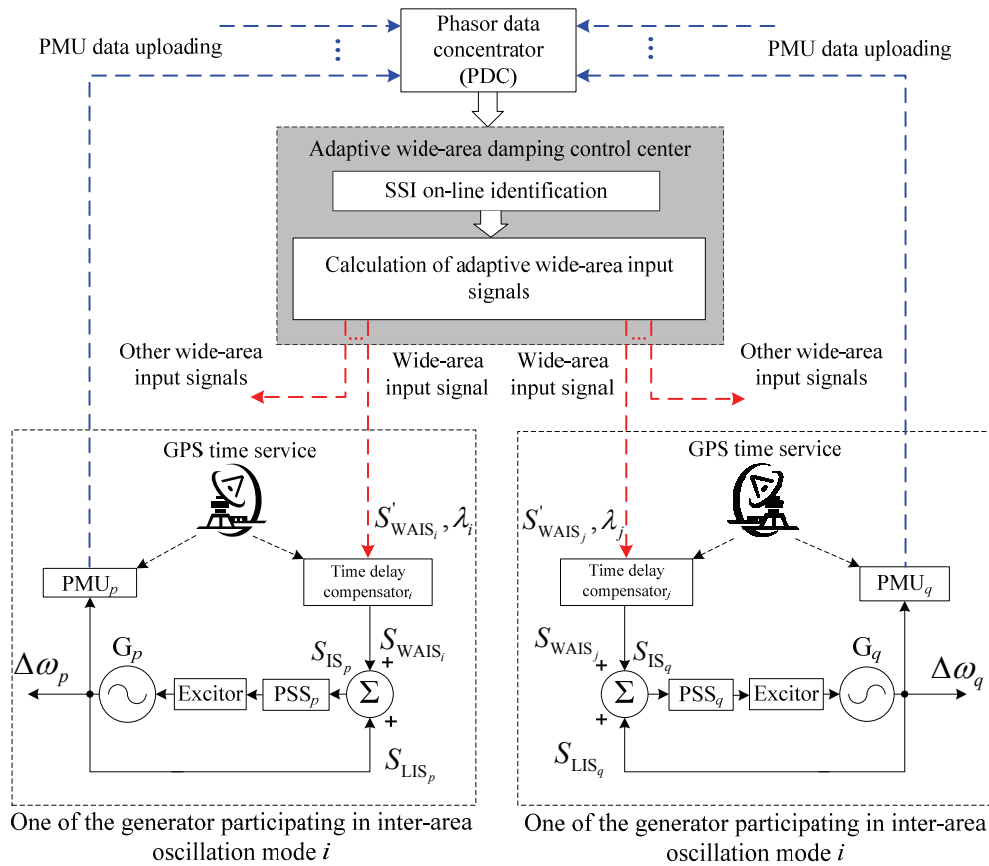


Fig. 7.1 Adaptive wide-area damping control Scheme

In case low-frequency oscillation arises, local signal and WAMS based wide-area signals would be combined as the input signal of PSS to suppress the local and inter-area oscillation modes. The suppression mechanism adopted here is that (1) low-frequency inter-area oscillation modes and the corresponding generator oscillation groups will first be identified online based on the SSI; (2) for each inter-area oscillation mode, a wide-area input signal (WAIS) will be derived to suppress the oscillation; and (3) this WAIS, S'_{WAIS} , will be combined with the local input signal (LIS) as the input signal of the PSSs installed in all the

generators participating in a specific inter-area oscillation mode and be compensated locally for the transmission time delay as shown in Fig. 7.2.

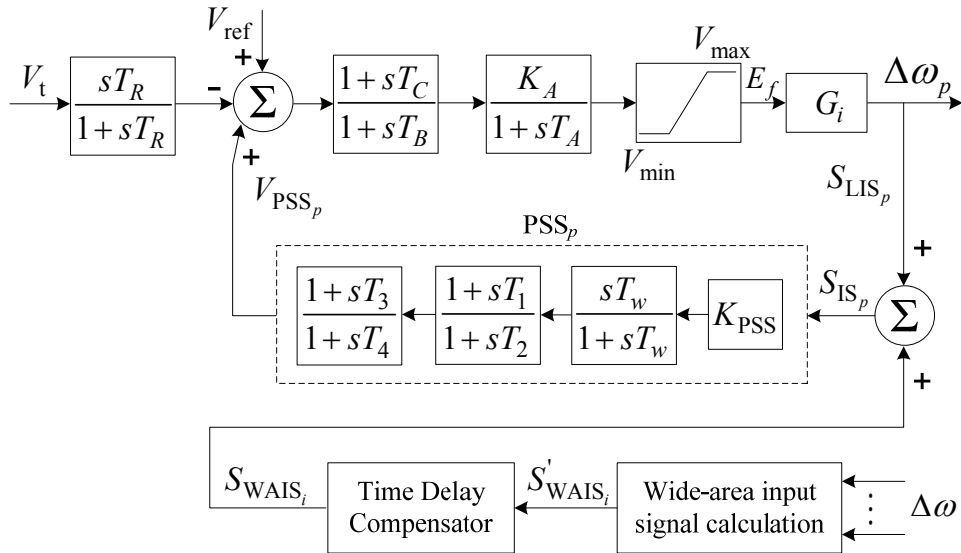


Fig. 7.2 Exciter model of one generator participating in a specific inter-area oscillation mode with PSS combining local and wide-area input signals

Fig. 7.2 shows the exciter model of one of the generators participating in the inter-area oscillation mode i with a PSS combining local and wide-area input signals. This PSS serves the following two functions [220]: (1) both local and inter-area oscillation modes can be suppressed; (2) in case the wide-area input signal fails because of lost of PMU data or communication network failure, the PSS with only the local input signal remains operational and capable to suppress local oscillation modes and supply damping to the inter-area oscillation modes. In case active power was selected instead of frequency as the local PSS input signal, an additional gain would be needed after the time delay compensator to ensure the compatibility of wide-area signal and the local signal.

The proposed adaptive wide-area damping control scheme mainly composes of following three parts: SSI algorithm, wide-area signal formulation and signal time delay compensation. While SSI algorithm has been introduced in the

previous chapter, detail description on the later two parts will be given in the following two sections.

7.3 WIDE-AREA INPUT SIGNAL FORMULATION

When low-frequency oscillations are detected and identified in the power system, a wide-area input signal will be fed to the PSSs installed in the generator oscillation clusters in order to reinforce the damping torque of the targeted inter-area oscillation modes which have insufficient damping.

Oscillating generator clusters would first be identified from the mode shape matrix Φ . For each oscillation mode i , signals from the corresponding cluster pair consisting of p and q generators would be used to synthesise the following wide-area control signal $\Delta\omega_i$ and feed to all the generators participating in oscillation mode i determined by the mode shape matrix Φ .

$$\Delta\omega_i = \frac{\sum_{j=1}^p H_j \Delta\omega_j}{\sum_{j=1}^p H_j} - \frac{\sum_{j=1}^q H_j \Delta\omega_j}{\sum_{j=1}^q H_j} \quad (7.1)$$

where H_j is the inertia constant of generator j .

7.4 SIGNAL TIME DELAY COMPENSATION

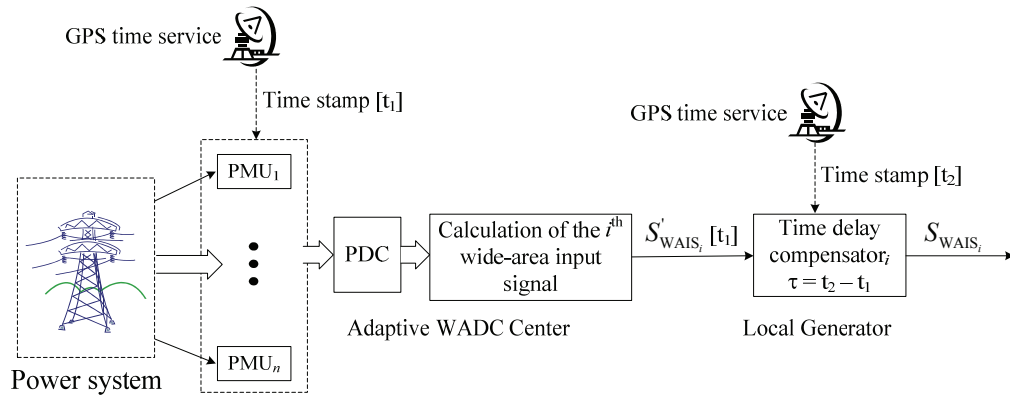


Fig. 7.3 Scheme of signal time delay compensator

The signal time delay, mainly introduced by the long distance transmission of

the wide-area input signal from the adaptive wide-area damping control center to the target generator, is significant and shall be compensated locally as shown in Fig. 7.1 and further illustrated in Fig. 7.3 with details.

Accurate time from the GPS would be received locally in both PMUs and time delay compensator. Wide-area phasors measured by the PMUs at time t_1 are collected and resynchronized by the PDC and in turn processed to generate the wide-area input signal S'_{WAIS_i} with time stamp $[t_1]$. When the local time delay compensator, which is installed close to the PSS, receives the input signal $S'_{\text{WAIS}_i}[t_1]$, the signal will be re-labeled with a new time stamp $[t_2]$ freshly obtained from the GPS and the exact time delay can be calculated accurately as $\tau = t_2 - t_1$ because of the high resolution time service provided by the GPS.

Once the exactly time delay is known, the time delay can be modeled and compensated as shown in Fig. 7.4.

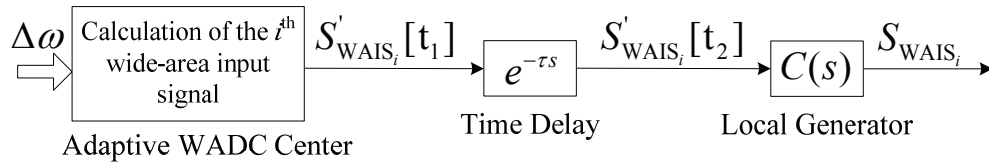


Fig. 7.4 Time delay modeling and compensation

When a PSS is added to the j^{th} generator, the change of the i^{th} eigenvalue λ_i associating with i^{th} oscillation mode is [215]:

$$\Delta\lambda_i = H_{\text{WADC}_i}(\lambda_i)R_i \quad (7.2)$$

With the time delay taking into consideration, the change of λ_i would become:

$$\begin{aligned} \Delta\lambda'_i &= e^{-\lambda_i\tau} H_{\text{WADC}_i}(\lambda_i)R_i \\ &= e^{-\lambda_i\tau} \Delta\lambda_i = e^{-\sigma_i\tau} e^{-j\omega_i\tau} \Delta\lambda_i = \gamma_i e^{-j\varphi_i} \Delta\lambda_i \end{aligned} \quad (7.3)$$

where $\gamma_i = e^{-\sigma_i\tau}$ and $\varphi_i = \omega_i\tau$. This means the signal time delay effects on the displacement of λ_i can be decomposed into gain drift of γ_i and phase lag of φ_i . If λ_i is passed to the local generator along with the wide-area input signal

$S'_{\text{WAIS}_i}[t_1]$, the time delay could be compensated locally using the following transfer function with parameters tuned as follows [221]:

$$C(s) = K_c \left(\frac{1 + sT_{C1}}{1 + sT_{C2}} \right)^2 \quad (7.3)$$

where $K_c = \frac{1}{\gamma_i}$, $\alpha_c = \frac{1 - \sin(\varphi_i/2)}{1 + \sin(\varphi_i/2)}$, $T_{C2} = \frac{1}{\omega_i \sqrt{\alpha_c}}$, $T_{C1} = \alpha_c T_{C2}$

7.5 CONTROL FLOW OF ADAPTIVE WIDE-AREA DAMPING CONTROL SCHEME

Fig. 7.5 shows the overall flow chart of the proposed adaptive wide-area damping control scheme which mainly consists of the SSI algorithm, calculation of wide-area input signal and time delay compensator outlined in previous sections. The control algorithm operates on windows of WAMS data with cycle time T_{SSI} (the width of the window) and could be triggered by timer, events or operator. The following are the major steps involved in a cycle.

- Step 1: Apply the SSI algorithm on a window of WAMS data collected in last cycle to identify the inter-area oscillation modes whose oscillation frequency is around 0.1-0.7 Hz.
- Step 2: If there are large oscillations with damping below, say 5% [13], proceed to the following step to activate the adaptive wide-area damping control; otherwise, wait till next cycle while collecting WAMS data and return to Step 1.
- Step 3: Identify the m inter-area oscillation modes with insufficient damping and the corresponding oscillation generator group pair for each oscillation mode.
- Step 4: Calculate the wide-area input signals $S'_{\text{WAIS}_i}[t_1]$ which will be sent to the corresponding PSSs installed in the generator oscillation clusters

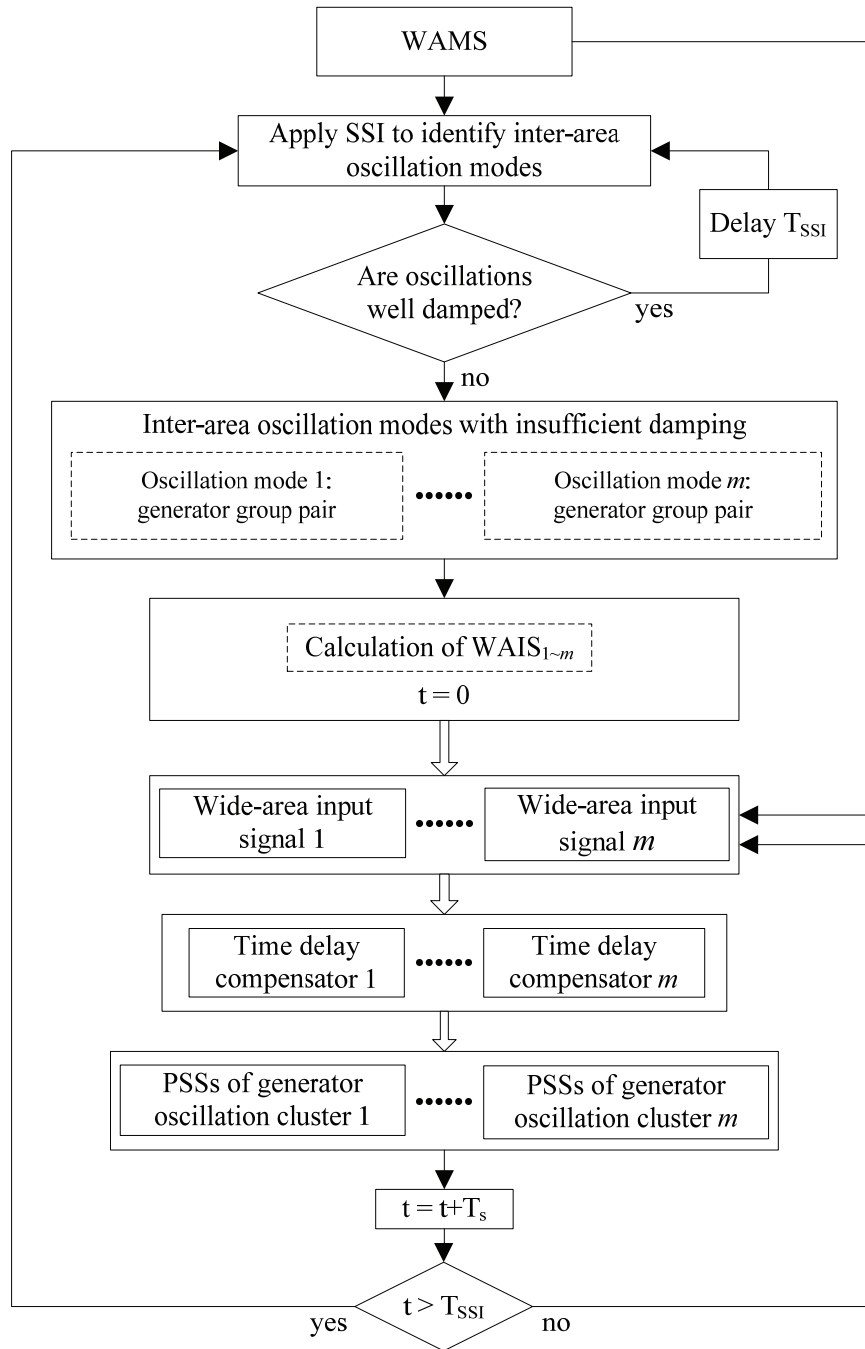


Fig. 7.5 Flow chart of the proposed adaptive wide-area damping control scheme together with λ_i , according to Equation (7.1) using the current WAMS information.

Step 5: Measure the signal time delay locally in the generator with the help of high resolution GPS time service and apply the signal time delay compensation to produce the required wide-area input signal S_{WAIS_i}

feeding to the PSSs installed in the generator oscillation clusters for the i^{th} inter-area oscillation mode in order to increase damping of the targeted inter-area oscillation mode.

Step 6: Increment t by one time-step T_s and go back to Step 4 to continue the control action until next cycle.

Step 7: Go back to Step 1 to start a new cycle of adaptive wide-area control.

7.6 CASE STUDIES

The IEEE 4-generator 2-area test system shown in Fig. 6.2 and the IEEE 16-generator 5-area test system shown in Fig. 6.6 were selected as the benchmark systems for evaluating the performance of the proposed adaptive wide-area damping control scheme with consideration of signal time delay.

7.6.1 4-GENERATOR 2-AREA TEST SYSTEM

This test system consists of two identical areas connected via two long transmission lines. In each area, there are two generators located at buses 1 and 2 in area 1 and at buses 11 and 12 in area 2. The loads are at bus 4 in area 1, and at bus 14 in area 2. Bus 1 is assigned as the swing bus. The four generators are equipped with static exciters, turbine/governors, and local PSSs. While the complete set of system data is taken from in [13], the gain of the PSS is modified to a relatively low value, i.e. $K_{\text{PSS}} = 30$, so as to clearly illustrate the effectiveness of WADC.

In order to fully test the effectiveness of the proposed adaptive wide-area damping control scheme, the following two representative disturbances are considered:

Case a: small disturbance – the active power load at bus 4 is increased by 20% at time $t = 1\text{s}$ and then restore back to the original value at time $t = 2\text{s}$.

Case b: large disturbance – a solid 3-phase fault occurs in the beginning of one of lines between bus 3 and 101 at time $t = 1s$ and is cleared with the faulty line tripped after 0.04s.

(1) SSI Low-frequency Oscillation Mode Identification

For the two simulation cases considered in the IEEE 4-generator 2-area test system, just as illustrated in the control flow of adaptive wide-area damping control scheme shown in Fig. 7.6, when oscillation is detected, SSI algorithm is used to identify the low-frequency oscillation modes. The identification results as listed in Table 7.1 match well with the ones obtained with the modal analysis.

Table 7.1 Identification results for IEEE 4-generator 2-area test system

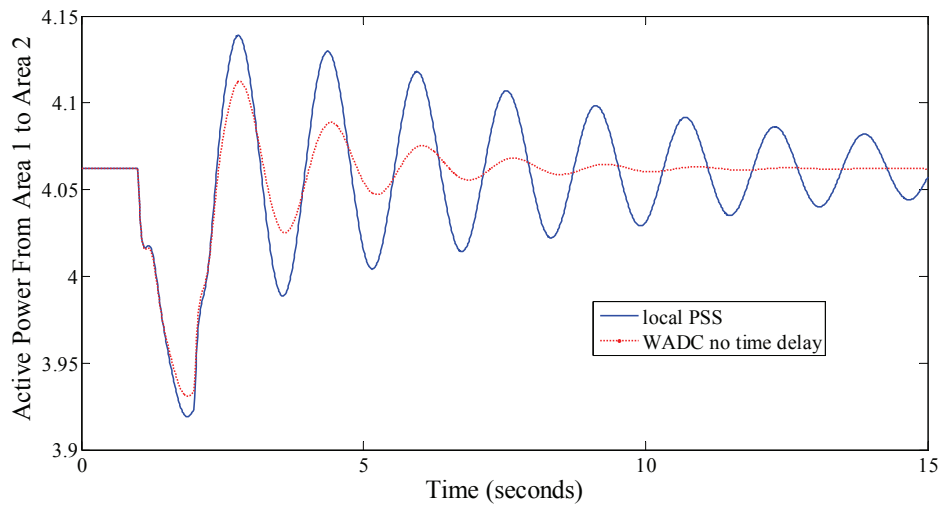
Inter-area oscillation mode	Case	Method	Frequency (Hz)	Damping (%)	Oscillation generator clusters
Inter-area mode	a	Modal Analysis	0.63051	3.1791	(G1,G2) vs (G3,G4)
		SSI	0.63087	3.1841	
	b	Modal Analysis (after line trip)	0.47694	4.3584	
		SSI	0.50022	4.1779	

(2) Effectiveness of Adaptive Wide-area Damping Control

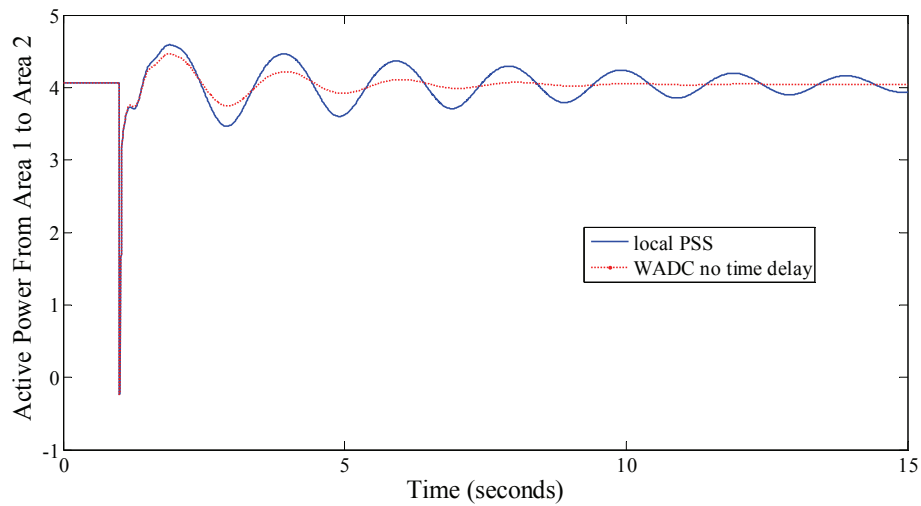
According to the results from SSI, it is shown that in the inter-area mode, generators (G1 and G2) in area 1 oscillate against generators (G3 and G4) in area 2. Thus WADCs are implemented on generators G1, G2, G3 and G4, and their inputs are set according to Equation (7.1), and the parameters of WADCs are the same as the local PSSs without considering signal transmission time delay. The active powers from area 1 to 2 in Case a and b with and without WADC are plotted in Figure 7.6.

It is clear that, because of insufficient damping in the inter-area oscillation

modes, the power system would take a long time to settle down in both Case *a* and *b* if only the local PSSs were installed. However, with the help of the proposed adaptive WADCs, oscillations were suppressed quickly in both cases in this IEEE 4-generator 2-area test system.



(a) Case a



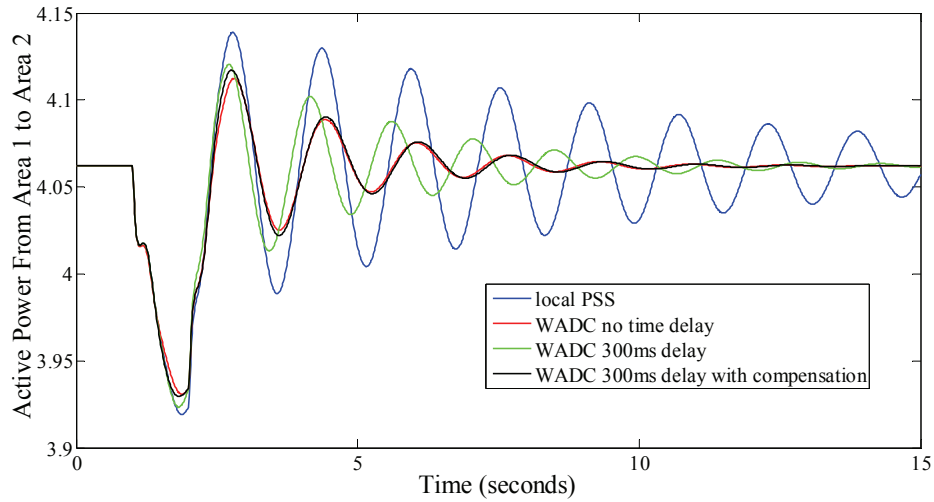
(b) Case b

Fig. 7.6 Active powers from area 1 to 2 in Case a and b

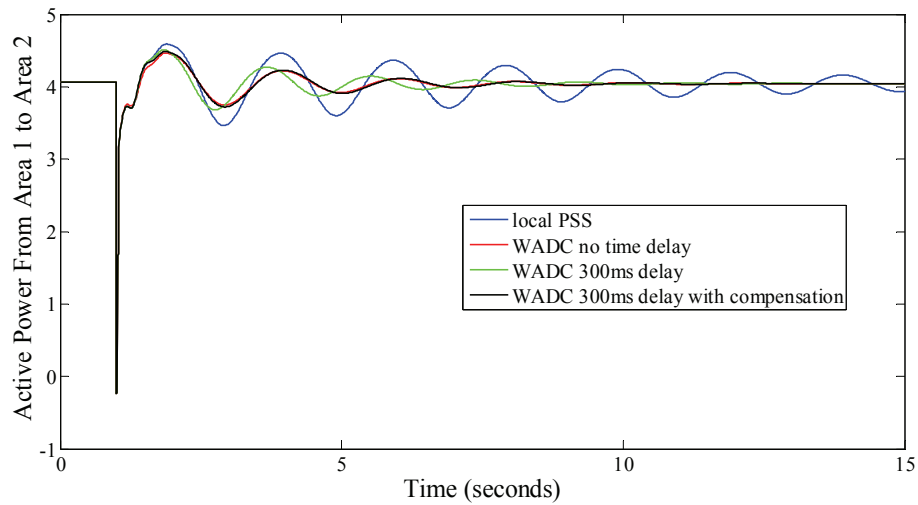
(3) Signal Time Delay Compensation

Because of the wide spread of the inter-connected power system, signal transmission delay cannot be ignored. Typically, the signal time delay in WAMS

is in the order of 100ms but could be longer if communication links are busy and congested. In this study, the signal time delay is set to 300ms. The active powers from area 1 to 2 in Case a and b with signal time delay are plotted in Figure 7.7.



(a) Case a



(b) Case b

Fig. 7.7 Active powers from area 1 to 2 in Case a and b with signal time delay

It is clear that, when the signal time delay was included but not compensated, the effectiveness of the wide-area control was severely deteriorated; whereas, the responses for including signal time delay and compensation was very close to the ones without including any signal time delay. This shows that the proposed

signal time delay compensation works well and is capable to produce good results in this IEEE 4-generator 2-area test system.

7.6.2 16-GENERATOR 5-AREA TEST SYSTEM

The large 16-generator 5-area test system as shown in Fig. 6.6 are then selected for further evaluating the performance of the proposed adaptive wide-area damping control scheme with consideration of signal time delay. Local PSSs are equipped in generator G1~G12.

It is noteworthy that because of the complex interactions of large power system, WADCs considering time delay may have adverse effect to the local modes, thus a low pass filter block is added in the WADC control loop to eliminate the adverse effect.

In order to fully test the effectiveness of the proposed adaptive wide-area damping control scheme, the following two operation scenarios are considered:

(A) Operation scenario 1:

In this operation scenario, the inter-area mode, (G1~G13) vs (G14~G16), is the critical mode and is excited by the following disturbances:

Case a: small disturbance – the active power load at bus 51 is increased by 20% at time $t = 0.6s$, and then restores to the original value after 1s.

Case b: large disturbance – a solid 3-phase fault occurs in the beginning of the line between bus 1 and 2 at time $t = 0.6s$, and is cleared with the faulty line tripped after 0.02s.

(B) Operation scenario 2:

In this operation scenario, the inter-area mode, (G1~G9) vs (G10~G13), is the critical mode and is excited by the following disturbances:

Case a: small disturbance – the active power load at bus 1 is increased by 20% at time $t = 0.1s$, and then restores to the original value after 1s.

Case b: large disturbance – a solid 3-phase fault occurs in the beginning of the line between bus 1 and 27 at time $t = 0.1$ s, and is cleared with the faulty line tripped after 0.1s.

In the following subsections, the above two operation scenarios would be analyzed as the previous study on the IEEE 4-generation 2-area test system.

(A.1) SSI Low-frequency Oscillation Mode Identification for Operation Scenario 1

Table 7.2 lists the SSI low frequency oscillation identification results obtained with SSI and modal analysis for the IEEE 16-generator 5-area test system in operation scenario 1. In Case a, the frequency and damping results from both methods are match well. In Case b, there is a slight discrepancy in the damping results while the frequency matches well.

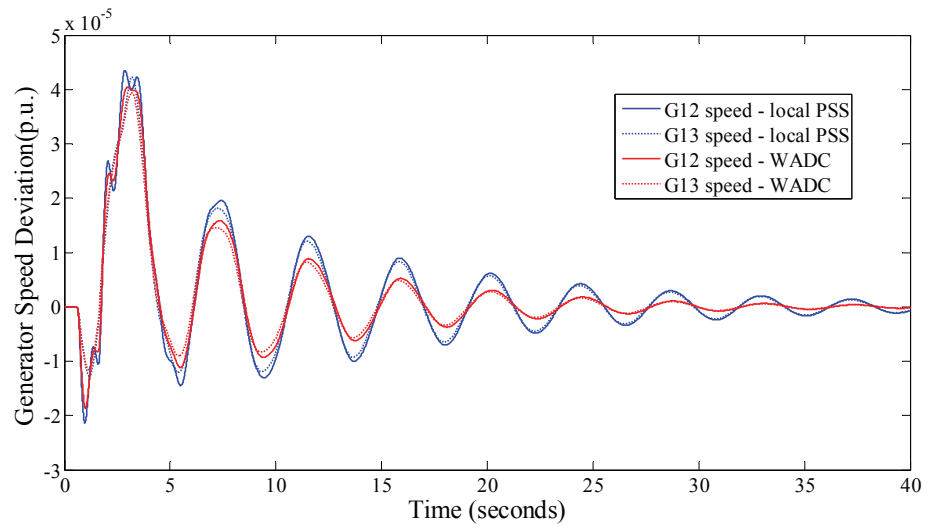
Table 7.2 Identification results for IEEE 16-generator 5-area test system in Scenario 1

Inter-area oscillation mode	Case	Method	Frequency (Hz)	Damping (%)	Oscillation generator clusters
Inter-area mode	a	Modal Analysis	0.23586	5.6477	(G1~G13) vs (G14~G16)
		SSI	0.23414	5.7648	
	b	Modal Analysis (after line trip)	0.22347	3.2303	
		SSI	0.22584	5.1423	

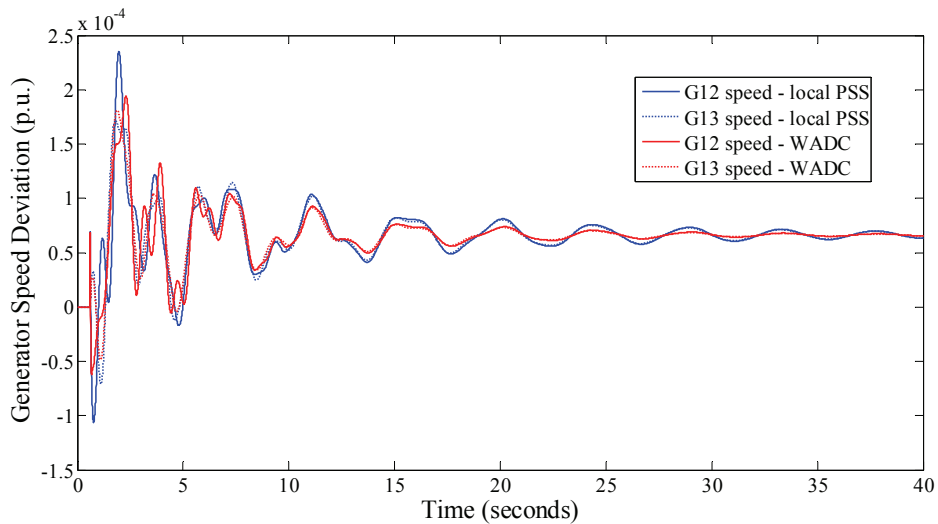
(A.2) Effectiveness of Adaptive Wide-area Damping Control for Operation Scenario 1

The results from SSI shows that generator cluster G1~G13 oscillates against generator cluster G14~G16 in this inter-area mode. Since only generators G1~G12 are equipped with local PSSs and the proposed WADC is built on the existing

local PSSs, WADCs are therefore implemented on generators G1~G12 with input set according to (7.1) and parameters being the same as the local PSSs, i.e. no signal time compensation. In addition, generators G1~G12 were the ones participated in the low-frequency oscillation mode identified by the SSI algorithm. In general, any generator equipped with local PSS and participates in a low-frequency oscillation mode should be controlled.



(a) Case a

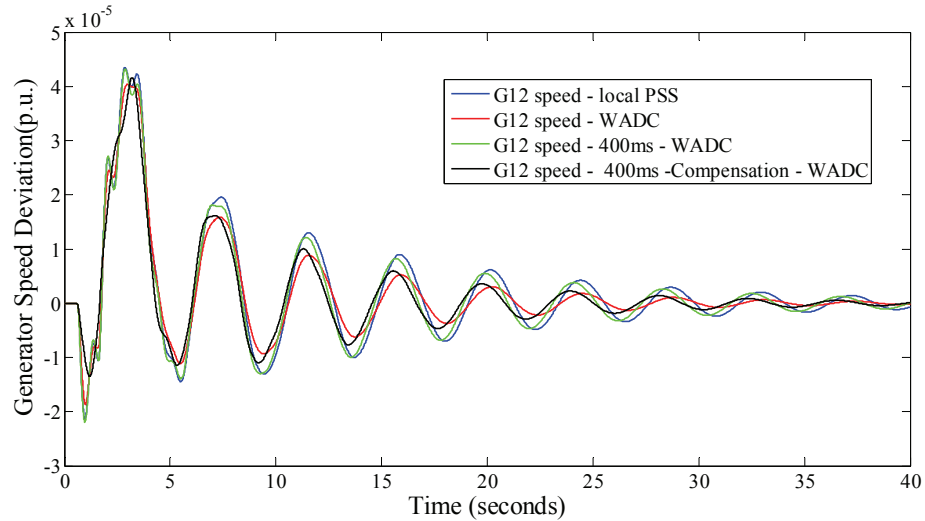


(b) Case b

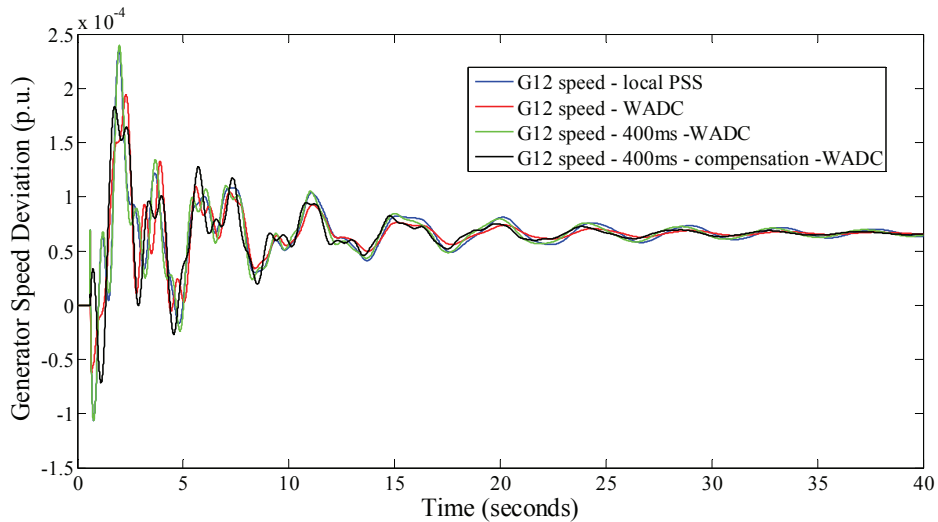
Fig. 7.8 Rotor speed deviations of G12 and G13 in Case a and b under operation scenario 1

The rotor speed deviations of G12 and G13 are plotted in Figure 7.8. While the system damping is improved with the help of WADCs, improvements in Case a are more noticeable.

(A.3) Signal Time Delay Compensation for Operation Scenario 1



(a) Case a



(b) Case b

Fig. 7.9 Rotor speed deviations of G12 in Case a and b under operation scenario 1 with signal time delay

In this simulation test, the signal time delay of 400ms is added. The rotor speed deviations of G12 with and without the addition of WADCs and the consideration

of signal time delay are plotted in Figure 7.9. It shows that the effectiveness of the WADCs is significantly deteriorated without the time delay compensation and the proposed time delay compensation scheme works well.

(B.1) SSI Low-frequency Oscillation Mode Identification for Operation Scenario 2

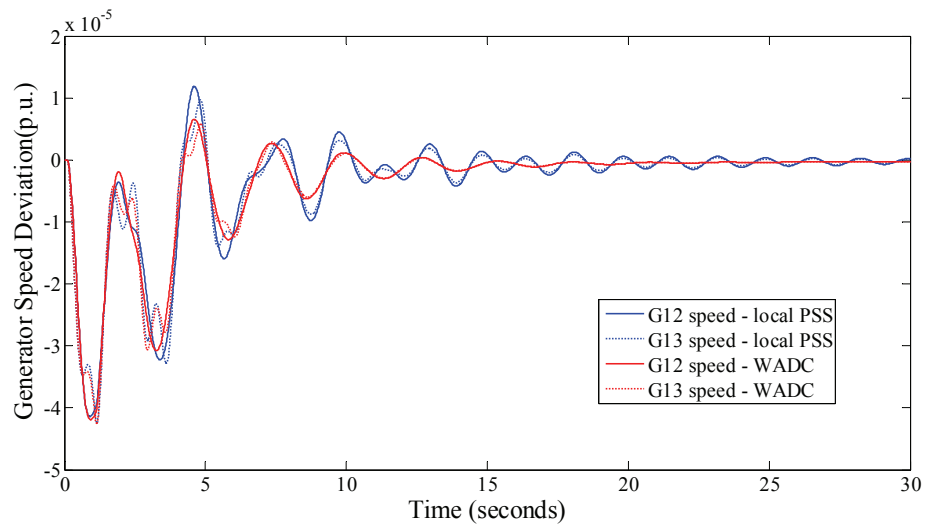
Table 7.3 lists the SSI low frequency oscillation identification results obtained with SSI and modal analysis for the IEEE 16-generator 5-area test system in operation scenario 2. In both cases, the frequency and damping results from both methods match well.

Table 7.3 Identification results for IEEE 16-generator 5-area test system in Scenario 2

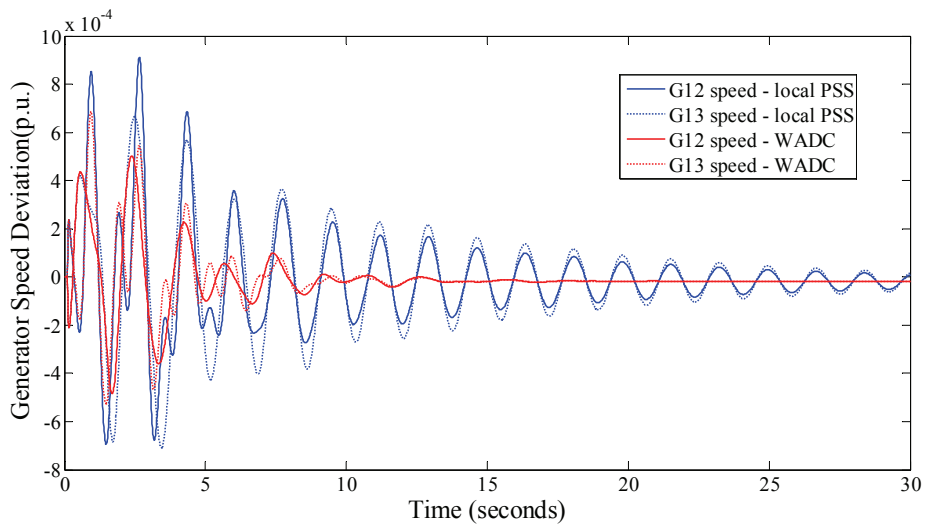
Inter-area oscillation mode	Case	Method	Frequency (Hz)	Damping (%)	Oscillation generator clusters
Inter-area mode	a	Modal Analysis	0.59228	2.605	(G1~G9) vs (G10~G13)
		SSI	0.59224	2.617	
	b	Modal Analysis (after line trip)	0.58071	2.719	
		SSI	0.58118	2.668	

(B.2) Effectiveness of Adaptive Wide-area Damping Control for Operation Scenario 2

The results from SSI shows that generator cluster G1~G9 oscillates against generator cluster G10~G13 in this inter-area mode. WADCs are therefore implemented on generators G1~G12 with input set according to Equation (7.1) and parameters being the same as the local PSSs, i.e. no signal time compensation. The rotor speed deviations of G12 and G13 are plotted in Figure 7.10. In both cases, the system damping is significantly improved with the help of WADCs.



(a) Case a

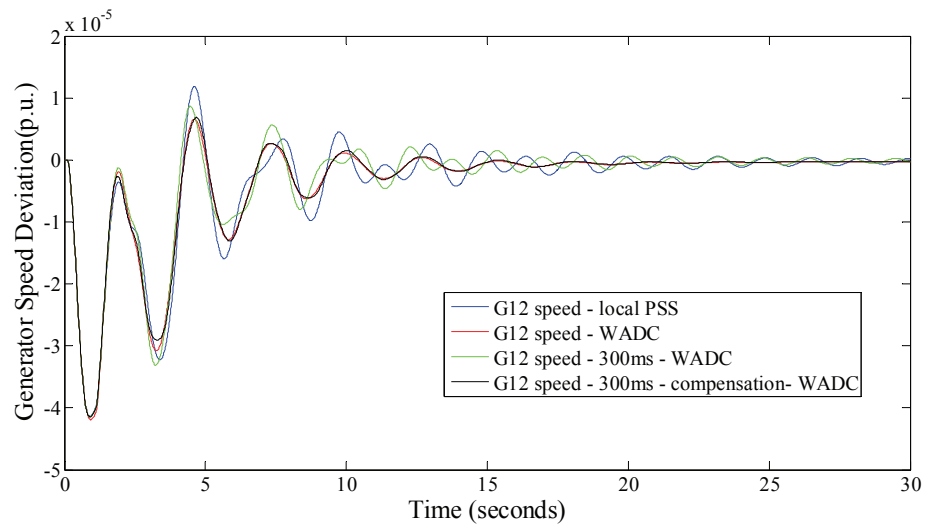


(b) Case b

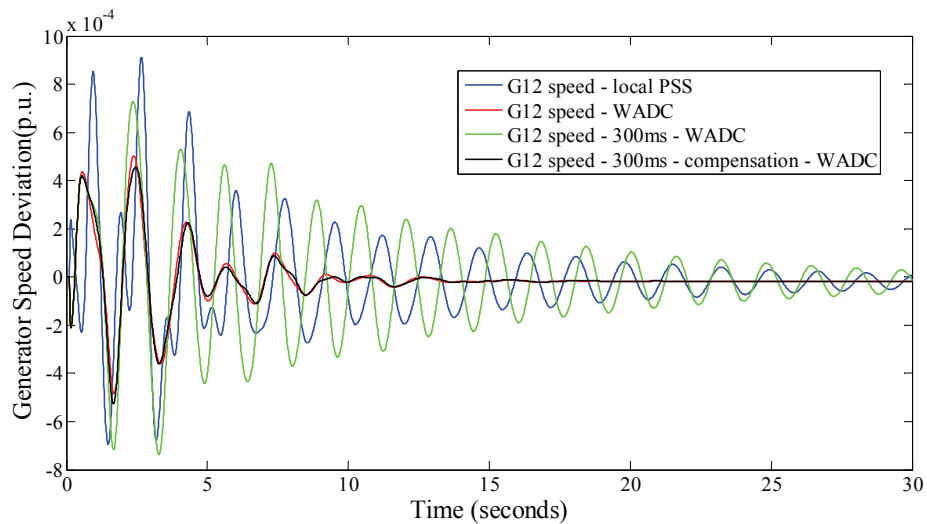
Fig. 7.10 Rotor speed deviations of G12 and G13 in Case a and b under operation scenario 2

(B.3) Signal Time Delay Compensation for Operation Scenario 2

In this simulation test, the signal time delay of 300ms is added. The rotor speed deviations of G12 with and without the addition of WADCs and the consideration of signal time delay are plotted in Figure 7.11. It shows that the effectiveness of the WADCs is significantly deteriorated without the time delay compensation and the proposed time delay compensation scheme works very well.



(a) Case a



(b) Case b

Fig. 7.11 Rotor speed deviations of G12 in Case a and b under operation scenario 2 with signal time delay

As shown in Table 2 and 3 and Fig. 7.8 ~ 7.11, it can be found that the proposed adaptive wide-area damping control scheme performs well in both operation scenarios for the IEEE 16-generator 5-area test system without and with signal time delay being considered.

7.7 IMPLEMENTATION ISSUES

On-line low-frequency oscillation suppression is a challenging and emergent issue to be addressed for large-scale interconnected power grids. The problem of on-line low-frequency oscillation suppression can be further divided into on-line low-frequency oscillation identification and on-line low-frequency oscillation control. Until now, there has not been any effective on-line low-frequency oscillation suppression scheme in practical implementation. The requirements for an effective on-line low-frequency oscillation suppression scheme lie in the following two aspects:

- (1) On-line, rapid, accurate and noise-free low-frequency oscillation mode identification.
- (2) On-line, adaptive and effective low-frequency oscillation control scheme which can compensate the adverse effect of varying signal time delay.

In this chapter, an adaptive WADC scheme is proposed to suppress the low-frequency oscillation online. This damping control scheme fulfills the requirements of an effective on-line low-frequency oscillation suppression scheme as follows:

- (1) The proposed SSI algorithm is able to rapidly and accurately identify all the low-frequency oscillation modes shape online with high noise resistance.
- (2) According to the identified inter-area oscillation modes shape, wide-area input signal can be calculated to suppress the oscillation. The adverse effect of varying signal time delay containing in WAMS data can be simply and effectively compensated by the designed signal time delay compensator.

Therefore, the adaptive WADC scheme proposed in this chapter is suitable for the on-line low-frequency oscillation suppression and could be applied in practice to solve the increasing low-frequency oscillation problem following the interconnection of large-scale power grids.

7.8 SUMMARY AND FUTURE WORK

In this chapter, a novel adaptive wide-area control scheme with SSI and signal time delay compensation is proposed. This control scheme mainly composes of three parts: SSI algorithm, wide-area input signal formulation and signal time delay compensation. When oscillation is detected in power system, SSI algorithm first effectively and robustly identifies the low-frequency oscillation mode on-line. Then, according to the identified inter-area oscillation modes with insufficient damping, wide-area input signals are calculated and combined with the local input signals as the input signal of PSS. In addition, signal time delay compensator is added to effectively eliminate the effects of signal time delay to the damping control.

Through the case studies conducted on the IEEE 4-generator 2-area and IEEE 16-generators 5-area test systems, the effectiveness of the proposed wide-area damping control scheme is proved. When signal time delay is considered in simulation, the proposed signal time delay compensator can effectively eliminate the effects of signal time delay on the performance of the adaptive WADC.

In this chapter, the parameters of WADCs are selected as the same as the local PSSs and remain unchanged throughout the entire low-frequency oscillation control operation. As the next stage of research, the parameters of WADCs shall be tuned optimally as well based on the online SSI identification results when the oscillation control operation starts and adjusted adaptively according to the updated SSI identification results during the course of control.

CHAPTER VIII CONCLUSION

With the interconnection of the regional power grids and the dissociation of power generations and transmission utilities, the operation of modern power system is becoming more and more complex and challenging. It is therefore imperative for the development of WAMS to facilitate wide-area supervision and control the power system in the coming era of smart grid.

As an emerging technology, WAMS can not only enhance the observability but also strengthen the safety and stability of power system. But, like any other rising technologies, the utilization of WAMS may also introduce new concerns in stability analysis and control of power grid while it does offer new possibilities for improvements. The concerns include investment, synchronization accuracy, signal time delay, reliability and risk of WAMS. It is therefore necessary to investigate these aspects of WAMS and their influence on power system stability analysis and control. This investigation is the primary focus of this research work which could be summarized as follows:

- 1) *Quantitative analysis of WAMS characteristics is the key preliminary work of any WAMS based stability analysis and control scheme with practical value.*

As an advanced and reliable information platform for power system real-time monitoring and control, many WAMS based stability analysis and control schemes have been proposed in recent years. However, most of these schemes have limited practical value because most of the WAMS characteristics including synchronization accuracy, signal time delay and reliability, which would have large effects on the performance of those WAMS based stability analysis and control schemes, were ignored in their design.

The first contribution of this thesis is to systematically and quantitatively

analyze the WAMS characteristics including synchronization accuracy, signal time delay and reliability. This thesis first discusses the causes and effects of synchronization inaccuracy and signal time delay, and then the synchronization accuracy and signal time delay are systematically studied and examined such that some recommendations could be made to improve the synchronization accuracy and reduce the signal time delay to meet the demand of wide-area stability analysis and control in practical use.

Reliability is a performance characteristic of WAMS that reflects the ability of WAMS to operate successfully long enough to supply enough synchronized phasors for the monitoring and control of power system. In this thesis, a comprehensive reliability evaluation method based on Monte Carlo Fault Tree Analysis is proposed for WAMS. As WAMS is a complex system which can be divided into several sub-systems including PMUs, PDC, communication networks (including local area communication network and wide area communication network), and control center, FT modeling method is first used to construct the reliability models of these sub-systems, and then Monte Carlo simulation approach is used to evaluate the reliability indices of these sub-systems. Finally, reliability of the whole WAMS can be evaluated using the reliability indices of its sub-systems. The main advantage for using the FT modeling method to construct the reliability model of WAMS is that it allows multiple fault patterns in WAMS to be considered in the reliability evaluation conveniently. Furthermore, the reliability of both PMU measurements uploading from PMUs to the control center and control instructions downloading from the control center to PMUs could be considered in the construction of reliability model of WAMS. The problem of state space explosion is overcome with the use of Monte Carlo simulation for evaluating the FT reliability model of WAMS. Not only the reliability indices of WAMS can be evaluated more accurately, but also additional

reliability indices such as importance indices, which cannot be easily obtained otherwise, can be deduced via the Monte Carlo simulation.

Comparison studies with the Markov-Enumeration method showed that the proposed reliability evaluation method is superior, in terms of both correctness and functionality, in particular for large-scale WAMS with high failure rate. A general guideline is also provided to improve the reliability of WAMS for online stability analysis and control. In addition, a simple example based on an adaptive wide-area damping control scheme has been given to show the application of the proposed WAMS reliability evaluation method.

2) *The investigation of which WAMS CN architecture would have better performance in the monitoring and control of power systems has been conducted on the aspects of investment, signal time delay, reliability and risk of CN.*

With the profound deregulation and the growing integration of renewable energies and intelligent controllers, new control strategies shall be adopted to control the increasingly complex power industries. There is an urgent need for high-performance CN which is an essential component of WAMS with different architecture to coordinate with the different control strategies of power systems.

By employing the proposed improved MST algorithm, the optimal communication networks with minimum investment in centralized and distributed WAMS of Shandong Power Grid are firstly constructed to facilitate the quantitative and comprehensive investigation of centralized and distributed CNs. The investigation results show that, while the investment is comparable, distributed CN has shorter signal time delay, higher reliability and lower risk than centralized one. This means that distributed CN has better performance in the monitoring and control of power systems than the centralized one.

Through the risk evaluation of centralized and distributed CNs by using MCDM approach combined with AHP and risk ranking technology, it can be seen that the same communication link in CN with different architecture could possess totally different risk to the power grid. This can be used to reduce the risk level of the existing CN and construct the new CN with lowest risk level.

3) *Adaptive wide-area damping control scheme with SSI and signal time delay compensation is taken as an example to demonstrate the influence of WAMS characteristics on power system stability analysis and control.*

Different WAMS characteristics have different influence on WAMS based stability analysis and control schemes. In order to demonstrate the influence of WAMS characteristics on stability analysis and control schemes, a novel adaptive wide-area control scheme with SSI and signal time delay compensation is proposed. This control scheme mainly composed of three parts: SSI algorithm, wide-area input signal formulation and signal time delay compensation. When oscillation is detected in power system, SSI algorithm can first effectively and robustly identify the low-frequency oscillation mode on-line. Then, according to the identified inter-area oscillation modes with insufficient damping, the wide-area input signals would be calculated and combined with local input signal to act as the input signal of PSSs to provide the necessary damping torque on demand to suppress the oscillations. In addition, a simple but effective signal time delay compensation scheme based on the GPS time measurements has been proposed to eliminate the effect of signal time delay to the damping control.

Case studies are conducted on IEEE 4-generator 2-area and IEEE 16-generators 5-area test systems. The effectiveness and robustness of the proposed wide-area damping control scheme has been illustrated with simulations on cases representing different disturbance scenarios. When signal

time delay is introduced in simulation, proposed signal time delay compensator can effectively eliminate the effect of signal time delay on the performance of the adaptive WADC.

APPENDICES

APPENDIX A IEEE 4-GENERATORS 2-AREA SYSTEM PARAMETERS

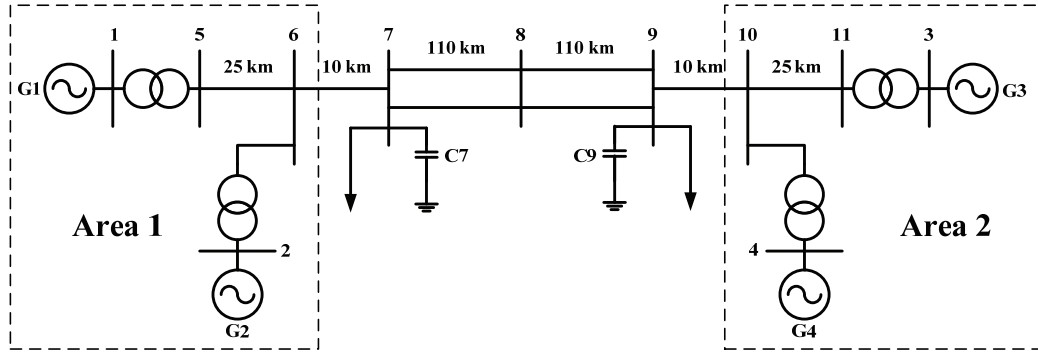


Fig. A.1 Single line diagram of IEEE 4-generator 2-area system

The single line diagram of IEEE 4-generator 2-area system is shown in Fig. A.1. This system consists of two similar areas connected by a weak tie. Each area consists of two coupled units, each having a rating of 900 MVA and 20 kV. The generator parameters in per unit on the rated MVA and kV base are as follows:

$$X_d = 1.8 \quad X_q = 1.7 \quad X'_d = 0.3 \quad X'_q = 0.55$$

$$R_a = 0.0025 \quad T'_d = 8.0s \quad T'_q = 0.4s \quad K_D = 0$$

$$H = 6.5 \text{ for G1 and G2}$$

$$H = 6.175 \text{ for G3 and G4}$$

Each step-up transformer has an impedance of $0+j0.15$ per unit on 900 MVA and 20/30kV base, and has an off-nominal ratio of 1.0.

The transmission system nominal voltage is 230 kV. The line lengths are identified in Fig. A.1. The parameters of the lines in per unit on 100 MVA, 230 kV base are:

$$r = 0.0001 \text{ pu/km} \quad x_L = 0.001 \text{ pu/km} \quad b_C = 0.00175 \text{ pu/km}$$

The system is operating with area 1 exporting 400 MW to area 2, and the generating units are loaded as follows:

$$G1: P = 700 \text{ MW}, Q = 185 \text{ MVAr}, E_t = 1.03 \angle 20.20^\circ$$

$$G2: P = 700 \text{ MW}, Q = 235 \text{ MVAr}, E_t = 1.01 \angle 10.5^\circ$$

$$G3: P = 719 \text{ MW}, Q = 176 \text{ MVAr}, E_t = 1.03 \angle -6.8^\circ$$

$$G4: P = 700 \text{ MW}, Q = 202 \text{ MVAr}, E_t = 1.01 \angle -17.0^\circ$$

The loads and reactive power supplied (Q_C) by the shunt capacitors at buses 7 and 9 area as follows:

$$\text{Bus 7: } P_L = 976 \text{ MW}, Q_L = 100 \text{ MVAr}, Q_C = 200 \text{ MVAr}$$

$$\text{Bus 9: } P_L = 1767 \text{ MW}, Q_L = 100 \text{ MVAr}, Q_C = 350 \text{ MVAr}$$

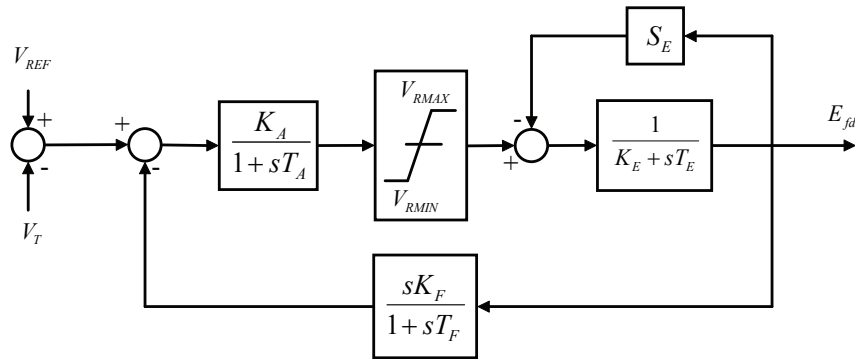


Fig. A.2 IEEE type 1 rotating excitation system model

In this system, uniform IEEE type 1 rotating excitation system is used. The model of IEEE type 1 rotating excitation system is shown in Fig. A.2 and the parameters are as follow:

$$\begin{array}{llll} K_A = 40.0 & V_{RMIN} = -10 & V_{RMAX} = 10 & K_E = 1.0 \\ T_E = 0.785 & K_F = 0.03 & T_F = 1.0 & C_1 = 0.07 \\ C_2 = 0.91 & & & \end{array}$$

APPENDIX B IEEE 16-GENERATOR 68-BUS SYSTEM

PARAMETERS

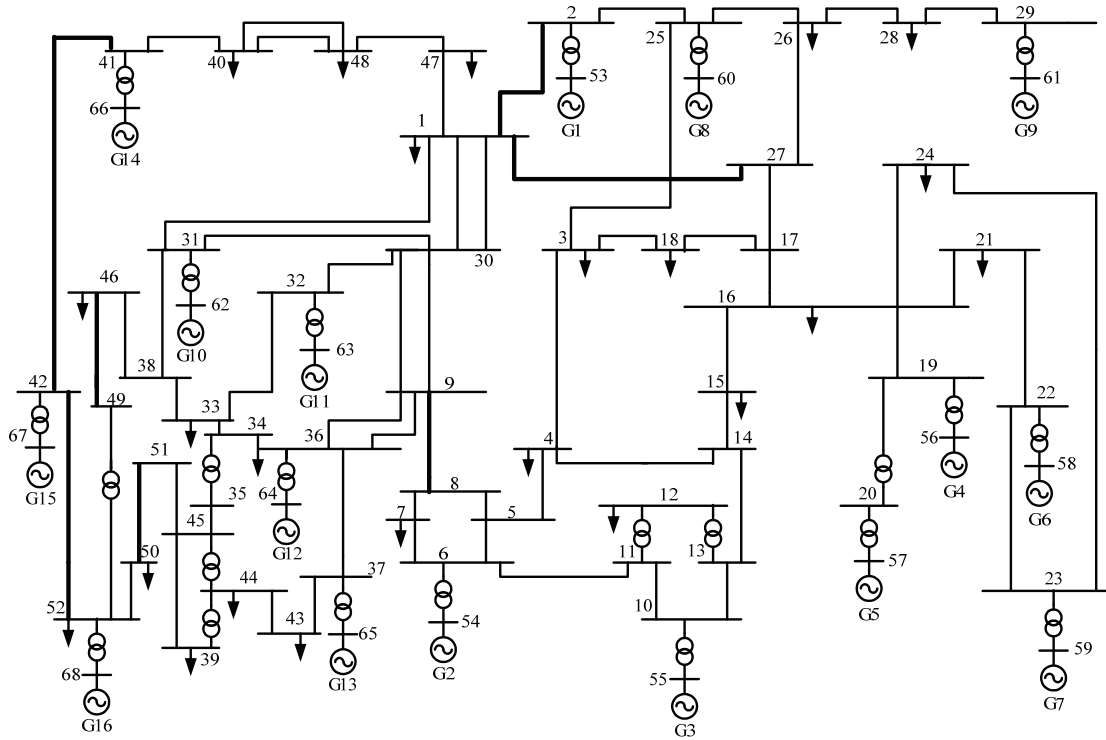


Fig. B.1 Single line diagram of IEEE 16-generator 68-bus system

The single line diagram of IEEE 16-generator 68-bus system is shown in Fig.

B.1 and the parameters of this system are divided in:

- Bus Data
- Branch Data
- Generation Data
- Regulator Data

Bus Data

Table B.1 represents the bus data of IEEE 16-generator 68-bus system. The nomenclature for the table headings is:

Bus No.	Number of the Bus
Bus Type	Bus type code:

(1) Load Bus, PQ Bus

(2) Generator Bus, PV Bus

(3) Slack Bus

Bus voltage

Bus voltage, in per unit

Load W

Real component of the Load, in per unit

Load VAR

Reactive component of the Load, in per unit

Gen W

Generator real power output, in per unit

Gen VAR

Generator reactive power output, in per unit

Table B. 1 Bus data of IEEE 16-generator 68-bus system

Bus No.	Bus type	Bus voltage	Load W	Load VAR	Gen W	Gen VAR
1	1	1.0	2.527	1.1856	-	-
2	1	1.0	0	0	-	-
3	1	1.0	3.22	0.02	-	-
4	1	1.0	5.0	1.84		
5	1	1.0	0	0		
6	1	1.0	0	0	-	-
7	1	1.0	2.34	0.84	-	-
8	1	1.0	5.22	1.77	-	-
9	1	1.0	1.04	1.25	-	-
10	1	1.0	0	0	-	-
11	1	1.0	0	0	-	-
12	1	1.0	0.09	0.88	-	-
13	1	1.0	0	0	-	-
14	1	1.0	0	0	-	-
15	1	1.0	3.2	1.53	-	-
16	1	1.0	3.29	0.32	-	-
17	1	1.0	0	0	-	-

18	1	1.0	1.58	0.3		
19	1	1.0	0	0		
20	1	1.0	6.8	1.03	-	-
21	1	1.0	2.74	1.15	-	-
22	1	1.0	0	0	-	-
23	1	1.0	2.48	0.85	-	-
24	1	1.0	3.09	-0.92	-	-
25	1	1.0	2.24	0.47	-	-
26	1	1.0	1.39	0.17	-	-
27	1	1.0	2.81	0.76	-	-
28	1	1.0	2.06	0.28	-	-
29	1	1.0	2.84	0.27	-	
30	1	1.0	0	0	-	
31	1	1.0	0	0	-	-
32	1	1.0	0	0		-
33	1	1.0	1.12	0		-
34	1	1.0	0	0	-	
35	1	1.0	0	0	-	
36	1	1.0	1.02	-0.1946	-	-
37	1	1.0	60	3	-	-
38	1	1.0	0	0	-	-
39	1	1.0	2.67	0.126	-	-
40	1	1.0	0.6563	0.2353	-	-
41	1	1.0	10	2.5	-	-
42	1	1.0	11.5	2.5	-	-
43	1	1.0	0	0	-	-
44	1	1.0	2.6755	0.0484	-	-
45	1	1.0	2.08	0.21	-	-

46	1	1.0	1.507	0.285	-	-
47	1	1.0	2.0312	0.3259	-	-
48	1	1.0	2.412	0.022	-	
49	1	1.0	1.64	0.29	-	
50	1	1.0	1	-1.47	-	-
51	1	1.0	3.37	-1.22	-	-
52	1	1.0	24.7	1.23	-	-
53	2	1.045	0	0	2.50	0
54	2	0.98	0	0	5.45	0
55	2	0.983	0	0	6.50	0
56	2	0.997	0	0	6.32	0
57	2	1.011	0	0	5.052	0
58	2	1.05	0	0	7.0	0
59	2	1.063	0	0	5.60	0
60	2	1.03	0	0	5.40	0
61	2	1.025	0	0	8.0	0
62	2	1.01	0	0	5.0	0
63	2	1.00	0	0	10.0	0
64	2	1.0156	0	0	13.5	0
65	3	1.011	0	0	35.91	0
66	2	1.00	0	0	17.85	0
67	2	1.00	0	0	10.0	0
68	2	1.00	0	0	40.0	0

Branch Data

Table B.2 represents the branch (transmission lines and transformers) data of IEEE 16-generator 68-bus system. The nomenclature for the table headings is:

Number Number of the branch
From Bus Branch starting bus number

To Bus	Branch ending bus number
Resistance	Branch resistance, in per unit
Reactance	Branch reactance, in per unit
Susceptance	Branch total charging susceptance, in per unit
Branch Tap	Transformer off-nominal turns ratio

Table B.2 Branch data of IEEE 16-generator 68-bus system

Number	From Bus	To Bus	Resistance	Reactance	Susceptance	Branch Tap
1	1	2	0.0035	0.0411	0.6987	-
2	1	30	0.0008	0.0074	0.48	-
3	2	3	0.0013	0.0151	0.2572	-
4	2	25	0.007	0.0086	0.146	-
5	2	53	0	0.0181	0	1.025
6	3	4	0.0013	0.0213	0.2214	-
7	3	18	0.0011	0.0133	0.2138	-
8	4	5	0.0008	0.0128	0.1342	-
9	4	14	0.0008	0.0129	0.1382	-
10	5	6	0.0002	0.0026	0.0434	-
11	5	8	0.0008	0.0112	0.1476	-
12	6	7	0.0006	0.0092	0.1130	-
13	6	11	0.0007	0.0082	0.1389	-
14	6	54	0	0.025	0	1.07
15	7	8	0.0004	0.0046	0.078	-
16	8	9	0.0023	0.0363	0.3804	-
17	9	30	0.0019	0.0183	0.29	-
18	10	11	0.0004	0.0043	0.0729	-
19	10	13	0.0004	0.0043	0.0729	-
20	10	55	0	0.02	0	1.07

21	12	11	0.0016	0.0435	0	1.06
22	12	13	0.0016	0.0435	0	1.06
23	13	14	0.0009	0.0101	0.1723	-
24	14	15	0.0018	0.0217	0.366	-
25	15	16	0.0009	0.0094	0.171	-
26	16	17	0.0007	0.0089	0.1342	-
27	16	19	0.0016	0.0195	0.3040	-
28	16	21	0.0008	0.0135	0.2548	-
29	16	24	0.0003	0.0059	0.0680	-
30	17	18	0.0007	0.0082	0.1319	-
31	17	27	0.0013	0.0173	0.3216	-
32	19	20	0.0007	0.0138	0	1.06
33	19	56	0.0007	0.0142	0	1.07
34	20	57	0.0009	0.0180	0	1.009
35	21	22	0.0008	0.0140	0.2565	-
36	22	23	0.0006	0.0096	0.1846	-
37	22	58	0	0.0143	0	1.025
38	23	24	0.0022	0.0350	0.3610	-
39	23	59	0.0005	0.0272	0	-
40	25	26	0.0032	0.0323	0.5310	-
41	25	60	0.0006	0.0232	0	1.025
42	26	27	0.0014	0.0147	0.2396	-
43	26	28	0.0043	0.0474	0.7802	-
44	26	29	0.0057	0.0625	1.0290	-
45	28	29	0.0014	0.0151	0.2490	-
46	29	61	0.0008	0.0156	0	1.025
47	9	30	0.0019	0.0183	0.29	-
48	9	36	0.0022	0.0196	0.34	-

49	9	36	0.0022	0.0196	0.34	-
50	36	37	0.0005	0.0045	0.32	-
51	34	36	0.0033	0.0111	1.45	-
52	35	34	0.0001	0.0074	0	0.946
53	33	34	0.0011	0.0157	0.202	-
54	32	33	0.0008	0.0099	0.168	-
55	30	31	0.0013	0.0187	0.333	-
56	30	32	0.0024	0.0288	0.488	-
57	1	31	0.0016	0.0163	0.25	-
58	31	38	0.0011	0.0147	0.247	-
59	33	38	0.0036	0.0444	0.693	-
60	38	46	0.0022	0.0284	0.43	-
61	46	49	0.0018	0.0274	0.27	-
62	1	47	0.0013	0.0188	1.31	-
63	47	48	0.0025	0.0268	0.40	-
64	47	48	0.0025	0.0268	0.40	-
65	48	40	0.0020	0.022	1.28	-
66	35	45	0.0007	0.0175	1.39	-
67	37	43	0.0005	0.0276	0	-
68	43	44	0.0001	0.0011	0	-
69	44	45	0.0025	0.073	0	-
70	39	44	0	0.0411	0	-
71	39	45	0	0.0839	0	-
72	45	51	0.0004	0.0105	0.72	-
73	50	52	0.0012	0.0288	2.06	-
74	50	51	0.0009	0.0221	1.62	-
75	49	52	0.0076	0.1141	1.16	-
76	52	42	0.0040	0.0600	2.25	-

77	42	41	0.0040	0.0600	2.25	-
78	41	40	0.0060	0.0840	3.15	-
79	31	62	0	0.026	0	1.04
80	32	63	0	0.013	0	1.04
81	36	64	0	0.0075	0	1.04
82	37	65	0	0.0033	0	1.04
83	41	66	0	0.0015	0	1
84	42	67	0	0.0015	0	1
85	52	68	0	0.0030	0	1
86	1	27	0.032	0.32	0.41	1

Note that: in Table B.2, there are several same branches which mean the double-circuit transmission lines.

Generation Data

Table B.3 represents the generation data of IEEE 16-generator 68-bus system.

The nomenclature of the table headings is:

Unit No.	Number of the generators
H	Inertia constant of generators, in second
R_a	Resistance, in per unit
X_l	Leakage reactance, in per unit
X_d	D-axis synchronous reactance, in per unit
X_q	Q-axis synchronous reactance, in per unit
X_d'	D-axis transient reactance, in per unit
X_q'	Q-axis transient reactance, in per unit
T_{d0}'	D-axis open-circuit time constant, in second
T_{q0}'	Q-axis open-circuit time constant, in second

Table B.3 Generator data of IEEE 16-generator 68-bus system

Unit No.	H (sec)	R _a	X _l	X _d	X _q	X _d '	X _q '	T _{d0} '	T _{q0} '
1	3.4	0	0.003	0.969	0.6	0.248	0.25	12.6	0.035
2	1.8	0	0.035	1.8	1.7207	0.4253	0.3661	6.56	1.5
3	4.9623	0	0.0304	1.8	1.7098	0.383	0.3607	1.5	1.5
4	4.1629	0	0.0295	1.8	1.7725	0.2995	0.2748	5.69	1.5
5	4.7667	0	0.027	1.8	1.6909	0.36	0.3273	5.4	0.44
6	4.9107	0	0.0224	1.8	1.7079	0.3543	0.3189	7.3	0.4
7	4.3267	0	0.0322	1.8	1.7817	0.299	0.2746	5.66	1.5
8	3.915	0	0.028	1.8	1.7379	0.3538	0.3103	6.7	0.41
9	4.0365	0	0.0298	1.8	1.7521	0.4872	0.4274	4.79	1.96
10	2.9106	0	0.0199	1.8	1.2249	0.4868	0.4793	9.37	1.5
11	2.0053	0	0.0103	1.8	1.7297	0.2531	0.2109	4.1	1.5
12	5.1721	0	0.022	1.8	1.6931	0.5525	0.4990	7.4	1.5
13	4.0782	0	0.003	1.8	1.7392	0.3345	0.3041	5.9	1.5
14	3	0	0.0017	1.8	1.73	0.285	0.25	4.1	1.5
15	3	0	0.0017	1.8	1.73	0.285	0.25	4.1	1.5
16	4.45	0	0.0041	1.8	1.6888	0.359	0.3034	7.8	1.5

Regulator Data

The regulators of generator used in this thesis include exciter and PSS, in the following, the parameters of these two regulators will be listed respectively.

Exciter Data

Exciter used in IEEE 16-generator 68-bus system is IEEE Type 1 rotating excitation system which is the same as IEEE 4-generator 2-area system depicted in APPENDIX A. The model of IEEE type 1 rotating excitation system is shown in Fig. A.2 and Table B.4 represents the exciter data of IEEE 16-generator 68-bus system. The nomenclature of the table headings is:

Unit No.	Number of the generators
K_A	Voltage regulator gain
T_A	Voltage regulator time constant, in second
V_{RMAX}	Maximum voltage regulator output
V_{RMIN}	Minimum voltage regulator output
K_E	Exciter constant
T_E	Exciter time constant, in second
K_F	Stabilizer gain
T_F	Stabilizer time constant, in second
C_1	Saturation function 1
C_2	Saturation function 2

Table B.4 Exciter data of IEEE 16-generator 68-bus system

Unit No.	K_A	T_A	V_{RMAX}	V_{RMIN}	K_E	T_E	K_F	T_F	C_1	C_2
1	30	0.02	10	-10	1.0	0.785	0.03	1.0	0.07	0.91
2	30	0.02	10	-10	1.0	0.785	0.03	1.0	0.07	0.91
3	30	0.02	10	-10	1.0	0.785	0.03	1.0	0.07	0.91
4	30	0.02	10	-10	1.0	0.785	0.03	1.0	0.07	0.91
5	30	0.02	10	-10	1.0	0.785	0.03	1.0	0.07	0.91
6	30	0.02	10	-10	1.0	0.785	0.03	1.0	0.07	0.91
7	30	0.02	10	-10	1.0	0.785	0.03	1.0	0.07	0.91
8	30	0.02	10	-10	1.0	0.785	0.03	1.0	0.07	0.91
9	30	0.02	10	-10	1.0	0.785	0.03	1.0	0.07	0.91
10	30	0.02	10	-10	1.0	0.785	0.03	1.0	0.07	0.91
11	30	0.02	10	-10	1.0	0.785	0.03	1.0	0.07	0.91
12	30	0.02	10	-10	1.0	0.785	0.03	1.0	0.07	0.91

PSS Data

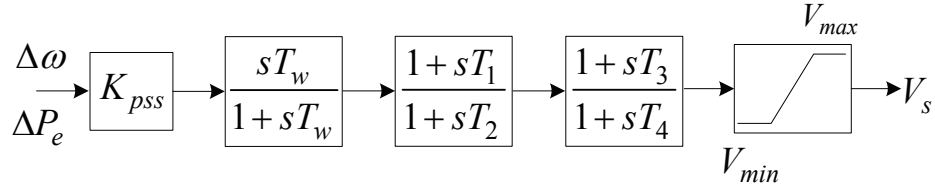


Fig. B.2 IEEE Type 1 rotating excitation system model

The model of PSS used in IEEE 16-generator 68-bus system is shown in Fig. B.2 and Table B.5 represents the PSS data of IEEE 16-generator 68-bus system.

The nomenclature of the table headings is:

Unit No.	Number of the generators
K_{PSS}	PSS gain
T_w	PSS washing time, in second
T_1	PSS leading time constant, in second
T_2	PSS lag time constant, in second
T_3	PSS leading time constant, in second
T_4	PSS lag time constant, in second
V_{max}	PSS maximum voltage output
V_{min}	PSS minimum voltage output

Table B.5 PSS data of IEEE 16-generator 68-bus system

Unit No.	K_{PSS}	T_w	T_1	T_2	T_3	T_4	V_{max}	V_{min}
1	100	10	0.1	0.02	0.08	0.02	0.02	-0.05
2	100	10	0.08	0.02	0.08	0.02	0.02	-0.05
3	100	10	0.08	0.02	0.08	0.02	0.02	-0.05
4	100	10	0.08	0.02	0.08	0.02	0.02	-0.05
5	100	10	0.08	0.02	0.08	0.02	0.02	-0.05
6	100	10	0.1	0.02	0.1	0.02	0.02	-0.05

7	100	10	0.08	0.02	0.08	0.02	0.02	-0.05
8	100	10	0.08	0.02	0.08	0.02	0.02	-0.05
9	100	10	0.08	0.03	0.05	0.01	0.02	-0.05
10	100	10	0.1	0.02	0.1	0.02	0.02	-0.05
11	50	10	0.08	0.03	0.05	0.01	0.02	-0.05
12	110	10	0.1	0.02	0.1	0.02	0.02	-0.05

REFERENCE

- [1] G. S. Vassell, "Northeast blackout of 1965," *IEEE Power Engineering Review*, vol. 11, no. 1, pp. 4, 1991.
- [2] R. Kearsley, "Restoration in Sweden and experience gained from the blackout of 1983," *IEEE Transactions on Power Systems*, vol. 2, no. 2, pp. 422-428, 1987.
- [3] G. Andersson, P. Donalek, R. Farmer, *et al.*, "Causes of the 2003 major grid blackouts in north America and Europe, and recommended means to improve system dynamic performance," *IEEE Transactions on Power Systems*, vol. 20, no. 4, pp. 1922-1928, 2005.
- [4] B. F. Wollenberg, "In my view - from blackout to blackout - 1965 to 2003: how far have we come with reliability?," *IEEE Power and Energy Magazine*, vol. 2, no. 1, pp. 88-86, 2004.
- [5] A. G. Phadke and de R. M. Moraes, "The wide world of wide-area measurement," *IEEE Power and Energy Magazine*, vol. 6, no. 5, pp. 52-65, 2008.
- [6] A. G. Phadke, "Synchronized phasor measurements - a historical overview," *IEEE/PES Transmission and Distribution Conference and Exhibition 2002: Asia Pacific*, vol. 1, pp. 476-479, 2003.
- [7] M. Begovic, D. Novosel, C. Henville, *et al.*, "Wide-area protection and emergency control," *Proceedings of the IEEE*, vol.93, no.5, pp. 876-891, 2005.
- [8] X. R. Xie, Y. Z. Xin, J. Y. Xiao, *et al.*, "WAMS applications in Chinese power systems," *IEEE Power and Energy Magazine*, vol. 4, no. 1, pp. 54-63, 2006.
- [9] W. X. Liu, N. Liu, Y. F. Fan, *et al.*, "Reliability analysis of wide area

- measurement system based on the centralized distributed model,” *Power System Conference and Exposition, PSCE’09*, pp. 1-6, 2009.
- [10] Y. Wang, W. Y. Li and J. P. Lu, “Reliability analysis of wide-area measurement system,” *IEEE Transactions on Power Delivery*, vol. 25, no. 3, pp.1483-1491, 2010.
- [11] E. S. Silva and P. M. Ochoa, “State space exploration in Markov models,” *ACM SIGMETRICS Performance Evaluation Review*, vol.20, no.1, pp. 152-166, 1992.
- [12] Q. Y. Jiang, Z. Y. Zou, Y. J. Cao, *et al.*, “Overview of power system stability analysis and wide-area control in consideration of time delay,” *Automation of Electric Power Systems*, vol. 29, no. 3, pp. 1-7, 2005.
- [13] G. Rogers, *Power system oscillations*, Kluwer Academic Publishers, 2000.
- [14] S. Chakrabarti, E. Kyriakides, G. Ledwich, *et al.*, “Inclusion of PMU current phasor measurements in a power system state estimator,” *IET Generation, Transmission & Distribution*, vol. 4, no. 10, pp. 1104-1115, 2010.
- [15] N. H. Abbasy and H. M. Ismail, “A unified approach for the optimal PMU location for power system state estimation,” *IEEE Transactions on Power Systems*, vol. 24, no. 2, pp. 806-813, 2009.
- [16] H. Xue, Q. Q. Jia and N. Wang, “A dynamic state estimation method with PMU and SCADA measurement for power systems,” *IPEC 2007 International Power Engineering Conference*, pp. 848-853, 2007.
- [17] S. Y. Hou, Z. X. Xu, H. Y. Lv, *et al.*, “Research into harmonic state estimation in power system based on PMU and SVD,” *PowerCon 2006 International Conference on Power System Technology*, pp. 1-6, 2006.
- [18] C. W. Taylor and D. C. Erickson, “Recording and analyzing the July 2

- cascading outage,” *IEEE Computer Applications in Power*, vol. 10, no. 1, pp. 26-30, 1997.
- [19] J. W. Balance, B. Bhargava and G. D. Rodriguez, “Monitoring power system dynamics using phasor measurement technology for power system dynamic security assessment,” *2003 Bologna IEEE Power Tech Conference Proceedings*, vol. 3, pp. 683-689, 2003.
- [20] R. O. Burnett, M. M. Butts, T. W. Cease, *et al.*, “Synchronized phasor measurements of a power system event,” *IEEE Transactions on Power Systems*, vol. 9, no. 3, pp. 1643-1650, 1994.
- [21] J. F. Hauer, “Validation of phasor calculations in the macrodyne PMU for California-Oregon transmission project tests of March 1993,” *IEEE Transactions on Power Delivery*, vol. 11, no. 3, pp. 1224-1231, 1996.
- [22] B. K. Kumar, S. N. Sighn and S. C. Srivastava, “A decentralized nonlinear feedback controller with prescribed degree of stability for damping power system oscillations,” *Electric Power System Research*, vol.77, no.3, pp. 204-211, 2007.
- [23] R. M. He, “Power system dynamics monitoring and management system,” *Automation of Electric Power Systems*, vol. 26, no. 5, pp. 1-4, 2002.
- [24] H. Ota, Y. Kitayama, H. Ito, *et al.*, “Development of transient stability control system (TSC system) based on on-line stability calculation,” *IEEE Transactions on Power Systems*, vol. 11, no. 3, pp. 1463-1472, 1996.
- [25] F. F. Song, T. S. Bi and Q. X. Yang, “Study on wide area measurement system based transient stability control for power system,” *The 7th International Power Engineering Conference, IPEC 2005*, vol. 2, pp. 757-760, 2005.

- [26] B. Milosevic and M. Begovic, "Voltage-stability protection and control using a wide-area network of phasor measurements," *IEEE Transactions on Power Systems*, vol. 18, no. 1, pp. 121-127, 2003.
- [27] R. F. Nuqui, A. G. Phadke, R. P. Schulz, *et al.*, "Fast on-line voltage security monitoring using synchronized phasor measurements and decision trees," *IEEE Power Engineering Society Winter Meeting*, vol. 3, pp. 1347-1352, 2001.
- [28] C. Rehtanz and J. Bertsch, "Wide area measurement and protection system for emergency voltage stability control," *IEEE Power Engineering Society Winter Meeting*, vol. 2, pp. 842-847, 2002.
- [29] K. Tomsovic, D. E. Bakken, V. Venkatasubramanian, *et al.*, "Designing the next generation of real-time control, communication, and computations for large power systems," *Proceeding of the IEEE*, vol. 93, no. 5, pp. 965-979, 2005.
- [30] J. C. Tan, P. A. Crossley, P. G. McLaren, *et al.*, "Application of a wide area backup protection expert system to prevent cascading outages," *IEEE Transactions on Power Delivery*, vol. 17, no. 2, pp. 375-380, 2002.
- [31] J. Tang and P. G. McLaren, "A wide area differential backup protection scheme for shipboard application," *IEEE Transactions on Power Delivery*, vol. 21, no. 3, pp. 1183-1190, 2006.
- [32] Y. Serizawa, M. Myoujin and K. Kitamura, "Wide-area current differential backup protection employing broadband communications and time transfer systems," *IEEE Transactions on Power Delivery*, vol. 13, no. 4, pp. 1046-1052, 1998.
- [33] J. D. McDonald, *Electric power substations engineering*, Second Edition, CRC Press, 2007.

- [34] H. Kirkham, A. R. Johnston and G. D. Allen, "Design considerations for a fiber optic communications network for power systems," *IEEE Transactions on Power Delivery*, vol. 9, no. 1, pp. 510-518, 1994.
- [35] K. W. Lu and R. S. Wolff, "Cost analysis for switched star broadband access," *International Journal of Digital & Analog Cabled Systems*, vol. 1, no. 3, pp. 139-147, 1988.
- [36] Z. Y. Huang, J. F. Hauer and K. E. Martin, "Evaluation of PMU dynamic performance in both lab environments and under field operating conditions," *IEEE Power Engineering Society General Meeting*, pp. 1-6, 2007.
- [37] G. Stenbakken and M. Zhou, "Dynamic phasor measurement unit test system," *IEEE Power Engineering Society General Meeting*, pp. 1-8, June 2007.
- [38] M. Sahinoglu and C. V. Ramamoorthy, "RBD tools using compression, decompression, hybrid techniques to code, decode, and compute reliability in simple and complex embedded systems," *IEEE Transactions on Instrumentation and Measurement*, vol. 54, no. 5, pp. 1789-1799, 2005.
- [39] R. Robidoux, H. Xu, L. Xing, M. Zhou, "Automated modeling of dynamic reliability block diagrams using colored Petri Nets," *IEEE Transactions on Systems, Man and Cybernetics, Part A: Systems and Humans*, vol. 40, no. 2, pp. 337-351, 2010.
- [40] S. Distefano and A. Puliafito, "Dependability evaluation with dynamic reliability block diagrams and dynamic fault trees," *IEEE Transactions on Dependable and Secure Computing*, vol. 6, no. 1, pp. 4-17, 2009.
- [41] C. E. Rago, C. M. Spencer, Z. Wolf, *et al.*, "High reliability prototype quadrupole for the next linear collider," *IEEE Transactions on Applied*

- Superconductivity*, vol. 12, no. 1, pp. 270-273, 2002.
- [42] S. M. Yacoub and H. H. Ammar, "A methodology for architecture-level reliability risk analysis," *IEEE Transactions on Software Engineering*, vol. 28, no. 6, pp. 529-547, 2002.
- [43] R. Bono, R. Alexander, A. Dorman, *et al.*, "Analyzing reliability-a simple yet rigorous approach," *IEEE Transactions on Industry Applications*, vol. 40, no. 4, pp. 950-957, 2004.
- [44] S. K. Chen, T. K. Ho, B. H. Mao, "Reliability evaluations of railway power supplies by fault-tree analysis," *IET Electric Power Applications*, vol. 1, no. 2, pp. 161-172, 2007.
- [45] R. T. Hessian, B. B. Salter, E. F. Goodwin, "Fault-tree analysis for system design, development, modification, and verification," *IEEE Transactions on Reliability*, vol. 39, no. 1, pp. 87-91, 1990.
- [46] K. Takaragi, R. Sasaki, S. Shingai, "A method of rapid Markov reliability calculation," *IEEE Transactions on Reliability*, vol. R-34, no. 3, pp. 262-268, 1985.
- [47] K. Siegrist, "Reliability of systems with Markov transfer of control I," *IEEE Transactions on Software Engineering*, vol. 14, no. 7, pp. 1049-1053, 1988.
- [48] K. Siegrist, "Reliability of systems with Markov transfer of control, II," *IEEE Transactions on Software Engineering*, vol. 14, no. 10, pp. 1478-1480, 1988.
- [49] Y. A. Katsigiannis, P. S. Georgilakis, G. J. Tsinarakis, "A novel colored fluid stochastic Petri Net simulation model for reliability evaluation of wind/PV/diesel small isolated power systems," *IEEE Transactions on Systems, Man and Cybernetics, Part A: Systems and Humans*, vol. 40, no. 6, pp.1296-1309, 2010.

- [50] W. G. Schneeweiss, ““Review of Petri Net picture book” and “Petri Nets for Reliability Modeling”,” *IEEE Transactions on Reliability*, vol. 55, no. 2, pp. 391-392, 2006.
- [51] D. C. Yu, T. C. Nguyen, P. Haddawy, “Bayesian network model for reliability assessment of power systems,” *IEEE Transactions on Power Systems*, vol. 14, no. 2, pp. 426-432, 1999.
- [52] H. Boudali and J. B. Dugan, “A continuous-time Bayesian network reliability modeling, and analysis framework,” *IEEE Transactions on Reliability*, vol. 55, no. 1, pp. 86-97, 2006.
- [53] M. M. Ahmad, A. Debs, Y. Wardi, “Estimation of the derivatives of generation system reliability indices in Monte Carlo simulation,” *IEEE Transactions on Power Systems*, vol. 8, no. 4, pp. 1448-1454, 1993.
- [54] R. Billinton and W. Wangdee, “Delivery point reliability indices of a bulk electric system using sequential Monte Carlo simulation,” *IEEE Transactions on Power Delivery*, vol. 21, no. 1, pp. 345-352, 2006.
- [55] A. Sankarakrishnan and R. Billinton, “Sequential Monte Carlo simulation for composite power system reliability analysis with time varying loads,” *IEEE Transactions on Power Systems*, vol. 10, no. 3, pp. 1540-1545, 1995.
- [56] N. Balijepalli, S. S. Venkata, R. D. Christie, “Modeling and analysis of distribution reliability indices,” *IEEE Transactions on Power Delivery*, vol. 19, no. 4, pp. 1950- 1955, 2004.
- [57] R. R. Lutz, G. G. Helmer, M. M. Moseman, *et al.*, “Safety analysis of requirements for a product family”, *Third International Conference on Requirements Engineering*, pp. 24-31, 1998.
- [58] G. Helmer, “Safety checklist for four variable requirements methods,” <http://archives.cs.iastate.edu/documents/disk0/00/00/01/63/00000163-01/>

TR98-01.pdf, 2011.

- [59] M. H. Mazouni and J. F. Aubry, "A PHA based on a systemic and generic ontology service operations and logistics, and informatics," *IEEE International Conference on Service Operations and Logistics, and Informatics*, pp. 1-6, 2007.
- [60] N. Zhao, T. Zhao, J. Tian, "Reliability dentered preliminary hazard analysis," *Reliability and Maintainability Symposium*, pp. 164-169, 2009.
- [61] M. H. Mazouni, D. Bied-Charreton, J. F. Aubry, "Proposal of a generic methodology to harmonize preliminary hazard analyses for guided transport system of systems engineering," *IEEE International Conference on System of Systems Engineering*, pp. 1-6, 2007.
- [62] A. Shafaghi and F. B. Cook, "Application of a hazard and operability study to hazard evaluation of an absorption heat pump," *IEEE Transactions on Reliability*, vol.37, no.2, pp. 159-166, 1988.
- [63] T. C. McKelvey, "How to improve the effectiveness of hazard and operability analysis," *IEEE Transactions on Reliability*, vol. 37, no. 2, pp. 167-170, 1988.
- [64] R. J. Mulvihill, "Design-safety enhancement through the use of hazard and risk analysis," *IEEE Transactions on Reliability*, vol.37, no.2, pp. 149-158, 1988.
- [65] X. Hong and J. B. Dugan, "Combining dynamic fault trees and event trees for probabilistic risk assessment," *Reliability and Maintainability 2004 Annual Symposium - RAMS*, pp. 214-219, 2004.
- [66] J. D. Andrews and S.J. Dunnett, "Event-tree analysis using binary decision diagrams," *IEEE Transactions on Reliability*, vol. 49, no. 2, pp. 230-238, 2000.
- [67] M. A. Mustafa and J. F. Al-Bahar, "Project risk assessment using the

- analytic hierarchy process,” *IEEE Transactions on Engineering Management*, vol. 38, no. 1, pp. 46-52, 1991.
- [68] P. K. Dey, “Decision support system for inspection and maintenance: a case study of oil pipelines,” *IEEE Transactions on Engineering Management*, vol. 51, no. 1, pp. 47-56, 2004.
- [69] R. Chedid, H. Akiki, S. Rahman, “A decision support technique for the design of hybrid solar-wind power systems,” *IEEE Transactions on Energy Conversion*, vol. 13, no.1, pp. 76-83, 1998.
- [70] T. J. Kull and S. Talluri, “A supply risk reduction model using integrated multicriteria decision making,” *IEEE Transactions on Engineering Management*, vol. 55, no. 3, pp. 409-419, 2008.
- [71] W. Liu, Y. Fan, L. Zhang, *et al.*, “WAMS information security assessment based on evidence theory,” *International Conference on Sustainable Power Generation and Supply*, pp. 1-5, 2009.
- [72] P. Kundur, *Power System Stability and Control*, New York: McGraw-Hill, 1994.
- [73] P. Eykhoff, *System identification parameter and state estimation*, John Wiley & Sons, 1974.
- [74] P. O’Shea, “The use of sliding spectral windows for parameter estimation in power system disturbance monitoring,” *IEEE Transactions on Power Systems*, vol. 15, no. 4, pp. 1261-1267, 2000.
- [75] K. C. Lee and K. P. Poon, “Analysis of power system dynamic oscillations with heat phenomenon by Fourier transformation,” *IEEE Transactions on Power Systems*, vol. 5, no. 1, pp. 148-153, 1990.
- [76] P. O’Shea, “A high-resolution spectral analysis algorithm for power system disturbance monitoring,” *IEEE Transactions on Power Systems*, vol. 17, no. 3, pp. 676-680, 2002.

- [77] M. Glickman, P. O'Shea and G. Ledwich, "Estimation of modal damping in power networks," *IEEE Transactions on Power Systems*, vol. 22, no. 3, pp. 1340-1350, 2007.
- [78] M. Bronzini, S. Bruno, M. D. Benedictis, *et al.*, "Power system modal identification via wavelet analysis," *Power Tech, IEEE Lausanne*, pp. 2041-2046, 2007.
- [79] D. S. Laila, A. R. Messina and B. C. Pal, "A refined Hilbert-Huang transform with applications to inter-area oscillation monitoring," *IEEE Transactions on Power Systems*, vol. 24, no. 2, pp. 610-620, 2009.
- [80] A. R. Messina and V. Vittal, "Nonlinear, non-stationary analysis of inter-area oscillations via Hilbert spectral analysis," *IEEE Transactions on Power Systems*, vol. 21, no. 3, pp. 1234-1241, 2006.
- [81] J. W. Pierre, D. J. Trudnowski and M. K. Donnelly, "Initial results in electromechanical mode identification from ambient data," *IEEE Transactions on Power Systems*, vol. 12, no. 3, pp. 1245-1251, 1997.
- [82] R. W. Wies, J. W. Pierre and D. J. Trudnowski, "Use of ARMA block processing for estimating stationary low-frequency electromechanical modes of power systems," *IEEE Transactions on Power Systems*, vol. 18, no. 1, pp. 167-173, 2003.
- [83] J. R. Smith, F. Fatehi, C. S. Woods, *et al.*, "Transfer function identification in power system applications," *IEEE Transactions on Power Systems*, vol. 8, no. 3, pp. 1282-1290, 1993.
- [84] J. C. -H. Peng and N. -K. C. Nair, "Adaptive sampling scheme for monitoring oscillations using Prony analysis," *IET Generation, Transmission & Distribution*, vol. 3, no. 12, pp. 1052-1060, 2009.
- [85] D. J. Trudnowski, J. R. Smith, T. A. Short, *et al.*, "An application of Prony methods in PSS design for multi-machine systems," *IEEE*

Transactions on Power Systems, vol. 6, no. 1, pp.118-126, 1991.

- [86] P. V. Overschee and B. D. Moor, *Subspace identification for linear system: theory-implementation-applications*. Dordrecht: Kluwer Academic Publishers, 1996.
- [87] A. R. Messina, J. M. Ramirez and J. M. Canedo, "An investigation on the use of power system stabilizers for damping inter-area oscillations in longitudinal power systems," *IEEE Transactions on Power Systems*, vol. 13, no. 2, pp. 552-559, 1998.
- [88] D. Jovicic, N. Pahalawaththa and M. Zavahir, "Novel current controller design for elimination of dominant oscillatory mode on an HVDC line," *IEEE Transactions on Power Delivery*, vol. 14, no. 2, pp. 543-548, 1999.
- [89] Y. Zhang and A. Bose, "Design of wide-area damping controllers for inter-area oscillations," *IEEE Transactions on Power Systems*, vol. 23, no. 3, pp. 1136-1143, 2008.
- [90] I. Kamwa, R. Grondin and Y. Hebert, "Wide-area measurement based stabilizing control of large power systems - a decentralized/hierarchical approach," *IEEE Transactions on Power Systems*, vol. 16, no. 1, pp. 136-153, 2001.
- [91] X. R. Xie and C. Lu, "Optimization and coordination of wide-area damping controls for enhancing the transfer capability of interconnected power systems," *Electric power systems research*, vol. 78, no. 6, pp. 1099-1108, 2008.
- [92] F. Okou, L. -A. Dessaint and O. Akhrif, "Power system stability enhancement using a wide-area signal based hierarchical controller," *IEEE Transactions on Power Systems*, vol. 20, no. 3, pp. 1465-1477, 2005.
- [93] C. X. Mao, K. S. Prakash, O. P. Malik, *et al.*, "Implementation and

- laboratory test results for an adaptive power system stabilizer based on linear optimal control,” *IEEE Transactions on Energy Conversion*, vol. 5, no. 4, pp. 666-672, 1990.
- [94] S. M. Back and J. W. Park, “Nonlinear parameter neuro-estimation for optimal tuning of power system stabilizers,” *The IEEE International Conference on Industrial informatics*, pp. 921-926, 2008.
- [95] Q. Lu, Y. Sun, Z. Xu, *et al.*, “Decentralized nonlinear optimal excitation control,” *IEEE Transactions on Power Systems*, vol. 11, no. 4, pp. 1957-1962, 1996.
- [96] B. Pal and B. Chaudhuri, *Robust control in power systems*, New York: Springer, 2005.
- [97] R. Majumder, B. C. Pal, C. Dufour, *et al.*, “Design and real-time implementation of robust FACTS controller for damping inter-area oscillation,” *IEEE Transactions on Power Systems*, vol. 21, no. 2, pp. 809-816, 2006.
- [98] C. J. Zhu, M. Khammash, V. Vittal, *et al.*, “Robust power system stabilizer design using H_∞ loop shaping approach,” *IEEE Transactions on Power Systems*, vol. 18, no. 2, pp. 810-818, 2003.
- [99] S. R. Zhang and F. L. Luo, “An improved simple adaptive control applied to power system stabilizer,” *IEEE Transactions on Power Electronics*, vol. 24, no.2, pp. 369-375, 2009.
- [100] Y. -Y. Hsu and T. -S. Luor, “Damping of power system oscillations using adaptive thyristor-controlled series compensators tuned by artificial neural networks,” *IEE Generation, Transmission and Distribution*, vol. 146, no. 2, pp. 1350-2360, 1999.
- [101] S. Mishra, P. K. Dash, P. K. Hota, *et al.*, “Genetically optimized neuro-fuzzy IPFC for damping modal oscillations of power system,”

- IEEE Transactions on Power Systems*, vol. 17, no. 4, pp. 1140-1147, 2002.
- [102] D. K. Chaturvedi, O. P. Malik and P. K. Kalra, "Generalised neuron-based adaptive power system stabiliser," *IEE Generation, Transmission and Distribution*, vol. 151, no. 2, pp. 213-218, 2004.
- [103] Z. Barton, "Robust control in a multimachine power system using adaptive neuro-fuzzy stabilisers," *IEE Generation, Transmission and Distribution*, vol. 151, no.2, pp. 261-267, 2004.
- [104] B. Naduvathuparambil, M. C. Valenti, A. Feliachi, *et al.*, "Communication delays in wide area measurement systems," *Proceedings of the 34th Southeastern Symposium on System Theory*, vol. 16, no. 1, pp. 136–153, 2002.
- [105] B. C. Pal, "Robust damping of inter-area oscillations with unified power-flow controller," *IEE Proceedings-Generation, Transmission and Distribution*, vol. 149, no. 6, pp. 733-738, 2002.
- [106] B. Chaudhuri, R. Majumder and B. C. Pal, "Wide-area measurement-based stabilizing control of power system considering signal transmission delay," *IEEE Transactions on Power Systems*, vol. 19, no. 4, pp. 1971-1979, 2004.
- [107] R. Majumder, B. Chaudhuri and B. C. Pal, "Implementation and test results of a wide-area measurement-based controller for damping inter-area oscillations considering signal-transmission delay," *IET Generation, Transmission and Distribution*, vol. 1, no. 1, pp. 1-7, 2007.
- [108] J. Qi, Q. Y. Jiang, G. Z. Wang, *et al.*, "Wide-area time-delay robust damping control for power system," *European transactions on electrical power*, vol. 19, pp. 899-910, 2009.
- [109] G. J. Li, T. T. Lie, C. B. Soh, *et al.*, "Decentralized nonlinear H_∞ control

- for stability enhancement in power systems,” *IEE Proceedings Generation, Transmission and Distribution*, vol. 146, no. 1, 2002.
- [110] H. X. Wu, K. S. Tsakalis and G. T. Heydt, “Evaluation of time delay effects to wide-area power system stabilizer design,” *IEEE Transactions on Power Systems*, vol. 19, no. 4, pp. 1935-1941, 2004.
- [111] J. He, C. Lu, X. Wu, *et al*, “Design and experiment of wide area HVDC supplementary damping controller considering time delay in China southern power grid,” *IET Generation, Transmission & Distribution*, vol. 3, no. 1, pp. 17-25, Dec. 2008.
- [112] P. Li, X. C. Wu, C. Li, *et al.*, “Implementation of CSG’s wide-area damping control system: overview and experience,” *Power systems Conference and Exposition, PSCE '09. IEEE/PES*, pp. 1-9, Mar. 2009.
- [113] H. J. Li, X. R. Xie, L. Y. Tong, *et al.*, “Implement of on-line transient stability control pre-decision in wide-area measurement system in Jiangsu power network,” *2005 IEEE/PES Transmission and Distribution Conference and Exhibition: Asia and Pacific*, pp. 1-4, 2005.
- [114] E. M. Martinez, “Wide area measurement & control system in Mexico,” *Third International Conference on Electric Utility Deregulation and Restructuring and Power Technologies, DRPT 2008*, pp. 156-161, 2008.
- [115] I. Kamwa, J. Beland, G. Trudel, *et al.*, “Wide-area monitoring and control at Hydro-Québec: past, present and future,” *IEEE Power Engineering Society General Meeting*, pp. 1-12, Oct. 2006.
- [116] P. Korba and K. Uhlen, “Wide-area monitoring of electromechanical oscillations in the Nordic power system: practical experience,” *IET Generation, Transmission & Distribution*, vol. 4, no. 10, pp. 1116-1126, Sep. 2010.
- [117] L. C. S, Y. Okada, M. Watanabe, *et al.*, “Analysis of Kita-Hon HVDC

- link for load frequency control of eastern Japan 50 Hz power system based on application of the Campus WAMS,” *Power and Energy Engineering Conference (APPEEC), 2010 Asia-Pacific*, pp. 1-4, Apr. 2010.
- [118] J. Y. Cai, Z. Y. H, J. Hauer, *et al.*, “Current status and experience of WAMS implementation in North America,” *2005 IEEE/PES Transmission and Distribution Conference and Exhibition*, pp. 1-7, Dec. 2005.
- [119] Ph. Denys, C. Counan, L. Hossenlopp, *et al.*, “Measurement of voltage phase for the French future defence plan against losses of synchronism,” *IEEE Transactions on Power Delivery*, vol. 7, no. 1, pp. 62-69, Jan. 1992.
- [120] K. K. Yi, J. B. Cho, S. H. Yoon, *et al.*, “Development of wide area measurement and dynamic security assessment systems in Korea,” *IEEE Power Engineering Society Summer Meeting*, vol. 3, pp. 1495-1499, Jul. 2001.
- [121] A. G. Phadke, B. Pickett, M. Adamiak, *et al.*, “Synchronized sampling and phasor measurements for relaying and control,” *IEEE Transactions on Power Delivery*, vol. 9, no.1, pp. 442-452, 1994.
- [122] A. F. Snyder, A. E. Mohammed, D. Georges, *et al.*, “A robust damping controller for power systems using linear matrix inequalities,” *Power Engineering Society Winter Meeting*, vol. 1, pp. 519-524, 1999.
- [123] S. E. Stanton, C. Slivinsky, K. Martin, *et al.*, “Application of phasor measurements and partial energy analysis in stabilizing large disturbances,” *IEEE Transactions on Power Systems*, vol. 10, no. 1, pp. 297-306, 1995.
- [124] V. Centeno, J. de la Ree, A. G. Phadke, *et al.*, “Adaptive out-of-step relaying using phasor measurement techniques,” *IEEE CAP*, vol. 6, no.

- 4, pp. 12-17, 1993.
- [125] N. R. Chaudhuri, B. Chaudhuri, S. Ray, *et al.*, “Wide-area phasor power oscillation damping controller: A new approach to handling time-varying signal latency,” *IET Generation, Transmission & Distribution*, vol. 4, no. 5, pp. 620-630, 2010.
- [126] Z. Y. Huang, J. F. Hauer and K. E. Martin, “Evaluation of PMU dynamic performance in both lab environments and under field operating conditions,” *IEEE Power Engineering Society General Meeting*, pp. 1–6, 2007
- [127] A. P. S. Meliopoulos, G. J. Cokkinides, O. Wasynczuk, *et al.*, “PMU data characterization and application to stability monitoring”, *Power Systems Conference and Exposition*, pp. 151-158, 2006.
- [128] J. Depablos, V. Centeno, A. G. Phadke, *et al.*, “Comparative testing of synchronized phasor measurement units,” *Power Engineering Society General Meeting*, vol.1, pp. 948 – 954, 2004.
- [129] K. Martin, T. Faris and J. Hauer, “Standard testing of phasor measurement unit,” *Fault and Disturbance Analysis Conference 2006*, Georgia Tech, Atlanta, GA, pp. 1-21, 2006.
- [130] C. S. Yu and W. H. Chen, “Removing decaying DC component in fault currents via a new modify discrete Fourier algorithm,” *IEEE Power Engineering Society General Meeting*, vol. 1, pp. 728-733, 2005.
- [131] A. G. Phadke, “Synchronized phasor measurements in power systems,” *IEEE Computer Application in Power*, vol. 6, pp, 10-15, 1993.
- [132] D. Fan and V. Centeno, “Phasor-based synchronized frequency measurement in power systems,” *IEEE Transactions on Power Delivery*, vol. 22, no.4, pp. 2010-2016, 2007.
- [133] A. G. Phadke and B. Kasztenny, “Synchronized phasor and frequency

- measurement under transient conditions,” *IEEE Transactions on Power Delivery*, vol. 24, no. 1, pp. 89-95, 2009.
- [134] C. W. Taylor, D. C. Erickson, K. E. Martin, *et al.*, “WACS wide-area stability and voltage control system: R&D and online demonstration,” *Proceeding of the IEEE*, vol. 93, no. 5, pp. 892-906, 2005.
- [135] J. Bertsch, C. Carnal, D. Karlson, *et al.*, “Wide-area protection and power system utilization,” *Proceedings of the IEEE*, vol. 93, no. 5, MAY 2005.
- [136] D. Karlsson, M. Hemmingsson and S. Lindahl, “Wide area system monitoring and control-terminology, phenomena, and solution implementation strategies,” *IEEE Power and Energy Magazine*, vol.2, no.5, pp. 68-76, 2004.
- [137] *WECC synchro-phasor project whitepaper*, version 3.0, July 17 2009.
- [138] (2002), ISA-TR84.00.02-2002, *The instruction, systems, and automation society (ISA)*, Available:
http://www.techstreet.com/standards/isa/tr84_00_02_2002_set?product_id=1035147
- [139] *IEEE guide for selecting and using reliability predictions based on IEEE 1413*, IEEE Std. 1413.1-2002
- [140] T. A. Mazzuchi and R. Soyer, “A Bayes method for assessing product-reliability during development testing,” *IEEE Transactions on Reliability*, vol. 42, no. 3, pp. 503-510, 1993.
- [141] R. Robidoux, H. P. Xu, L. D. Xing, *et al.*, “Automated Modeling of Dynamic Reliability Block Diagrams Using Colored Petri Nets,” *IEEE Transactions on System, Man and Cybernetics, part A: Systems and Humans*, vol. 40, no. 2, pp. 337-351, 2010.
- [142] S. Distefano and A. Puliafito, “Dependability evaluation with dynamic reliability block diagrams and dynamic fault trees,” *IEEE Transactions*

- on Dependable and Secure Computing*, vol. 6, no. 1, pp. 1545-5971, 2009.
- [143] E. J. Henley and H. Kumamoto, *Reliability engineering and risk assessment*, Englewood Cliffs: Prentice Hall, 1981.
- [144] N. G. Leveson, *Safeware: system safety and computers*, Addison Wesley, 1995.
- [145] W. S. Lee, D. L. Grosh, F. A. Tillman, *et al.*, "Fault tree analysis methods and applications: a review," *IEEE Transactions on Reliability*, vol. R-34, no. 3, pp. 194-203, 1985.
- [146] K. Durga Rao, V. Gopika, V. V. S. Sanyasi Rao, *et al.*, "Dynamic fault tree analysis using Monte Carlo simulation in probabilistic safety assessment," *Reliability Engineering & System Safety*, vol. 94, pp. 872-883, Apr. 2009.
- [147] W. E. Vesely, F. F. Goldberg, N. H. Robert, *et al.*, *Fault tree handbook* (NUREG-0492), US Nuclear Regulatory Commission, 1981.
- [148] S. B. Akers, "Binary decision diagrams," *IEEE Transactions on Computers*, vol. C-27, pp. 509-516, 1978.
- [149] X. Q. Bian, C. H. Mou, Z. P. Yan, *et al.*, "Simulation model and fault tree analysis for AUV," *Proceedings of the 2009 IEEE, international conference on macaronis and automation*, pp. 4452-4457, 2009.
- [150] J. B. Dugan, S. J. Bavuso and M. A. Boyd, "Dynamic fault-tree for fault-tolerant computer systems," *IEEE Transactions on Reliability*, vol. 41, no. 3, pp. 363-76, 1992.
- [151] R. Yanson and B. D. Joanne, "Design of reliable systems using static and dynamic fault trees," *IEEE Transactions on Reliability*, vol. 47, no. 3, pp. 234-244, 1998.
- [152] S. P. L and Z. Q. H, "Reliability analysis of transformer based on FTA

- and Monte Carlo method,” *Power and Energy Engineering Conference 2009*, pp. 1-3, 2009.
- [153] A. R. Karen and J. D. Andrews, “A fault tree analysis using binary decision diagrams,” *Reliability Engineering and System Safety*, pp. 45-56, 2002.
- [154] Y. Y. Wang, J. J. Zhou and W. G. Chen, “Assessment method for the reliability of power transformer based on fault-tree analysis,” *High Voltage Engineering*, vol. 35, no. 3, March 2009.
- [155] Y. Y. Hong, L. H. Lee and H. H. Cheng, “Reliability assessment of protection system for switchyard using fault-tree analysis,” *2006 International Conference on Power System Technology*, pp. 1-8, 2006.
- [156] G. Merle, J. M. Roussel, J. J. Lesage, *et al.*, “Probabilistic algebraic analysis of fault trees with priority dynamic gates and repeated events,” *IEEE Transactions on Reliability*, vol. 59, no. 1, pp. 250-261, March 2010.
- [157] R. Yansong and J. Bechta Dugan, “Design of reliable systems using static & dynamic fault trees,” *IEEE Transactions on Reliability*, vol. 47, no. 3, Sep. 1998.
- [158] J. Yuan, Y. Long, Y. L. Li, *et al.*, “A comparison of load models for composite reliability evaluation by nonsequential Monte Carlo simulation,” *IEEE Transactions on Power Systems*, vol. 25, no. 2, pp. 649-656, May 2010.
- [159] M. Zima, M. Larsson, P. Korba, *et al.*, “Design aspects for wide-area monitoring and control systems,” *Proceedings of the IEEE*, vol. 93, no. 5, pp. 980-996, 2005.
- [160] Y. Wang, W. Y. Li and J. P. Lu, “Reliability analysis of phasor measurement unit using hierarchical Markov modeling,” *Electric Power*

Components and Systems, vol. 37, pp. 517-532, 2009.

- [161] F. Aminifar, S. Bagheri-Shouraki, M. Fotuhi-Firuzabad, *et al.*, “Reliability modeling of PMUs using fuzzy sets,” *IEEE Transactions on Power Delivery*, vol. 25, no. 4, pp. 2384-2391, Oct. 2010.
- [162] J. A. Buzacott, “Network approaches to finding the reliability of repairable systems,” *IEEE Transactions on Reliability*, vol. R-19, no. 4, pp. 140-146, Aug. 2009.
- [163] R. N. Allan, R. Billinton and M. F. De Oliveira, “An efficient algorithm for deducing the minimal cuts and reliability indices of a general network configuration,” *IEEE Transactions on Reliability*, vol. R-25, no. 4, pp. 226-233, Aug. 2009.
- [164] “User’s manual and technology specification for SMU-2 Phasor Measurement Unit”, NR Electric Co. Ltd., April 2008.
- [165] “The technology specification for CSS-200/1 distributed Phasor Measurement Unit”, Beijing Sifang Automation Co. Ltd., June 2006.
- [166] “The technology specification for PAC-2000 power system Phasor Measurement Unit”, China Electric Power Research Institute, Aug. 2008.
- [167] D. Itagaki, K. Ohashi, I. Shuto and H. Ito, “Field experience and assessment of GPS signal receiving and distribution system for synchronizing power system protection, control and monitoring”, *2006 IEEE Power India Conference*, June 2006.
- [168] “Standard PMU definition”, version 6.4, Midwest Independent Transmission System Operator, Inc., August 26, 2011.
- [169] “Digital Fault Recorder SIMEAS R-PMU Manual”, Siemens Aktiengesellschaft, May 2011.
- [170] “SEL-487E Relay Current Differential and Voltage Protection Instruction Manual”, Schweitzer Engineering Laboratories, Inc., August 2, 2011.

- [171] L. Wang, J. Zhou, S. X. Zhu, *et al.*, “Distributed channel recorder of power grids protection and stability control system”, *Automation of Electric Power Systems*, vol.30, no.1, Jan.2006.
- [172] Y. K. Malaiya, M. N. Li, J. M. Bieman, *et al.*, “Software reliability growth with test coverage,” *IEEE Transactions on Reliability*, vol. 51, no. 4, pp. 420-426, Dec. 2002.
- [173] M. S. Ding, G. Wang and X. H. Li, “Reliability analysis of digital relay”, *2004 Eighth IEE International Conference on Developments in Power System Protection*, vol. 1, pp. 268-271, 2004.
- [174] A. Antonopoulos, J. J. O’Reilly and P. Lane, “A framework for the availability assessment of SDH transport networks”, *2nd IEEE Symposium on Computers and Communications*, Alexandria, Egypt, pp. 666–670, July 1997.
- [175] A. C. G. Melo and M. V. F. Pereira, “Sensitivity analysis of reliability indices respect to equipment failure and repair rates”, *IEEE Transactions on Power Systems*, vol. 10, no. 2, pp. 1014-1021, 1995.
- [176] I. Rados, T. Sunaric and P. Turalija, “Availability comparison of different protection mechanisms in SDH ring network”, *Proceedings of the International Conference on Modern Problems of Radio Engineering, Telecommunications and Computer Science*, pp. 287-290, 2002.
- [177] M. G. Adamiak, A. P. Apostolov, M. M. Begovic, *et al.*, “Wide-area protection-technology and infrastructures”, *IEEE Transactions on Power Delivery*, vol. 21, no. 2, pp. 601-609, 2006.
- [178] H. Cancela and M. El Khadiri, “A recursive variance-reduction algorithm for estimating communication-network reliability”, *IEEE Transactions on Reliability*, vol. 44, no. 4, pp. 595-602, Dec. 1995.
- [179] R. Suresh, “A cut set approach to reliability evaluation in communication

- networks”, *IEEE Transactions on Reliability*, vol. R-31, no. 5, pp. 428-431, Aug. 2009.
- [180] P. Zhang, D. Y. Yang, K. W. Chan, *et al.*, “Self-adaptive wide-area damping control based on SSI and WAMS”, *International Conference on Electrical Engineering, Korea*, 11-14 Jul. 2010.
- [181] M. Shahidehpour and Y. Y. Wang, *Communication and control in electric power systems: applications of parallel and distributed processing*, Wiley-Interscience IEEE Press, 2003.
- [182] O. Gehrke, S. Ropenus and P. Venne, “Distributed energy resources and control: a power system point of view”, in *Proc. Risø Energy Conf.* Roskilde, Denmark, pp. 248-257, 2007.
- [183] M. Chenine and L. Nordstrom, “Simulation of wide-area communication for centralized PMU-based applications”, *IEEE Trans. Power Deliv.*, vol. 26, no. 3, pp. 1372-1380, July 2011.
- [184] W. Y. Li, *Risk assessment of power systems: models, methods, and applications*. IEEE Press, 2005.
- [185] F. Lambert and V. Gungor, “A survey on communication networks for electric system automation”, *Computer networks*, vol. 50, no. 7, pp. 877-897, 2006.
- [186] Y. Deng, H. Lin, A. G. Phadke *et al.*, “Research of risk-based security assessment of power system”, *2011 4th International Conference on Electric Utility Deregulation and Restructuring and Power Technologies*, pp. 1335-1340, July 2011.
- [187] N. Liu, H. Zhang and W. X. Liu, “Security assessment for communication networks of power control systems using attack graph and MCDM”, *IEEE Trans. Power Deliv.*, vol. 25, no. 3, pp. 1492-1500, 2010.

- [188] Y. Deng, H. Lin, A. G. Phadke *et al.*, “Communication network modeling and simulation for wide area measurement applicaitons”, *Proceedings of 2nd IEEE International Conference on Smart Grid Communications*, pp. 1-6, Oct. 2011.
- [189] Y. Deng, H. Lin, A. G. Phadke *et al.*, “Reliability evaluation of the communication network in wide-area protection”, *IEEE Trans. Power Deliv.*, vol. 26, no. 4, pp. 2523-2530, 2011.
- [190] M. Khosrow and K. Ranjit, “A reliability perspective of the smart grid”, *IEEE Trans. Smart grid*, vol. 1, no. 1, pp. 57-64, June, 2010.
- [191] M. Shahraeini, M. H. Javidi and M. S. Ghazizadeh, “Comparison between communication infrastructures of centralized and decentralized wide area measurement systems”, *IEEE Trans. Smart Grid*, vol. 2, no. 1, pp. 206-211, March, 2011.
- [192] W. H. Zhang, “Calculation and analysis about transmission time delay of SDH self-healing loop network”, *Telecommunications for Electric Power System*, vol. 26, no. 154, pp. 54-60, Aug. 2005.
- [193] D. K. Mynbaev and L. L. Scheiner, *Fiber-optic communications technology*. Prentice Hall: 2002
- [194] J. D. Andrews and T. R. Moss, *Reliability and risk assessment*. Professional Engineering Publishing Limited, 2002.
- [195] R. Billinton and R. N. Allan, *Reliability evaluation of engineering systems: concepts and techniques*, second edition, plenum press, New York and London, 1992.
- [196] T. L. Saaty, “How to make a decision: the analytic hierarchy process”, *Europ. J. Operat. Res.*, vol. 48, pp. 9-36, 1990.

- [197] T. L. Saaty, "Absolute and relative measurement with the AHP: the most livable cities in the United States", *Europ. J. Operat. Res.*, vol. 22, pp. 347-358, 1986.
- [198] GB/T 20984-2007, *Information security technology-risk assessment specification for information security*, 2007.
- [199] Y. J. Lee and M. Atiquzzaman, "Exact algorithm for delay-constrained capacitated minimum spanning tree network", *IET Communications*, vol. 1, no. 6, pp. 1238-1247, Dec. 2007.
- [200] S. W. Chung, E. S. Jung, E. Kim, *et al.*, "An MST-based network architecture for sharing broadcast TV programs", *IEEE Communications Magazine*, vol. 48, no. 6, pp. 82-91, June 2010.
- [201] I. Cahit and R. Cahit, "Minimum spanning tree", *Proceedings of the Institution of Electrical Engineers*, vol. 122, no. 5, pp. 496, May 1975.
- [202] L. Li and Y. T. Liu, "Out-of-step splitting scheme based on coherency identification and self-adaptive power system separation criteria", *Journal of Shandong university (Engineering Science)*, vol. 37, no. 6, pp. 49-53, Dec. 2007.
- [203] I. Cahit and R. Cahit, "Structural reliability of centralized tree network", *Electronic Letters*, vol. 9, no. 26, pp. 621-622, Dec. 1973.
- [204] F. P. Demello and C. Concordia, "Concept of synchronous machine stability as affected by excitation control," *IEEE Transactions on Power Apparatus and Systems*, vol. 88, no. 4, pp. 316-329, 1969.
- [205] C. E. Grund, J. J. Paserba, J. F. Hauer, *et al.*, "Comparison of Prony and eigenanalysis for power system control design," *IEEE Transactions on Power Systems*, vol. 8, no. 3, pp. 964-971, 1993.
- [206] D. J. Trudnowski, J. W. Pierre, N. Zhou, *et al.*, "Performance of three mode-meter block-processing algorithms for automated dynamic stability

- assessment,” *IEEE Transactions on Power Systems*, vol. 23, no. 2, pp. 680-690, 2008.
- [207] H. Ghasemi, C. Canizares and A. Moshref, “Oscillatory stability limit prediction using stochastic subspace identification,” *IEEE Transactions on Power Systems*, vol. 21, no. 2, pp. 736-745, 2006.
- [208] S. Y. Kung, “A new identification method and reduction algorithm via singular value decomposition,” *12th Asilomar Conference on Circuits, Systems and Computer, CA*, 1978.
- [209] B. Peeters and G. De Roeck, “Comparison of system identification methods using operational data of a bridge test,” *Proceeding of the 23rd ISMA, Noise and Vibration Engineering*, pp. 923-930, 1998.
- [210] B. Peeters and G. De Roeck, “Reference based stochastic subspace identification in civil engineering,” *Proceedings of the 2nd international conference on identification engineering systems, Swansea*, pp. 639-648, 1999.
- [211] E. Reynders and G. D. Roeck, “Reference-based combined deterministic-stochastic subspace identification for experimental and operational modal analysis,” *Mechanical Systems and Signal Processing*, vol. 22, pp. 617-637, 2008.
- [212] P. Bart and D. R. Guido, “Reference-based stochastic subspace identification for output-only modal analysis,” *Mechanical Systems and Signal Processing*, vol. 13, no. 6, pp. 855-878, 1999.
- [213] R. Brincker and P. Andersen, “Understanding stochastic subspace identification,” *Conference & Amp, Exposition on Structural Dynamics*, pp. 1-6, 2006.
- [214] G. T. Heydt, C. C. Liu, A. G. Phadke, *et al.*, “Solutions for the crisis in electric power supply,” *IEEE Control System Magazine*, vol.20, pp. 22-30,

2000.

- [215] A. Magdya, A. Sallam, J. McCalley, *et al.*, “Damping controller design for power system oscillations using global signals,” *IEEE Transactions on Power Systems*, vol.11, no. 2, pp.767-773, 1996.
- [216] W. Masayuki, H. Takuhei, I. Takanori, *et al.*, “Power system stabilization control based on the wide area phasor measurement,” *Transactions of the Institute of Electrical Engineers of Japan*, vol.163, no.1, pp.16-24, 2008.
- [217] D. Ruiz-Vega, A. R. Messina and M. Pavella, “Online assessment and control of transient oscillations damping,” *IEEE Transactions on Power Systems*, vol. 19, no. 2, pp. 1038-1047, 2004.
- [218] A. F. Komla, N. Yorino and H. Sasaki, “Design of H_{∞} -PSS using numerator-denominator uncertainty representation,” *IEEE Transactions on Energy Conversion*, vol. 12, no. 1, pp. 45-50, 1997.
- [219] S. Ray and G. K. Venayagamoorthy, “Real-time implementation of a measurement-based adaptive wide-area control system considering communication delay,” *IET Generation Transmission & Distribution*, vol. 2, no. 1, pp. 62-70, 2008.
- [220] D. Dotta, A. S. e Silva and I. C. Decker, “Wide-area measurements-based two-level control design considering signal transmission delay,” *IEEE Transactions on Power Systems*, vol. 24, no. 1, 2009.
- [221] N. Yang, Q. Liu and J. D. McCalley, “TCSC controller design for damping interarea oscillations,” *IEEE Transactions on Power Systems*, vol. 13, no. 4, pp. 1304-1310, 1998.